

BYG•DTU

DANMARKS
TEKNISKE
UNIVERSITET



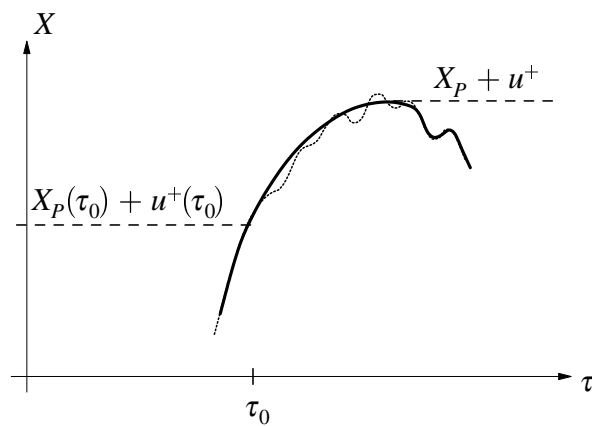
Niels Jacob Tarp-Johansen

Two Problems in Stochastic Structural Dynamics

Rapport
BYG•DTU R-026
2001
ISSN 1601-2917
ISBN 87-7877-085-8

Two Problems in Stochastic Structural Dynamics

Niels Jacob Tarp-Johansen



Department of Civil Engineering
DTU-bygning 118
2800 Kgs. Lyngby
<http://www.byg.dtu.dk>

2001

Preface

This thesis is submitted as a partial fulfillment of the requirements for the Danish Ph.D. degree.

The work leading to this thesis was carried out as a part of a Ph.D.-study at the Department of Structural Engineering and Materials (BKM), Technical University of Denmark, during the period October 1, 1995 to May 1, 2000. Professor at BKM Ove Ditlevsen supervised the study.

During the study a total of about one and a half year of absence was spent in various research positions at BKM and on the EU-programme: Human Capital and Mobility Research Network. The latter with Professor R. Rackwitz at the Institut für Massivbau, Technical University of Munich, Germany as supervisor.

Work different from that leading to this thesis has also been carried out during the study and the periods of leave. Research has been conducted in the area of stochastic FEM [9], in the area of positive random fields [15] and in the area of Bayesian Statistics applied to censored data [11]. It appears from the references that all this research work was done in close collaboration with O. Ditlevsen. Finally work within the field of computer methods in structural safety was carried out in Munich.

Hellerup, Copenhagen, May 8, 2000

Niels Jacob Tarp-Johansen

Acknowledgements

First of all my supervisor, professor at the Department of Structural Engineering and Materials (BKM) at the Technical University of Denmark Ove Ditlevsen is thanked. His professional skills, enthusiasm, always hard working attitude, willingness to let his students accompany him when going to conferences all over the world, his understanding in stressed situations and his humanity, are all qualities for which I value him highly.

Associated professor at BKM Lars Damkilde is thanked for being the first that by his enthusiasm drew my attention to the field of applied mechanics, especially the advanced topics of structural mechanics such as dynamics, plasticity, structural stability and FEM.

Steen Krenk, Professor at BKM, is thanked for taking the time to have talks with me, that, though not directly related to the project, were inspiring and have contributed to my attitude and approach to problems in the field of applied mechanics.

The Technical University of Denmark is gratefully acknowledged for granting me a ph.d.-scholarship. The Danish Research Council and the European Human Capital and Mobility EU-Programme are acknowledged for, when on leave from my project, providing me with the financial support that gave me the opportunity to work with and gain more insight into the field and methods of stochastic mechanics and reliability theory.

Finally, I am deeply indebted to my family and my beloved Lise for their support, interest, understanding and encouragement during the study and its ending.

Abstract

This thesis treats two different subjects within the field of random vibrations of structural systems. For this reason the thesis falls in two parts and consequently this abstract is also split into two parts.

Part I

The first part concerns a fast simulation technique useful for the examination of the stochastic characteristics of the random development of the plastic displacement processes of elasto-plastic oscillators (EPOs) driven by Gaussian white noise. These oscillators are specific examples of the more general class of systems with hysteresis. The results obtained herein are, however, valid for general hysteretic systems.

The simulation procedure consists in simulating clumps of plastic displacement increments by use of the so-called Slepian model and simulating, by simple means, the inter-clump waiting times. The Slepian model has earlier been applied to ideal EPOs for which analytical results have been derived. Similar results cannot be derived for non-ideal EPOs, why simulations are required. In the present work the analytical results valid for the ideal EPO forms the basis of a semi-analytical simulation scheme used for non-ideal EPOs with strain hardening and softening. The simulation algorithm, which is basically a time integration algorithm, is fast as it takes time-steps of half a period or larger. Especially when simulating waiting times it may use time steps of the same magnitude as the mean waiting time, which gives a considerable time gain compared to traditional direct numerical time integration.

In former works an approximate waiting time distribution based on asymptotic analytical results has been suggested. Here an improved waiting time description accounting for the fact that convergence to the asymptotic result is slow is presented. The problem is that for realistic yield levels clumps arrive in groups. A phenomenon which is not properly accounted for by the asymptotic results. For the waiting time simulation a model for the amplitude process of a linear oscillator driven by white noise is applied. It is derived from two simple Slepian models for the displacement and velocity processes. In order that the Slepian model simulation of the clumps be sufficiently simple to code and the computation of the plastic increments not too time costly, a simplification of the general hysteretic restoring force diagram is suggested and proved

useful. Since yield levels are generally asymmetric with respect to the equilibrium point the notion of symmetrized yield levels is introduced as they simplify the waiting time simulation. This implies the so-called clump definition different from what has traditionally been used. It is demonstrated that the simulation scheme proves well using these symmetrized yield levels without limiting the applicability of the algorithm.

As the results obtained by the Slepian Model Simulation Method are compared to results obtained by direct time integration a thorough discussion of the applied direct time integration scheme is given. It is proven that the scheme is at the same time a fair and a realistic benchmark for the Slepian Model Simulation Method with respect to time consumption and accuracy. Finally, simulation results are presented. These proves that the Slepian Simulation Method gives good approximate results and that it exhibits good time gain factors. Especially it is proven that the merging of clump simulations and waiting time simulations, due to the suggested waiting time distribution works notably better than results obtained by exponentially distributed waiting times.

Part II

The second part deals with the random response of a certain class of structures with random properties subjected mainly to deterministic excitation.

In investigations of noise radiated from submerged ship hulls it turns out that the vibrations of the ship hull are influenced by the presence of numerous minor devices elastically attached to the hull. Furthermore, information about the entity of the devices is uncertain, why the devices are termed fuzzy substructures. The fuzzies are most realistically modeled by stochastic means. Thus the ship hull, the so-called master, may be considered a structure with random vibration properties.

Herein it is investigated whether the dynamical damping effect that the master experiences due to the fuzzies, is obtained if the fuzzies are modeled by a continuous random field. Some researches have claimed that this is not the case. Constructing, step by step, a piecewise continuous one-dimensional Poisson square wave field from a discrete model of the fuzzies, and further proving a certain asymptotic equivalence of the discrete model and the field, it is shown that continuous fields lead to damping effects too.

Furthermore, a specific example is given in which quantification of the damping effect is obtained by use of Winterstein approximations to the distribution of the change-in-impedance of the master as caused by the fuzzies. The strength of these results is that, via the Winterstein approximations, a mapping from standard Gaussian variables to the change-in-impedance quantities is obtained thus opening for possible applications in numerical reliability methods.

Though the theory of fuzzy substructures has arisen in the field of submarine engineering the authors of [22] see potential use of this theory in structural engineering as well.

Resumé

Denne afhandling er indleveret som et led i erhvervelsen af den tekniske ph.d.-grad ved Danmarks Tekniske Universitet. Afhandlingen bærer titlen: To Problemer i Stokastisk Strukturel Dynamik, og den behandler to forskellige problemstillinger inden for stokastiske svingninger i bærende konstruktioner, hvorfor afhandlingen falder i to dele.

Del I

Den første del omhandler en effektiv simuleringsmetode, der er anvendelig ved undersøgelsen af de stokastiske karakteristika for den tidlige udvikling af den plastiske flytning i elastisk-plastiske oscillatorer (EPOer) belastet med gaussisk hvid støj. Elastisk-plastiske oscillatorer er specielle eksempler fra den generelle klasse af systemer med hysteres. Resultaterne beskrevet i nærværende afhandling er dog også gyldige for hysterese-systemer i almindelighed.

Simuleringsmetoden består i, ved brug af den såkaldte Slepian-model, at simulere klumper af plastiske flytningsinkremitter og på simpel måde at simulere ventetiden mellem klumperne. Tidligere har Slepianmodellen været anvendt på ideelle EPOer, for hvilke det er muligt at udlede analytiske resultater. Tilsvarende resultater kan ikke udledes for ikke-ideelle EPOer, hvorfor simuleringer er påkrævede. I nærværende arbejde udnyttes de analytiske resultater for den ideelle EPO som grundlag for en semianalytisk simuleringsalgoritme anvendelig på ikke-ideelle EPOer med strain hardening og softening. Simuleringsalgoritmen, der grundlæggende er en tidsintegrationsalgoritme, er hurtig, fordi den anvender tidskridt af størrelse en halv svingningstid eller mere. Specielt ved simulering af ventetiderne kan der anvendes tidsskridt af samme størrelsesorden som middelvektiden, hvilket giver en anseelig tidsbesparelse i forhold til traditionel direkte numerisk tidsintegration.

I tidligere arbejder er en approksimativ ventetidsfordeling baseret på asymptotiske resultater blevet foreslået. Heri beskrives en forbedret ventetidsfordeling, som tager hensyn til det faktum, at konvergens til det asymptotiske resultat er langsom. Problemet er, at for realistiske flydeniveauer forekommer klumperne i grupper. Et fænomen som de asymptotiske resultater ikke inkluderer. Til anvendelse ved ventetidssimuleringen benyttes en model for amplitudeprocessen for en lineær oscillator belastet med hvid støj. Denne model dannes udfra to simple Slepianmodeller for flytningen og hastigheden. For at sikre at Slepianmodelsimuleringerne af de plastiske inkremitter hverken bliver for komplicerede eller for beregningsmæssige tunge indføres en

simplificering af det generelle arbejdsdiagram, og det vises, at denne simplifikation er brugbar. Idet flydegrænserne generelt er asymmetriske mht. ligevægtspunktet, introduceres de såkaldte symmetriserede flydegrænser. Dette medfører, at den såkaldte klumpdefinition ændres i forhold til den traditionelle. Det vises, at simuleringsmetoden på tilfredsstillende måde kan håndtere disse symmetriserede flydegrænser, uden at det begrænser metodens anvendelsesområde.

Da resultaterne, der opnåes ved anvendelse af Slepianmodelsimuleringsmetoden, sammenlignes med resultater opnået ved direkte numerisk tidsintegration, gives en grundig gennemgang af metoden anvendt ved direkte tidsintegration. Det vises, at denne direkte metode giver et rimeligt og realistisk sammenligningsgrundlag for Slepianmodelsimuleringsmetoden mht. tidsforbrug og nøjagtighed. Sluttelig præsenteres simuleringsresultater. Disse viser, at Slepianmodelsimuleringsmetoden giver gode approximative resultater, og at den udviser gode beregningstidsbesparelser.

Del II

Den anden del af afhandlingen angår det stokastiske respons af en bestemt klasse af konstruktioner med stokastiske egenskaber og som drives af en deterministisk last.

I forbindelse med undersøgelser af støj udsendt fra ubåde viser det sig, at svingningerne i ubådens skrog påvirkes af alle de mindre instrumenter, der er elastisk fastgjort til skroget. Desuden er den tilgængelige information om instrumenterne forbundet med usikkerhed. Af samme grund kaldes instrumenterne på engelsk under ét fuzzy substructures. Det er derfor kun rimeligt at anvende en stokastisk modellering af fuzzy'erne. Således kan man betragte skroget (kaldet masteren) som en konstruktion med stokastiske svingningsegenskaber.

I afhandlingen undersøges det hvorvidt den dynamiske dæmpning, som masteren påvirkes af pga. fuzzy'erne, kan beskrives hvis fuzzy'erne modelleres som et kontinuert stokastisk felt. Nogle forskere hævder, at dette ikke er muligt. Ved, skridt for skridt, at konstruere et stykkevis kontinuert endimensionelt Poisson square-wave felt fra en diskret model, og desuden bevise at der eksisterer en anden-moment-ækvivalens mellem Poisson square-wave feltet og det diskrete felt, vises det, at kontinuerte felter også kan give en dæmpningseffekt.

Endvidere gives et specifikt eksempel, i hvilket en kvantificering af dæmpningseffekten opnåes vha. Wintersteinapproximationer til impedansændringerne pga. fuzzy'erne. Disse resultaters styrke er, at der opnåes en afbildning fra gaussiske stokastiske variable til de størrelser, der beskriver impedansændringerne. Derved er der åbnet mulighed for anvendelser inden for numerisk sikkerhedsanalyse.

Selvom teorien for fuzzy substructures oprindeligt udvikledes inden for ubåddesign ser forfatterne af [22] mulighed for anvendelse af teorien inden for bærende konstruktioners sikkerhed.

Table of Contents

Background and Organization	1
I Slepian Modeling of Random Vibrations in Systems with Hysteresis	7
1 Introduction	9
1.1 Background and Mechanical Modeling	9
1.2 The Equation of Motion for the SDOF EPO	12
1.2.1 The Gaussianity of the White Noise	13
1.2.2 The Scaled Equation of Motion	15
1.2.3 The Amplitude Process	17
1.3 Historical Review	18
1.4 The Slepian Model Simulation Method for the SDOF EPO	19
1.5 Outline of the Following Chapters	21
1.6 Summary	22
2 Modeling and Simulating Clumps	23
2.1 Clump Definition	23
2.2 Definition of The ALO Response Process	27
2.3 Modeling the Plastic Increments	28
2.4 ALO Response Properties and Slepian Modeling	30
2.4.1 Upcrossings and Maxima of Stationary Gaussian Processes	30
2.4.2 The ALO Maxima	32
2.4.3 First Maximum in a Clump	33
2.4.4 Second and Following Maxima in a Clump	34
2.5 From ALO to EPO Response	36
2.6 Simulation Scheme	40
2.6.1 Computational Aspects	43
2.7 Simulations of Clumps for the Bilinear EPO	45

2.8	Summary	48
3	Modeling and Simulation of Inter-clump Waiting Times	53
3.1	Main Characteristics of the Distribution	53
3.1.1	Quantities on which the Distribution Depends and Symmetrization . . .	53
3.1.2	The Amplitude Process	54
3.1.3	Transient Lower Tail	55
3.1.4	Exponential Upper Tail	56
3.2	Simulating the Waiting Time	58
3.2.1	Simulating the Transient Lower Tail	58
3.2.2	Simulating the Exponential Upper Tail	65
3.3	Summary	72
4	Simulation by Direct Numerical Time Integration	75
4.1	White Noise Approximation	76
4.2	Time Integration	77
4.2.1	Linear States: Exact Time-Stepping	77
4.2.2	Non-Linear States: Approximate Time-Stepping	79
4.3	Stochastic Properties of the Time-Stepping Process	81
4.3.1	Pulse Distribution	82
4.3.2	Power Spectrum	82
4.4	Algorithm – Discussion	89
4.4.1	Time-Step Size – Again	89
4.4.2	The Algorithm in Short	91
4.5	Summary	91
5	Simulation Results	95
5.1	The Plastic Displacement Process	95
5.2	Initial Conditions	96
5.3	Strain Hardening and Softening for the Bilinear EPO	97
5.3.1	Hardening	97
5.3.2	Softening	102
5.4	Non-Ideal EPO	106
5.5	Time Gain Factor	108
5.6	Summary	109
6	Conclusions	115

A	Restoring Force Diagrams	119
A.1	The Bilinear EPO	119
A.2	A Non-Idealized EPO	121
A.2.1	The Simplified Restoring Force Diagram	122
A.2.2	The Non-Simplified Restoring Force Diagram	123
A.3	A Few Phrases used in the Theory of Plasticity.	125
II	Vibrations in Systems with Fuzzy Sub-Systems	127
1	Introduction	129
1.1	Background and Mechanical Modeling	129
1.1.1	Modeling the Master and the Fuzzies	130
1.1.2	Governing Equations, Impedance and Frequency Response	132
1.2	Outline of the Following Chapters	135
1.3	Summary	135
2	Modeling the Fuzzies	137
2.1	A Discrete Fuzzy Model	137
2.2	A Non-Discrete Field Fuzzy Model	139
2.3	Distributional Properties of R and V and Winterstein Approximations	142
2.4	Summary	145
3	Quantification of Vibration Damping	147
3.1	Amplification Factor and Phase Angle	147
3.2	The Example	148
3.3	Summary	153
4	Conclusions	155
A	Statistical Moments of Integrals of Poisson Fields	157
A.1	The Square-Wave Field	157
A.2	The Point Pulse Field	160
	Bibliography	163

Background and Organization

This first chapter gives a survey of the very background of the field to which the problems treated in this thesis belong. In addition it presents the outline of the thesis and also a few remarks concerning the nomenclature used are given.

Background

Basically, any design problem a structural engineer is faced with involves randomness. There are different sources of randomness of which one or more may be relevant to the design problem at hand.

One of the sources is the inherent randomness of nature itself which is easily appreciated, accepted and understood even by non-professionals. Almost anyone knows, by some sort of experience, that two wooden sticks, though geometrically alike, may exhibit considerable differences with respect to flexibility and strength properties. Further, we all understand that not only structural properties are affected by the randomness of nature. The actions that structures are subjected to are also random. Obvious examples of such actions are forces due to wind and sea waves. More rare, but at the same time with the risk of being of more devastating nature, are earthquake loads.

Less familiar to layman is randomness due to insufficient information about various parameters going into the design process. For instance, these parameters are distribution parameters of the distributions that describe the randomness of structural properties and actions. Such insufficient knowledge, or in other words: uncertain information, is usually reflected as stochastic uncertainty. However, it need not be distribution parameters that are assessed with uncertainty. As it is discussed later, it might simply be deterministic quantities like the mass of some part of the structure that is not well defined.

Also the human factor plays a role. Generally structures are designed for human use. Take furniture in apartments as an example. They are, from a technical point of view, randomly scattered over floors, walls and ceilings. Thus, designing structures for human living involves a contribution to uncertainty in addition to that due to the randomness of nature. Another example of the effect of human activity is traffic on bridges.

Model uncertainty is yet another contributor to uncertainty that must be mentioned here to complete the picture. It arises from the fact that in all design situations a simplified model is set up in order to make computations practicable or simply because the amount of information available does not allow a more complicated model. The simple model excludes quantities (physical, geometrical etc.) that may randomly influence the performance of the system. Thus, as a consequence of the design process itself, unclarified uncertainty is present.

Though randomness appears everywhere it is not necessarily justifiable from an engineering point of view to always include it in the design process. Actually an engineer may account for randomness by simply stating that it is negligible as fluctuations are small or it appears in places where even severe randomness does not affect the design significantly because the system is maybe dominated by deterministic effects that are orders of magnitude more important to system behavior than those due to randomness. The engineer may even for simplicity reasons choose to replace random quantities by deterministic quantities that results in a design that in his judgement is on the safe side.

As design demands tend to favor optimized structures to those that results from very conservative assessments neglecting randomness, there is a need for studies in stochastic mechanics. Especially studies of computational methods in stochastic mechanics are relevant, as the complexity of the computations in stochastic design problems is in general greater than those of computations in deterministic problems as adding randomness to a given problem seldom reduces the governing equations. This problem may of course be circumvented by lowering the demands on the amount of information on system behaviour required to make design decisions. One may decide to use only information about, say, expectations and scatter of the random system behaviour in terms of mean values, standard deviations and correlations. However, even obtaining this limited information may be difficult - or if not difficult then at least cumbersome.

Following the same line of argumentation as above, it is clear that almost all mechanical systems are dynamic as well as random. They respond dynamically since loads are applied or removed over some finite time. But, then again, many systems are from an engineering point of view most reasonably considered quasi-static as the duration of load application is long compared to the relevant characteristic time-scale of the load carrying mechanism.

Though a lot randomness and uncertainty effects as well as dynamic effects may be neglected, systems still exist that are only given a proper treatment if they are analyzed applying methods from the field of stochastic dynamics. This may be so because of significantly temporal and/or spatial random fluctuations of the driving forces and/or system properties.

In the present thesis two problems within the field of random vibrations of engineering systems are treated. Firstly one, in which temporal random loading is essential and system properties are considered deterministic, and secondly one, where random system properties is brought into focus, whereas the driving forces may or may not be random.

Random Temporal Forcing

A classical case study in the field of random loading is the single degree of freedom (SDOF) oscillator subjected to some random driving force which, with almost equal power, in the long run excites the oscillator at many different frequencies around its resonant frequency at which amplification is strongest. As the response is dominated by the amplified frequencies, one usually does in these studies, with only small error, replace the forcing process by the white noise process that is characterized by containing, in the long run, equal power at all frequencies.

Herein such a hysteretic, i.e. non-linear, SDOF oscillator subjected to white noise is studied. As opposed to linear oscillators closed form solutions for the joint distribution or even the second moment structure of the response process do seldom exist. Therefore one is faced with the above mentioned computational problem. In [6] it is presented how one by approximate reasoning in terms of the so-called Slepian model is able to obtain analytical expressions for the probabilistic characteristics of different quantities associated with the response of a linear-elastic-ideal-plastic SDOF oscillator excited by Gaussian white noise. If the linear-elastic-ideal-plastic strain-stress relation is replaced by a stress-strain relation of general hysteresis type the simplifications obtained in the linear-elastic-ideal-plastic case do not carry through. It may then seem necessary to resort to Monte Carlo simulation. Such simulations can become quite time costly if they are performed by straight-forward numerical time integration. However, some of the analytical results from the linear-elastic-ideal-plastic case may form the basis of a fast semi-analytical simulation scheme which makes the simulation time for a single response path sample become conveniently small. As it will be shown this is done without losing essential features of the response. The simulation strategy is termed the *Slepian Model Simulation Method*.

Random System Properties

During the design process of complicated structures or mechanical systems one often encounter situations where either statements about the system must be given, even though the final configuration of the systems is unknown, or it is known that the configuration changes unpredictably during use. As it is pointed out below these situations may be considered as examples of systems with random properties.

The area of research that has initiated investigations of the kind of problem considered herein is submarine engineering. In that field one needs to give statements about the dynamical characteristics of the submarine before all details concerning the equipment of the submarine is well known. In one of the previous sections it was mentioned, that in the field of structural engineering buildings and bridges can be thought of as structures of which the configuration changes during use. Characteristic of the described problems is that they involve a larger main structure and several minor structures or mechanical devices such as the equipment attached to the main structure. It is the ensemble of the minor structures that is not well-defined and for that reason it is termed a *fuzzy sub-system*. The main structure, the so-called master structure, on the other

hand is well-defined. Clearly the dynamical properties of the complete system depends on the interaction between the master structure and the fuzzy sub-system.

Usually some information is available about the dynamical properties of the fuzzy sub-system. Assume that it is possible to quantify this information by density functions for the random distribution of the properties of the fuzzy sub-system over the master structure. Then one can simply consider the fuzzy sub-system as giving rise to random system properties of the master structure. It is this line of reasoning that is investigated herein. Especially the case study of a master structure being a linear SDOF oscillator and a fuzzy sub-system of likewise linear SDOF oscillators which is considered. The aim is to compute the stochastic properties of the frequency response function of the complete system.

Organization of the Thesis

As the consequence of having two different subjects in the field of random vibrations treated in the present thesis, the thesis is split into two parts. The first part concerns the efficient Slepian model simulation technique for systems with hysteresis driven by certain types of random loading, while the second part treats the stochastic properties of the frequency response function of a linear SDOF oscillator having a fuzzy sub-system attached.

Nomenclature

The nomenclature applied in the thesis generally follows the most commonly used nomenclature in the theory of stochastic mechanics. It is, however, considered worthwhile to explain the conventions used herein. The table below lists the typography. The typographic rules used are not very strict, S_w , for instance, denotes a power spectrum rather than a random variable. However, the context will warrant that no misunderstandings occur.

Variable type	Typography	Example
Random variable	Capital italics	<i>X</i>
Random matrix/vector	Capital boldface roman	Y
Realization of random variables	Small italics	<i>x</i>
Deterministic variable	Small italics	<i>z</i>
Deterministic matrix	Capital boldface sans serif	A
Deterministic vector	Small boldface sans serif	b

Part I

Slepian Modeling of Random Vibrations in Systems with Hysteresis

Chapter 1

Introduction

This introductory chapter gives a thorough discussion of the physical background and the basic assumptions leading to the model used for the considered mechanical problem. Next it briefly presents the main features of the simulation technique which is the subject of this first part of the thesis. Finally a short outline of the following chapters is given.

1.1 Background and Mechanical Modeling

Randomly dynamically loaded deterministic mechanical systems with hysteresis is the background of the work presented here. Figure 1.1 shows schematics of a few cycles in typical hysteretic displacement/restoring-force diagrams representing kinematic strain hardening and softening. The first case, the so-called strain hardening case, is well-known from the theory of plasticity which deals with the behaviour of elasto-plastic materials. The latter case, typically

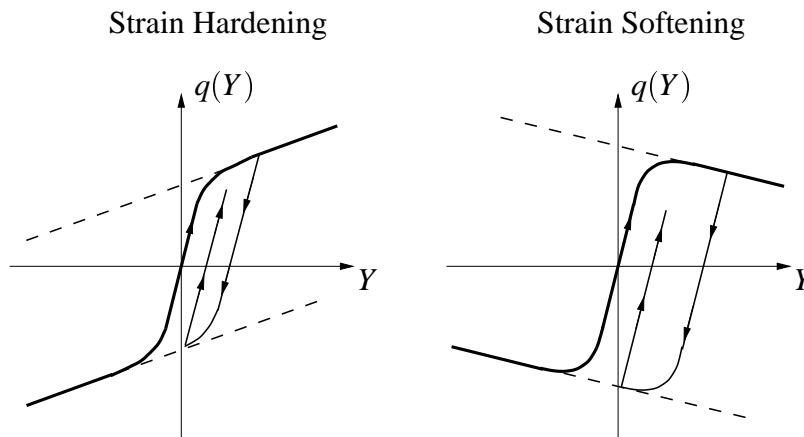


Figure 1.1: Schematics of a few cycles in typical hysteretic displacement/restoring-force diagrams.

is derived from the first. It arises when structural elements like a column, made out of a plastic material with almost no strain hardening, is subject to compressive normal forces. These forces reduce stiffness and may thus bring an otherwise up-going hardening branch into a down-going softening branch. In the remainder of this part of the thesis the hysteretic systems are in fact exemplified by such elasto-plastic structural systems. The obtained results are, however, still generally valid for any hysteretic system that comply with the assumptions made.

For elasto-plastic structures like frames and trusses a common design criterion is that the probability of the formation of a mechanism should be below some specific value. However, such mechanism formations need not be catastrophic for a dynamically loaded structure. It is catastrophic only if the structure starts moving and collapses. Due to the dynamical load the elements of the structure may for a short while move in a mechanism pattern and shortly after move in another pattern bringing the mechanism formation to an end. Thus an important design issue is rather the degradation of the structure due to several mechanism formations than the mere formation of a mechanism. Therefore the response process of the structural system is of interest.

An important implication of the considered physical systems being mechanical is that they may exhibit resonant behaviour when dynamically loaded. For strongly non-linear or heavily damped systems resonance may not be an important issue. Here damping is taken light and viscous in accordance with the reality of structural systems (typically the damping ratios are 0.005–0.05). Furthermore it follows from design practice that structural systems are highly reliable, why the presence of hysteresis is assumed not dominating for the response. As it will show, these assumptions imply that many of the features of the response of lightly viscously damped linear systems, with some approximation carry over to the considered hysteretic systems. For this reason the notions of an *elasto-plastic oscillator* (EPO) and its *associated linear oscillator* (ALO) are introduced. The ALO is defined as the linear oscillator obtained by linearizing the EPO at the zero-point.

What is meant by 'not dominating hysteresis' needs some clarification. Clearly the interplay between the power of the driving force and the dynamical characteristics of the system influences the magnitude of the response and thereby also the possibility of having response realizations that will pass through the hysteretic branches in the restoring force diagram. Consequently a quantitative discussion of the 'not dominating hysteresis' phrase certainly requires a specification of the type of loading considered.

The origin of the kind of problem treated in the next chapters is for instance earthquake loaded structures. A record of the ground acceleration in the east-west direction during the Loma Prieta earthquake in the Santa Cruz Mountains on October 17, 1989 is shown in Fig.1.2 (data was sampled at a rate of 200 Hz.) A zoom of the central part of the record is also shown. This zoom shows that the frequency content of the record is rich. This is a typical feature of dynamical loading of mechanical systems and is termed *broad banded load*. As it is assumed that the mechanical systems regarded here are only little and at most moderately non-linear, they exhibit resonant behaviour. This means that there are generally two possibilities. Either, the load process covers a frequency range that falls outside the critical frequency domain of the

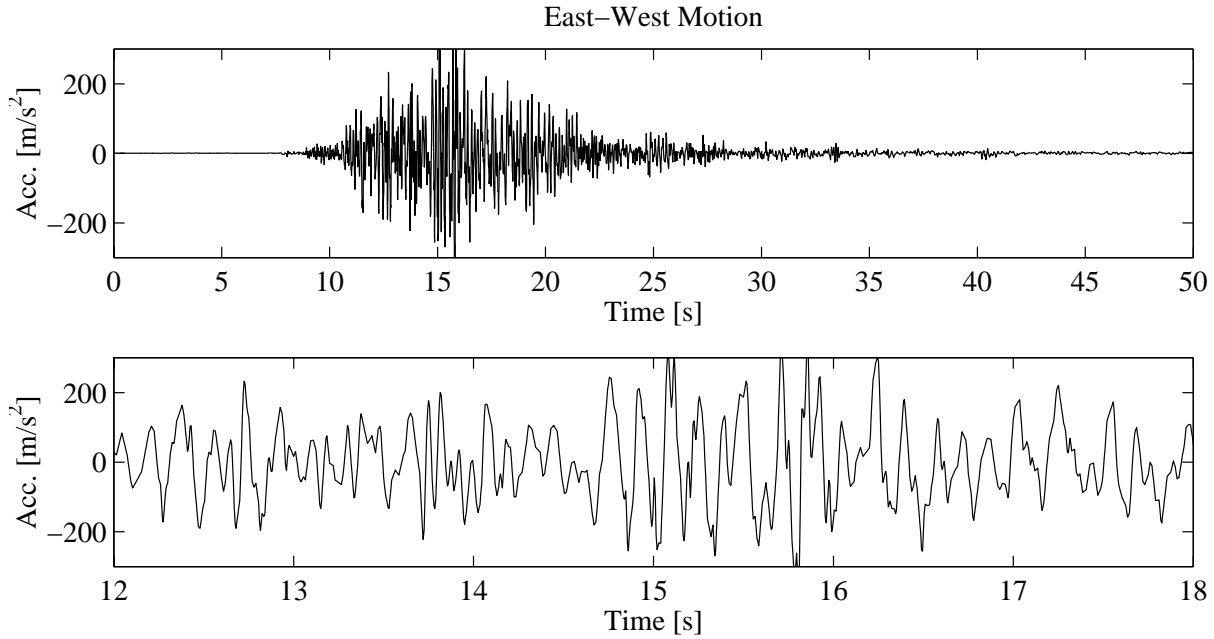


Figure 1.2: Measured ground acceleration record from the Loma Prieta earthquake (top) and a zoom of the central part of this record (bottom).

mechanical system, or a considerable part of the input excites the resonant frequencies. The first event is not critical, whereas the latter calls for further investigation as unwanted large deflections and internal forces in the mechanical system will occur.

The following chapter will bring focus on structures driven by broad banded stochastic process that has its main power input around the resonant frequencies of the mechanical system. This implies that with only small error the load process can be replaced by a process that has power input at all frequencies. This is due to the frequency content of the response be almost insensitive to the extra power input as the amplification declines rapidly outside the resonant domain. White noise processes are such processes that on the average inputs equal power at all frequencies. This is an idealization as it implies infinite average power input. The implications of the idealization is discussed later. If the power input of the driving process is not homogeneously spread over the resonant frequencies, a more realistic modeling of the input process is still obtainable by application of white noise processes. One simply passes a properly scaled white noise process through a filter that in some way amplifies those frequencies that are present in the real input process. Since mechanical systems themselves amplify input at resonant frequencies, they may be used for such filtering purposes.

Though load processes are generally non-stationary, there are often time intervals during which the processes are almost stationary. Figure. 1.2 illustrates by plots such stationary parts of a load process are typically present where the input is most powerful. The studies presented herein therefore consider systems at a time when stationarity is reached. It is obvious from the figure

that in the case of earthquakes the duration of the stationary load history part is rather short. One may thus argue that it gives unrealistic modeling to consider stationarity. However, in other cases, like fatigue loading, wind and ocean wave loads, the extent of the stationary intervals is much longer. For the earthquake case the stationarity model is not useful for predicting the time from the quake starts to the first excursion of the response outside the elasticity limits. It is still useful, though, in modeling the response that follows. This is important too, as it is during this phase that degradation of the structure takes place.

The above discussion motivates investigations of the stationary response of mechanical systems with hysteresis excited by white noise processes and answers the question regarding the kind of load applied to the mechanical systems. Thus time is due to return at the initial question of what is meant by 'not dominating hysteresis'.

If hysteresis is not dominating it must be so that the response path only seldom reaches the hysteresis branches of the restoring force diagrams. Now, since the resonant frequencies of the system are excited, one must for a given structure and load relate the elasticity limits to the response peaks which are due to resonance and depend on the intensity of the input. These peaks are random, and for that reason some averaged value for the size of the peaks is required. The stationary standard deviation, σ_{ALO} , of the response of the ALO reflects the peaks in the ALO's frequency response function together with the intensity of the load. If hysteresis is not dominating σ_{ALO} is a good average value for the EPO response peaks as well. Scaling the response by σ_{ALO} the scaled elasticity limits become meaningful relative measures of the degree of hysteresis present. As it is discussed later the white noise process is assumed Gaussian. For the ALO this implies that the response is Gaussian too. Hence, if the scaled limits are of magnitude 1 one may, using the Gaussian distribution for guidance, state that with probability approx. 30% of the response is outside the elasticity limits. This is dominating hysteresis. For scaled limits of magnitude 2 the corresponding probability is approx. 5% which is little. The conclusion is, that for scaled elasticity limits above 2 hysteresis is not dominating. For limits between 1.5 and 2, hysteresis is moderate, and any limit below 1.5 means dominating hysteresis. Since structural systems are very reliable, scaled elasticity limits below 2 seldom occurs, so the assumption about non-dominating hysteresis is not unrealistic.

1.2 The Equation of Motion for the SDOF EPO

Having now clarified the basic assumptions about the driving load process and the dynamical properties of the hysteretic systems the implications of these assumptions on the treatment of the problem may be discussed. To that end, a good understanding of the stationary response of the viscously damped single degree of freedom (SDOF) oscillator with weak hysteresis and driven by white noise is useful. This is due to the experience reported in [18] of a multi degree of freedom (MDOF) oscillator with localized hysteresis. This MDOF oscillator is an example of a structure with added mechanical filtering of the white noise process as mentioned above. It is in the MDOF case assumed too that hysteresis is weak, and therefore application of modal

analysis to the ALO response gives good results. The SDOF oscillator is therefore the main subject of this part of the thesis.

At this point some equations are now required to facilitate the further development of the considered problem. The mass normalized equation of motion for an SDOF oscillator with viscous damping and a non-linear restoring force is (c = mass normalized coefficient of damping, $q(y)$ = mass normalized restoring force as function of the displacement y , $F(t)$ = mass normalized dynamical load as function of the unscaled time t)

$$\ddot{Y} + c\dot{Y} + q(Y) = F(t) \quad (1.1)$$

Another way of expressing the equation of motion, that will prove useful in the discussion of the load process and the scaling of the response, is the so-called phase-space (or better state-space) formulation. There exist several possible state vectors and the state formulation we need here is

$$\frac{d}{dt} \begin{bmatrix} Y \\ \dot{Y} \end{bmatrix} = \begin{bmatrix} \dot{Y} \\ -c\dot{Y} - q(Y) \end{bmatrix} + \begin{bmatrix} 0 \\ F \end{bmatrix} \quad (1.2)$$

in which the state vector $[Y \ \dot{Y}]^T$ directly reflects the second order nature of Newton's second law and the first term on the right-hand side gives the free response state change rate as function of the system parameters.

1.2.1 The Gaussianity of the White Noise

Up till now it has been decided to model the load as process of white noise type. The actual distribution of $F(t)$ has not been discussed. The following discussion is partly taken from [13][pp. 80-83]. From physics one knows that for non-idealized load process the response Y and the velocity \dot{Y} develop continuously in time. We will demand that the same holds true for the response to the idealized white noise load process. This requirement will induce the distribution of $F(t)$. The state space equation (1.2) clearly states that the load influences the rate of the velocity change directly and the rate of the response change only indirectly. Taking the last equation of Eq. (1.2) one has

$$\dot{Y}(t) = \int_{t_0}^t (-c\dot{Y} - q(Y)) ds + \int_{t_0}^t F ds \quad (1.3)$$

It is, as $q(Y)$ is always at least continuous, apparent from this equation that the continuity demand is fulfilled only if the integral $\Psi(t) = \int_{t_0}^t F ds$ of the white noise process is continuous. It is easily realized that Ψ is a continuous Markov process, for what reason a Fokker-Planck equation (FPE) for Ψ exists. The white noise process is characterized by an average power input that is the same at all frequencies. This implies infinitely rapidly fluctuating samples, which in turn implies that the process has zero correlation length and infinite variance. Therefore it turns out that, except for a constant factor dependent on the intensity of the power of F , the FPE for Ψ is equal to the FPE for the Brownian motion process. Consequently the stationary distribution of

Ψ is Gaussian with zero mean and variance proportional to $t - t_0$. As $d\Psi = Fdt$, it is concluded that $F(t)$ must have Gaussian distribution of zero mean too.

As it is implicitly indicated above, the idealized white noise process may be obtained as the limit of a sequence of processes with decreasing correlation length. Thereby the variance becomes infinite, which changes the infinitesimal order of the terms in which the idealized process appears. Therefore one has to decide precisely how to integrate the stochastic differential equation (SDE) of motion under these conditions. There are infinitely many different ways of doing so, implying equally many different solutions. Two of those, however, stand out as especially useful. One uses the Itô stochastic integral, the other uses the Stratonovich stochastic integral. The Itô integral is algebraically simple whereas the Stratonovich integral gives a physically meaningful result. There is a way to transform the SDE such that applying the Itô integral gives the same result as applying the Stratonovich integral to the original SDE. The Wong-Zakai Limit Theorem gives a statement about this. If the idealized process is multiplied by a factor depending non-linearly on the response process the equation has to be corrected – otherwise not. Hence, the equations considered herein give the same result whether they are interpreted in the Itô or the Stratonovich sense. The Itô formula leading to the Fokker-Planck equation and the moment equations which give physically meaningful results is thus (see Eq. (1.2))

$$df = \left[\frac{\partial f}{\partial t} + \dot{Y} \frac{\partial f}{\partial y} + (-c\dot{Y} - q(Y)) \frac{\partial f}{\partial \dot{y}} + \frac{1}{2} \sigma_F^2 \frac{\partial^2 f}{\partial^2 \dot{y}} \right] dt + \sigma_F \frac{\partial f}{\partial \dot{y}} dB \quad (1.4)$$

In which the constant σ_F is $\sqrt{2\pi S_F}$ and dB is the increment of the Brownian motion.

The Gaussian distribution of $F(t)$ was derived from a continuity requirement for the response caused by the idealized white noise excitation. The Gaussianity of $F(t)$ also has its algebraic advantages which are extensively exploited in the sequel. For the ALO, the property of the set of Gaussian distributions as being closed with respect to linear operations, yields the convenient result that the ALO response process becomes Gaussian too. Therefore all joint distributions of the ALO response are known and of simple type – a considerable advantage. How it is utilized is revealed later on.

Had one not assumed the white noise property of the input the continuity requirement would itself had been insufficient to ensure Gaussianity of $F(t)$. One may ask if the idealization has too big impact on the response distribution, by bringing it too far away from the real distribution. Consider the ALO again. The intuitive result, connected to the Central Limit Theorem, that the stationary response of linear systems with light damping excited by weakly correlated non-Gaussian processes is approximately Gaussian indicates that the assumption does not lead to results that are completely off.

Turning the above discussion up-side-down one may from an engineering point of view simply state that substituting the real non-Gaussian broad banded load process by Gaussian white noise is an obvious model choice. The choice is obvious because it makes the ALO response process become algebraically tractable at the same time as having the nice implication that the response and velocity processes become continuous. No matter which line of attack one prefers,

it clearly relevant to investigate the response due to Gaussian white noise. The author prefers the approach of the derivation in the previous sections as it shows clearly what assumptions are made.

1.2.2 The Scaled Equation of Motion

The different terms of the governing equation has now been discussed, why the afore mentioned scaling can be carried out. For convenience of notation the scaling is first carried out for the ALO equation, then, afterwards the EPO equation is set up as a generalization of the scaled ALO equation. The standard normalized equation of motion for the SDOF ALO corresponding to Eq.(1.1) has the form (ω_0 = undamped eigenfrequency, ζ = damping ratio, $F(t)$ = mass normalized load)

$$\ddot{Y} + 2\zeta\omega_0\dot{Y} + \omega_0^2 Y = F(t) \quad (1.5)$$

As explained the response is scaled by the stationary response standard deviation σ_{ALO} . Denoting by S_F the constant double sided power spectrum density of F the stationary variance becomes

$$\sigma_{ALO}^2 = \frac{\pi S_F}{2\zeta\omega_0^3} \quad (1.6)$$

In addition to the response scaling, a temporal scaling is carried out too. This is not because different time scales are to be compared, as it has already been decided that the load predominantly excites the resonant frequency. It is for the purpose of ensuring generality of the results by eliminating the frequency ω_0 . Time is scaled by the damped eigenfrequency of the ALO yielding the time scale

$$\tau = t \sqrt{1 - \zeta^2} \omega_0 \quad (1.7)$$

After some simple manipulations the following scaled equation of motion for the SDOF ALO, in which $X(\tau) = Y(t)/\sigma_{ALO}$ is reached:

$$\ddot{X} + 2\alpha\dot{X} + (1 + \alpha^2)X = W(\tau) \quad (1.8)$$

Two new symbols have been introduced in the equation. One symbol is the scaled damping ratio α given by

$$\alpha = \zeta / \sqrt{1 - \zeta^2} \quad (1.9)$$

The other is the load process $W(\tau)$ which equals $F(t)(1 + \alpha^2)/\sigma_{ALO}\omega_0^2$. Accounting for the difference in time scale of $W(\tau)$ and $F(t)$ the spectral intensity of W can be found as

$$S_W = \frac{2}{\pi} \alpha (1 + \alpha^2) \quad (1.10)$$

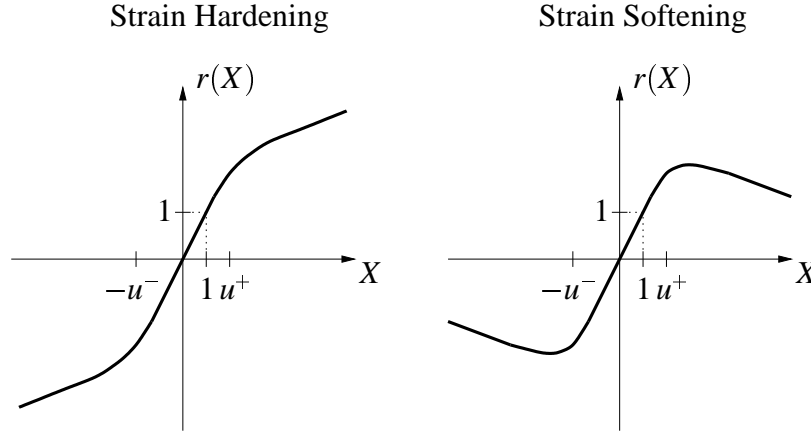


Figure 1.3: Schematics of the non-linear restoring force diagram with scaled elasticity limits u^+ and $-u^-$ of larger absolute value than 1.

This last result enables a discussion of the relative order of magnitude of the different terms in the equation of motion. Noting that (1.10) implies that the load is of order $\alpha^{1/2}$, one sees that the choice of scaling has made it explicit that for the considered resonant phenomenon the load process is half an order of magnitude larger than the damping term and half an order of magnitude smaller than the inertia and restoring force terms. This is usually termed *weak excitation*. It does, however, not mean that the load is vanishing, it simply underlines the fact that for weak damping, resonance amplifies the excitation considerably.

The statistical moments of the scaled SDOF ALO response are heavily used in the following. These moments are computed using the relevant Itô formula. According to the earlier discussion one finds that for the scaled SDOF ALO equation the Itô formula becomes

$$df = \left[\frac{\partial f}{\partial t} + \dot{X} \frac{\partial f}{\partial x} + (-2\alpha\dot{X} - (1+\alpha^2)X) \frac{\partial f}{\partial \dot{x}} + \alpha(1+\alpha^2) \frac{\partial^2 f}{\partial^2 \dot{x}} \right] dt + \sqrt{\alpha(1+\alpha^2)} \frac{\partial f}{\partial \dot{x}} dB \quad (1.11)$$

Finally, the equation of motion for the SDOF EPO is reached by simply replacing the displacement X in the third term of Eq. (1.8) by a non-linear function $r(X)$ which is a scaled restoring force function that is related to the mass-normalized restoring force $q(Y)$ in Eq. (1.1) by

$$r(X) = \frac{q(\sigma_{ALO} X)}{\omega_0^2 \sigma_{ALO}} \quad (1.12)$$

In this way the scaled SDOF EPO equation writes

$$\ddot{X} + 2\alpha\dot{X} + (1+\alpha^2)r(X) = W(\tau) \quad (1.13)$$

Schematics of the scaled hardening and softening restoring force diagrams are shown in Fig. 1.3. As shown the absolute values of the upper and lower elasticity limits are denoted u^+ and u^-

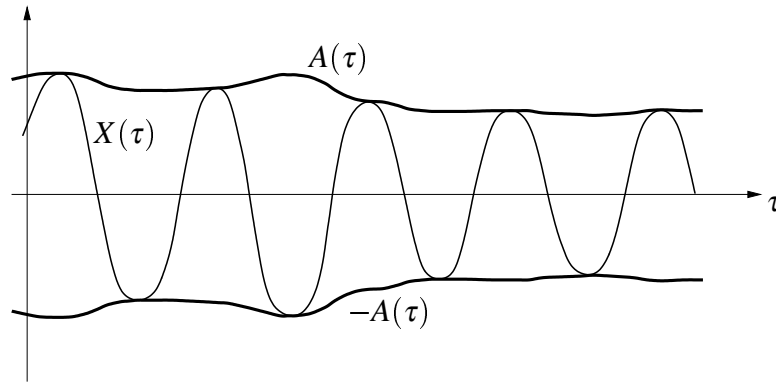


Figure 1.4: The energy based envelope defining the amplitude process.

respectively. It is noted that they due to hardening/softening depend on time and further that they are generally not of the same size, except when the plastic displacement is zero as is the case in the figure.

1.2.3 The Amplitude Process

For the description of the time development of the response process it is useful to consider also the mechanical energy process of the ALO. The mechanical energy E corresponding to the scaled ALO equation is given by

$$\begin{aligned} E &= \frac{1}{2}(1 + \alpha^2)X^2 + \frac{1}{2}\dot{X}^2 \\ &= \frac{1}{2}(1 + \alpha^2) \left(X^2 + \left(\frac{\dot{X}}{\sqrt{1 + \alpha^2}} \right)^2 \right) \end{aligned} \quad (1.14)$$

The square root of the larger parenthesis defines yet another process which touches all extremes of the response and hence is called the amplitude process A :

$$A = \sqrt{X^2 + \left(\frac{\dot{X}}{\tilde{\omega}_0} \right)^2}, \quad \tilde{\omega}_0^2 = 1 + \alpha^2 \quad (1.15)$$

As sketched in Fig. 1.4 the amplitude process defined by Eq. (1.15) gives a certain envelope of the process. If the response process crosses out of the elasticity domain any envelope process does so too. Though the opposite does not necessarily hold true the time development of the amplitude process, or equivalently the energy process, can give valuable information about the behaviour of the outcrossings of the response process. The mechanical energy does not oscillate in time like the response does. It develops much slower reflecting the energy drain due to damping and the energy input due to the driving force. To see how this quantitatively affects the amplitude process another set of state variables than $[X \ \dot{X}]^T$ is considered. If one chooses

A as the one state variable and in accordance with the relation $E = \frac{1}{2}(1 + \alpha^2)A^2$ introduces the transformation

$$X = A \cos(\tilde{\omega}_0 \tau + \Phi) \quad (1.16)$$

$$\dot{X} = -A\tilde{\omega}_0 \sin(\tilde{\omega}_0 \tau + \Phi) \quad (1.17)$$

then the phase drift Φ is defined as the second state variable. Combining the state equations for $[X \ \dot{X}]^T$ and the transformation (1.16) the equations for this set of state variables become

$$\dot{A} = 2\alpha A \sin^2(\tilde{\omega}_0 \tau + \Phi) - \frac{\sqrt{2\alpha} V}{\tilde{\omega}_0} \sin(\tilde{\omega}_0 \tau + \Phi) \quad (1.18)$$

$$\dot{\Phi} = 2\alpha \sin(\tilde{\omega}_0 \tau + \Phi) \cos(\tilde{\omega}_0 \tau + \Phi) - \frac{\sqrt{2\alpha} V}{A\tilde{\omega}_0} \cos(\tilde{\omega}_0 \tau + \Phi) \quad (1.19)$$

in which the load process $W(\tau)$ has been replaced by the process $\sqrt{2\alpha} V(\tau)$ to make it explicit that the load is of order $\alpha^{1/2}$ as the result of scaling. Since the scaled damping ratio α is small compared to 1 and all other terms in the equations are of order 1, Eqs. (1.18) and (1.19) show quantitatively that the amplitude process develops slowly in time. The slow variation of A and Φ makes it possible to average the deterministic terms in Eqs. (1.18) and (1.19) over a period of oscillation simplifying the equations considerably. Furthermore the zero correlation length of the white noise process $V(\tau)$ allows averaging of the driving terms according to the Stratonovich-Khasminski stochastic averaging technique. In addition to a simplification of the equations the result of the averaging is that the amplitude becomes independent of the phase drift as expressed by the following diffusion equations:

$$dA = \alpha \left(-A + \frac{1}{A}\right) d\tau + \sqrt{2\alpha} dB_A \quad (1.20)$$

$$d\Phi = \frac{\sqrt{2\alpha}}{A} dB_\Phi \quad (1.21)$$

in which the B 's denote independent standard Brownian motion processes. Later Eq. (1.20) will be referred to when discussing the time development of the mechanical energy and the amplitude of the ALO response.

1.3 Historical Review

The above presented problem has been examined by many different researches in the field of applied stochastic mechanics following different lines of attack. The problem is twofold: the determination of the response process, and the isolation of the non-elastic part of the response. One of the first to look into the problem was Caughey [1] who examined the response of a bilinear hysteretic system to stationary Gaussian white noise. In his work he used the Kryloff-Bogoliubov averaging method to obtain equations for the amplitude and phase drift,

and he applied an equivalent linearization technique to these equations. Others have exercised the equivalent linearization and 'non-linearization' techniques, but the main drawback of these methods is that only second order information about the response is obtained. Response distributions and especially stochastic information about the non-elastic displacements are not obtainable. Employing the Stratonovich-Khasminski stochastic averaging technique leading to diffusion equations, as seen above, calls for the application of the Fokker-Planck-Kolmogorov equation. Hence Roberts does in [19] (among several papers) obtain distributions for the plastic displacement increments.

In stead of averaging, Karnopp & Scharon in their pioneer work [16] go in the opposite direction and make use of the fact that between the oscillations causing the plastic displacements the hysteretic oscillator behaves as a linear oscillator. In this way the plastic displacements get special attention. Based on the same idea, but avoiding some of the approximations introduced by Karnopp & Scharon and others extending the work of Karnopp & Scharon, Ditlevsen has applied the so-called Slepian model approach to the stationary Gaussian ALO response and thereby reached very good results for the distribution of the plastic displacements of the ideal EPO. A comprehensive presentation of these results is given in [6]. It is based on the success of this approach that the work on non-ideal EPOs with hardening and softening presented in this part of the thesis is developed.

None of the different classes of methods mentioned in this overview section are of simulation type. When non-linearity becomes too complicated, one usually has to resort to direct simulations of the response and then extract the plastic displacement process. This is where the work presented here comes into the picture. In order to reduce simulation time a semi-analytical simulation scheme which uses the results known from [6] and which simulates directly the plastic displacement process is derived. It is named the *Slepian Model Simulation Method* all though it includes simulations from other distributions than those obtained from the Slepian model.

1.4 The Slepian Model Simulation Method for the SDOF EPO

It was mentioned early in this chapter that the important design issue is degradation of the mechanical system. Hence, it is the plastic displacement process, denoted $X_p(\tau)$, which is of interest as it is this process that monitors how degradation evolves in time. In Fig. 1.5 the bold curve shows two sections of a possible sample path of the SDOF EPO response to white noise. The dashed curves show how elasticity limits develop in time. First of all it is noted, that the assumption about light damping and non-dominating hysteresis implies that the EPO response process is narrow banded and very close to the response of a linear oscillator. Next it is seen, that it is characterized by regions of one or several, in time closely positioned, consecutive excursions of the response beyond the elasticity limits, and regions where the response stays inside the limits (this is for typographical reason shown by curved cut lines). The first regions are termed *clumps*. The others are called *inter-clump* regions, and the time from one clump to another is named the *inter-clump waiting time*.

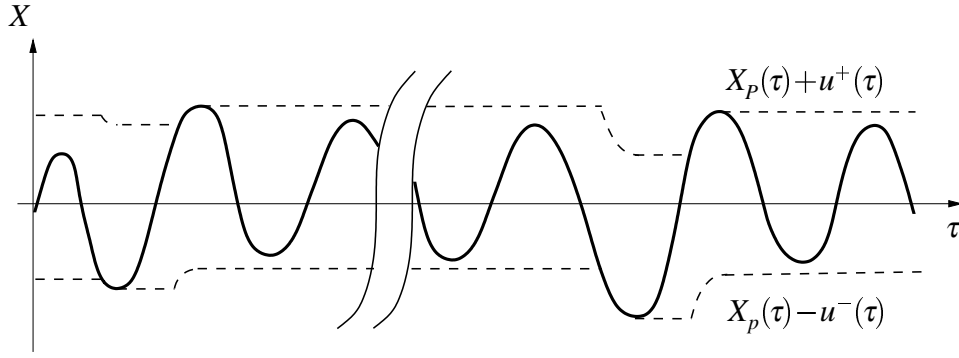


Figure 1.5: Two sections of a possible stationary sample path of the SDOF EPO excited by white noise.

The aim of this first part of the thesis is to present a semi analytical simulation scheme that can produce approximate sample curves of the plastic displacement process by an approximate time integration scheme. Traditional numerical time integration evaluates the sample curves at discrete points separated in time by about one tenth of the natural period of the ALO. Based on the assumptions: light damping and non-dominating hysteresis, the samples are computed at discrete points, separated by either half a period or several periods depending on the relevant time scale at a given point of the sample.

The choice of relevant time scale depends on whether the response process is in a region where the plastic displacement changes or not. The clumps are regions where the plastic displacement changes. In these regions oscillations are essential why it is reasonable to use a fast time scale of magnitude some few natural periods of oscillation. Between clumps the plastic displacement process is constant and because such inter-clump regions for weak hysteresis can have considerable duration, the relevant time scale in these regions is a slow time scale (reflecting damping) of much larger magnitude than that used for the clumps. The conclusion is that it is a natural thought to divide the simulation of a plastic displacement process sample into the simulation of clumps and inter-clump waiting times.

The simulation of the clumps is based on the so-called Slepian model which models the response process of the ALO after an outcrossing through the elasticity limits. Simulating the ALO response extreme by use of the Slepian model and next transforming this extreme into an extreme for the EPO response employing the so-called Karnopp-Scharton hypothesis (the more justifiable the weaker the hysteresis) the change of the plastic displacement process is approximately simulated. This carries on until the clump is ended. Postponing details till later, it is here only noted that in this way the real plastic displacement process during a clump is approximated by a jump process with jumps separated in time precisely by half a period of the ALO.

Depending on the elasticity limit and the damping ratio, the inter-clump waiting time distribution $F_T(\tau)$ will, due to transients, have significant jumps at the first few integer multiples of half natural period of the ALO. In accordance with asymptotic results, the upper tail of $F_T(\tau)$

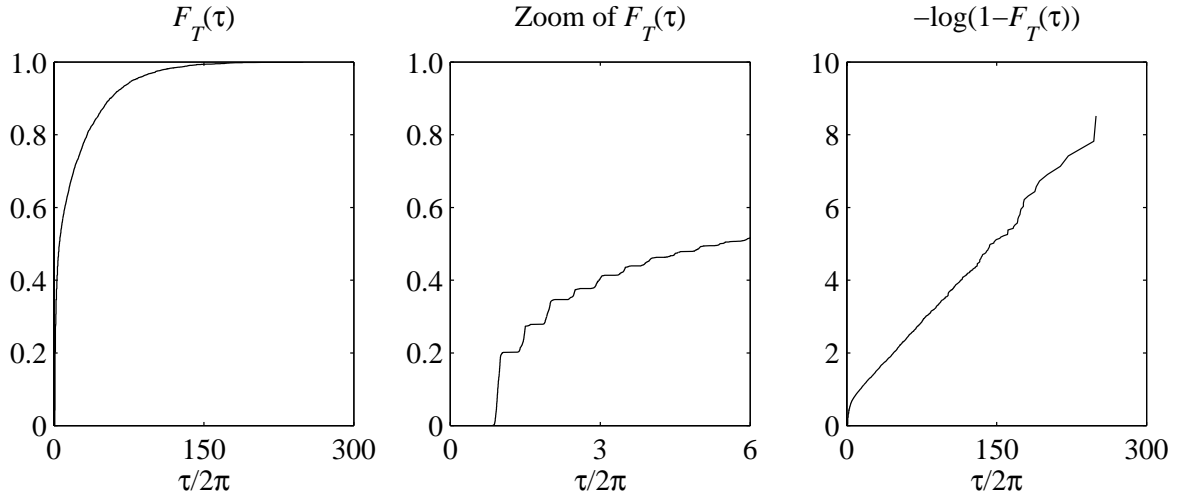


Figure 1.6: A typical inter-clump waiting time distribution for the scaled elasticity limit equal 2 and $\zeta = 0.01$. Left plot: full waiting time distribution, middle plot: zoom on transient tail, right plot: logarithmic plot showing exponential upper tail.

is exponential. Figure 1.6 shows a plot of a typical waiting time distribution. Outcomes of the waiting time belonging to the lower transient tail or the upper exponential tail of $F_T(\tau)$ is simulated by simple means exploiting that until the next outcrossing the response is governed by the ALO. It is the simulation of the waiting time that is the real strength of the simulation scheme. For high elasticity limit levels the average duration of the inter-clump regions is very large compared to the duration of the clumps. Thus a lot of simulation time is saved by simulating the waiting time in only a few steps rather than in steps of one tenth of a period.

1.5 Outline of the Following Chapters

- Chapter 2.** presents the Slepian model for the clumps of excursions in the SDOF EPO response as well as the simulation of those.
- Chapter 3.** deals with the related waiting time distribution and its simulation.
- Chapter 4.** explains the direct numerical time integration scheme employed as the tool of verification of the Slepian model simulation method.
- Chapter 5.** presents simulation results for the SDOF EPO, with hardening and softening.
- Chapter 6.** presents the conclusions.
- Appendix A.** presents two restoring force diagrams

1.6 Summary

It has been made clear that the investigation of the response of oscillators – especially single degree of freedom oscillators – with light damping and weak hysteresis and excited by a white noise process is a relevant problem. The applicability of the idealized white noise process is justified by the presence of only light damping.

The relevant governing equations for different stochastic quantities of the response have been set up – including the scaled equation of motion and a related envelope process defined as an amplitude process based on the mechanical energy of the oscillator.

The main features of the approximate semi-analytical numerical simulation strategy, which is the subject of this part of thesis, has been presented. The concept is quite simple. One observes that in certain regions of time the response experiences several excursions beyond the elasticity limits and in others it does not. The regions of excursions are called *clumps* and the time between clumps is called the *inter-clump waiting time*. As degradation of the mechanical system, which is the result of excursions, is considered the main design issue, the simulation scheme divides the simulation procedure into simulation of the clumps and inter-clump waiting times.

Chapter 2

Modeling and Simulating Clumps

The degradation of the white noise excited SDOF EPO is not a continuously ongoing process. Degradation takes place only in limited intervals of time. In this chapter those parts of the response path which contributes to the plastic displacement process $X_p(\tau)$ are considered. Plastic displacements are due to the excursion of the response outside the elasticity limits. Thus plastic displacements occur when the energy level of the oscillator is sufficiently high for excursions to take place. Due to the random loading and damping the energy level drifts and diffuses in time. It builds up and decreases slowly compared to the fast time scale of the oscillations. Consequently plastic displacements are most likely to arrive in clumps. How to model and simulate these clumps in the SDOF case is the subject of the present chapter.

2.1 Clump Definition

The following discussion reflects the difficulties in introducing a precise and at the same time universal definition of a clump. Defining a clump is, however, unavoidable as simulating a plastic displacement increment depends on whether it is the first after an interval of oscillations inside the elasticity limits, i.e. if it is the first in a clump, or it follows one or several closely preceding plastic displacement increments. It is shown later that the first plastic displacement increment is on the average smaller than the following increments. The question is simply: how close do two plastic increments have to be in time as to be considered belonging to the same clump?

Though it was ensured by the continuity requirement for the velocity (Sec. 1.2.1) that the response is continuous and smooth, the continuity condition did not put any restrictions on how wiggled the response path can possibly be. Thus, the response process is regular, meaning that only finitely many outcrossings occur per unit time, but due to the white noise excitation a lot of wiggles are, however, present in the response. Figure 2.1 shows how the response crosses out of and in to the elasticity domain several times on its way to a crest maximum outside the elasticity domain. Between each out- and incrossing a plastic displacement increment is generated.

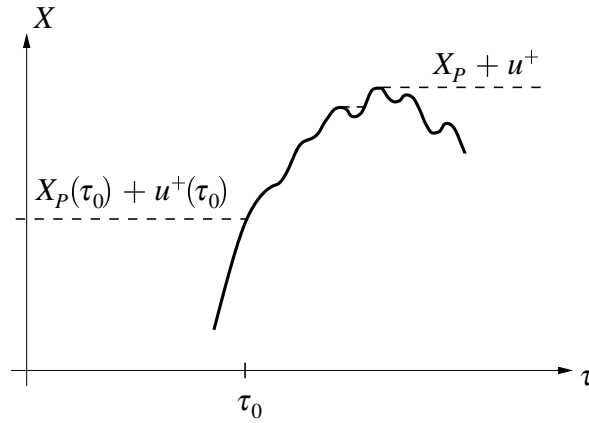


Figure 2.1: Zoom of the response path on its way to a crest maximum above the upper elasticity limit $X_P(\tau_0) + u^+(\tau_0)$.

Thus plastic increments can arrive very closely in time. The terms *crest maximum* and *trough minimum* are introduced to avoid confusion with the terms global maximum and minimum, respectively. A crest maximum is the global maximum within a single crest of the response, and a trough minimum is the global minimum within a single trough.

From an engineering point of view it is the crest/trough extremes outside the elasticity domain that are important. Each of the small wiggles contributes to the plastic displacement process, but it is sufficient to know the grand total of these plastic displacement increments generated on the way to a crest/trough extreme, as this is a satisfactory measure of degradation. This is a very important observation that we will return to over and over again because it simplifies the modeling of the plastic displacement process considerably. The argument is supported by the fact that wiggles may not be present in reality but simply be the result of the white noise modeling of the real load. Consequently the above question should be rephrased: how close must a crest and a trough, both outside the elasticity limits, be in time as if to be considered belonging to the same clump?

Look at the schematics in Fig. 2.2. They show the response (neglecting the wiggles) in situations where the energy level is high and some plastic deformation has already taken place. I.e. they show different possible clump candidates. The upper schematic shows that due to strain hardening or softening the upper and lower elasticity limits u^+ and u^- are not of the same size and dependent on time. The asymmetry of the elasticity limits makes it most likely that every second crest/trough is outside the elasticity limits, whereas every other second is not. Hence it is reasonable to argue that the clump is not terminated until at least *two* consecutive crest/trough extremes are inside the elasticity limits.

The lower schematic in Fig. 2.2 illustrates how the drifting of the amplitude process makes it likely that the amplitude at high energy levels drifts forth and back around the elasticity limits, until it finally fades away so much that several crests and troughs exclusively inside the elasticity limits follow. During the drifting forth and back of the amplitude process consecutive

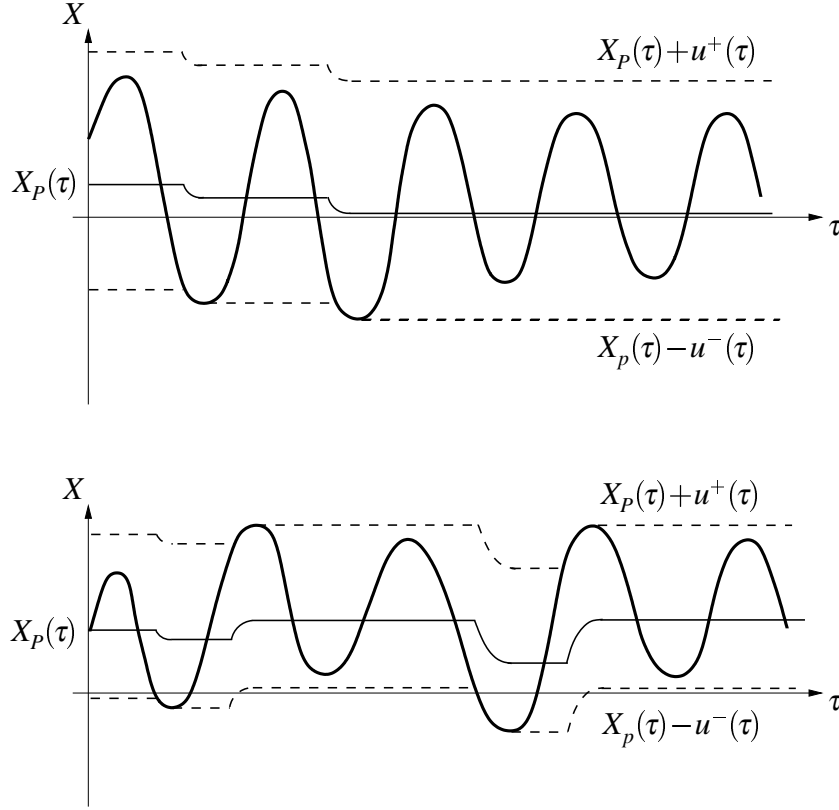


Figure 2.2: Different clump candidates.

crest/trough extremes outside the elasticity limits are followed by consecutive crests/troughs inside the elasticity limits, which are then again followed by crests/troughs outside the elasticity limits and so forth. Whether to regard the entire drifting phase as a single clump or an ensemble of clumps is a somewhat open question. It has been custom in works like [16] and [6], to consider the above described phenomenon an ensemble of clumps. Then each clump is terminated at the moment when a crest or trough inside the elasticity limits is met. It is from a time scale point of view (as discussed in Sec. 1.4) tempting to consider the entire drifting phase as one single clump. It rises one problem, though: how many crests and troughs inside the elasticity limits must follow the last crest/trough outside the elasticity limits before a clump is considered ended and one shifts to the inter-clump waiting time simulation? There is not a simple rational way to decide this. Guidelines are: the amplitude drifting is the more pronounced the lower the yield levels u^+ , u^- and the weaker the damping. The reasons are as follows. Equation 1.20 shows that for low damping the rate of change of the amplitude is low. Hence, when a large amplitude is first build up it takes long time for it to fade away. With lower yield limits, the probability of being outside the elasticity limits increases, causing crossings out and in the elasticity domain to become more frequent. Though guidelines are understandable, laying down rules – as function of u^+ , u^- and the damping ratio α – for the number of crests and troughs inside the elasticity limits required to end the clump, is not straightforward. To be able to handle

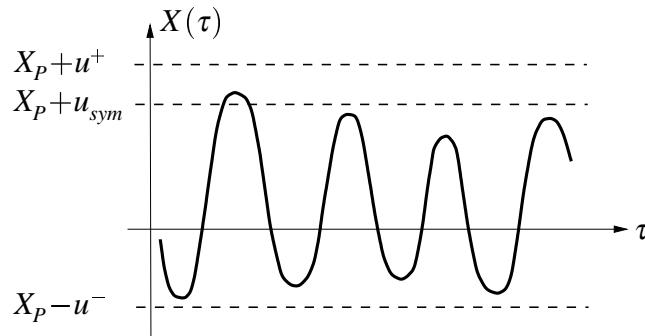


Figure 2.3: An example of an empty clump in the case $u_{sym} = u^- < u^+$ and $X_P > 0$.

at least the asymmetry problem, one therefore resolves that, a clump is terminated when, after a crest/trough inside the elasticity limits, two consecutive crests/troughs are inside the elasticity limits. The consequence is that the inter-clump waiting time simulation will include simulations of short waiting times as well as long waiting times. That is, the waiting time simulation will have to operate on both the slow *and* the fast time scale. This will be the subject of the next chapter.

In stead of defining a clump as terminated when two consecutive crests/troughs are inside the elasticity limits, there is a way to introduce a single yield limit, u_{sym} that makes it possible to define the clump as terminated, when the first crest/trough inside this yield limit is encountered. The problem regarding the asymmetric yield limits u^+ and u^- is, that the one limit might be so much smaller than the other, that crossings of the smallest is notably more likely than the crossings of the largest. If one defines

$$u_{sym} = \min(u^+, u^-) \quad (2.1)$$

then it is ensured that the crest/trough is inside the lowest, i.e. the most critical, yield limit if the crest/trough is inside the so-called symmetrized yield limit u_{sym} . Thus the condition of having two consecutive crests/troughs inside the elasticity limits to end a clump can be replaced by a condition that a clump is ended when a crest/trough inside u_{sym} is met. Clearly the introduction of u_{sym} simplifies the clump termination criterion. However, the real advantage of the notion of a symmetrized yield level becomes apparent, when in Chapter 3 the inter-clump waiting time is treated. The reason is that it is more simple to consider crossings of a process out of symmetric domains, than crossing out of asymmetric domains. Therefore it becomes natural to use u_{sym} not only for the clump termination criterion, but for the clump initiation criterion too. Summing up, the clump definition becomes (this definition was first given in [12]):

Clump Definition

A clump is defined by: a crest/trough outside the symmetrized yield level $u_{sym} = \min(u^+, u^-)$ followed by crests and troughs until the moment when a crest/trough inside the symmetrized limit is encountered.

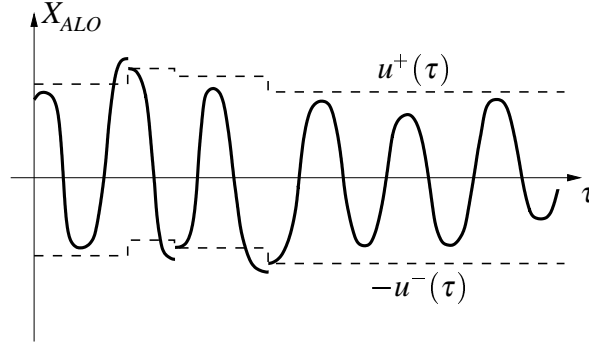


Figure 2.4: Schematic of a possible sample of the ALO response process.

It is noted that the consequence of the present clump definition is that clumps with no plastic displacement increments at all may occur, i.e. an empty clump. Say, as shown in Fig. 2.3, that $u_{sym} < u^+$ then the first excursion in a clump is, according to the definition, of course above u_{sym} , but it may be below u^+ . The following trough may be below u_{sym} . Thus the clump is initiated and ended without any yielding taking place. In the following excursions of u_{sym} not causing any yielding are termed *empty excursions*, whereas excursions causing yielding are termed *genuine excursions*.

2.2 Definition of The ALO Response Process

The next section deals with the modeling of the plastic displacement increment. To that end a precise definition of how the ALO is associated to the EPO is required. The definition used in this thesis is given in the present section. To keep the discussion in Sec. 1.1 simple, the ALO was represented by the equation of motion

$$\ddot{X} + 2\alpha\dot{X} + (1 + \alpha^2)X = W(\tau) \quad (2.2)$$

What was not made clear was that the ALO response has some jumps. This is depicted in Fig. 2.4. After a crest/trough outside the elasticity limits, the EPO behaves like a linear oscillator with equilibrium position $X_p(\tau)$ and initial conditions $X = u^+, \dot{X} = 0$ or $X = -u^-, \dot{X} = 0$. The idea is that the ALO shall reproduce this response, because it is the EPO response relative to X_p that defines the time to the next excursion and the mechanical energy of the EPO at this time. Consequently, after each crest/trough of the EPO response outside the elasticity limits, the ALO is restarted with initial conditions $X = u^+, \dot{X} = 0$ or $X = -u^-, \dot{X} = 0$. This is what causes the jumps. Approximations to the crest/trough extremes of the ALO response outside the elasticity limits will later prove useful in the computation of the plastic displacement increments. Therefore the ALO response process includes these crest and trough extremes, which appear right before each of the jumps.

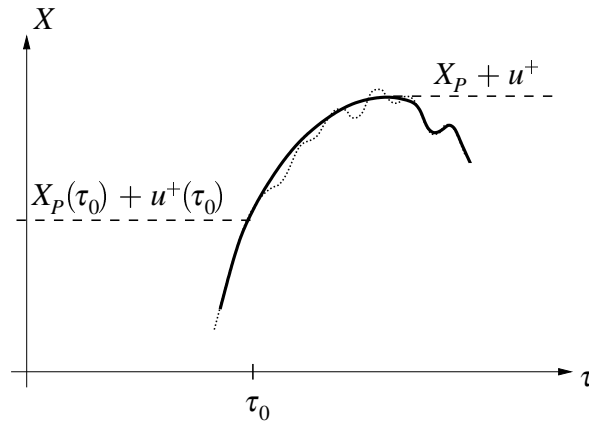


Figure 2.5: The response approximation according to the Karnopp-Scharton approximation (based on Fig. 2.1)

2.3 Modeling the Plastic Increments

It has already been pointed out that it is the sum of the plastic displacement increments generated on the way to a crest/trough and not each of the increments that is of interest. For weakly hysteretic systems an excursion of the elasticity limit is in the first place the result of a resonant buildup of the amplitude. I.e. it is mainly the result of energy put into the system during longer time and not the present forcing. As the driving force $W(\tau)$ is of order $\alpha^{1/2}$ the effect of this relatively small force in the short time interval during which the yielding takes place is insignificant in comparison to the effect of the restoring force which at the same time near is its maximum. Thus, neglecting $W(\tau)$ during yielding will introduce a very small error in assessing the extreme and it will remove the wiggles, which by this argument are seen to be unimportant – supporting the previously mentioned engineering point of view further. Figure 2.5 illustrates this. Likewise the velocity proportional viscous damping force is negligible compared to the restoring force, as velocity is close to zero and damping is of order α . The approximations suggested here were first presented by Karnopp and Scharton in their joint paper [16]. Hence, in the following they are phrased the Karnopp-Scharton hypothesis. Clearly the error by the Karnopp-Scharton hypothesis gets smaller the weaker the hysteresis, because the higher the yield levels the shorter the duration of the yielding and the more dominating the restoring force.

One is now in a position where one can relate the plastic increment ΔX_p to the response before yielding starts. As shown to the right in Fig. 2.6 ΔX_p is a function of the crest/trough extreme value M_{EPO} of the EPO response during yielding. Employing the Karnopp-Scharton approximation the approximate extreme value depends solely on the mechanical energy in the EPO the moment yielding begins. Since damping and driving forces are neglected during yielding, the mechanical energy present in the SDOF EPO when yielding begins, is at the time yielding stops fully transferred into potential energy and plastic dissipation, as the velocity is zero at this time.

Applying the notion of the ALO, the above energy considerations may be rephrased in a way that will turn out useful. Until yielding the ALO and the EPO response processes are identical

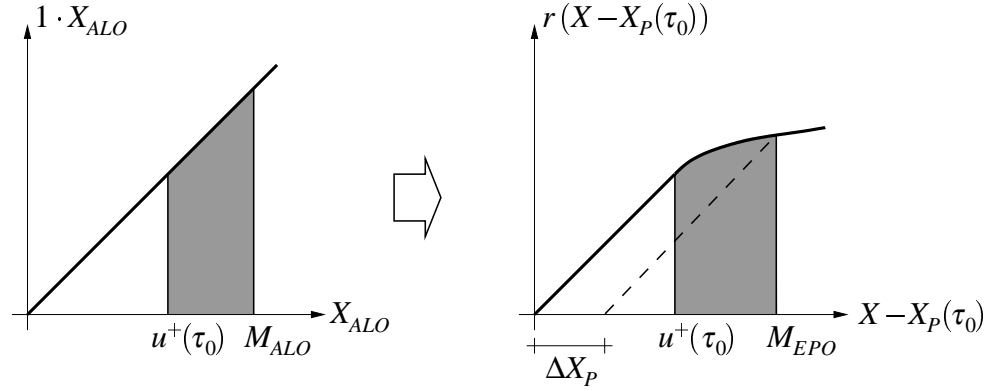


Figure 2.6: The computation of the approximate crest maximum M_{EPO} and the corresponding plastic displacement increment ΔX_p . The excess potential energy of the ALO is transferred into excess potential energy and plastic work of the EPO. Note that the restoring force diagrams are scaled. τ_0 denotes the time yielding begins.

except for a translation by X_p . Therefore they possess the same mechanical energy at the time τ_0 yielding commences. Neglecting damping and driving forces after τ_0 , an approximate extreme value M_{ALO} of the ALO is obtained. By this approximation the potential energy at the approximate extreme M_{ALO} equals the mechanical energy in the EPO when yielding begins. Therefore the potential energy at M_{ALO} in excess of the potential energy at the yield level equals the potential excess energy *plus* the plastic work of the EPO. Figure 2.6 illustrates, in the case where the extreme is a maximum that the excess potential energy of the ALO is transferred into excess of the EPO. Referring to Fig. 2.6 the plastic displacement increment ΔX_p in the specific case of a maximum is determined by the equations (note that $r(M_{EPO})$ equals the new elasticity limit u^+ after yielding):

$$\Delta X_p = M_{EPO} - r(M_{EPO}) \quad (2.3)$$

$$\int_{u^+(\tau_0)}^{M_{EPO}} r(\tau, x) dx = \frac{1}{2} (M_{ALO}^2 - u^{+2}(\tau_0)) \quad (2.4)$$

where the τ in $r(\tau, x)$ underlines that the restoring force diagram depends on time in the sense that it depends on the past displacement history, τ_0 is the time yielding begins and M_{EPO} denotes the maximum value of the EPO response relative to the plastic displacement $X_p(\tau_0)$. The corresponding equations in the case of a minimum are:

$$\Delta X_p = -M_{EPO} - r(-M_{EPO}) \quad (2.5)$$

$$\int_{-u^-(\tau_0)}^{-M_{EPO}} r(\tau, x) dx = \frac{1}{2} (M_{ALO}^2 - u^{-2}(\tau_0)) \quad (2.6)$$

in which, anticipating events, M_{EPO} denotes the absolute value of the minimum of the EPO response relative to $X_p(\tau_0)$. Therefore the lower elasticity limit u^- after yielding equals $-r(-M_{EPO})$.

2.4 ALO Response Properties and Slepian Modeling

It follows from the previous section that the simulation of a plastic displacement increment ΔX_p can be carried out by first simulating an approximate extreme M_{ALO} of the ALO response. Some process theory for the ALO response is a prerequisite for the description of the simulation of the approximate extremes. Since the ALO response is Gaussian the so-called Slepian Model process, which is the subject of this section, proves useful.

The first observation one makes is that it is sufficient to consider upcrossings of the Gaussian process through some positive level u . Downcrossings of the ALO response through a negative level $-u$ is simply obtained by changing the sign of the ALO response and considering upcrossings of the corresponding positive level u . This is permissible, as changing the sign of the ALO response does not destroy Gaussianity. Thus, in the following we consider only upcrossings of positive levels u and the related approximate maxima which are denoted M_{ALO} .

Obviously the ALO response is non-stationary. However, by use of conditioning, one can transform the results obtained from a stationary process into statements valid for the non-stationary process. Therefore in the following we consider firstly level crossings of the stationary Gaussian response process of the linear oscillator (LO) without the jumps of the ALO response. To keep notation simple X will throughout this section temporarily denote the LO response and not the EPO response.

2.4.1 Upcrossings and Maxima of Stationary Gaussian Processes

Since we are interested in upcrossings and the matching maxima, it is natural to study the non-stationary process that arises from the stationary process by conditioning on either the occurrence of an upcrossing or a maximum. Conditioning on an upcrossing or a maximum at time τ_0 can be fully expressed by conditioning on X and its derivatives at τ_0 . Exploiting that the stationary LO process is Gaussian its derivatives are Gaussian too, why the process conditional on $X(\tau_0), \dot{X}(\tau_0), \ddot{X}(\tau_0), \dots$ is Gaussian and identical to the linear regression of the process on $X(\tau_0), \dot{X}(\tau_0), \ddot{X}(\tau_0), \dots$ added with a zero mean non-stationary Gaussian residual process. Since the linear regression for Gaussian variables coincides with the conditional mean, the non-stationary conditioned process is written

$$X_{\text{cond}}(\tau, \tau_0) = E[X(\tau)|X(\tau_0), \dot{X}(\tau_0), \ddot{X}(\tau_0), \dots] + R(\tau - \tau_0) \quad (2.7)$$

Due to the white noise excitation the derivatives of order higher than one does not exist. One may show that for this reason all possible linear regressions appearing in 2.7 are identical to $E[X(\tau)|X(\tau_0), \dot{X}(\tau_0)]$. This is in agreement with intuition. Since the governing equation represents a mechanical system, any state of this system is fully defined by position and velocity. Adding to this that the load is independent of the past, it is always sufficient to condition on $X(\tau_0)$ and $\dot{X}(\tau_0)$ in order to obtain full probabilistic information about the process conditional on the process at time τ_0 . The point of this argument, we return to later when the approximate simulation of the separate extremes in a clump is treated.

Before writing out the linear regression in full, its structure is easily realized. Since the linear regression operator is linear in its arguments, taking the linear regression $E[\bullet|X(\tau_0), \dot{X}(\tau_0)]$ on each side of the LO's equation of motion shows, that the linear regression of the stationary LO response process on $X(\tau_0), \dot{X}(\tau_0)$ satisfies the homogeneous equation of motion. The equation is homogeneous because the load process $W(\tau)$ has zero mean and is independent of the response process X . Stated in other words: the linear regression $E[X(\tau)|X(\tau_0), \dot{X}(\tau_0)]$ equals the free damped response with initial conditions $X(\tau_0), \dot{X}(\tau_0)$. It is therefore clear that the residual process R represents the wiggles of the conditional response, thus accounting for the part of the response due to the load. For a more detailed discussion refer to [10].

To write down the expression for the linear regression, the means $E[X(\tau)]$ and $E[\dot{X}(\tau)]$ and the covariance function $c(\tau) = \text{Cov}[X(0), X(\tau)]$ of the stationary LO response are required. From the equation of motion or from the Itô formula Eq.(1.11) one derives that the means are both zero. Thus the linear regression becomes

$$E[X(\tau)|X(\tau_0), \dot{X}(\tau_0)] = c(\tau - \tau_0)X(\tau_0) - \frac{\dot{c}(\tau - \tau_0)}{\lambda_2}\dot{X}(\tau_0) \quad (2.8)$$

in which λ_2 denotes the second spectral moment of X and equals $\text{Var}[\dot{X}(\tau)]$. Since the linear regression equals free response with initial conditions $X(\tau_0), \dot{X}(\tau_0)$ it follows that $c(\tau)$ is identical to the free response with initial conditions $c(0) = 1$ and $\dot{c}(0) = 0$, which complies with normalization and stationarity. This is a standard problem giving:

$$c(\tau) = e^{-\alpha\tau}(\cos \tau + \alpha \sin \tau), \quad \tau \geq 0 \quad (2.9)$$

Combining (2.7) and (2.8) one finds that the covariance function of R which is needed later is given by:

$$\text{Cov}[R(\tau_1 - \tau_0), R(\tau_2 - \tau_0)] = c(\tau_1 - \tau_2) - c(\tau_1 - \tau_0)c(\tau_2 - \tau_0) - \frac{\dot{c}(\tau_1 - \tau_0)\dot{c}(\tau_2 - \tau_0)}{\lambda_2} \quad (2.10)$$

One can now turn to the question of choosing the proper conditioned process $X_{\text{cond}}(\tau)$. In the linear regression $E[X(\tau)|X(\tau_0), \dot{X}(\tau_0)]$ the variables $X(\tau_0)$ and $\dot{X}(\tau_0)$ are Gaussian, because this is the distribution of these variables if sampled at all points in time. However, for the upcrossings, the distribution of $X(\tau_0)$ and $\dot{X}(\tau_0)$ conditional on $X(\tau_0) \geq 0$ and $\dot{X}(\tau_0) = u$ is much more relevant. For the maxima the distribution conditional on $\dot{X}(\tau_0) = 0$ is relevant. If these conditional distributions are substituted into the expression for the linear regression in the place of $X(\tau_0)$ and $\dot{X}(\tau_0)$ a generally non-Gaussian distribution of $X_{\text{cond}}(\tau)$ is generated. In this way a model for the process under the given conditions is obtained. This model is the so-called Slepian model taking its name from the mathematician D. Slepian who was the first to work on this kind of modeling.

Consider first conditioning on a maximum. Then the model becomes

$$X_{\max}(\tau - \tau_{\max}) = c(\tau - \tau_{\max})M + R(\tau - \tau_{\max}) \quad (2.11)$$

in which M is distributed as the maxima of X , and τ_{\max} is the time of the maximum. If one samples all maxima of the stationary LO response process their distribution becomes standard Gaussian, i.e. of mean zero. This is useless, as we seek a model that describes what happens after an upcrossing of level u . One should rather sample only the largest maxima above u . In stead of doing this it turns out to be more fruitful to sample the normalized velocity $Z = \dot{X}(\tau_0)/\sqrt{\lambda_2}$ conditional on upcrossings and to evaluate the approximate maximum from the following Slepian model

$$X_u(\tau - \tau_0) = c(\tau - \tau_0)u - \frac{\dot{c}(\tau - \tau_0)}{\sqrt{\lambda_2}}Z + R(\tau - \tau_0) \quad (2.12)$$

If $\dot{X}(\tau_0)$ is sampled at time points τ_0 for which $X(\tau_0) = u$ and $\dot{X}(\tau_0) > 0$, then the normalized velocity Z has standard Rayleigh distribution independent of u (see e.g. [5]):

$$f_Z(z) = ze^{-\frac{1}{2}z^2}, \quad z > 0 \quad (2.13)$$

Neglecting, in accordance with the discussion in Sec.2.3, the wiggles due to the driving force and the damping a model for the approximate response after an outcrossing is obtained by:

$$X_u(\tau - \tau_0) \approx u \cos(\tau - \tau_0) + Z \sin(\tau - \tau_0), \quad \tau > \tau_0 \quad (2.14)$$

Denoting the first maximum of this model M one finds that this approximation to the maximum of the stationary LO response process obeys the equation

$$M^2 = u^2 + Z^2 \quad (2.15)$$

which is simply a restatement of the energy equation

$$\frac{1}{2}(1 + \alpha^2)M^2 = \frac{1}{2}(1 + \alpha^2)u^2 + \frac{1}{2}\dot{X}^2(\tau_0|X(\tau_0) = u) \quad (2.16)$$

showing that M , as wanted, represents the energy in the oscillator right before the outcrossing. By use of $P(Z > z) = e^{-\frac{1}{2}z^2}$, it follows from Eq.(2.15) that the approximate maximum has truncated standard Rayleigh distribution

$$P(M > m|M > u) = \frac{e^{-\frac{1}{2}m^2}}{e^{-\frac{1}{2}u^2}}, \quad m > u \quad (2.17)$$

2.4.2 The ALO Maxima

Next step is to find the distribution of the approximate maxima M_{ALO} over u of the ALO response by use of the distribution of the approximate maxima M over u of the stationary LO response.

There are two different kinds of such maxima. Those that corresponds to the first extreme in a clump and those corresponding to the following extremes in the clump. In the case of the first kind of maxima, all one knows is that, according to the clump definition, the response before the outcrossing lies inside the symmetric limits $-u$ and u . In the second case one knows, due to the narrow banded response, that approximately half a period before the maxima the response is at the opposite elasticity limit. Comparing the two cases it is clear that the mechanical energy of the oscillator before an outcrossing is smaller in the first case than in the second case. Therefore the first kind of maxima are on the average smaller than in the second case, which must be reflected by their distributions. Thus we seek the distribution of the maxima conditioned on the response being inside $[-u, u]$ in the time up to the outcrossing and the distribution of the maxima conditioned on the response being at a fixed value approximately half a period before. These distributions are obtained by long run sampling in the stationary LO response the first upcrossings that follow after time points at which $X = \pm u$ and $\dot{X} = 0$ (in accordance with Fig.2.4). In stead of reconsidering the sampling process, which led to the distribution of Z and M , an alternative simple approach giving approximations to these two distributions by use of Bayes' formula and the already established distribution $f_M(m)$ is employed.

2.4.3 First Maximum in a Clump

If the response is inside $[-u, u]$ in the time up to the outcrossing, then the minimum before the maximum is of course inside this interval. The opposite is not true. However, as the minimum equals the energy in the oscillator it may for practical purposes be expected that it is sufficiently accurate to condition on the minimum. Furthermore, as the response is narrow banded the minimum occurs approximately half a period before the maximum. Therefore, conditioning on the response half a period before the maximum being inside $[-u, u]$, rather than conditioning on the entire process up till the upcrossing may be expected to work fine. This has in [4] been proven to hold true. It is this line of reasoning which shows why it is useful to consider the approximate maxima of the ALO response rather than the energy at the time of outcrossing. Due to the narrow band characteristic of the response the time distance between two consecutive extremes scatters only little around half a period. The time distance from a minimum preceding an upcrossing is, however, less well-defined rendering the conditioning on a minimum before an upcrossing more complicated than conditioning on a minimum before a maximum.

Setting the time of the maximum to 0 one can write the density that is sought

$$f_M(m | X(-\pi) \in [-u, u]) \quad (2.18)$$

By Bayes' formula this is rewritten into

$$f_M(m | X(-\pi) \in [-u, u]) \propto P(X(-\pi) \in [-u, u] | M = m) f_M(m), \quad m > u \quad (2.19)$$

The unconditional density of the approximate maximum follows from Eq. (2.17):

$$f_M(m) = \frac{me^{-\frac{1}{2}m^2}}{e^{-\frac{1}{2}u^2}}, \quad m > u \quad (2.20)$$

Assuming, as an approximation, that renormalization of the process has taken place, the displacement conditional on a maximum half a period before is approximated using the linear regression (2.8) rendering

$$\begin{aligned}
P(X(-\pi) \in [-u, u] | M = m) &\approx P(X(-\pi) \in [-u, u] | X(0) = m, \dot{X}(0) = 0) \\
&= P(c(-\pi)m + R(-\pi) \in [-u, u]) \\
&= \Phi\left(\frac{u + \mu m}{\sigma}\right) - \Phi\left(\frac{-u + \mu m}{\sigma}\right) \\
&\approx \Phi\left(\frac{u - \mu m}{\sigma}\right)
\end{aligned} \tag{2.21}$$

in which

$$\mu = -c(-\pi) = e^{-\alpha\pi} \tag{2.22}$$

$$\sigma^2 = \text{Var}[R(-\pi)] = 1 - e^{-2\alpha\pi} \tag{2.23}$$

The variance σ^2 is obtained from Eq. (2.10). Substituting Eq. (2.20) and Eq. (2.21) into Eq. (2.19) then gives conditional density

$$f_M(m | X(-\pi) \in [-u, u]) \propto \Phi\left(\frac{u - \mu m}{\sigma}\right) m e^{-\frac{1}{2}m^2}, \quad m > u \tag{2.24}$$

and the corresponding complementary distribution function

$$\begin{aligned}
1 - F_M(m | X(-\pi) \in [-u, u]) &= \frac{\int_m^\infty \Phi\left(\frac{u - \mu z}{\sigma}\right) z e^{-\frac{1}{2}z^2} dz}{\int_u^\infty \Phi\left(\frac{u - \mu z}{\sigma}\right) z e^{-\frac{1}{2}z^2} dz} \\
&= \frac{\varphi(m) \Phi\left(\frac{u - \mu m}{\sigma}\right) - \mu \varphi(u) \Phi\left(\frac{\mu u - m}{\sigma}\right)}{\varphi(u) \Phi\left(\frac{u - \mu u}{\sigma}\right) - \mu \varphi(u) \Phi\left(\frac{\mu u - u}{\sigma}\right)}, \quad m > u
\end{aligned} \tag{2.25}$$

2.4.4 Second and Following Maxima in a Clump

After the first extreme in a clump the ALO starts at rest at a fixed value equal to one of the yield limits. Therefore the distribution of an approximate maximum after a fixed minimum is sought. Due to the narrow banded response the maximum is encountered very close to half a period after the minimum. Consequently an approximate conditional distribution fit for the simulation of an approximate ALO maximum following a fixed minimum is derived from

$$f_M(m | X(-\pi) = -\xi) \tag{2.26}$$

in which $\xi > 0$ denotes the absolute value of the fixed minimum at which the ALO starts. Similarly to the derivation in the previous section one obtains

$$f_M(m | X(-\pi) = -\xi) \propto \varphi\left(\frac{\xi - \mu m}{\sigma}\right) m e^{-\frac{1}{2}m^2} \propto m \varphi\left(\frac{m - \mu \xi}{\sigma}\right), \quad m > u \tag{2.27}$$

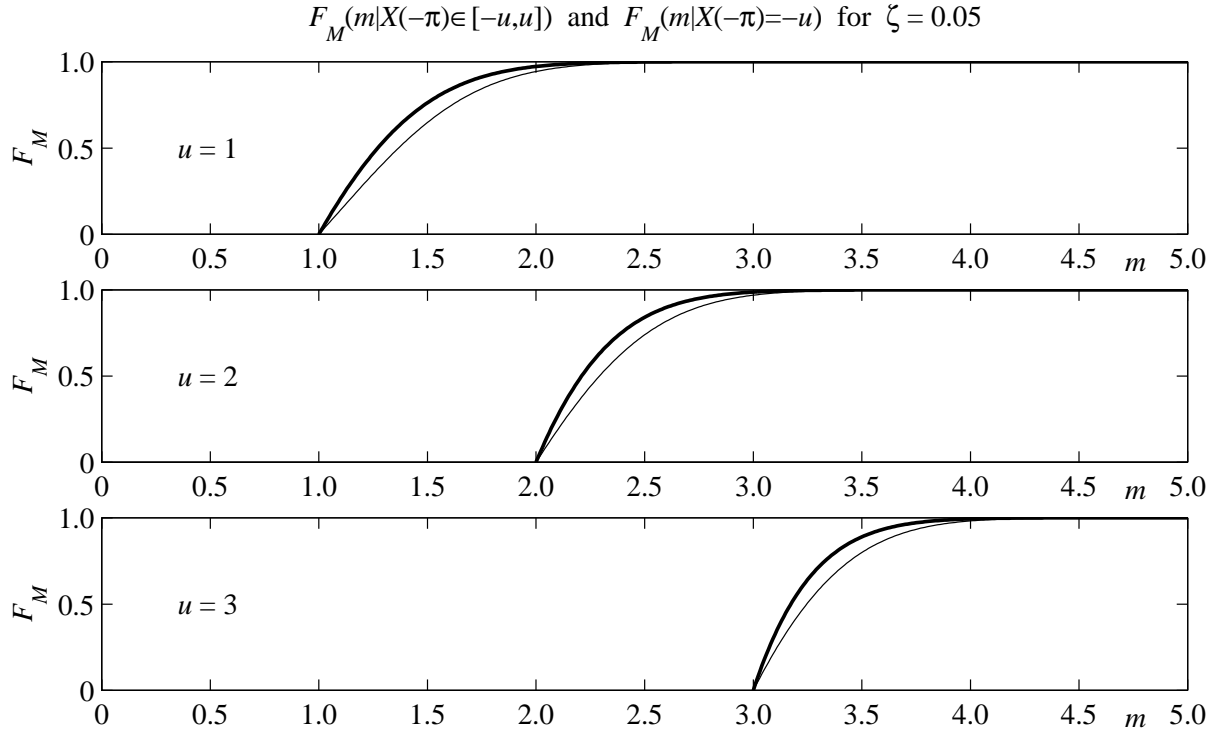


Figure 2.7: Comparison of the distribution of the first approximate ALO maximum in a clump (thick curves) and the distribution of the second and following approximate ALO maxima in a clump (thin curves). See discussion in the text.

and thereby the corresponding complementary distribution function

$$\begin{aligned}
 1 - F_M(m|X(-\pi) = -\xi) &= \frac{\int_m^\infty z \varphi\left(\frac{z-\mu_\xi}{\sigma}\right) dz}{\int_u^\infty z \varphi\left(\frac{z-\mu_\xi}{\sigma}\right) dz} \\
 &= \frac{\varphi\left(\frac{m-\mu_\xi}{\sigma}\right) + \frac{\mu_\xi}{\sigma} \Phi\left(-\frac{m-\mu_\xi}{\sigma}\right)}{\varphi\left(\frac{u-\mu_\xi}{\sigma}\right) + \frac{\mu_\xi}{\sigma} \Phi\left(-\frac{u-\mu_\xi}{\sigma}\right)}, \quad m > u
 \end{aligned} \tag{2.28}$$

The plots in Fig. 2.7 compare the distributions (2.25) and (2.28) to each other for $\zeta = 0.05$, different values of u , and $\xi = u$ in (2.28). The conditioning is seen to have the wanted effect and it is observed that the higher the level u the smaller the standard deviation. This conforms to intuition, as the distribution of the velocity and consequently the kinetic energy is independent of u , whereas the potential energy is quadratic in u .

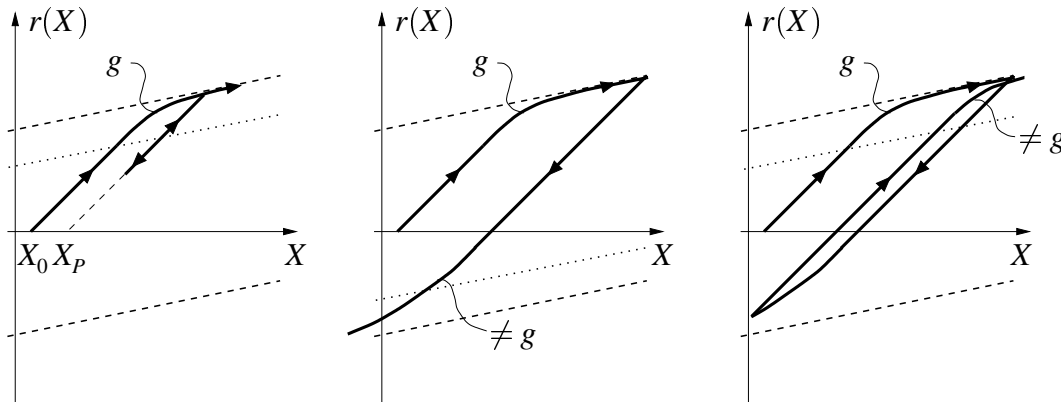


Figure 2.8: Non-ideal kinematic hardening. To the left: uploading, unloading and reloading paths. In the middle: the Bauschinger effect for reversed loading. To the right: Partial reversed loading followed by uploading.

2.5 From ALO to EPO Response

Having simulated an approximate maximum M_{ALO} from one of the conditional distributions (2.25) and (2.28) an approximate extreme of the EPO is obtained by substitution M_{ALO} in one of the energy equations (2.4) or (2.6) and solving with respect to M_{EPO} . Depending on the complexity of the restoring force function $r(\tau, x)$ the equations for M_{EPO} are solved analytically or numerically. The more complex the more time consuming the computation of M_{EPO} becomes. In order to minimize the complexity in computing M_{EPO} a simplified model for non-ideal plasticity with strain hardening/softening is presented in this first study of how to deal with non-ideal plasticity combined with hardening/softening in Slepian Model simulations. In [8] and [12], respectively, non-ideal plasticity without hardening/softening and ideal plasticity with hardening/softening have been treated in the context of Slepian Model Simulations, but never joined.

In Appendix A some of the phrases defined in the theory of plasticity and used in the following, are shortly reviewed. In modeling the restoring force diagram there are two effects to take into consideration: unloading/reloading and reversed loading (the so-called Bauschinger effect). The diagram to the left in Fig. 2.8 shows unloading/reloading effect. As indicated by X_0 this effect is easily accounted for by a zero point variable, i.e. X_0 , the current plastic displacement X_p and some function g for the curve describing the non-ideal behaviour above the yield limit (defined by the dotted line). In the diagram in the middle of Fig. 2.8 the Bauschinger effect is shown. In the case of kinematic strain hardening yielding starts at a lower level than that indicated by the dotted line. This dotted line corresponds to the dotted line in the left diagram. Thus, if strain hardening is assumed kinematic, the curved part on the reversing path is not identical to the one given by g on the uploading path. Furthermore the shape of the curve depends on how far the uploading reaches on the branch defined by g . Finally the diagram to the right in Fig. 2.8 shows partial reversed loading followed by uploading. Assuming kinematic

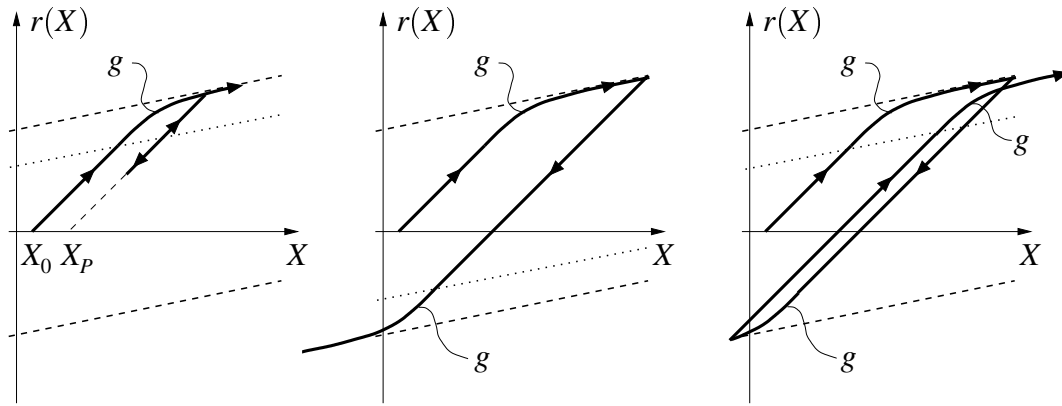


Figure 2.9: A simplified model for non-ideal strain hardening. To the left: uploading, unloading and reloading paths. In the middle: the Bauschinger effect for reversed loading. To the right: Partial reversed loading followed by uploading.

strain hardening, yielding during the second uploading starts above the dotted line which is identical to the one in the left diagram. Thus the curved part on the second uploading path is also different from the one defined by g . Clearly carrying on like this will complicate the hole matter even more. Thus one will need several different functions g to describe the many different curved parts of the restoring force diagram. This again implies that several different implementations for the solution of the energy equations may be needed. To avoid this the following approach is suggested.

One fixes some function g as shown in the uploading/unloading/reloading diagram to the left in Fig. 2.9 which is identical to the left diagram in Fig. 2.8. This function is then used in the case of reversed loading too. As is shown in the diagram in the middle of Fig. 2.9 this implies that yielding in reversed loading begins at the dotted line. Thus hardening is not kinematic nor isotropic, but independent. However, for curved parts of smaller and smaller extend the simplified diagram approaches ideal plastic hardening with kinematic hardening. Since for bending in slender frames made out of metal the curved parts of the restoring force diagram are usually small, the simplification is, from an engineering point of view, acceptable. To the right in Fig. 2.9 the case of partial reversed loading followed by an uploading is reconsidered. As shown, it is suggested that the onset of yielding during the second uploading is defined by the same dotted line as in the left diagram, such that g is used for the curved part in this case too. This simplification is based on the assumption that if the material experiences reversed yielding, even if it is only partial, the material has recovered sufficiently to exhibit full non-ideal plasticity during the following uploading. Again this assumption gets less problematic the closer one is to ideal plasticity. The zero point is introduced for the purpose of handling the unloading/reloading situation as shown to the left in Fig. 2.9. This means that whenever the load is reversed, the zero point is set equal to the current plastic displacement X_p . Then the zero point stays unchanged during succeeding unloadings/reloadings until the next reversed loading appears and so forth. It is noted that the definition given here applies to strain softening as well.

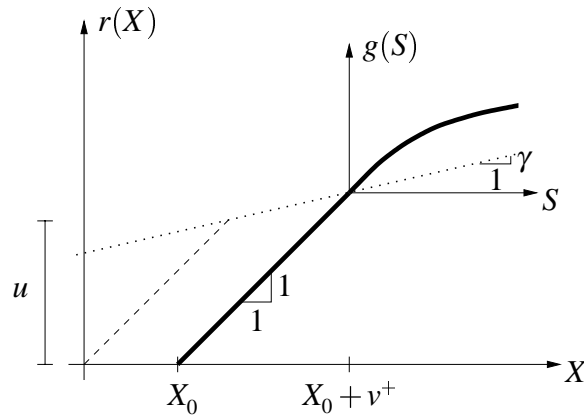


Figure 2.10: The characterization of the simplified restoring force diagram.

Having decided on the simplified model it is time to set up expressions for the evaluation of the plastic increments ΔX_p , and the updating of the yield limits u^+ and u^- . Figure 2.10 shows the case of strain hardening. The force diagram of the simplified model is defined by the inclined dotted line defining the yield limit at which the curved parts begin, the function $g(s)$ for the curved part and the zero point X_0 . In turn the inclined lines are defined by their inclination γ and the initial yield levels $u^+ = u$. In addition to the actual yield levels u^\pm two assisting levels v^\pm connected to the zero point X_0 are introduced. The level v^+ is shown in the figure too. The levels are given by the formulas

$$v^+ = u + \frac{\gamma}{1-\gamma} X_0, \quad v^- = u - \frac{\gamma}{1-\gamma} X_0 \quad (2.29)$$

It is noted that strain softening is obtained for $\gamma < 0$, which does not change the validity of the formulas for the assisting levels v^\pm .

Say we consider the i 'th excursion of the elasticity limits. Furthermore say this is a maximum. Then the situation is as shown to the left in Fig. 2.11. The plastic displacement and the yield levels before the yielding is denoted $X_{P,i}$ and u_i^\pm , respectively. After the yielding the new plastic displacement and the yield levels are denoted $X_{P,i+1}$ and u_{i+1}^\pm , respectively. The plastic increment $\Delta X_{P,i}$ is in the following denoted D_i and equals

$$D_i = X_{P,i+1} - X_{P,i} \quad (2.30)$$

It follows from the figure that the energy equation which transforms the simulated approximate M_{ALO} into M_{EPO} becomes

$$v^+ (M_{EPO} - u_i^+) + \int_{(X_{P,i} + u_i^+) - (X_0 + v^+)}^{(X_{P,i+1} + M_{EPO}) - (X_0 + v^+)} g(s) ds = \frac{1}{2} (M_{ALO}^2 - u_i^{+2}) \quad (2.31)$$

From this equation it is observed that the function g defining the non-ideal part of the force diagram must be of simple form, such that the integral is easily evaluated by analytical means.

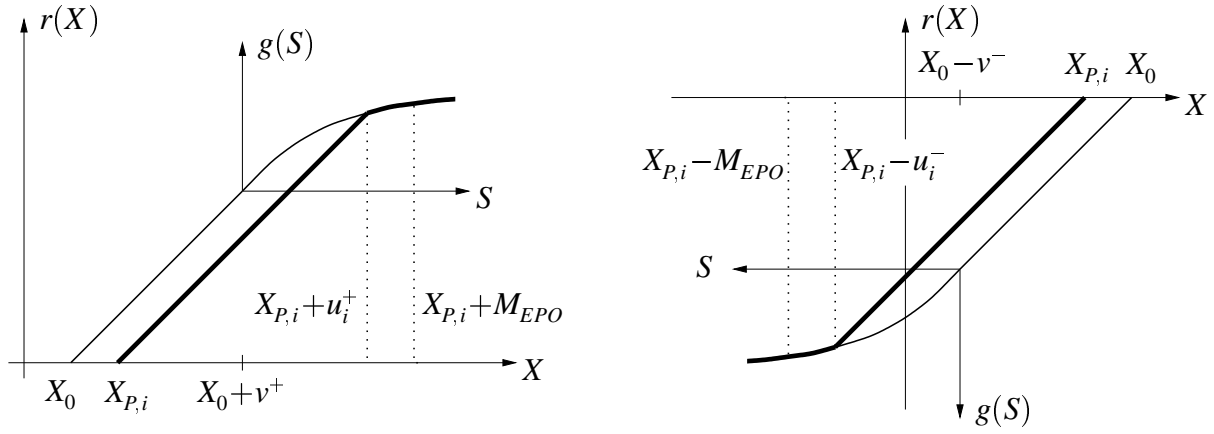


Figure 2.11: The computation of M_{EPO} and updating of the plastic displacement and the yield levels using the simplified restoring force diagram.

Otherwise, the integral is numerically evaluated and it becomes too time consuming to numerically solve the non-linear energy equation with respect to M_{EPO} , and some of the advantage of the Slepian Simulation Method is lost. After M_{EPO} is computed the yield limits and the plastic displacement are computed by

$$u_{i+1}^+ = v^+ + g((X_{P,i} + M_{EPO}) - (X_0 + v^+)) \quad (2.32a)$$

$$X_{P,i+1} = X_{P,i} + M_{EPO} - u_{i+1}^+ \quad (2.32b)$$

$$u_{i+1}^- = u - \frac{\gamma}{1-\gamma} X_{P,i+1} \quad (2.32c)$$

Where the last equation follows from Eq. (2.29) as this is the yield limit met in reversed loading where $X_0 = X_{P,i+1}$. Finally the plastic displacement increment becomes

$$D_i = M_{EPO} - u_{i+1}^+ \quad (2.33)$$

If the i 'th excursion of the elasticity limits is a minimum then the situation is as shown to the right in Fig. 2.11. The energy equation becomes:

$$v^- (M_{EPO} - u_i^-) + \int_{(X_0-v^-)-(X_{P,i}-u_i^-)}^{(X_0-v^-)-(X_{P,i}-M_{EPO})} g(s)ds = \frac{1}{2}(M_{ALO}^2 - u_i^{-2}) \quad (2.34)$$

and the updating formulas become

$$u_{i+1}^- = v^- + g((X_0 - v^-) - (X_{P,i} - M_{EPO})) \quad (2.35a)$$

$$X_{P,i+1} = X_{P,i} - M_{EPO} + u_{i+1}^- \quad (2.35b)$$

$$u_{i+1}^+ = u + \frac{\gamma}{1-\gamma} X_{P,i+1} \quad (2.35c)$$

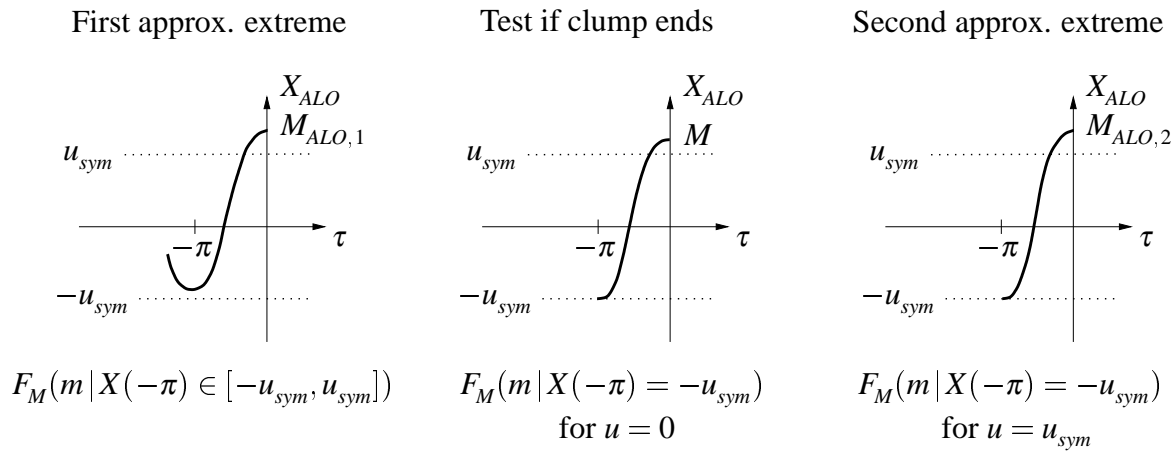


Figure 2.12: Simulating the two first extremes in a clump.

and the plastic displacement increment is computed by

$$D_i = -M_{EPO} + u_{i+1}^- \quad (2.36)$$

It is noted that the above equations are valid for strain softening also, i.e. for $\gamma < 0$. The only difference is that, because of the softening, the restoring force is actually no longer restoring when the displacement exceeds certain bounds. Beyond these bounds inertia and restoring forces act in the same direction, why the displacement grows to infinity and the oscillator collapses when these bounds are passed. These bounds are, however, seldom met in reality but for the sake of completeness their approximate assessment is presented. Due to the symmetry of the restoring force diagram the positive and negative collapse bounds are of the same size. Denoting the positive collapse bound X_{collap} one has the following equation:

$$u + g(X_{collap} - u) = 0 \quad (2.37)$$

2.6 Simulation Scheme

The elements of the clump simulation is now at hand. All that is needed is to link them together. The linking is quite easy. Having simulated the first extreme in a clump the next extreme is simulated independently of that first extreme, and so forth. Simulating the extremes independently is possible for two reasons. An extreme depends on the initial conditions after the previous extreme in the clump and on the load process. The initial conditions are accounted for by the conditioning in the distribution $F_M(m | X(-\pi) = -\xi)$ for M_{ALO} , and the load process, which is the source of the randomness described by this distribution, is white noise and thus independent of the past. Since the clumps are not of infinite duration one must after each simulation

```

IF simulating first clump
    Simulate first extreme according to Table 2.2.
ELSE
    Simulate first extreme according to Table 2.3.
ENDIF
DO
    Simulate extreme according to Table 2.4.
UNTIL clump terminated.

```

Table 2.1: Simulation of a clump by the Slepian model.

of an extreme decide, by simulation, whether the clump continues or it terminates. In [6] it is shown that if one generates an outcome M of $F_M(m | X(-\pi) = -\xi)$ for $u = 0$, then the condition $M < u_{sym}$ is a good clump termination criterion. Finally it is noted, that in going through the simulation one must keep track of whether the EPO is experiencing a reloading or a reversed loading, and in the case of strain softening if the oscillator collapses.

After this outline, an example of the simulation of a single clump is given. To keep it simple only the ALO response is considered. The EPO response is obtained by the energy transformation. Assume that the first extreme $M_{ALO,1}$ is a maximum (see Fig. 2.12). It is simulated from $F_M(m | X(-\pi) \in [-u_{sym}, u_{sym}])$. Either $M_{ALO,1} < u_1^+$ or not. If $M_{ALO,1} < u_1^+$ there is no plastic deformation and one puts $\xi = M_{ALO,1}$, otherwise there is a plastic deformation and one puts $\xi = u_2^+$, the updated yield limit. Next simulate M from $F_M(m | X(-\pi) = -\xi)$, setting $u = 0$ in formula (2.28). If $M < u_{sym}$ the clump ends. Otherwise the clump continues and the following minimum $-M_{ALO,2}$ is obtained by simulating $M_{ALO,2}$ from $F_M(m | X(-\pi) = -\xi)$, setting $u = u_{sym}$ in formula (2.28). If $M_{ALO,2} < u_2^-$ the excursion is empty and one puts $\xi = M_{ALO,2}$. Else one sets $\xi = u_3^-$. Then, again, simulate M from $F_M(m | X(-\pi) = -\xi)$, setting $u = 0$ in formula (2.28). If $M < u_{sym}$ the clump ends. Otherwise one carries on simulating the next maximum $M_{ALO,3}$ like one simulated $M_{ALO,2}$ except for the appropriate changes of sign and indices. This goes on till the clump terminates. If the first extreme is a minimum, the simulation is similar to the above, except for changes of sign.

The time development of the simulated plastic displacement process has not been explicitly discussed. In the true plastic displacement process each phase of yielding has small but finite duration. In the Slepian Model simulation, the plastic increment is computed in a single step localized at a single time point. The result is that plastic displacement process is discretized. Thus, during a clump, the plastic displacement process is discretized as a step-process of consecutive localized plastic displacement increments separated in time by a half period. It is noted

$$X_0 = X_{P,0} = 0.$$

$$u^+ = u^- = u.$$

Decide by uniform simulation if the first extreme is a maximum or minimum.

Simulate M_{ALO} from $F_M(m | X(-\pi) \in [-u, u])$.

IF simulating maximum

Compute M_{EPO} , $X_{P,1}$, u_1^+ and u_1^- from M_{ALO} and Eqs. (2.31) and (2.32).

$$\xi = u_1^+.$$

$$D_1 = X_{P,1}.$$

ELSE simulating minimum

Compute M_{EPO} , $X_{P,1}$, u_1^+ and u_1^- from M_{ALO} and Eqs. (2.34) and (2.35).

$$\xi = u_1^-.$$

$$D_1 = X_{P,1}.$$

ENDIF

Increment time by half a period.

Table 2.2: Simulation of the first extreme in the first clump.

that in the real process phase drift is present. This is too neglected in the Slepian clump simulation. Thus it is a requirement that simulation of the inter-clump waiting time shall introduce phase drift.

To give a more explicit formulation of the simulation algorithm a recapitulation in terms of pseudo code is given in tables 2.2, 2.3 and 2.4. One table for each of the three special cases of extreme simulations. The first case concerns the first extreme in the first clump. This extreme always causes a plastic displacement and the EPO experiences its first uploading. This is treated in Tab. 2.2. The second case concerns the first extreme in the second and following clumps. This extreme does not necessarily cause a plastic increment, i.e. an empty excursion may be encountered (see note after the clump definition on page 26). Furthermore, if the extreme does cause a plastic displacement, whether the EPO experiences a reloading or a reversed loading then depends on the past displacement history. Therefore this case is different from the case of the first clump treated in Tab. 2.2. The simulation of the first extreme in the second and following clumps is given in Tab. 2.3. The third case concerns the simulation of the possible second and following extremes in a clump. This simulation includes the test of whether the clump terminates or not, and the simulation distribution is not the same as for the first extreme in the clump. Therefore this is a case different from the two others. See Tab. 2.4. Finally Table 2.1 gives the overall outline of the simulation of a clump.

$$u_{sym} = \min(u_i^+, u_i^-).$$

Dependent on the waiting time simulation (Tab. 3.2 p. 73) simulate a max. or a min.

Simulate M_{ALO} from $F_M(m | X(-\pi) \in [-u_{sym}, u_{sym}])$.

IF simulating maximum

IF an empty excursion – i.e. $M_{ALO} < u_i^+$

$$\xi = M_{ALO}.$$

$$D_i = 0.$$

ELSE a genuine excursion

If load reversed set $X_0 = X_p$.

Compute M_{EPO} , $X_{P,i+1}$, u_{i+1}^+ and u_{i+1}^- from Eqs. (2.31) and (2.32).

$$\xi = u_{i+1}^+.$$

$$D_i = X_{P,i+1} - X_{P,i}.$$

ENDIF

ELSE simulating minimum

IF an empty excursion – i.e. $M_{ALO} < u_i^-$

$$\xi = M_{ALO}.$$

$$D_i = 0.$$

ELSE a genuine excursion

If load reversed set $X_0 = X_p$.

Compute M_{EPO} , $X_{P,i+1}$, u_{i+1}^+ and u_{i+1}^- from Eqs. (2.34) and (2.35).

$$\xi = u_{i+1}^-.$$

$$D_i = X_{P,i+1} - X_{P,i}.$$

ENDIF

ENDIF

Increment time by half a period.

Table 2.3: Simulation of the first extreme in the second and following clumps.

2.6.1 Computational Aspects

Finally some comments on the computational aspects of the Slepian Model clump simulation scheme are relevant. Simulating first M_{ALO} and then next computing M_{EPO} involves solving two equations numerically. In the present implementation first an interval bracketing the solution is found and next bisection is used. This is quite simple and avoids the divergence problem that may appear when using Newton-Raphson – especially so when computing M_{ALO} because of the small slopes in the tails of the distribution functions $F_M(m | \dots)$. The time consumption of

$$u_{sym} = \min(u_i^+, u_i^-).$$

Whether to simulate a maximum or a minimum depends on the previous extreme.

Simulate M from $F_M(m | X(-\pi) = -\xi)$ setting $u = 0$ in (2.28).

IF clump ended – i.e. $M < u_{sym}$

Store M in M_{term} for later use in waiting time simulation (Tab. 3.2 p. 73).

STOP clump simulation.

ELSE IF simulating maximum

IF an empty excursion – i.e. $M < u_i^+$

$$\xi = M.$$

$$D_i = 0.$$

Increment time by half a period.

ELSE a genuine excursion

Simulate M_{ALO} from $F_M(m | X(-\pi) = -\xi)$ setting $u = u_i^+$ in (2.28).

If load reversed set $X_0 = X_P$.

Compute M_{EPO} , $X_{P,i+1}$, u_{i+1}^+ and u_{i+1}^- from Eqs. (2.31) and (2.32).

$$\xi = u_{i+1}^+.$$

$$D_i = X_{P,i+1} - X_{P,i}.$$

Increment time by half a period.

ENDIF

ELSE simulating minimum

IF an empty excursion – i.e. $M < u_i^-$

$$\xi = M.$$

$$D_i = 0.$$

Increment time by half a period.

ELSE a genuine excursion

Simulate M_{ALO} from $F_M(m | X(-\pi) = -\xi)$ setting $u = u_i^-$ in (2.28).

If load reversed set $X_0 = X_P$.

Compute M_{EPO} , $X_{P,i+1}$, u_{i+1}^+ and u_{i+1}^- from Eqs. (2.34) and (2.35).

$$\xi = u_{i+1}^-.$$

$$D_i = X_{P,i+1} - X_{P,i}.$$

Increment time by half a period.

ENDIF

ENDIF

Table 2.4: Simulation of the second and following extremes in a clump.

this approach is to be compared with the time consumption of a direct time-stepping procedure which usually spends (see Chap. 4) five time-steps to reach from one extreme to the next, and ten, twenty or thirty small time-steps during yielding to obtain a refined computation of the plastic displacement increment.

Each function evaluation of the distribution functions $F_M(m | \dots)$ is quite expensive, and iterations are required to obtain M_{ALO} . Thus the computation of M_{ALO} may become expensive. On top of this comes the iterations needed to compute M_{EPO} from M_{ALO} . On the other hand, depending on the complexity of the restoring force diagram the refined stepping during yielding involves solving a non-linear equation in each time-step too. Clearly it is difficult to say which approach is the most expensive. We will return to this issue in Sec. 5.5. At this stage it is, however, natural to answer a question that will rise under circumstances, where the Slepian Model clump simulation is more expensive than the direct clump simulation: is the Slepian Model Simulation Method really useful? Yes, it is. As it is shown in Chap. 3 the real time gain is due to the inter-clump waiting time simulation. This simulation does, however, not provide sufficient information to compute the first plastic displacement in a clump. Therefore, in order to initiate the clump, one has to simulate from $F_M(m | X(-\pi) \in [-u_{sym}, u_{sym}])$ to obtain M_{ALO} and thereby M_{EPO} . Thus the time gain due to the waiting time simulation is not obtainable unless a stand-alone simulation procedure for the clumps exists.

As a closing remark it is noted that though it does not appear so, it is simpler to code the Slepian Model Simulation Method without making errors, than it is to code the direct simulation method. For direct numerical time integration it is – in the author’s experience – difficult to extract from the samples information about plastic displacement increments, clump lengths etc.. This is because one has to be careful about the phase drift and the wiggles which are of course present in these samples.

2.7 Simulations of Clumps for the Bilinear EPO

In this section different simulation results for the clumps of the idealized bilinear EPO is presented for the purpose of comparing results obtained by Slepian simulation and direct simulation. The restoring force diagram of the bilinear EPO is reviewed in Appendix A. For easy reference the diagram is depicted in Fig. 2.13. An example of a non-idealized restoring force diagrams is given in Chapter 5. The simulations are conducted in the following way. Only the first clump in samples which have initial displacement inside the symmetrized yield limits is considered. For the direct simulation scheme this is obtained by generating a truncated Gaussian initial displacement inside the symmetric yield limits and a Gaussian velocity independent of the displacement. Then a sample with this set of initial conditions is simulated and traced until the first clump ends. The Slepian clump simulations simply follow Tab. 2.1. The number of simulations is 10000.

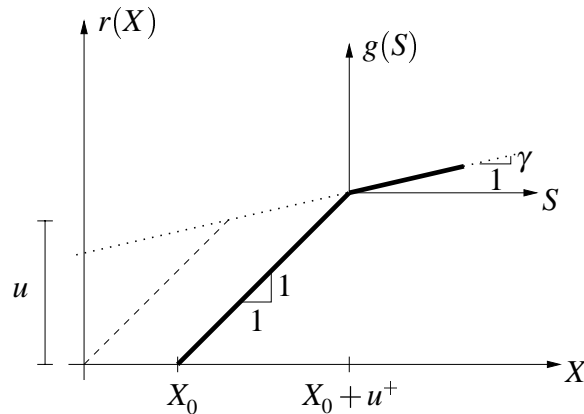


Figure 2.13: The characterization of the ideal bilinear restoring force diagram.

A set of four parameters characterizes each simulation. Three of them are system parameters: the initial yield level u , the hardening/softening parameter γ and the damping ratio ζ . As the plastic displacements in a clump depend on the value of the plastic displacement before the clump begins, a fourth parameter $X_{P,\text{initial}}$ is introduced. Choosing this last parameter a good way from zero, considerable asymmetric yield levels are present. In this way it may be tested how well the notion of symmetric yield limits works – for instance how well empty excursions are captured. It is noted that in case $X_{P,\text{initial}} \neq 0$ one enters Tab. 2.1 as if one is *not* simulating the first clump and the probabilities that the first extreme in the clump be a maximum or minimum are equal. It is noted that since it has become practice in papers [6], [19], [12] and others to present results as function of ζ in stead of the scaled damping ratio α it has been decided to do likewise herein (as $\alpha \approx \zeta$ it is not very confusing).

For each parameter set four plots are shown. The left most plot shows the histogram of the clump length measured by the number of extremes N in the clump. The two middle plots show histograms of the first and the second plastic displacement in a clump. These histograms do not include empty excursions. These are accounted for in the right most plot which shows the probability of having an empty excursion at the i 'th extreme in a clump, $i = 1, 2, 3, 4$. Slepian model results are shown with a thick line, while direct simulation results are shown with a thin line.

In Fig. 2.14 (found at the end of the chapter, page 50) only the initial yield level u varies. This shows how well the Slepian Simulation Method performs at different levels of hysteresis. As one should expect (in accordance with the discussion on page 12), clearly the moderately low level $u = 1.5$ is the limit of the method. One sees that the variance of the (approximately) true distributions of D_1 and D_2 as obtained by direct time integration are larger than the variance of those obtained by Slepian simulation. This is due to the Karnopp-Scharton hypothesis. Neglecting the load process after outcrossing means neglecting a source of randomness. Therefore in general the variance of the plastic displacements obtained by Slepian simulation is smaller than

the true variance. The more so, the longer the duration of the yielding, i.e. the lower the yield level. The errors in clump length estimation and the errors in the estimated number of empty excursions show the same trend. Due to hardening there will be no empty excursions until the third excursion in a clump. It is seen that the ratio of empty excursions is well approximated for levels above 1.5. Thus for levels $u = 2.0$ and higher the Slepian method produces very good results. Let us, in continuation of this conclusion, turn to the simplified restoring force diagram to give a short remark related to the performance of the Slepian Method demonstrated here. In the definition of the simplified diagram it was implicitly assumed that a linear part is always present. It is now seen clearly that this assumption is necessary for the Slepian Model Simulation Method to give reliable results for non-linear plasticity. In the simplified non-linear restoring force diagram there must always be a linear part of reasonable extend. Otherwise, if the linear part, and thereby the yield limit, is too small the simulated plastic displacement increments will be in error, even if the hardening/softening branch starts out all most linearly. The error will simply be due to the approximations of the Karnopp-Scharton hypothesis and not the non-linearity. Also another remark is appropriate. Anticipating the discussion of the inter-clump waiting time distribution it is noted that the clump size decreases with increasing yield level. This is in accordance with asymptotic results. It is, however, also noted that clump sizes larger than 1 are very likely for realistic levels like $u = 2$ and $u = 3$. Thus, it is already here noted, that the convergence to the asymptotic limit is too slow for asymptotic results to be valid for realistic yield levels. A similar experience is reported for the waiting time distribution.

In Fig. 2.15 (found also at the end of the chapter, page 51) $u = 2$ in all cases. In stead the other parameters are varied such that the plots may be compared to the plots for $u = 2$ in Fig. 2.14. The top most plots show that even for higher damping the Slepian method gives good results. As one should expect the clumps become shorter for higher damping as higher damping implies less narrow banded response, i.e. a more rapidly varying amplitude process. Therefore also the variance of D_i increases with increasing damping. The second row of plots treats the case of strain softening. Good agreement between simulation results is apparent. Due to the destabilizing effect of the softening, the variance of D_i is larger in the case of softening than in the case of hardening. Furthermore softening implies that, contrary to hardening, empty excursions may occur already at the second extreme in a clump. The Slepian simulation captures this very well, too. In the last two rows the case of considerable asymmetric yield limits is considered. Still there is a very good agreement between the results. The distributions are very asymmetric due to the presence of asymmetric yield limits. Considering how very well the asymmetry of the distributions is captured by the Slepian Simulation Method one can conclude, that the notion of symmetrized yield limits is very successfully managed. It is noted that in the second last and the last rows the initial symmetrized yield levels are 1.14 and 1.54, respectively. This is quite low, why an error in terms of a too small variance like in the first row of Fig. 2.14 must be expected. The error is of course largest in the second last row.

Concluding on the basis of Figs. 2.14 and 2.15 one has that the Slepian clump simulation in general provides results in very good agreement with the direct simulation results – as long as the assumption about non-dominating hysteresis is not violated, of course. Especially it is noted that the notion of the symmetrized yield level does not give rise to any problems.

2.8 Summary

The Slepian modeling and simulation of the clumps of plastic displacement increments in the response of SDOF EPOs has been presented. The Slepian model approach to the clump modeling of the ideal EPO, as known from [6], is recapitulated and extended to non-ideal plasticity with hardening or softening. In extending from ideal to non-ideal EPOs it becomes apparent that some simplifications of the restoring force diagram are required, otherwise the Slepian Model clump simulation will be too time costly. To that end a simplified, yet, from an engineering point of view acceptable, model for the non-ideal restoring force diagram is introduced. The corner stone of the simplification is the treatment of unloading/reloading and the Bauschinger effect. A specific implication of the Slepian Model approach is that the simplified non-ideal diagram must have a linear part of reasonable extend.

A detailed presentation of the Slepian Model clump simulation is given in terms of tables of pseudo code. Though it may not appear so at a first glance, the algorithm is simpler to implement than direct numerical time integration algorithms.

The definition of clumps differs from what has been used in former works such as [16] and [6] dealing with the ideal EPO. What is new here is that the problem of asymmetric yield levels is considered. Due to this asymmetry it becomes convenient to define clumps such that they include excursions above a so-called symmetrized yield level, even though these excursions do necessarily not cause plastic displacements. The symmetrized yield level simply equals the narrowest of the asymmetric yield levels. The notion of a symmetrized yield level is actually motivated by the simplifications obtained in the inter-clump waiting time simulation described in Chapter 3. Handling the excursions of a symmetric domain is considerably simpler than it is for asymmetric domains.

Another important point about clumps is that they appear in groups of clumps, i.e. in clumps of clumps. By the clump definition introduced here it is required that the inter-clump simulation procedure be capable of simulating both the short waiting times between the clumps that appear in the clumps of clumps as well as the much longer waiting times between the clumps of clumps. Yet another aspect concerning the simulation of waiting times is that the simulation of the plastic displacement process implies a discretization of the process into a discontinuous step process with increments separated in time by half a period. Therefore it is left to the inter-clump waiting time simulation procedure to account for the phase drift which is present in response, but is neglected in the clump simulation.

Finally simulation results for the bilinear EPO verify how very well the Slepian model simulates the development of the plastic increment process even for notably asymmetric yield levels. These results prove that the introduction of the symmetrized yield level does not cause any restrictions on the applicability of the Slepian Model Simulation Method.

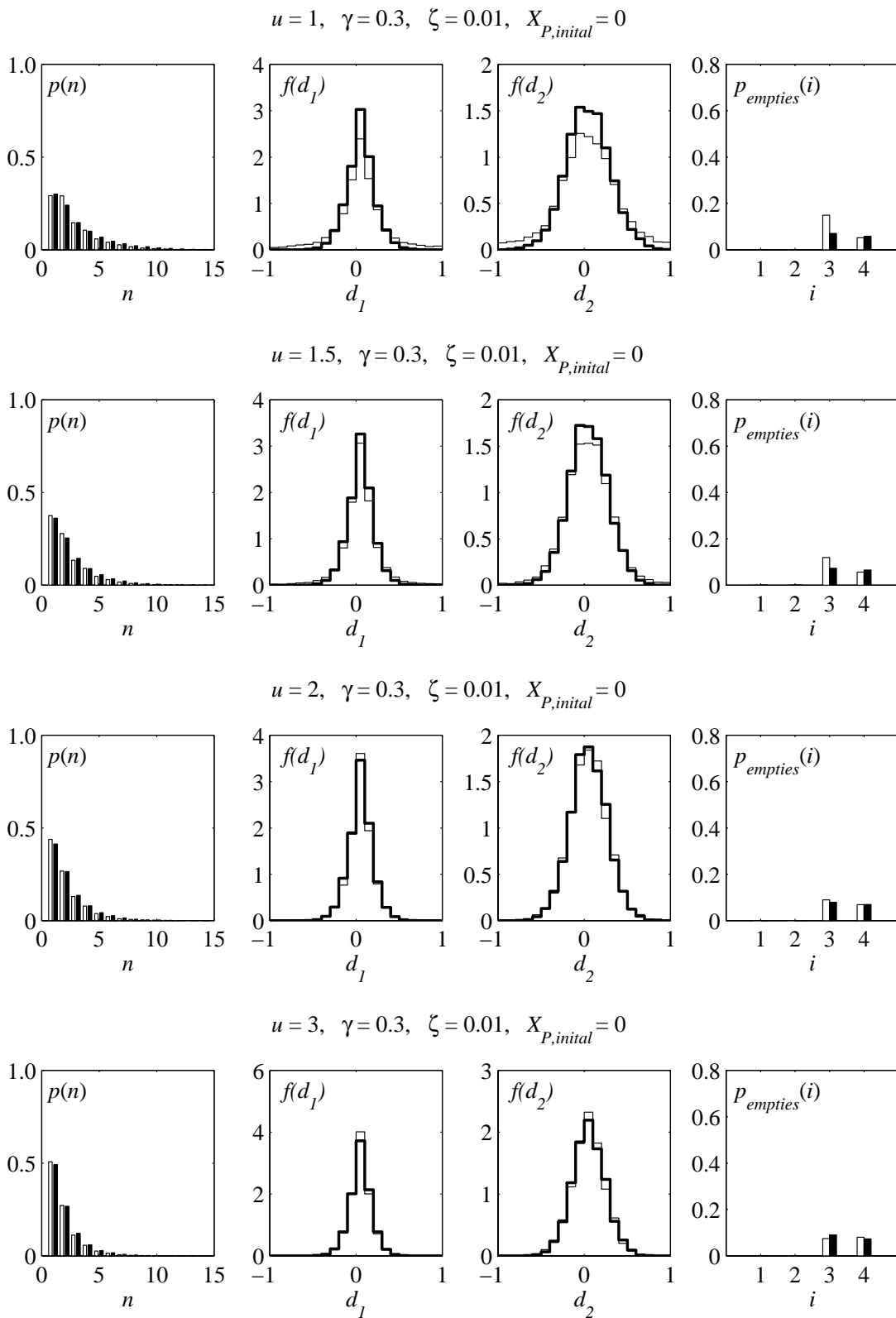


Figure 2.14: Comparison of clump simulation results obtained by Slepian simulation (thick curves) and direct simulation (thin curves). See discussion at p. 45.

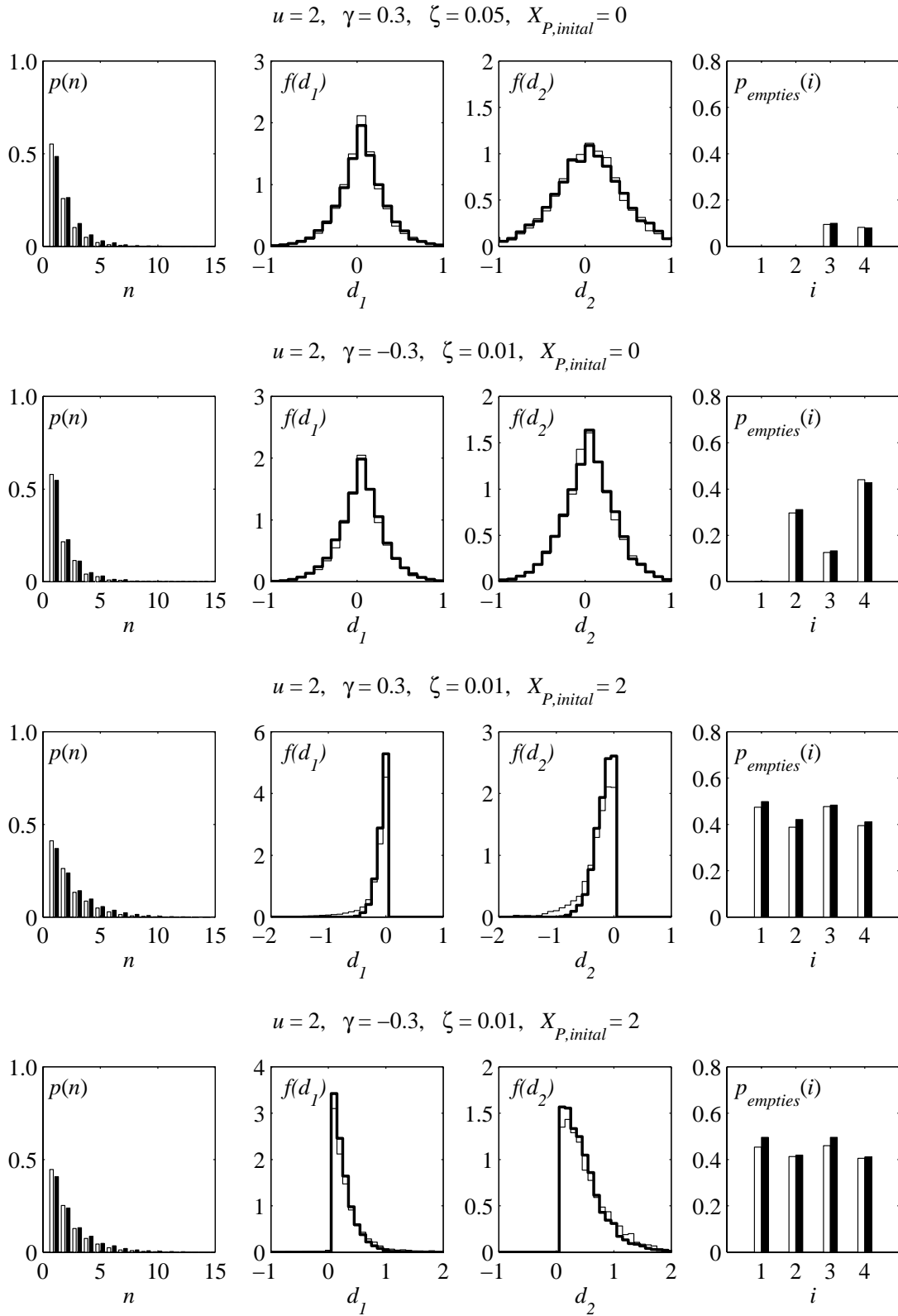


Figure 2.15: Comparison of clump simulation results obtained by Slepian simulation (thick curves) and direct simulation (thin curves). See discussion at p. 45.

Chapter 3

Modeling and Simulation of Inter-clump Waiting Times

As described in the previous chapter the degradation of the EPO takes place only in limited time intervals which for short are termed clumps. In this chapter the remaining response outside the clumps is in focus. Since no degradation takes place in these time intervals it is sufficient for the description of the plastic process to establish a model for the duration of the response between the clumps. It is the modeling and simulation of the inter-clump waiting times for the SDOF EPO that is the subject of this chapter.

3.1 Main Characteristics of the Distribution

There does not exist analytical expressions for the inter-clump waiting time distribution. However, some considerations about the general features of the distribution may be given. Based on these considerations a fast simulation scheme can be derived. Therefore this first section provides a general discussion of the characteristics of the distribution.

3.1.1 Quantities on which the Distribution Depends and Symmetrization

Clearly the waiting time depends on all parameters of the system: driving force, damping and the non-linear restoring force diagram, as they all appear in the governing equation. However, due to the scaling of the equation of motion and the symmetrized yield limits introduced in the previous chapter it is in the following shown, that it is possible to work with waiting time distributions of rather general type, depending only on the scaled damping ratio α and the symmetrized yield level u_{sym} .

Since the response in the time between clumps is inside the elasticity limits u^+ and u^- the inter-clump response which is decisive for the waiting time fulfills the equation of motion for the ALO:

$$\ddot{X} + 2\alpha\dot{X} + (1+\alpha^2)X = W(\tau). \quad (1.8)$$

Consequently the only way non-linearity influences the waiting time distribution is through the asymmetric elasticity limits. Due to the scaling of the equation of motion the influence of the load process is accounted for by the elasticity limits as well. Damping is simply described by α .

The way in which the waiting time depends on the elasticity limits deserves some attention. When yielding ends, the ALO is restarted with initial conditions $X = u^+, \dot{X} = 0$ or $X = u^-, \dot{X} = 0$. Onset of yielding is then the next time at which $X = u^+$ or $X = u^-$. This means, since generally $u^+ \neq u^-$, that there is essentially two different combinations of initial and stopping conditions for the inter-clump sample paths: starting at one level and crossing out the same level, or: starting at one level and crossing out the opposite level, which is generally of different absolute value. Clearly both crossing problems are of non-stationary nature, why the first cannot be considered a special case of the second. Without going into details, it is here mentioned that one of the computations appearing later in this chapter becomes considerably simpler by use of symmetric yield limits. Further more it eliminates the problem of assessing whether the outcrossing is an outcrossing of the upper or lower yield limit. This is a task for the clump simulation procedure to take care of. It is recalled that in the previous chapter it was shown that symmetrized limits can successfully be included in the clump simulation. Thus it is not a restriction to introduce symmetrized yield limits, merely a computational ease.

3.1.2 The Amplitude Process

If the response crosses out of the elasticity domain the amplitude process does so too. However, the processes do not cross at the same time. Furthermore, since the amplitude process expresses the energy, it may cross out without the response crossing out. The waiting time to the first outcrossing of the amplitude process therefore is not identical to the waiting time to the first outcrossing of the response. The two different waiting times do not differ much so the equation for the amplitude process derived in Sec. 1.2.3 does provide useful information about the characteristics of the waiting time distribution. For easy reference the amplitude diffusion equation is repeated below:

$$dA = \alpha(-A + \frac{1}{A})d\tau + \sqrt{2\alpha} dB_A \quad (1.20)$$

A way to find an approximate waiting time distribution would be to find the amplitude distribution as function of time by solving the Fokker-Planck equation associated with Eq. (1.20) using absorbing boundaries. Based on the amplitude distribution $F_A(\tau, a) = P(A(\tau) \leq a)$ the waiting time distribution is given by $F_T(\tau) = 1 - F_A(\tau, u)$. Computing $F_A(\tau, a)$ involves absorbing

boundaries and initial density $f_A(\tau = 0, a) = \delta(a - u)$, $a \in [0, u]$. This is not easy and computationally expensive, so no attempts are made here to solve the amplitude diffusion equation.

How the waiting time distribution depends on the symmetrized yield level u_{sym} and the damping ratio α can, however, be discussed on the basis of Eq. (1.20). Clearly, the lower the damping the lower the rate of change of the amplitude. As discussed in Sec. 2.1, dealing with the clump definition, the fact that the amplitude drifts slowly causes the existence of short and long waiting times of principally different character. For given damping the yield level influences the amount of short waiting times relative to the amount of long waiting times. The drift coefficient $\alpha(-A + \frac{1}{A})$ shows that the amplitude fades away faster for higher yield levels than for lower levels, making short waiting times become less likely. This is due to imbalance between energy input and drain for oscillations with large amplitudes. The viscous energy drain per cycle increases proportionally with the square of the amplitude, while the energy input due to the forcing is directly proportional to the amplitude. This imbalance is expressed by the two terms $-A$ and $\frac{1}{A}$ appearing in the drift coefficient.

3.1.3 Transient Lower Tail

Right after the termination of a clump the amplitude is close to the symmetrized yield limit. Since the amplitude process drifts and diffuses on slow time scales the amplitude stays close to u_{sym} for a while. Thus short waiting times to the first outcrossing after clump termination are quite likely. This issue was one of the key points in the discussion of the clump definition in Chap. 2, where a distinction between separate clumps, and clumps of clumps was made. It was at that time pointed out, that the simulation scheme for the waiting time should account for the presence of clumps of clumps. Therefore the characteristics of the short waiting times giving the time separation of the clumps inside the clumps of clumps is treated separately here.

The distribution of the short waiting times relates to the fast time scale of the oscillations as described in the following. As it takes an extreme inside the symmetrized yield limit to terminate the clump, the first crossing after a clump is determined from the second extreme after the clump. Thus the first possible crossing time will, due to the narrow banded response, be very close to the natural period of the ALO. The second possible crossing time is close to one and a half period, and so on. This means that the lower tail of the waiting time distribution is step-like. The larger the waiting time is, the less pronounced the steps are as the phase drift causes the waiting time to scatter more and more about integer multiples of half a period. The step shape suggests that short waiting times may be simulated by a stepping procedure which uses steps of size half a period.

Since the lower tail of the waiting time distribution results from the ALO response shortly after the clump termination, it is termed the *transient lower tail*. This subsection is closed by showing some typical transient lower tails. Figure 3.1 shows a few transient tails in which the steps appear very clearly in the beginning, and where the smoothing effect of the phase drift takes over after a while. As explained above the amplitude fades away faster for higher yield

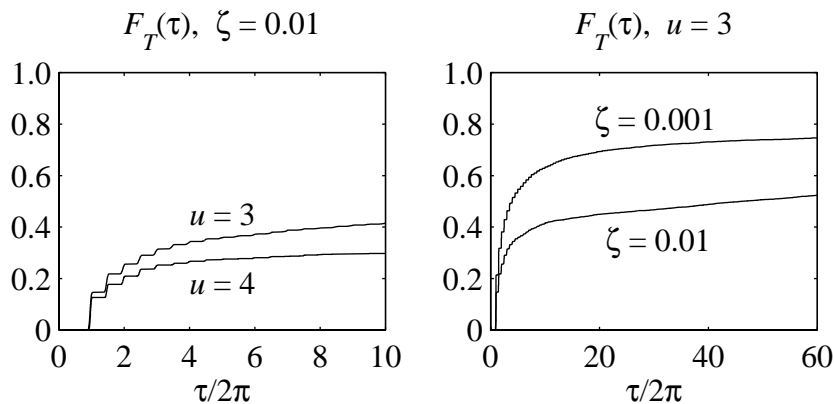


Figure 3.1: A few transient tails. See discussion in the text.

levels than for lower levels, making short waiting times more likely for low levels than for high levels as shown in the left plot in Fig. 3.1. The amplitude also fades away faster for increasing damping, so, as shown in the plot to the right in Fig. 3.1, this results in increasing probabilities of having short waiting times as damping decreases.

3.1.4 Exponential Upper Tail

During transients, which causes the short waiting times, the crossing rate is strongly varying with high peaks. The peaks are present because the phase drift has not yet set through, while the considerable size of the peaks is due to the high level of energy. If the oscillator has passed through transients without outcrossings the energy in the oscillator has become low relatively to the yield level and the phase drift has become more pronounced. This implies that the crossing rate is low and slowly varying. According to the slow time scale of the amplitude process it will take some time before the energy builds up again and an outcrossing will occur. Thus the natural time scale of the large waiting times which expresses the time between the clumps of clumps is the slow scale $\alpha\tau$. This means that the time distance between the clumps of clumps is so large that the response in two consecutive clumps of clumps are virtually independent. Therefore all non-transient outcrossings are approximately independent. On the slow time scale where the short waiting times vanish, outcrossings are therefore approximately independent events. Consequently the outcrossings corresponding to the large waiting times fulfill approximately the Poisson model, and hence the upper tail is approximately exponential. In other words, the distribution of the waiting times beyond a certain value $\tau_{\text{transients}}$ is most reasonably modeled by an exponential distribution. Writing this in terms of a formula it becomes

$$F_T(\tau) = \begin{cases} G(\tau) & , \text{for } \tau \leq \tau_{\text{transients}} \\ 1 - (1 - G(\tau_{\text{transients}})) e^{-\lambda(\tau - \tau_{\text{transients}})} & , \text{for } \tau > \tau_{\text{transients}} \end{cases} \quad (3.1)$$

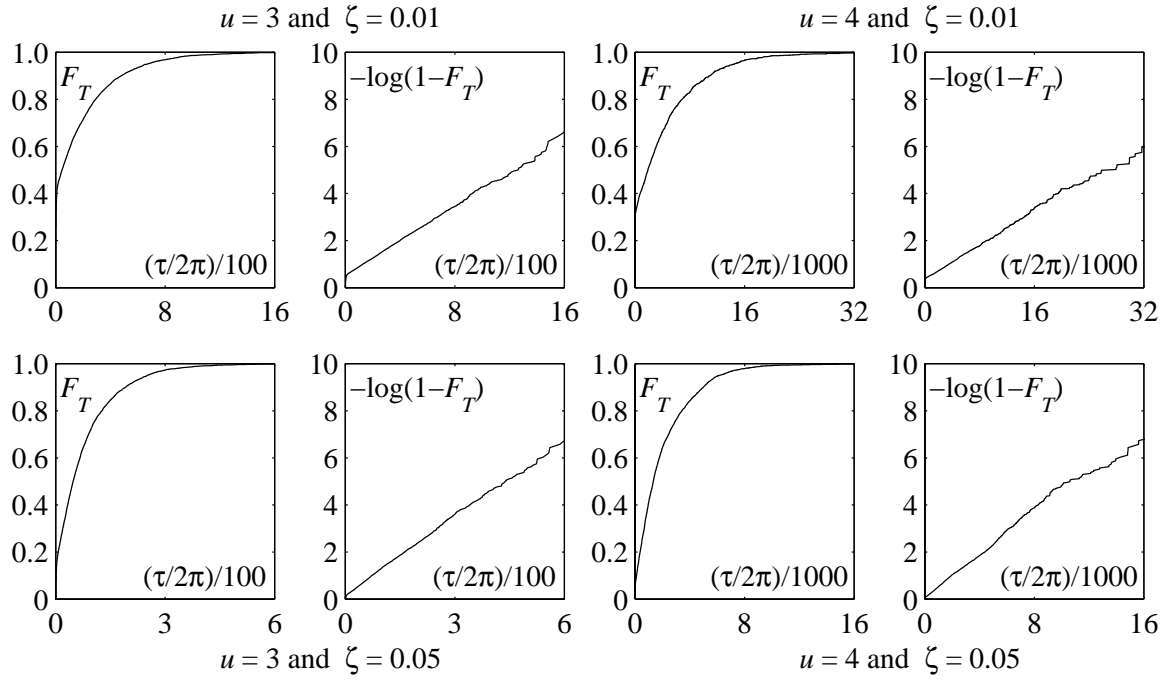


Figure 3.2: A few distributions showing exponential upper tails. See discussion in the text.

in which λ denotes the stationary mean crossing rate given that $\tau > \tau_{\text{transients}}$. As the distribution of the large waiting times may be modeled by an exponential distribution the upper tail is called the *exponential upper tail*.

Figure 3.2 shows plots of the waiting time distribution for different parameters. To make the exponential tail become apparent the plots show $-\log(1 - F_T(\tau))$ too. Clearly the plots verify that modeling the upper tail as an exponential distribution works fine. The plots also demonstrate the balance between the transient lower tail and the exponential upper tail in dependence of damping ratio and yield level. The upper row shows, as mentioned in the previous section, that for increasing yield levels short waiting times become less likely. This behaviour is a realization of the asymptotic Poisson character of the stream of upcrossings when the crossing level tends to infinity [2][Chap. 12]. In previous works like [6] and [8] transients were neglected and the entire distribution assumed exponential in accordance with the asymptotic result by Cramér and Leadbetter. As supported by the plots, the Poisson model is asymptotically correct. It however further appears from the plots that the convergence is slow, why the asymptotic result is not very useful for realistic yield levels. In [12] the appreciation of this fact led to the first steps in the direction of accounting for transients, but a systematic treatment like here was not given. For high damping the amplitude fades fast why transients gets less important. The lower row in Fig. 3.2 shows this in the case $\zeta = 0.05$. Compared to the upper row it may be concluded that transients is more dominant in the realistic case of $\zeta = 0.01$. This supports further the above statement that transients cannot be neglected.

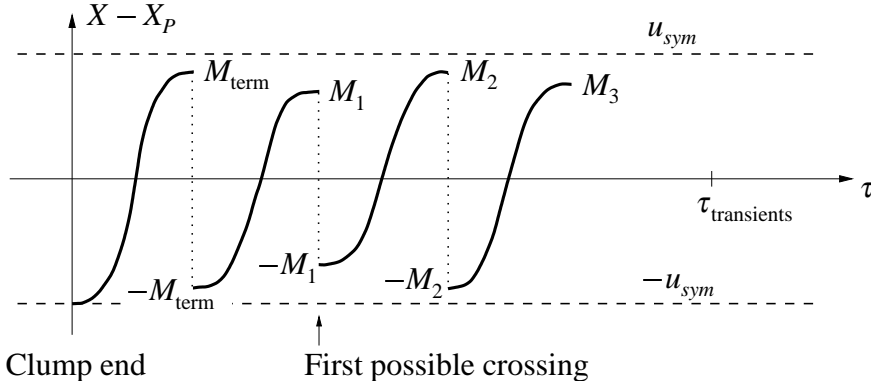


Figure 3.3: The simulation of the transient tail by use of a conditional distribution $F_M(m | X(-\pi) = -M_{i-1})$.

3.2 Simulating the Waiting Time

3.2.1 Simulating the Transient Lower Tail

As mentioned the step shape of the transient tail suggests that short waiting times are simulated by a stepping procedure which uses steps of size half a period. The approach suggested here consists in simply continuing the clump simulation until either an outcrossing is detected or a certain time $\tau_{\text{transients}}$ after the clump end is elapsed. If an outcrossing is detected before the time $\tau_{\text{transients}}$ after the clump end, then a new clump simulation is initiated. Else the waiting time falls outside the transient tail and a waiting time from the exponential tail is simulated as described in the next section.

Each step is simulated as a maximum M_i above zero conditional on the previously simulated maximum M_{i-1} . That is, M_i is simulated from some distribution $F_M(m | X(-\pi) = -M_{i-1})$ which is not necessarily identical to the Slepian model based distribution defined in formula (2.28) in Sec. 2.4.4. In the first step after the clump, M_1 is simulated conditional on the extreme $M_{\text{term}} < u_{\text{sym}}$ which terminated the clump. Figure 3.3 illustrates this.

Slepian Modeling

Since a formula for the distribution of an approximate maximum of the ALO given the previous minimum is already derived in Sec. 2.4.4, it is natural to try to use this in simulating the sequence of extremes trailing the clump. In the plot to the left in Fig. 3.4 the thick curve shows an example of the result of the simulation of short waiting times as obtained by use of formula (2.28) with $u = 0$, i.e. for zero-level crossings. In comparison to the waiting times obtained by direct simulation, shown by a thin line, an underestimation is apparent. This error is detected for all other combinations of the parameters u , ζ and it is due to the Karnopp-Scharton hypoth-

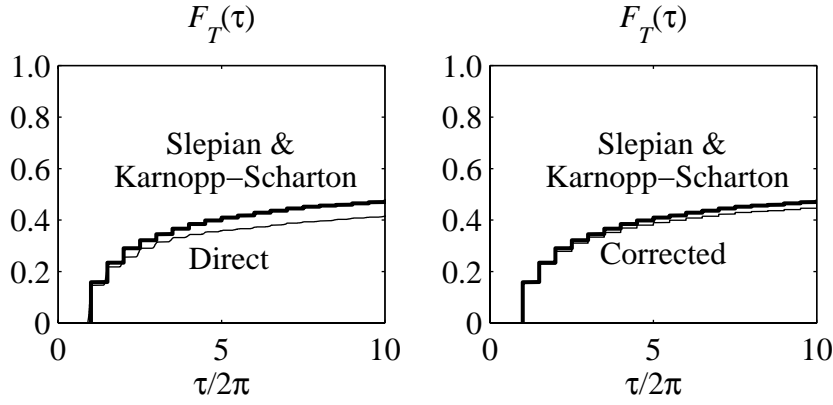


Figure 3.4: Simulation of transient waiting times by use of the Slepian model. Left: Slepian model simulation (thick curve) and direct simulation (thin curve). Right: Slepian model simulation (thick curve) and damping corrected Slepian model simulations (thin curve). The curves are obtained from those waiting times out of 5000 which are less than 20π . Parameters are $u = 3$, $\zeta = 0.01$.

esis. In the derivation of the unconditional distribution F_M of the approximate ALO maximum, damping and driving forces were neglected. These approximations are acceptable if the duration of the response from the outcrossing to the extreme is small. Simulating extremes above zero implies that the duration of the response from the crossing, i.e. the zero level-crossing, to the extreme is approximately half a period, which is not small. Therefore modifications of formula (2.28) are required. Regard damping first. In the derivation of the conditional distribution $F_M(m | X(-\pi) = -\xi)$ the conditional probability $P(X(-\pi) \in [-\xi, -\xi + d\xi] | M = m)$ is used. The formula for this distribution already includes damping (see Eqs. (2.21–2.23)). Thus it is only the unconditional distribution F_M which has to be corrected with respect to damping. Since we consider an extreme after a zero level crossing the reduction of the extreme caused by damping is approximately accounted for by multiplying the unconditional maximum M by $e^{-\frac{1}{2}\alpha\pi}$. Denoting the inverse of this factor v one finds analogously to Eqs. (2.27) and (2.28) that

$$f_M(m | X(-\pi) = -\xi) \propto \varphi\left(\frac{\xi - \mu m}{\sigma}\right) m e^{-\frac{1}{2}v^2 m^2} \propto m \varphi\left(\frac{\kappa^2 m - \mu \xi}{\kappa \sigma}\right), \quad m > 0 \quad (3.2)$$

in which $\kappa^2 = \mu^2 + v^2 \sigma^2$ and that the corresponding complementary distribution function is given by

$$\begin{aligned} 1 - F_M(m | X(-\pi) = -\xi) &= \frac{\int_m^\infty z \varphi\left(\frac{\kappa^2 z - \mu \xi}{\kappa \sigma}\right) dz}{\int_0^\infty z \varphi\left(\frac{\kappa^2 z - \mu \xi}{\kappa \sigma}\right) dz} \\ &= \frac{\varphi\left(\frac{\kappa^2 m - \mu \xi}{\kappa \sigma}\right) + \frac{\mu \xi}{\kappa \sigma} \Phi\left(-\frac{\kappa^2 m - \mu \xi}{\kappa \sigma}\right)}{\varphi\left(\frac{\kappa^2 u - \mu \xi}{\kappa \sigma}\right) + \frac{\mu \xi}{\kappa \sigma} \Phi\left(-\frac{\kappa^2 u - \mu \xi}{\kappa \sigma}\right)}, \quad m > 0 \end{aligned} \quad (3.3)$$

The lower step curve to the right in Fig. 3.4 shows the simulated distribution obtained by use of the damping corrected distribution. The upper curve shows the result obtained using non-corrected distribution. Only a slight improvement is obtained. Clearly neglecting the driving force, i.e. the source of randomness, causes the main error. Another modification of (2.28) would thus be the inclusion of the forcing. This is not easy to carry out, why the idea is given up in the favor of the approach presented below.

Amplitude Model

In the Slepian simulation approach a model for the response was obtained by substituting in the conditional mean $E[X_{LO}(\tau)|X_{LO}(\tau_0), \dot{X}_{LO}(\tau_0)]$ for the random variable $X_{LO}(\tau_0)$ a constant value and for $\dot{X}_{LO}(\tau_0)$ a non-Gaussian distribution established by long run sampling of upcrossings in the stationary response (subscript LO = linear oscillator, see Sec. 2.4). One might instead try to simulate directly from the Slepian model

$$\begin{aligned} X_{\max}(\tau - \tau_0) &= E[X_{LO}(\tau) | X_{LO}(\tau_0) = -M_{i-1}, \dot{X}_{LO}(\tau_0) = 0] + R(\tau - \tau_0) \\ &= -c(\tau - \tau_0)M_{i-1} + R(\tau - \tau_0), \quad \tau \geq \tau_0 \end{aligned} \quad (3.4)$$

Setting the time lag $\tau - \tau_0 = \pi$ in this model, a model for the next extreme is obtained. An extreme M_i is then easily simulated by first simulating a standard Gaussian variable independently of M_{i-1} , then scaling this outcome by the standard deviation of $R(\tau - \tau_0)$ and finally adding $-c(\tau - \tau_0)M_{i-1}$. For the same parameters as in Fig. 3.4 the left plot in Fig. 3.5 shows the simulated distribution when using the X_{\max} model. Though the residual term ensures that the X_{\max} model includes the randomness due to the driving force, an overestimation of the waiting times is now present. The reason is that the smoothing effect of the Karnopp-Scharton hypothesis in combination with the energy/amplitude representation by Z in the Slepian model is lost. Because of the phase drift an extreme may occur either earlier or later than one half period after the previous extreme. Obviously the X_{\max} model, simulating the conditional outcome of the response process exactly half a period after the previous extreme, may miss the current extreme. Therefore waiting times are overestimated.

The key to the problem is to find a better way to simulate the amplitude process, i.e. the current mechanical energy of the EPO, than done by the Slepian model when combined with the Karnopp-Scharton hypothesis. A very simple approach would be to discretize the amplitude diffusion equation (1.20) into steps of half a period, integrate the drift by the Runge-Kutta method and simulate the diffusion by a standard Gaussian variable scaled by $\sqrt{2\alpha\pi}$. As the amplitude drifts on a slow time scale this might work. It does for small damping ratios, but not in general. Especially the non-linearity of the drift coefficient $\alpha(-A + \frac{1}{A})$ causes trouble. Alternatively Slepian modeling of the amplitude process may be an option. However, it is not simple as A is a non-Gaussian process.

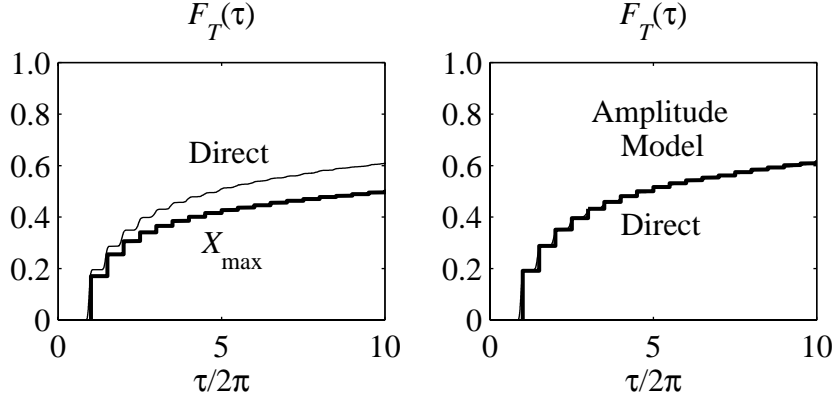


Figure 3.5: To the left: simulation of transient waiting times by use of the X_{\max} model (thick step curve) and by direct simulation (thin curve). To the right: simulation of transient waiting times by use of the amplitude model (thick step curve) and by direct simulation (thin curve) – note that the curves collapse. For both plots: the curves are obtained from those waiting times out of 5000 which are less than 20π . Parameters are $u = 2, \zeta = 0.01$. See discussion in the text.

Still the amplitude process may be simulated by simple means, if in addition to the X_{\max} model for the response, a Slepian model \dot{X}_{\max} for the velocity is introduced. Then A defined by

$$A^2 = X_{\max}^2 + \frac{\dot{X}_{\max}^2}{\lambda_2} \quad (3.5)$$

is a model for the amplitude process in which the problem about the drift in the X_{\max} model is avoided. Clearly A is not a Slepian model, but one is still in the context of Slepian modeling, as A is derived from the Slepian model pair $(X_{\max}, \dot{X}_{\max})$. The \dot{X}_{\max} model is completely analogous to the X_{\max} model. It uses the conditional mean

$$E[\dot{X}_{\text{LO}}(\tau) | X_{\text{LO}}(\tau_0), \dot{X}_{\text{LO}}(\tau_0)] = \dot{c}(\tau - \tau_0) X_{\text{LO}}(\tau_0) - \frac{\ddot{c}(\tau - \tau_0)}{\lambda_2} \dot{X}_{\text{LO}}(\tau_0) \quad (3.6)$$

which leads to the model

$$\begin{aligned} \dot{X}_{\max}(\tau - \tau_0) &= E[\dot{X}_{\text{LO}}(\tau) | X_{\text{LO}}(\tau_0) = -M_{i-1}, \dot{X}_{\text{LO}}(\tau_0) = 0] + Q(\tau - \tau_0) \\ &= -\dot{c}(\tau - \tau_0) M_{i-1} + Q(\tau - \tau_0), \quad \tau \geq \tau_0 \end{aligned} \quad (3.7)$$

where Q denotes the Gaussian velocity residual process of mean zero and covariance

$$\begin{aligned} \text{Cov}[Q(\tau_1), Q(\tau_2)] &= \\ &= -\ddot{c}(\tau_1 - \tau_2) - \dot{c}(\tau_1 - \tau_0)\dot{c}(\tau_2 - \tau_0) - \frac{\ddot{c}(\tau_1 - \tau_0)\ddot{c}(\tau_2 - \tau_0)}{\lambda_2}, \quad \tau_1 \geq \tau_2 \geq \tau_0 \end{aligned} \quad (3.8)$$

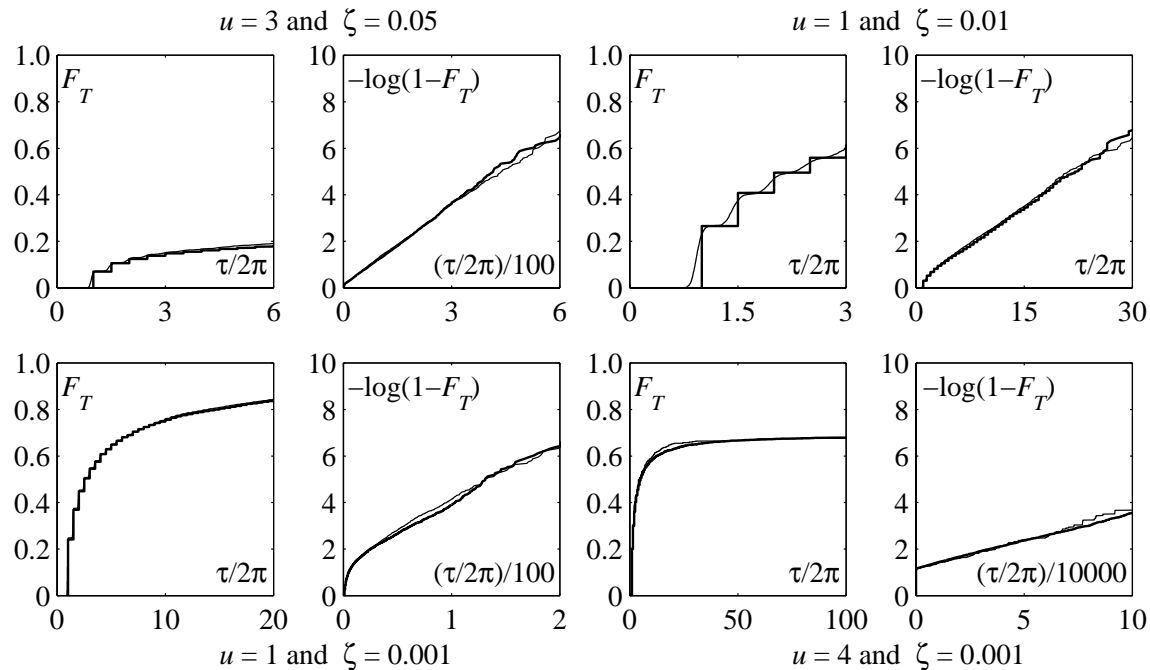


Figure 3.6: Simulation of short and long waiting times by use of the amplitude model (thick curves) and by direct simulation (thin curves) using time step of size one hundredth of the natural period. For all plots: 5000 samples. Parameters are given at the plots.

When generating an outcome of the amplitude model A , outcomes of the residual processes R and Q must be generated. Therefore their cross covariance function must be known too. It turns out that it suffices to know:

$$\text{Cov}[R(\tau_1), Q(\tau_1)] = -\dot{c}(\tau_1 - \tau_0) \left[c(\tau_1 - \tau_0) + \frac{1}{\lambda_2} \ddot{c}(\tau_1 - \tau_0) \right], \quad \tau_1 \geq \tau_0 \quad (3.9)$$

In order to make steps of half a period, one considers as usual the models at time lag $\tau - \tau_0 = \pi$. One easily finds that

$$A^2 = (\mu M_{i-1} + \sigma \Psi_X)^2 + (\sigma \Psi_{\dot{X}})^2 \quad (3.10)$$

in which $\mu = e^{-\alpha\pi}$ and $\sigma^2 = 1 - e^{-2\alpha\pi}$ and the Ψ 's are independent standard Gaussian variables. Note the convenient fact that the conditional response and velocity are uncorrelated at time lags equal integer multiples of π . Since the amplitude measures the mechanical energy in the oscillator, the value of A half a period after the extreme M_{i-1} , will be very close to the next extreme of the response, M_i . The difference is small because the extreme M_i occurs close to half a period after M_{i-1} . Therefore, when using the amplitude model (3.10) the next extreme M_i is simply computed by

$$M_i = \sqrt{(\mu M_{i-1} + \sigma \Psi_X)^2 + (\sigma \Psi_{\dot{X}})^2} \quad (3.11)$$

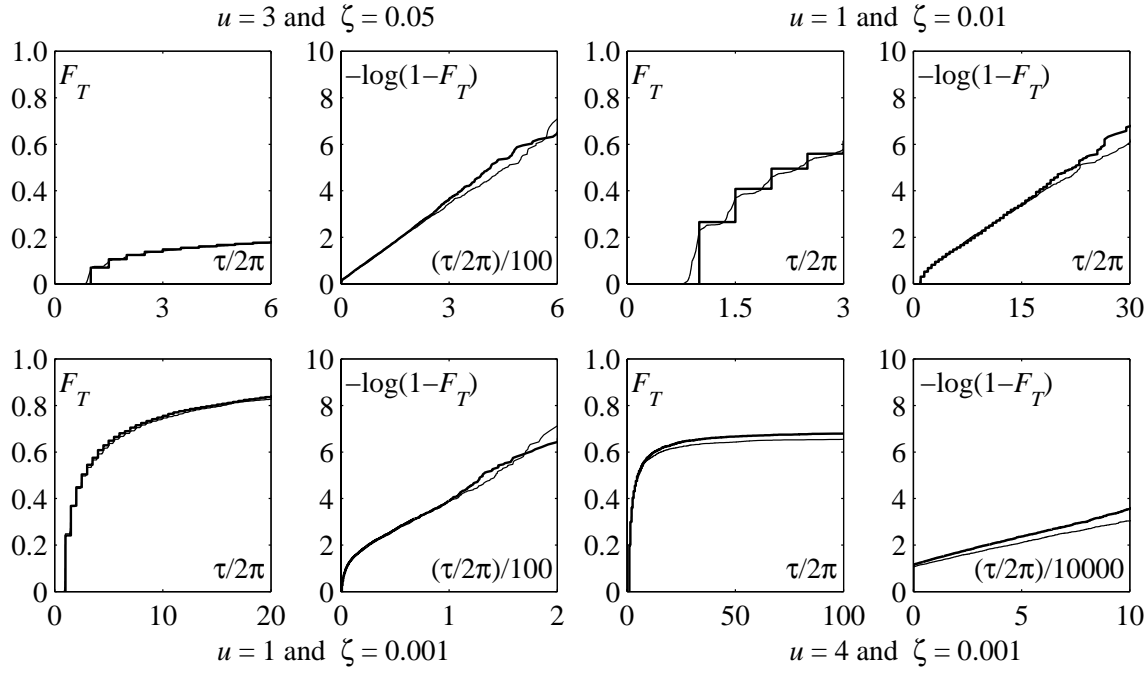


Figure 3.7: Simulation of short and long waiting times by use of the amplitude model (thick curves) and by direct simulation (thin curves) using time step of size one tenth of the natural period. For all plots: 5000 samples. Parameters are given at the plots.

It has not been explicitly stated yet, but clearly the amplitude model possesses, for the same reasons as for the conditional distribution $F_M(m|X(-\pi) = -M_{i-1})$ (Eq. (2.28)), the feature that two consecutive extremes may be simulated independently, i.e. Ψ_X and $\Psi_{\dot{X}}$ are independent of M_{i-1} . Furthermore it is faster to simulate an outcome of A , than an outcome of $F_M(m|X(-\pi) = -M_{i-1})$ given by (2.28). To the right in Fig. 3.5 the simulated transient tail of the waiting time distribution is shown together with the result obtained by direct simulation. Clearly a good agreement is obtained. To demonstrate the strength of the amplitude model Fig. 3.6 shows several plots of waiting time simulations of both short *and* long waiting times using only the amplitude model, that is, without exploiting the exponential tail property. It is interesting to note, that the inclination of the exponential tail in the logarithmic plot equals the inclination obtained by direct simulation. This indicates that the amplitude model may be useful in the computation of the crossing rate λ in (3.1). In Sec. 3.2.2 it is shown how this may be used.

The amplitude process model does not exploit any smoothing like the Karnopp-Scharton hypothesis. Therefore wiggles are present in the amplitude model which can cause errors similar to those experienced for X_{\max} model. When the amplitude process is close to the yield level the wiggles may cause the process to cross in and out of the elastic domain several times during half a period. There is no guarantee that any of these outcrossings will cause the amplitude to be above the yield level exactly half a period after the previously simulated outcome of the am-

plitude process. Therefore the amplitude model may miss outcrossings too, which should lead to an overestimation of waiting times. However, the plots in Fig. 3.6 show that in general the amplitude model does not lead to such an overestimation of waiting times. To explain this one has to consider the method used to obtain the direct simulation results. As explained in Chap. 4 Sec. 4.4.1 the direct simulation method may overlook excursions too. This is why it seems as if no overestimation of waiting times is obtained by the amplitude model. All plots of direct simulation results shown in the graphs in this chapter are obtained using small time steps of size one hundredth of the natural period. In Sec. 4.4.1 it is shown that almost equally good results may be obtained by simulations using time steps of size one tenth of the natural period. However, more excursions are lost. Figure 3.7 illustrates that using time steps of one tenth of the natural period causes gaps to arise between the graphs obtained using direct simulations and using the amplitude model. An investigation with smaller time steps has not been carried out as it would be rather time costly and because it is judged from Figs. 3.6 and 3.7 that it would not alter the results shown in Fig. 3.6 much. Returning to Fig. 3.6 the conclusion is that the amplitude model gives satisfactorily good results. It is, however, noted that an alternative to the amplitude process considered here that might improve the amplitude simulation but is analytically more difficult to apply, and which is left for future work, is the Cramér-Leadbetter envelope. This is a process more smooth than the amplitude process, because the artificial velocity process used is obtained by a time shift of the response process, why it has the same correlation structure as the response process.

Realizing that the amplitude model performs better for the waiting time simulations than the Slepian model based distribution (2.28) does, one may ask: why not apply the amplitude model to the extremes of the clumps? The answer is the same as given before: the distribution of the plastic displacement which initiates the clumps after an inter-clump interval is needed, and a simple result similar to (2.25) for the distribution of the ALO maximum, conditional on the response being inside the elasticity limits half a period before outcrossing, cannot be derived by means of the amplitude model. Furthermore, when simulating the plastic increments, Eqs. (2.25) and (2.28) are not used for zero-level crossings, so the error due to the Karnopp-Scharton hypothesis is not severe.

Drift, $\tau_{\text{transients}}$ and Initiation of a Clump Following a Short Waiting Time

A few matters need attention before closing the discussion about the simulation of the transient waiting times. Phase drift is present in the response but it is omitted during clump simulations and short waiting time simulations. In case the waiting time becomes larger than $\tau_{\text{transients}}$, the waiting time is simulated from the exponential tail which is continuous. In that way a continuously distributed waiting time is generated. If, on the other hand, the waiting time is less than $\tau_{\text{transients}}$ then one can include phase drift approximately by adding to the already simulated waiting time a number simulated uniformly from the interval $[-\frac{\pi}{2}, \frac{\pi}{2}]$. In the waiting time simulations shown in this chapter the phase drift correction is omitted so that the steps in the distributions simulated by the procedure described in this chapter can be directly compared to the steps in the distributions obtained by direct time integration.

The time $\tau_{\text{transients}}$, which defines the length of the maximal short waiting time, must be assessed. The quantity $\tau_{\text{transients}}$ depends on the level u as well as the damping ratio α . The time $\tau_{\text{transients}}$ is smaller the higher the level u and bigger the smaller the damping ratio α . A rough estimate neglects the dependence on u and assumes that transients is passed when the influence of initial values is negligible. Usually the duration of transients is determined by assuming that the amplitude damping factor in free response $e^{-\alpha\tau}$ is small. Setting $e^{-\alpha\tau_{\text{transients}}} = 0.1$ may be a reasonable choice. Below (Sec. 3.2.2 p. 69) it is, however, shown that it is sufficient to set $e^{-\alpha\tau_{\text{transients}}} = 0.3$, i.e.,

$$\tau_{\text{transients}} = -\frac{\log(0.3)}{\alpha} \quad (3.12)$$

Initiating a clump following a short waiting time is carried out as follows. First a remark on technicalities: because the simulation of the first plastic increment in a clump includes a time increment π (see Tabs. 2.2 and 2.3) one must subtract π from the simulated waiting time. During the waiting time simulation one keeps in each step track of whether a minimum or a maximum is simulated. Thus, when entering a clump after a short waiting time it is known whether the load is reversed or reloading is taking place. To understand why this is done regard first long waiting times. After a long waiting time stationarity is reached and the phase has drifted so much that outcrossings occur uniformly spread in time – regardless of whether the outcrossing is an up- or downcrossing. Thus it is equally probable that the outcrossing (of a symmetric domain) is due to a maximum or a minimum. On the other hand, for short waiting times the phase drift has not yet had a significant effect why crossings happen at almost discrete points in time. Therefore, for a given short waiting time the outcrossing is either with probability 1 due to a maximum or with probability 1 due to a minimum. In table 3.2 the waiting time simulation procedure is recapitulated in pseudo code.

3.2.2 Simulating the Exponential Upper Tail

Simulating outcomes of the exponential upper tail is very easy when one knows the stationary crossing rate $\lambda = \lambda(u, \alpha)$. Even though the waiting time distribution is only partially exponential the well-known lack of memory property of the exponential distribution is still valid for waiting times beyond $\tau_{\text{transients}}$. This follows from the computation below in which $\tau > \tau_{\text{transients}}$:

$$\begin{aligned} P(T > \tau | T > \tau_{\text{transients}}) &= \frac{P(T > \tau \wedge T > \tau_{\text{transients}})}{P(T > \tau_{\text{transients}})} \\ &= \frac{P(T > \tau, \tau > \tau_{\text{transients}})}{P(T > \tau_{\text{transients}})} \\ &= \frac{(1 - G(\tau_{\text{transients}})) e^{-\lambda(\tau - \tau_{\text{transients}})}}{1 - G(\tau_{\text{transients}})} \\ &= e^{-\lambda(\tau - \tau_{\text{transients}})}, \quad \tau > \tau_{\text{transients}} \end{aligned} \quad (3.13)$$

So, if the simulation of the transient tail shows that a waiting time beyond $\tau_{\text{transients}}$ should be simulated, then one simulates an additional waiting time $\delta\tau$ from the exponential distribution with parameter λ and adds it to $\tau_{\text{transients}}$. Thus the purpose of the simulation of the short waiting times is twofold: approximate the step-like distribution of the short waiting times and ensure that the fraction of long waiting times simulated is correct.

For the mean crossing rate λ one cannot use the mean crossing rate of the Cramér-Leadbetter envelope corrected with respect to the fraction of empty envelope upcrossings (see e.g. [6]). This crossing rate is too high because it is the mean crossing rate of all outcrossings including those that appear during transients. As argued above it is only the outcrossings corresponding to the long waiting times between clumps of clumps that are approximately independent and it is the mean rate of these crossings that is needed. Or in other words: it is the intensity of the arrivals of clumps of clumps that is the parameter to use in the exponential distribution which approximates the upper tail. This intensity is computed as the mean crossing rate conditional on the event that the waiting time is larger than $\tau_{\text{transients}}$, i.e., the event that no outcrossings have appeared in the time interval of length $\tau_{\text{transients}}$ before the outcrossing. By this conditioning the appropriate thinning of the arrivals of outcrossings is obtained as it is ensured that the distance to the previous crossing is at least $\tau_{\text{transients}}$. The intensity λ may be evaluated for different values of $\tau_{\text{transients}}$. It is the lowest value of $\tau_{\text{transients}}$ for which λ becomes stationary that defines $\tau_{\text{transients}}$. Clearly a stationary value of λ does not exist in a strict sense as increasing $\tau_{\text{transients}}$ always makes the conditional crossings become less and less dependent on each other, so for increasing values of $\tau_{\text{transients}}$ the intensity λ decreases. However, after a certain point, λ becomes practically stationary as it decreases only slowly after this point. It is so, because in the correlation structure of the response, and consequently in the correlation structure of the amplitude, the dominating factor is $e^{-\alpha\tau}$ which goes to zero relatively fast.

Computing the Conditional Mean Crossing Rate

The computation of λ as the conditional mean crossing rate is not a small, simple task. The amplitude model (3.10), used for the simulation of the transient tail, was seen in Fig. 3.6 to perform well for large waiting times too. Therefore a numerical approach based on the amplitude model is proposed here. This implies that waiting times are discretized to integer multiples of π and therefore some care has to be taken when computing the conditional crossing rate. To understand this consider $-\log(1 - F_T(\tau))$. Define the quantities $\tau_i = i\pi, i = 0, 1, 2, \dots$ and $P_i = P\{T \leq \tau_i\} = F_T(\tau_i)$. Then

$$\lambda_i = \frac{-\log(1 - P_{i+1}) + \log(1 - P_i)}{\pi} \quad (3.14)$$

is an approximation to λ . Rearranging terms and introducing $\Delta P_i = P_{i+1} - P_i$ leads to

$$\lambda_i = -\frac{1}{\pi} \log \left(1 - \frac{\Delta P_i}{1 - P_i} \right) \quad (3.15)$$

Since ΔP_i is the probability of having an outcrossing in the interval $]\tau_i, \tau_{i+1}]$ and no outcrossings in the interval $[0, \tau_i]$, and $1 - P_i$ is the probability of having no outcrossings in the interval $[0, \tau_i]$ the ratio $\frac{\Delta P_i}{1 - P_i}$ is the conditional probability of an outcrossing in the interval $]\tau_i, \tau_{i+1}]$ given no outcrossings before that interval. In the limit, when this ratio goes to zero, one finds

$$\lambda_i \approx \frac{1}{\pi} \frac{\Delta P_i}{1 - P_i} \quad (3.16)$$

as an approximation to the conditional crossing rate. So, except for the presence of the logarithm in Eq. (3.15), the computation of λ_i is basically a computation of the conditional crossing rate of the amplitude model. The logarithm is necessary in order to compensate for the discretization.

Denoting by $f_A(a|A_{-\pi} = a_0)$ the conditional density of A given the amplitude $A_{-\pi}$ half a period before, the probability P_i is given by the convolution

$$1 - P_i = \frac{\int_0^u \left[\cdots \int_0^u \left[\int_0^u f_A(a_i|A_{-\pi} = a_{i-1}) da_i \right] f_A(a_{i-1}|A_{-\pi} = a_{i-2}) da_{i-1} \cdots \right] f_A(a_1|A_{-\pi} = u) da_1}{\int_0^u f_A(a_1|A_{-\pi} = u) da_1} \quad (3.17)$$

The denominator is a normalization constant which gives the probability of not having an outcrossing at time π . The outcrossing at time π is excluded since waiting times equal $2\pi, 3\pi, \dots$. It follows from (3.10) that the conditional distribution $F_A(a|A_{-\pi} = a_0)$ is given by

$$\begin{aligned} F_A(a|A_{-\pi} = a_0) &= P((a_0\mu + \sigma\Psi_X)^2 + (\sigma\Psi_X)^2 \leq a^2) \\ &= P(\sigma^2\Psi_X^2 \leq a^2 - (a_0\mu + \sigma\Psi_X)^2) \\ &= \int_{(-a-a_0\mu)/\sigma}^{(a-a_0\mu)/\sigma} \left[1 - 2\Phi\left(-\frac{1}{\sigma} \sqrt{a^2 - (a_0\mu + \sigma\Psi_X)^2}\right) \right] \varphi(\psi_X) d\psi_X \\ &= \Phi\left(\frac{a-a_0\mu}{\sigma}\right) - \Phi\left(\frac{-a-a_0\mu}{\sigma}\right) \\ &\quad - 2 \int_{(-a-a_0\mu)/\sigma}^{(a-a_0\mu)/\sigma} \Phi\left(-\frac{1}{\sigma} \sqrt{a^2 - (a_0\mu + \sigma\Psi_X)^2}\right) \varphi(\psi_X) d\psi_X \end{aligned} \quad (3.18)$$

From formulas (3.17) and (3.18) it is clear that the probability P_i cannot be computed analytically. Some numerical approach is required. The convolutions in Eq. (3.17) follow from the Markov property of the amplitude model. So, instead of conducting numerical integration, an approximate propagation in time of the distribution of the amplitude is applied. It is done in the following way. The amplitude is given a discrete representation. Since one needs the distribution of the amplitude only over the interval $[0, u]$, the amplitude is discretized in terms of n states $z_i = ih, i = 1, \dots, n$ where $h = u/n$. Therefore, in order to propagate the amplitude distribution

in time, only a finite number of transition probabilities are needed. Using the continuous conditional distribution function $F_A(a|A_{-\pi} = a_0)$ the transition probability p_{ij} of going from state z_j to state z_i is approximated by

$$p_{ij} = \begin{cases} F_A(\frac{3}{2}h|A_{-\pi} = z_j) & \text{for } i = 1 \\ F_A((i + \frac{1}{2})h|A_{-\pi} = z_j) - F_A((i - \frac{1}{2})h|A_{-\pi} = z_j) & \text{for } 1 < i < n \\ F_A(nh|A_{-\pi} = z_j) - F_A((n - \frac{1}{2})h|A_{-\pi} = z_j) & \text{for } i = n \end{cases} \quad (3.19)$$

To initiate the computation of the propagation of the density, the initial distribution of the amplitude is needed. Since the oscillator starts at rest at the yield limit, the initial distribution is

$$\begin{bmatrix} p_1(\tau_0) \\ \vdots \\ p_{n-1}(\tau_0) \\ p_n(\tau_0) \end{bmatrix} = \begin{bmatrix} 0 \\ \vdots \\ 0 \\ 1 \end{bmatrix} \quad (3.20)$$

Recalling that in Eq. (3.17) a normalization is included to compensate for those outcrossings that occur before time τ_2 , it is clear that the first step in the propagation of the density leads to the following amplitude distribution

$$\begin{bmatrix} p_1(\tau_1) \\ \vdots \\ p_n(\tau_1) \end{bmatrix} = \frac{1}{\sum_{i=1}^{n-1} p_{in} + p_{nn}} \begin{bmatrix} p_{1n} \\ \vdots \\ p_{nn} \end{bmatrix} \quad (3.21)$$

After this first step the distribution $p_i(\tau_k)$ in step k is obtained by

$$p_i(\tau_k) = \sum_{j=1}^n p_{ij} p_j(\tau_{k-1}) \quad (3.22)$$

Knowing the approximate density of the amplitude, an approximation to the probability ΔP_k of having an outcrossing in the interval $[\tau_k, \tau_{k+1}]$ and no outcrossing in the interval $[0, \tau_k]$ is computed by

$$\Delta P_k = \sum_{j=1}^n \varepsilon_j p_j(\tau_k) \quad , \quad \varepsilon_j = 1 - \sum_{i=1}^n p_{ij} \quad (3.23)$$

and the probability $1 - P_k$ of no outcrossings in the interval $[0, \tau_k]$ is computed by

$$1 - P_k = \sum_{i=1}^n p_i(\tau_k) \quad (3.24)$$

It is finally noted that the above numerical scheme corresponds to solving the Fokker-Planck equation for the amplitude process with an absorbing boundary at $A = u$. Clearly non-symmetrized yield levels would lead to a non-stationary absorbing boundary complicating the picture

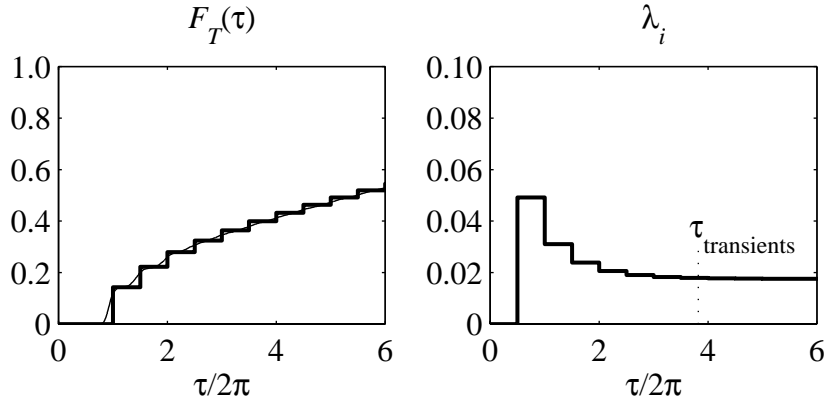


Figure 3.8: A transient lower tail and the corresponding approximate conditional mean crossing rate obtained by propagation of the amplitude distribution (thick curves). The left plot also shows the distribution obtained by direct simulation (thin curve). Parameters are: $u = 2$ and $\zeta = 0.05$

considerably. This is the main reason why the notion of the symmetrized yield level is so advantageous.

As an illustration of the results obtained by the propagation of the discretized amplitude density Fig. 3.8, shows the transient lower tail and the corresponding approximate intensity λ_i for the case $u = 2$ and $\zeta = 0.05$. In the left plot the distribution obtained by direct simulation is depicted for comparison. The good performance of the amplitude model is observed again. The time $\tau_{\text{transients}} = -\frac{\log(0.3)}{\alpha}$ is shown in the right plot, and it is clear that this is a good approximation to the time when stationarity is reached. Investigating other combinations of u and ζ shows that $\tau_{\text{transients}} = -\frac{\log(0.3)}{\alpha}$ is generally a good approximation to the time when transients end.

The computation of the conditional mean crossing rate by the propagation of the discretized amplitude density is quite expensive for low damping ratios and high yield levels as in those cases a rather dense discretization z_i is required. Therefore, computing the mean crossing rate for each simulation of long waiting times is not a reasonable way to go if one wants to save time. In stead one may resort to interpolation between the mean crossing rates shown in Table 3.1 (p. 70) and obtained by the above described numerical method. Before conducting the interpolating it is fruitful to plot $\log \lambda$ against u for given ζ . One then obtains the left plot in Fig. 3.9 (p. 71) showing almost straight lines. If next one plots $\log \lambda$ against $\log \zeta$ the plot to the right is obtained. This plot also exhibits almost straight lines. Thus, conducting linear interpolation in these plots is much more reasonable than conducting linear interpolating directly between the values in Table 3.1. Finding $\lambda(u, \zeta)$ may be done in many different ways. In the implementation used here one first interpolates $\log \lambda$ with respect to $\log \zeta$ in the right plot and then, according to the left plot, one interpolates with respect to u .

	ζ				
	0.001	0.005	0.01	0.02	0.05
u	0.5	$1.75 \cdot 10^{-2}$	$7.52 \cdot 10^{-2}$	$1.27 \cdot 10^{-1}$	$2.08 \cdot 10^{-1}$
	1.0	$4.35 \cdot 10^{-3}$	$1.91 \cdot 10^{-2}$	$3.47 \cdot 10^{-2}$	$6.07 \cdot 10^{-2}$
	1.5	$1.55 \cdot 10^{-3}$	$6.94 \cdot 10^{-3}$	$1.28 \cdot 10^{-2}$	$2.28 \cdot 10^{-2}$
	2.0	$6.05 \cdot 10^{-4}$	$2.71 \cdot 10^{-3}$	$4.99 \cdot 10^{-3}$	$8.89 \cdot 10^{-3}$
	2.5	$2.26 \cdot 10^{-4}$	$1.00 \cdot 10^{-3}$	$1.83 \cdot 10^{-3}$	$3.21 \cdot 10^{-3}$
	3.0	$7.36 \cdot 10^{-5}$	$3.19 \cdot 10^{-4}$	$5.74 \cdot 10^{-4}$	$9.85 \cdot 10^{-4}$
	3.5	$1.94 \cdot 10^{-5}$	$8.19 \cdot 10^{-5}$	$1.44 \cdot 10^{-4}$	$2.40 \cdot 10^{-4}$
	4.0	$3.96 \cdot 10^{-6}$	$1.61 \cdot 10^{-5}$	$2.77 \cdot 10^{-5}$	$4.48 \cdot 10^{-5}$

Table 3.1: Conditional mean crossing rates.

Two comments to the above are appropriate. First it is noted, that the very simple shape of the plots in Fig. 3.9 indicates that there might be a simple relation between λ and u, ζ . According to the right plot one may conjecture that

$$\lambda(u, \zeta) = \zeta^a e^{b(u)} \quad (3.25)$$

and from the left plot one may conjecture that

$$b(u) = -cu + d \quad (3.26)$$

all together leading to the possible approximation

$$\lambda(u, \zeta) = k\zeta^a e^{-cu} \quad (3.27)$$

However, though the curves in Fig. 3.9 are almost straight, they are too curved to allow such an approximation to be used as an alternative to linear interpolation in Fig. 3.9. The second comment concerns the computation of λ . It was mentioned that a satisfactory value of $\tau_{\text{transients}}$ is $-\frac{\log(0.3)}{\alpha}$. This is true as long as one considers the simulation of the long waiting times. When evaluating the conditional mean crossing rates for high yield levels and low damping ratios one has to propagate the amplitude distribution longer in time than $-\frac{\log(0.3)}{\alpha}$, as it takes longer time before satisfactory stationary values of λ are obtained. E.g. for $u = 4, \zeta = 0.01$ propagation was continued until $-\frac{\log(0.001)}{\alpha}$ (which was plentifully). The time $\tau_{\text{transients}} = -\frac{\log(0.3)}{\alpha}$ is, however, applicable for the simulations as the deviation of the waiting time distribution from the exponential distribution is sufficiently small for waiting times larger than $-\frac{\log(0.3)}{\alpha}$.

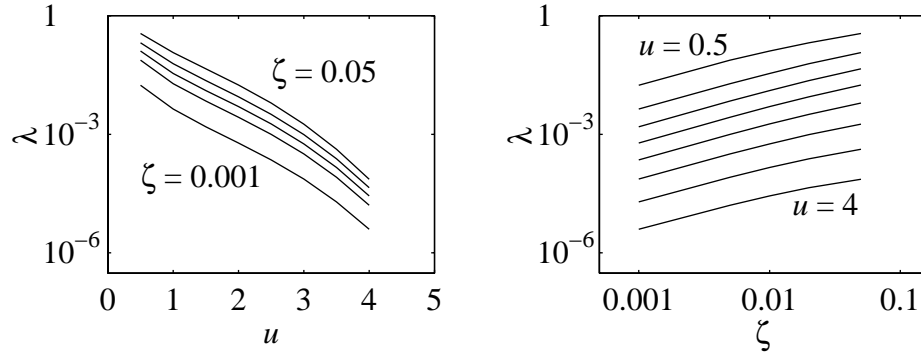


Figure 3.9: To the left: semi-log plot of λ against u for given ζ 's. To the right: log-log plot of λ plotted against ζ for given u 's.

Some Simulation Results

At the end of this section a few simulation results obtained by merging the two simulation procedures for the transient lower tail and the exponential upper tail are shown in Fig. 3.10 (p. 72). There is not much to add to what has already been said, except that the combination of the simulation of the lower and the upper tail works fine together. The figure shows other combinations of parameters than those that appear in the previous figures. Especially attention is drawn to the plot for $u = 1, \zeta = 0.05$ and $u = 0.5, \zeta = 0.01$. Unlike the Slepian Model simulations used for the clumps giving errors for such low levels, there are no errors in the waiting time simulations (except for the discretization error in the transient tail). In accordance with the discussion in connection to Figs. 3.6 and 3.7 a slight underestimation is observed in the plots in the lower row.

Initiation of a Clump Following a Long Waiting Time

As explained at the end of Sec. 3.2.1 an outcrossing after a long waiting time is with equal probability due to a maximum or a minimum. Therefore the simulation of a long waiting time is ended by deciding uniformly randomly whether the first extreme of the following clump is a maximum or a minimum.

Closing Remark

Due to the definition of the symmetrized yield limit the last excursion in a clump may not give a plastic displacement increment, i.e., it is an empty excursion (see page 26). If so, the last extreme in the clump is above u_{sym} , and therefore the EPO possesses more mechanical energy when it leaves the clump than if the last extreme had been a genuine excursion. On the average larger mechanical energy implies shorter waiting times than those obtained by the algorithm

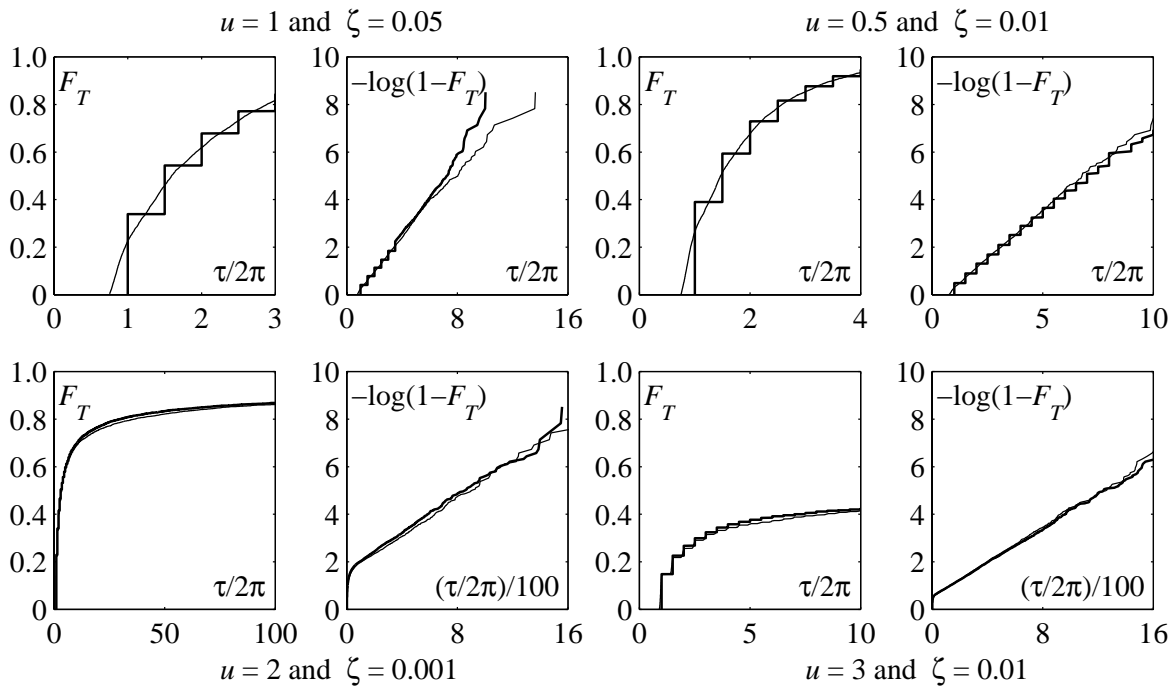


Figure 3.10: Simulation of the waiting time distribution according to table 3.2 (thick curves) and by direct simulation (thin curves). 5000 samples were conducted. Parameters are given at the plots.

described in this chapter. However, the extreme corresponding to the empty excursion cannot be much above u_{sym} , because otherwise it is unlikely that the clump would end after that extreme. Thus the energy in the EPO after an empty excursion is on the average not much higher than if the excursion had been genuine. Consequently it is reasonable to use the waiting time simulation procedure presented here also in case the clump ends with an empty excursion. A compensation for the error is obtained by setting $M_0 = M_{term}$ (see Fig. 3.3), where M_{term} is the ALO extreme which terminates the clump simulation. The full waiting time simulation algorithm is in Table 3.2 recapitulated in pseudo code.

3.3 Summary

In continuation of the previous chapter the present chapter deals with the waiting time between clumps of plastic displacements. As the clumps arrive in groups, that is, as clumps of clumps, it is natural to distinguish between, on the one hand the short waiting times from one clump to the next clump inside a clump of clumps, and on the other hand the long waiting times from one clump of clumps to the next. The short waiting times are due to the transient response right after clump termination. Therefore the lower tail of the waiting time distribution is named the transient lower tail. The long waiting times are so large that the arrivals of the clumps

Put $M_0 = M_{\text{term}}$ (see Tab. 2.4 p. 44) and increment time by half a period.

DO simulation of short waiting time

 Simulate M_i from M_{i-1} by use of the amplitude model (3.11).

 Increment time τ by half a period.

IF $M_i > u_{\text{sym}}$

 Introduce phase drift by adding U simulated uniformly from $[-\frac{\pi}{2}, \frac{\pi}{2}]$.

 Subtract π (in accordance with Tabs. 2.2 and 2.3 pp. 42 and 43).

STOP simulation.

ENDIF

WHILE $\tau < \tau_{\text{transients}}$

IF simulation of long waiting time

 Assess conditional mean crossing rate λ by interpolation in Fig. 3.9.

 Simulate additional waiting time $\delta\tau$ with distribution $1 - e^{-\lambda \delta\tau}$.

 Add $\delta\tau$ to $\tau_{\text{transients}}$ exploiting the lack of memory property.

 Decide uniformly randomly whether first extreme in next clump is a min. or a max.

 Subtract π (in accordance with Tabs. 2.2 and 2.3 pp. 42 and 43).

ENDIF

Table 3.2: Simulation of waiting times.

of clumps are approximately independent. Consequently they obey approximately the Poisson model, and therefore the long waiting times become approximately exponentially distributed. For that reason the upper tail of the waiting time distribution is called the exponential upper tail.

An analytical expression for the transient lower tail does not exist. In stead the amplitude process is simulated using time steps of half a natural period of the oscillator. If an outcrossing of this discretized amplitude process is detected before a certain time $\tau_{\text{transients}}$, a short waiting time is simulated. Otherwise a long waiting time should be simulated as explained in the next paragraph. The amplitude process defined by $A^2 = X^2 + \dot{X}^2/\lambda_2$ is discretized by use of the linear regression of (X, \dot{X}) on the response state half a period before plus their corresponding residual processes. This gives an amplitude model based on a pair of Slepian models for X and \dot{X} . It turns out that a very good agreement with simulation results obtained by direct time integration is reached. An alternative to the simulation of the amplitude would be the simulation of the extremes by use of the conditional distribution $F_M(m | X(-\pi) = -M_{i-1})$ (formula (2.28)) for crossings of the zero-level. However, this gives a considerable underestimation of the waiting times due to the neglected driving force after the zero-level crossing.

As mentioned the long waiting times are approximately exponentially distributed. The assessment of the parameter of this distribution is simplified if one considers symmetric yield levels. The symmetrized yield level is defined by $u_{sym} = \min(u^+, u^-)$. As shown in Chapter 2 this does not induce any limitations to the simulation of the clumps and it is therefore an acceptable approach. Due to the exponential distribution of the long waiting times it is possible to show that the lack of memory property, typical of the exponential distribution, carry over to the exponential upper tail. Thus a long waiting time is obtained by simulating an additional waiting time $\delta\tau$ from an exponential distribution with some parameter λ and adding it to $\tau_{transients}$. The parameter λ gives the intensity of arrivals of clumps of clumps which is obtained by a thinning of the arrivals of all crossings. Thus λ is not the mean crossing rate of the response out of $[-u_{sym}; u_{sym}]$, as that will include all crossings. The intensity λ is instead the mean crossing rate conditional on the event that the waiting time is larger than $\tau_{transients}$. Such a conditional crossing rate may be computed using the discretized amplitude process. Since this is a computationally expensive procedure a table of crossing rates are computed and the crossing rate λ is then obtained by non-linear interpolation in this table.

Finally it is mentioned that the time $\tau_{transients}$ is naturally linked to the correlation structure of the response which in turn reflects the time change rate of amplitude fade in free damped response. It turns out that satisfactory results are obtained if $\tau_{transients}$ is determined from the formula

$$\tau_{transients} = -\frac{\log(0.3)}{\alpha}. \quad (3.12)$$

Chapter 4

Simulation by Direct Numerical Time Integration

Inevitably this chapter is somewhat technical. However, the subject of the chapter is too important to be expelled to an appendix. It provides the documentation of the verification method used in testing the results of the Slepian Model Simulation Method with respect to accuracy and time consumption. The Slepian Simulation Method is faster than those from the traditional class of simulation methods to which the verification method belongs. A detailed discussion of the verification method thus gives a firm basis for the judgement of the time gain obtained by use of the Slepian simulation method.

Clearly only approximate means of verification of the semi analytical Slepian Model simulation method can be found. As in so many other cases a fully numerical method is just such an approximate tool which in principle can produce arbitrarily accurate results by letting certain parameters come close to given limit values. The Slepian Simulation Method itself is a Monte Carlo Method. In general one sample is insufficient to obtain the stochastic properties of the response. Likewise the validation method consists in simulating, over and over again, outcomes of the response by the more accurate simulation method followed by an ensemble average computation.

Details and approximations of the numerical method employed to obtain the individual response samples are discussed here. Basically the method is an approximate direct time integration method using finite time-steps. For that reason mainly two approximations occur in the algorithm: band width approximation of the white noise process and time integration errors due only to the discretized representation of the state variables. It turns out, however, that the latter approximation may be significantly reduced.

For easy reference the scaled equation of motion of the SDOF oscillator is repeated here:

$$\ddot{X} + 2\alpha\dot{X} + (1 + \alpha^2)r(X) = W(\tau). \quad (1.13)$$

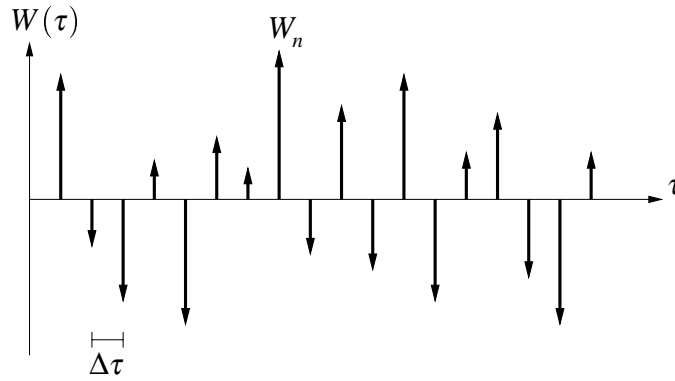


Figure 4.1: Schematic of the discretized sequence that simulates the white noise process.

4.1 White Noise Approximation

Due to the infinite variance characteristic of the white noise process, it is impossible to simulate exact white noise. There exists, however, different ways of simulating approximations to white noise. Common to all of these simulation schemes is that they cannot reproduce the constant power spectrum which characterizes white noise. Often they give a power spectrum that is almost flat in the lower frequency-range, the extent of which typically depends on the time-step size used in the – in the one way or the other – discretized representation of the white noise. It is not a big problem that the spectrum is only approximately constant in a finite frequency range, because the white noise is a driving process that is filtered by the mechanical system it drives. In engineering problems like those considered in the present work it is the response of the mechanical system that is in focus – not the white noise process itself. The measure of applicability of the white noise representation then becomes a question of how well the response of the mechanical system is reproduced. Generally it may be stated that for reasonable time-steps any simulation scheme produces an acceptable response of the mechanical system. Thus the choice of simulation scheme is not very crucial, though not completely trivial. In any case it should be proven that the chosen scheme implies a satisfactory response of the mechanical system under consideration.

Here a simulation scheme which is inspired by one of the physical phenomena that led to the introduction of white noise processes in physics is chosen. Brownian motion is the motion that particles subjected to pulses occurring infinitely close in time experiences. This phenomenon was the first that led to the definition of white noise. One cannot simulate pulses occurring infinitely close in time. Instead the continuous white noise process is approximated by pulses separated in time by $\Delta\tau$. This clearly implies a scaling of the pulses so that the approximating process feeds the same energy into the EPO as the real white noise process does. As it will be shown in the following the two advantages of the chosen white noise approximation are: time integration is exact for linear response and the error at the dominating resonant frequency is almost vanishing.

Figure 4.1 shows a schematic of the discretized sequence of pulses. Denoting by W_n the impulse transferred by the pulse occurring at time $\tau_n = n\Delta\tau$, the load term $W(\tau)$ in Eq. (1.13) reads

$$W(\tau) = \sum_{n=0}^{\infty} W_n \delta(\tau - \tau_n) \quad (4.1)$$

4.2 Time Integration

The choice of white noise approximation induces a straightforward numerical scheme by which an approximate integral of the equation of motion is obtained. As the pulses are applied at time distances $\Delta\tau$ the integral is computed using a time-stepping algorithm that steps ahead in time using steps of length $\Delta\tau$.

The following discussion distinguishes between time-stepping through linear states and through non-linear states. The reason is that the linearity of the equation of motion at linear states may be exploited so that the computational costs and approximations of the more generally applicable time-stepping procedure used at non-linear states are avoided. It is worthwhile putting focus on minimizing computational expenses and inaccuracies at linear states since these states in the majority of the cases studied in this work dominate the response. Also this effort provides a fair background for the comparison of the simulation time consumption of the Slepian Simulation Method and the direct numerical time integration scheme presented here.

4.2.1 Linear States: Exact Time-Stepping

What we are after is a time-stepping formula that relates the state at time $\tau_n = n\Delta\tau$ to the state at time τ_{n-1} a time-step $\Delta\tau$ earlier. Recalling that at linear states the oscillator behaves like a linear oscillator with the current plastic displacement X_p as equilibrium position, it follows that the state of the dynamic system is fully defined by the relative displacement $X^* = X - X_p$, the velocity $\dot{X}^* = \dot{X}$ and X_p . The plastic displacement is constant why we are only in need of a time-stepping formula describing the development of the random relative state vector

$$\mathbf{X}^* = \begin{bmatrix} X^* \\ \dot{X}^* \end{bmatrix} \quad (4.2)$$

The wanted formula is derived from the linearized form of the governing equation (1.13) which is restated in terms of the relative displacement X^* . For the free response between two pulses the equation of motion becomes

$$\ddot{X}^* + 2\alpha\dot{X}^* + (1 + \alpha^2)X^* = 0 \quad (4.3)$$

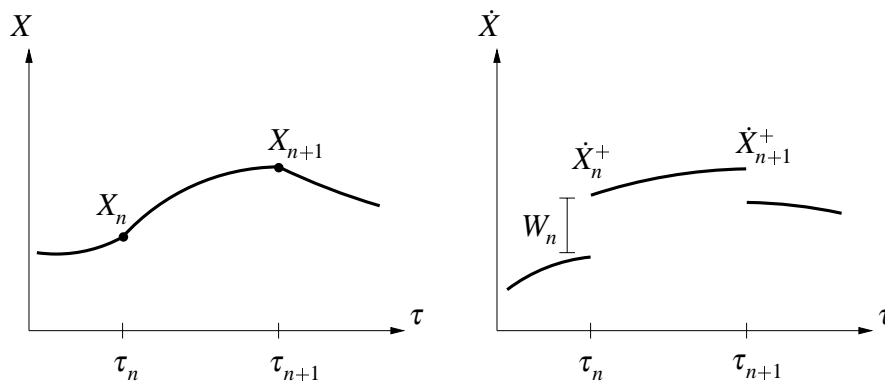


Figure 4.2: Schematic of displacement and velocity.

If \dot{X}_n^{*+} denotes the velocity right after the n 'th pulse while \dot{X}_{n+1}^{*-} denotes the velocity just before the $n+1$ 'th pulse (see Fig. 4.2) the exact definite integral of (4.3) is given by

$$X_{n+1}^* = X_n^* e^{-\alpha\Delta\tau} (\cos\Delta\tau + \alpha\sin\Delta\tau) + \dot{X}_n^{*+} e^{-\alpha\Delta\tau} \sin\Delta\tau \quad (4.4)$$

$$\dot{X}_{n+1}^{*-} = -X_n^* (1 + \alpha^2) e^{-\alpha\Delta\tau} \sin\Delta\tau + \dot{X}_n^{*+} e^{-\alpha\Delta\tau} (\cos\Delta\tau - \alpha\sin\Delta\tau) \quad (4.5)$$

In order to have a compact notation for the time-stepping formula the random vector \mathbf{Y}_n and the state transition matrix \mathbf{A} are defined by

$$\mathbf{Y}_n = \begin{bmatrix} X_n^* \\ \dot{X}_n^{*+} \end{bmatrix}, \quad \mathbf{A} = e^{-\alpha\Delta\tau} \begin{bmatrix} \cos\Delta\tau + \alpha\sin\Delta\tau & \sin\Delta\tau \\ -(1 + \alpha^2)\sin\Delta\tau & \cos\Delta\tau - \alpha\sin\Delta\tau \end{bmatrix} \quad (4.6)$$

leading to the formula

$$\mathbf{Y}_{n+1} = \mathbf{A}\mathbf{Y}_n + \mathbf{Z}_{n+1} \quad (4.7)$$

where the matrix \mathbf{A} accounts for the free response and

$$\mathbf{Z}_n = \begin{bmatrix} 0 \\ W_n \end{bmatrix} \quad (4.8)$$

is a random vector that gives the change in velocity due to the random pulse, of impulse W_n , at time τ_n . By (4.7) the wanted formula is reached.

The time-stepping formula (4.7) obtained by exact time integration has two advantages in comparison to the procedure presented in the following subsection. The evaluation of the time-stepping formula is fast once the matrix \mathbf{A} is computed, that is, it is sufficiently simple to allow direct implementation. Secondly the time-stepping does not introduce any further time discretization approximations in addition to that due to the white noise approximation. Hence the name *exact time-stepping*. The discussion of choice of time-step and the assessment of the variance of the intensity W_n of the pulses in dependence of the time-step is postponed till later.

4.2.2 Non-Linear States: Approximate Time-Stepping

At non-linear states the equation of motion does not in general reduce to a simple form that is solvable by analytical means. Therefore in contrast to the previous section we now put up a time-step *procedure* rather than a time-step formula. Essentially two things are done. As state variables are computed only at discrete instances in time, approximate formulas are used to link the acceleration to the position and velocity at these time instances. Further the resulting equation of motion is solved approximately numerically. The simple, yet effective, Newmark algorithm commonly used in structural dynamics is applied here. In the light of the present setting of a pulse load the implementation of the Newmark algorithm is shortly reviewed. The Newmark rule approximates the integrals in the Taylor expansions of velocity and position over a single time-step. The expansions are

$$\dot{X}(\tau_{n+1}) = \dot{X}(\tau_n) + \int_{\tau_n}^{\tau_{n+1}} \ddot{X}(\tau) d\tau \quad (4.9)$$

$$X(\tau_{n+1}) = X(\tau_n) + \Delta\tau \dot{X}(\tau_n) + \int_{\tau_n}^{\tau_{n+1}} (\tau_{n+1} - \tau) \ddot{X}(\tau) d\tau \quad (4.10)$$

The way of approximation is by use of appropriate weighted averages of the accelerations at the interval end-points [14, pp. 374]. The notation introduced in the previous section using + and - superscripts denoting states just before and right after a pulse is adopted here too (see Fig. 4.2). Following [14] the approximation formulas read

$$X_{n+1} = X_n + \Delta\tau \dot{X}_n^+ + \left(\frac{1}{2} - \beta\right) \Delta\tau^2 \ddot{X}_n^+ + \beta \Delta\tau^2 \ddot{X}_{n+1}^- \quad (4.11)$$

$$\dot{X}_{n+1}^- = \dot{X}_n^+ + (1 - \gamma) \Delta\tau \ddot{X}_n^+ + \gamma \Delta\tau \ddot{X}_{n+1}^- \quad (4.12)$$

When the weight parameters γ and β are assigned specific values the formulas give a discretized relation between the positions, velocities and accelerations at the interval end-points. To complete the time discretization scheme it lacks to choose a point in time at which the equation of motion should be satisfied. In the straightforward implementation of the Newmark algorithm employed herein this point is chosen identical to the interval end-point τ_{n+1} – just before the pulse. Substituting Eqs. (4.12) and (4.11) into the equation of motion gives

$$\begin{aligned} & \ddot{X}_{n+1}^- + 2\alpha (\dot{X}_n^+ + (1 - \gamma) \Delta\tau \ddot{X}_n^+ + \gamma \Delta\tau \ddot{X}_{n+1}^-) \\ & + (1 + \alpha^2) r (X_n + \Delta\tau \dot{X}_n^+ + \left(\frac{1}{2} - \beta\right) \Delta\tau^2 \ddot{X}_n^+ + \beta \Delta\tau^2 \ddot{X}_{n+1}^-) = 0 \end{aligned} \quad (4.13)$$

This equation in \ddot{X}_{n+1}^- can be cast in a more compact and computational useful form in terms of the acceleration increment $\Delta\ddot{X}_n = \ddot{X}_{n+1}^- - \ddot{X}_n^+$. If one introduces the so-called position and velocity predictors

$$X_{n+1}^{\text{pre}} = X_n + \Delta\tau \dot{X}_n^+ + \frac{1}{2} \Delta\tau^2 \ddot{X}_n^+ \quad (4.14)$$

$$\dot{X}_{n+1}^{\text{pre}} = \dot{X}_n^+ + \Delta\tau \ddot{X}_n^+ \quad (4.15)$$

the equation for the acceleration increment reads

$$(1 + 2\alpha\gamma\Delta\tau)\Delta\ddot{X}_n + \ddot{X}_n^+ + 2\alpha\dot{X}_{n+1}^{\text{pre}} + (1 + \alpha^2)r(X_{n+1}^{\text{pre}} + \beta\Delta\tau^2\Delta\ddot{X}_n) = 0 \quad (4.16)$$

Assuming that this equation is solved the next set of state variables are determined by the so-called corrector step. This step accounts for the difference between the predictors and the approximation formulas Eqs. (4.12) and (4.11). The pulse, that has not yet appeared in the above equations, is included in the corrector step too. The corrections become

$$X_{n+1} = X_{n+1}^{\text{pre}} + \beta\Delta\tau^2\Delta\ddot{X}_n \quad (4.17)$$

$$\dot{X}_{n+1}^+ = \dot{X}_{n+1}^{\text{pre}} + \gamma\Delta\tau\Delta\ddot{X}_n + W_n \quad (4.18)$$

$$\ddot{X}_{n+1}^+ = -2\alpha\dot{X}_{n+1}^+ - (1 + \alpha^2)r(X_{n+1}) \quad (4.19)$$

To end the presentation of the implementation of the Newmark algorithm the choice of the weight parameters β and γ is discussed. They are set to $\gamma = \frac{1}{2}$ and $\beta = \frac{1}{4}$ rendering the well-known average acceleration scheme that is unconditionally stable for linear systems. The system considered here is only moderately non-linear why it is assumed that one should not encounter stability problems. It is noted that stability problems have not been detected.

To avoid confusion in the survey given above on the Newmark implementation, the question about solving equation (4.16) for the acceleration increment was skipped. The method of solution requires a few remarks. Since the equation is non-linear it is solved approximately iteratively by use of the modified Newton-Raphson scheme using the initial tangent slope

$$\hat{m} = 1 + 2\alpha\gamma\Delta\tau + (1 + \alpha^2)\dot{r}(X_{n+1}^{\text{pre}})\beta\Delta\tau^2 \quad (4.20)$$

throughout the entire iteration. The stop-criterion used to terminate the iterations is based on a relative measure of the change of the iterate. Iterations stop when change of the iterate relative to the iterate itself is less than 10^{-4} . This is adequate as the time-steps are so short that the first iterate is generally quite close to the exact solution. Consequently only small successive corrections are needed. This also explains why the modified Newton-Raphson scheme is preferred to the full scheme. The slope \hat{m} changes only little during the iteration. Therefore, saving the unnecessary expense of recomputing \hat{m} in each iteration step fully compensates the slightly lower convergence rate of the modified scheme in the present context.

The main features of the described time-stepping procedure may be summarized as follows. On top of the white noise approximation error it introduces mainly an error because of the position and velocity approximations that prevent exact time integration. Minor errors are introduced by the approximate solution of the non-linear incremental equation of motion. Hence the term *approximate time-stepping*. The latter error is minimized by time costly iterations. For these reasons exact time-stepping is preferable to approximate time-stepping whenever applicable. Table 4.1 summarizes the steps of the implemented Newmark algorithm.

1) Prediction step:

$$\begin{aligned} X_{n+1}^{\text{pre}} &= X_n + \Delta\tau \dot{X}_n^+ + \frac{1}{2}\Delta\tau^2 \ddot{X}_n^+ \\ \dot{X}_{n+1}^{\text{pre}} &= \dot{X}_n^+ + \Delta\tau \ddot{X}_n^+ \end{aligned}$$

2) Compute acceleration increment $\Delta\ddot{X}_n$ by solving

$$(1 + 2\alpha\gamma\Delta\tau)\Delta\ddot{X}_n + \ddot{X}_n^+ + 2\alpha\dot{X}_{n+1}^{\text{pre}} + (1 + \alpha^2)r(X_{n+1}^{\text{pre}} + \beta\Delta\tau^2\Delta\ddot{X}_n) = 0$$

Apply modified Newton-Raphson with the tangent slope

$$\hat{m} = 1 + 2\alpha\gamma\Delta\tau + (1 + \alpha^2)\dot{r}(X_{n+1}^{\text{pre}})\beta\Delta\tau^2$$

3) Correction step:

$$\begin{aligned} X_{n+1} &= X_{n+1}^{\text{pre}} + \beta\Delta\tau^2\Delta\ddot{X}_n \\ \dot{X}_{n+1}^+ &= \dot{X}_{n+1}^{\text{pre}} + \gamma\Delta\tau\Delta\ddot{X}_n + W_n \\ \ddot{X}_{n+1}^+ &= -2\alpha\dot{X}_{n+1}^+ - (1 + \alpha^2)r(X_{n+1}) \end{aligned}$$

4) Return to 1) or stop.

Table 4.1: The present implementation of the Newmark algorithm.

4.3 Stochastic Properties of the Time-Stepping Process

Two aspects of the time-stepping procedure still need to be addressed. The one concerns the question of choosing the time-step size, and the other concerns the distribution of the load pulses. Both issues are important because the step size, as well as the pulse distribution, influence the stochastic properties of the response process simulated by the time-stepping algorithm. Due to the discretization this process is not identical to the real response process. The aim is to choose a suitably big time-step that will at the same time give reasonable simulation times and keep the difference, i.e. the error, between these two processes at an acceptably low level.

The comparison of the simulated process with the real response process must show how well the white noise process is approximated in a sense that reflects important features of the considered problem. There are two such features of which one is that white noise gives power input at all frequencies, and the other feature is the oscillatory characteristic of the mechanical system causing amplification of the power input at frequencies around the eigenfrequency. To test whether these features are satisfactorily represented in the simulated response or not, the simulation of a *linear* oscillator is considered. This is simply because, in the linear case analytical results for the power spectrum of the real stationary response and the simulated response process are obtainable. Reflecting the above mentioned features the spectrum of the real response

is smooth with a peak around the eigenfrequency. If the simulation scheme works properly its spectrum is smooth too and with an almost identical peak. If it is so, it is then assumed that the response of the EPO is satisfactorily reproduced also. This assumption is reasonable as, in consequence of the assumption about non-dominating hysteresis, the response of the EPO will deviate only little from the ALO response. Especially simulation of waiting times depends only on the simulation of linear response.

It is noted that, in recalling that the ALO response is Gaussian, it is clear that the spectrum, being the Fourier transform of the stationary correlation function, does not only reflect important features of the problem. It also becomes a direct measure of how close the distribution of the simulated response process is to the real response process.

4.3.1 Pulse Distribution

Choosing the distribution type of the pulses is straightforward as the white noise excitation is Gaussian resulting in a normally distributed response of the ALO. Thus the pulses must have Gaussian distribution too. Otherwise, even the simulation of the linear oscillator response would result in an only approximately normally distributed process. The mean of the pulses must be zero as any other choice would cause a shift of the mean response away from zero. Furthermore the pulses are uncorrelated. The only distribution parameter left is the variance σ_W^2 of the pulses. It can be qualitatively understood how σ_W must depend on the time-step size. Each pulse gives a change in velocity and thereby a change in kinetic energy causing a change in mechanical energy. Stationarity implies that the average energy input over time must be constant. Consequently the average energy input of each pulse must be proportional to the time-step length. As the average pulse energy input is proportional to σ_W^2 one concludes that $\sigma_W \propto \sqrt{\Delta\tau}$. In other words:

$$\sigma_W^2 = \text{Var}[\text{impulse}] = \text{Var}\left[\int_{\tau_n}^{\tau_{n+1}} W(\tau) d\tau\right] = I \Delta\tau \quad (4.21)$$

4.3.2 Power Spectrum

An approximate expression for the power spectrum of the simulated response process is obtained by deriving first the stationary correlation function of the simulated response. The following derivation is an extended and more direct version of the derivation given in [3, pp. 374–377]. The time-stepping formula (4.7), which is valid for the linear case, defines an autoregressive vector process that is clearly discrete. On the basis of this process solely the correlation between points separated in time by integer multiples of $\Delta\tau$ can be established. One needs, however, the correlation between points that are separated arbitrarily in time in order to compute the correlation function. Obtaining the simulated continuous process from the autoregressive process is easy, making the derivation of the correlation function from the correlation structure of the autoregressive process – as it will appear below – a simple task.

To see how the continuous response sample is related to the autoregressive process let, in accordance with the notation introduced above, \mathbf{Y}_n denote a state right after the application of a pulse. Free response follows and $\mathbf{A}\mathbf{Y}_n$ is then the response just before the next pulse. Defining the matrix \mathbf{A}_κ as the matrix obtained by replacing in the formula for \mathbf{A} the time-step $\Delta\tau$ by the scaled time-step $\kappa\Delta\tau$, $0 < \kappa < 1$, the development of the free response between any two consecutive pulses, say from time τ_n till any point in time before τ_{n+1} , is given by

$$\mathbf{A}_\kappa \mathbf{Y}_n, \quad 0 < \kappa < 1. \quad (4.22)$$

Before computing the correlation function some few results from the theory of stationary autoregressive processes are briefly repeated with emphasis on characteristics of the present problem. First of all it is noted that since \mathbf{A} represents the unforced development of the response of an oscillator with damping, the eigenvalues λ_1 and λ_2 of \mathbf{A} have modulus less than 1 implying that the process can actually reach stationarity. Due to the zero mean of the pulses the mean value vector obey the relation

$$E[\mathbf{Y}_n] = \mathbf{A}E[\mathbf{Y}_n] \quad (4.23)$$

As $|\lambda_i| < 1$ the mean value vectors become $E[\mathbf{Y}_n] = \mathbf{0}$. By recursion it follows that the correlation matrix $\mathbf{C}_k = \text{Cov}[\mathbf{Y}_n, \mathbf{Y}_{n-k}^T]$, $k = 0, 1, \dots$ between two states separated in time by k time-steps is given by the equations

$$\mathbf{C}_k = \mathbf{A}^k \mathbf{C}_0 \quad (4.24)$$

$$\mathbf{C}_0 = \mathbf{A} \mathbf{C}_0 \mathbf{A}^H + \mathbf{C}_Z \quad (4.25)$$

where

$$\mathbf{C}_Z = \text{Cov}[\mathbf{Z}_n, \mathbf{Z}_n] = \begin{bmatrix} 0 & 0 \\ 0 & \sigma_W^2 \end{bmatrix} \quad (4.26)$$

and the superscript H means the Hermitian, i.e., the transpose complex conjugate matrix. Though \mathbf{A} is real, the introduction of the Hermitian is needed later because the eigenvalue decomposition of \mathbf{A} is complex. Eq. (4.25) may be solved by replacing \mathbf{A} by its eigenvalue decomposition $\mathbf{A} = \mathbf{V}\mathbf{L}\mathbf{V}^{-1}$. Doing so one then finds that the following relations hold

$$\mathbf{C}_0 = \mathbf{V}\hat{\mathbf{C}}_0\mathbf{V}^H, \quad \{\hat{\mathbf{C}}_{0,nm}\} = \left\{ \frac{\hat{\mathbf{C}}_{Z,nm}}{1 - \lambda_n \bar{\lambda}_m} \right\}, \quad \hat{\mathbf{C}}_Z = \mathbf{V}^{-1}\mathbf{C}_Z(\mathbf{V}^{-1})^H \quad (4.27)$$

where the overbar means complex conjugate and $n, m = 1, 2$

After this short recapitulation of some basic results about stationary autoregressive processes it is time to turn to the evaluation of the correlation function of the simulated response process. First step is to relate the correlation structure of the simulated response process to the correlation structure \mathbf{C}_k of the autoregressive process. Combining the transition formula Eq. (4.22) and the

equation for \mathbf{C}_k Eq. (4.24), yields an expression for the correlation $\mathbf{C}_{k+\kappa}$ between two points separated in time by $(k+\kappa)\Delta\tau$:

$$\mathbf{C}_{k+\kappa} = \text{Cov}[\mathbf{A}_\kappa \mathbf{Y}_n, \mathbf{Y}_{n-k}^T] = \mathbf{A}_\kappa \mathbf{A}^k \mathbf{C}_0, \quad 0 < \kappa < 1 \quad (4.28)$$

The computation of the cumulative transition matrix $\mathbf{A}_\kappa \mathbf{A}^k$ is easily conducted by use of the eigenvalue decompositions of the individual transition matrices. The eigenvalues of \mathbf{A}_κ and \mathbf{A} are $\lambda_{\kappa;1,2} = e^{(-\alpha \pm i)\kappa\Delta\tau}$ and $\lambda_{1,2} = e^{(-\alpha \pm i)\Delta\tau}$ respectively. As one should intuitively expect they account for the development of the damped unforced response over a given time-step, why they are identical except for the step length. On the other hand the eigenvectors of the two matrices are identical and *independent* of the time-step. One finds

$$\mathbf{V} = \mathbf{V}_\kappa = \begin{bmatrix} 1 & 1 \\ -\alpha + i & -\alpha - i \end{bmatrix} \quad (4.29)$$

The fact that $\mathbf{V} = \mathbf{V}_\kappa$ is very useful in the evaluation of $\mathbf{C}_{k+\kappa}$. Denoting by θ the time lag $(k+\kappa)\Delta\tau$, and introducing the notation $\mathbf{R}(\theta)$ for the correlation function matrix of the simulated continuous state vector process one has

$$\begin{aligned} \mathbf{R}(\theta) &= \mathbf{C}_{k+\kappa} \\ &= \mathbf{A}_\kappa \mathbf{A}^k \mathbf{C}_0 \\ &= \mathbf{V}_\kappa \mathbf{L}_\kappa \mathbf{V}_\kappa^{-1} (\mathbf{V} \mathbf{L} \mathbf{V}^{-1} \dots \mathbf{V} \mathbf{L} \mathbf{V}^{-1}) \mathbf{C}_0 \\ &= \mathbf{V} \mathbf{L}_\kappa \mathbf{L}^k \mathbf{V}^{-1} \mathbf{C}_0 \\ &= \mathbf{V} \begin{bmatrix} e^{(-\alpha+i)\theta} & 0 \\ 0 & e^{(-\alpha-i)\theta} \end{bmatrix} \mathbf{V}^{-1} \mathbf{C}_0 \end{aligned} \quad (4.30)$$

The above expression tells us that the dependence of \mathbf{R} on the step size is isolated in \mathbf{C}_0 . Thus the next step naturally becomes an investigation of how \mathbf{C}_0 depends on $\Delta\tau$. Evaluating the formulas in Eq. (4.27) yields

$$\mathbf{C}_0 = \frac{(\sigma_w/\sqrt{\Delta\tau})^2}{8} \mathbf{V} \begin{bmatrix} \frac{2\Delta\tau}{1-e^{-2\alpha\Delta\tau}} & \frac{-2\Delta\tau}{1-e^{-2(\alpha-i)\Delta\tau}} \\ \frac{-2\Delta\tau}{1-e^{-2(\alpha+i)\Delta\tau}} & \frac{2\Delta\tau}{1-e^{-2\alpha\Delta\tau}} \end{bmatrix} \mathbf{V}^H \quad (4.31)$$

Note that σ_w has been divided by $\sqrt{\Delta\tau}$. According to the discussion in Sec. 4.3.1 about the dependence of σ_w on $\Delta\tau$, $(\sigma_w/\sqrt{\Delta\tau})^2$ is a scalar independent of $\Delta\tau$. All dependence on the time-step is thus isolated to the matrix between \mathbf{V} and \mathbf{V}^H in Eq. (4.31). Carrying on from now by analytical means is not easy without approximations. A Taylor expansion in $\Delta\tau$ is therefore considered. After some simple manipulations one obtains the below formulas in which $\mathbf{o}(\Delta\tau^2)$

denotes a matrix of little oh functions $o(\Delta\tau^2)$.

$$\begin{aligned}
\mathbf{C}_0 &= \frac{(\sigma_W/\sqrt{\Delta\tau})^2}{8} \mathbf{V} \left\{ \begin{bmatrix} \frac{1}{\alpha} & \frac{-i-\alpha}{1+\alpha^2} \\ \frac{i-\alpha}{1+\alpha^2} & \frac{1}{\alpha} \end{bmatrix} + \begin{bmatrix} 1 & -1 \\ -1 & 1 \end{bmatrix} \Delta\tau \right. \\
&\quad \left. + \frac{1}{3} \begin{bmatrix} \alpha & -\alpha+i \\ -\alpha-i & \alpha \end{bmatrix} \Delta\tau^2 \right\} \mathbf{V}^H + \mathbf{o}(\Delta\tau^2) \\
&= \frac{(\sigma_W/\sqrt{\Delta\tau})^2}{4\alpha(1+\alpha^2)} \left\{ \begin{bmatrix} 1 & 0 \\ 0 & 1+\alpha^2 \end{bmatrix} + 2\alpha(1+\alpha^2) \begin{bmatrix} 0 & 0 \\ 0 & 1 \end{bmatrix} \Delta\tau \right. \\
&\quad \left. + \frac{\alpha(1+\alpha^2)}{3} \begin{bmatrix} 0 & -1 \\ -1 & 4\alpha \end{bmatrix} \Delta\tau^2 \right\} + \mathbf{o}(\Delta\tau^2)
\end{aligned} \tag{4.32}$$

The latter of the above two formulas shows that if one puts

$$\sigma_W^2 = 4\alpha(1+\alpha^2)\Delta\tau \tag{4.33}$$

then, as $\Delta\tau$ tends to zero, the stationary variance of $X(\tau)$, $\dot{X}(\tau)$ and their zero covariance in the case of a continuous white noise forcing is recovered. Hence the simulation scheme is in this respect asymptotically correct.

The final step is to construct the power spectrum. By substitution of Eq. (4.32) into Eq. (4.30) and defining σ_W by Eq. (4.33) the Taylor expansion of the correlation function matrix $\mathbf{R}(\theta)$ becomes

$$\begin{aligned}
\mathbf{R}(\theta) &= e^{-\alpha\theta} \begin{bmatrix} \cos\theta + \alpha\sin\theta & (1+\alpha^2)\sin\theta \\ -(1+\alpha^2)\sin\theta & (1+\alpha^2)(\cos\theta - \alpha\sin\theta) \end{bmatrix} \\
&\quad + 2\alpha(1+\alpha^2) e^{-\alpha\theta} \begin{bmatrix} 0 & \sin\theta \\ 0 & \cos\theta - \alpha\sin\theta \end{bmatrix} \Delta\tau \\
&\quad + \frac{\alpha(1+\alpha^2)}{3} e^{-\alpha\theta} \begin{bmatrix} -\sin\theta & -\cos\theta + 3\alpha\sin\theta \\ -\cos\theta + \alpha\sin\theta & (1-3\alpha^2)\sin\theta + 4\alpha\cos\theta \end{bmatrix} \Delta\tau^2 \\
&\quad + \mathbf{o}(\Delta\tau^2)
\end{aligned} \tag{4.34}$$

Again it is seen that asymptotically for $\Delta\tau \rightarrow 0$ the simulation procedure reproduces the stationary response correlation structure of a white noise excited SDOF oscillator. The only spectrum that will be considered here is the displacement spectrum S_X . It is computed as

$$\begin{aligned}
S_X(\omega) &= \frac{1}{\pi} \int_0^\infty \mathbf{R}_{11}(\theta) \cos(\omega\theta) d\theta \\
&= \frac{1}{\pi} \frac{2\alpha(1+\alpha^2)}{((1+\alpha^2) - \omega^2)^2 + 4\alpha^2\omega^2} \left(1 - \frac{1}{6}(1+\alpha^2 - \omega^2)\Delta\tau^2 \right) + o(\Delta\tau^2)
\end{aligned} \tag{4.35}$$

The fraction in front of the parenthesis is the exact response spectrum. The second term in the parenthesis gives an approximation to the error due to the discretization. One observes that the error is of second order in the time-step $\Delta\tau$ and without noticeable influence from damping. The ω^2 in the inner-parenthesis shows that there will be some high frequent noise in the simulated process and almost no error at the peak. Clearly there must be some high-frequency noise, as the pulses give instant changes in velocity leading to non-differentiable displacement sample curves. Predicting the precise kind of high-frequency noise appearing in the second order Taylor series approximation is not easy, why no further discussion of the error term is given. The importance of the result is, however, that an acceptable error is obtained – independent of the damping ratio – by choosing $\Delta\tau$ equal one tenth of the period of oscillation.

Figures. 4.3 and 4.4 document the conclusions reached above. Figure 4.3 shows plots of the exact spectrum and the second order Taylor expansion of the spectrum of the simulated response. Both spectra are shown for different values of the damping ratio $\zeta = 0.001, 0.01, 0.05$ and for $\Delta\tau = 2\pi/10$, i.e., one tenth of the period. Figure 4.4 shows similar plots for the same damping ratios but with $\Delta\tau = 2\pi/5$. In both figures the left-hand plots show the logarithm of the spectrum in the vicinity of the peak. From these plots it is clear that the error at the peak is negligible. The right-hand plots show the scaled spectrum $S_X^*(\omega)$ in the domains next to the peak. This spectrum is defined by

$$S_X^*(\omega) = \frac{(1 + \alpha^2)\pi}{2\alpha} S_X(\omega) \quad (4.36)$$

which ensures that the plots always go through $(0, 1)$. In this way the plots will show the relative error. Note that not showing the peak makes the error appear more clearly than if the peak was included. As concluded above the error appears virtually independent of the damping ratio. As the variance and thus the energy content of the exact response and the simulated response are equal the presence of high-frequency noise in the simulated response is compensated by a reduced low-frequency content. The errors for a time-step of size one tenth of the natural period are acceptable. On the other hand comparing Figs. 4.3 and 4.4 proves considerable errors for a time-step of size one fifth of the natural period.

A time-step of size one tenth of the natural period as discussed above is not – as it may appear – an arbitrary choice. This step size is one of the most commonly used in simulations of the response of dynamically loaded structural systems. Therefore, in judging how fast the Slepian simulation scheme is relatively to direct numerical time integration simulations, it seems most relevant to use this time-step as this is usually the alternative. The conclusion of this section is that the direct simulation strategy presented in this chapter provides a satisfactory frequency content representation when a step size of one tenth of the natural period is used. Especially the dominating resonant frequency, important for the time scaling, has virtually no error. Thus it produces reliable results at the same time as it is fit for computation time comparisons.

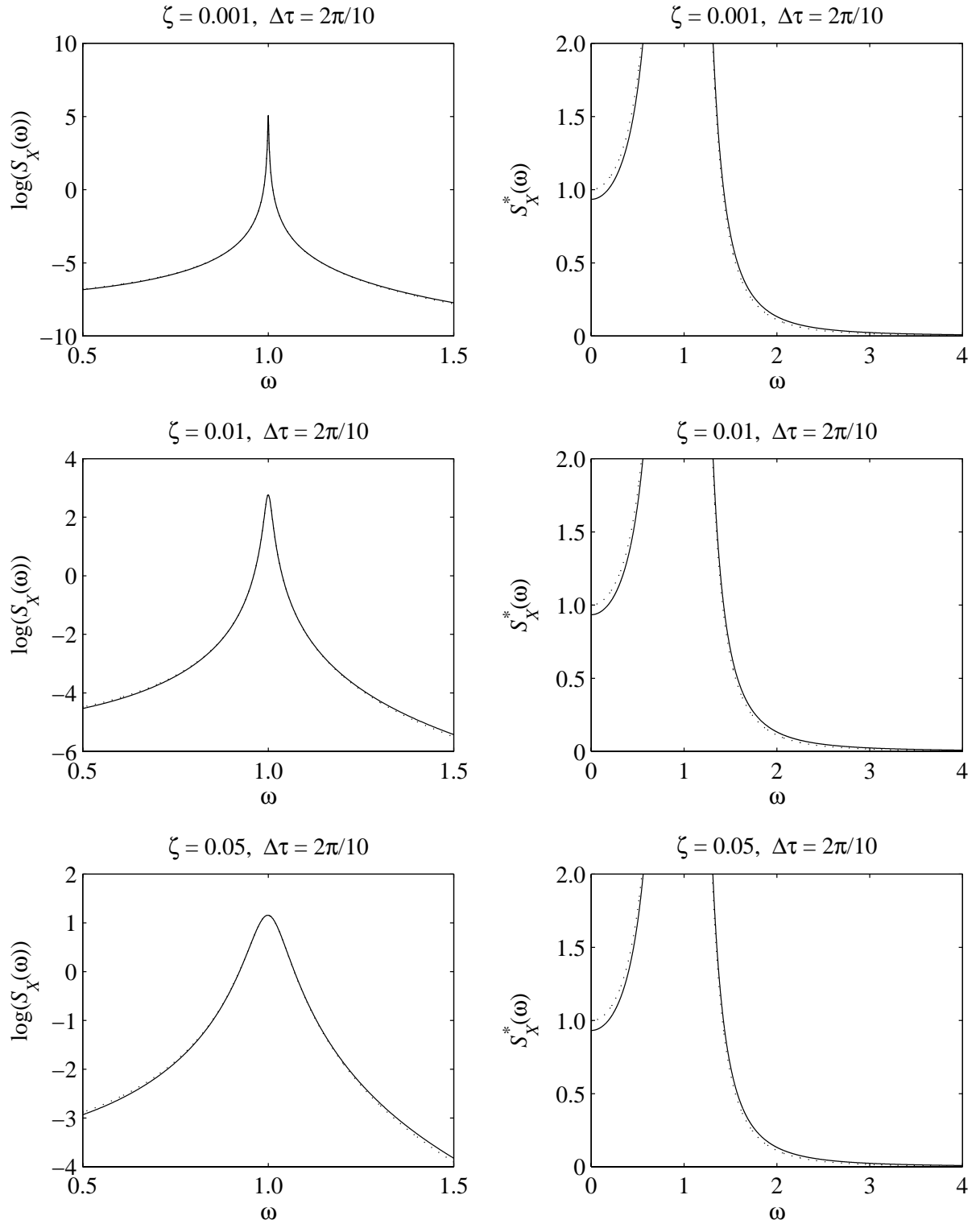


Figure 4.3: Comparison of the power spectra of the exact response (dotted curves) and the simulated response (full curves). See discussion in the text.

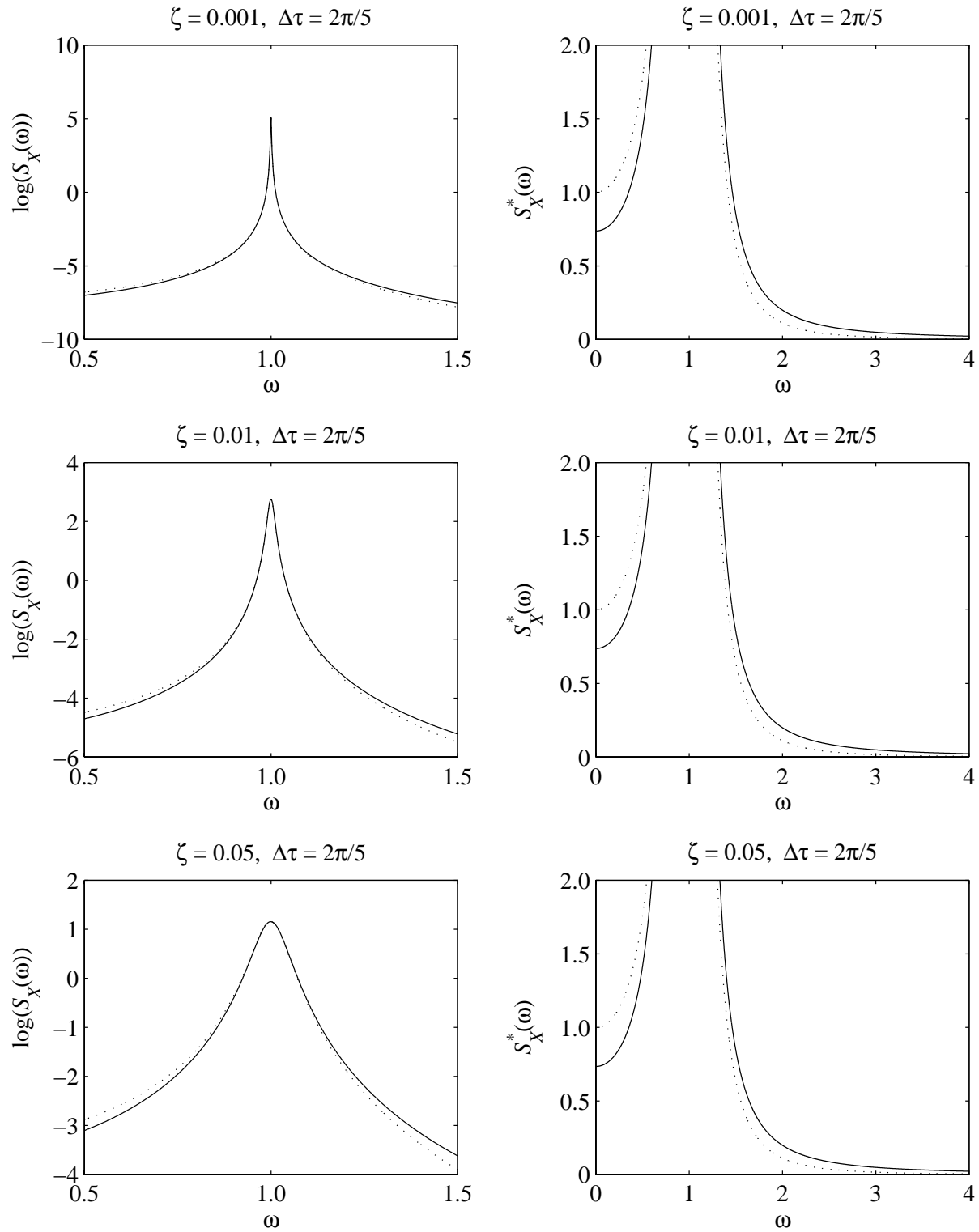


Figure 4.4: Comparison of the power spectra of the exact response (dotted curves) and the simulated response (full curves). See discussion in the text.

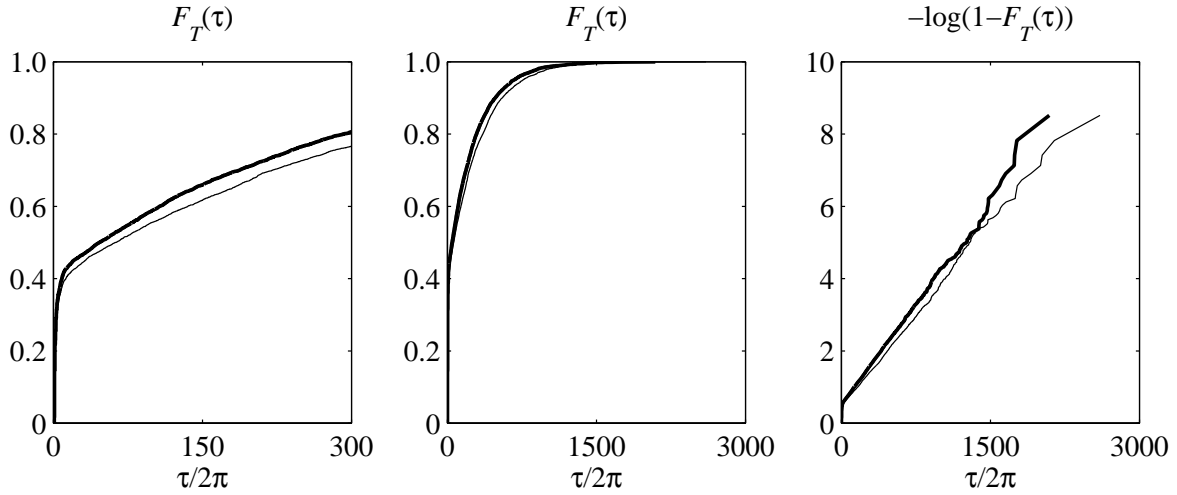


Figure 4.5: Waiting time distribution simulations by direct time integration with step size one tenth (thin curves) and one hundredth (thick curves) of the period. 5000 samples for $u = 3$ and $\zeta = 0.01$.

4.4 Algorithm – Discussion

In this section the complete algorithm is shortly recapitulated and enhanced a little. The enhancement follows from an additional discussion of the time-step size given below.

4.4.1 Time-Step Size – Again

When simulating waiting time distributions in the context of direct numerical time integration the simulation proceeds until the first time one detects that the response exceeds the elasticity limits. With probability one outcrossings occur between the pulses. Most likely an outcrossing is not followed by an incrossing until after the next pulse. Thus detecting outcrossings by detecting only outcrossings of the discrete autoregressive process will give a good estimate of the waiting time distribution. However, there might be samples with outcrossings of duration less than the step-size. Furthermore these outcrossings can take place between pulses. The more likely the larger the time-step size, of course.

The discussion in Sec. 4.3.2 led to the conclusion that simulations with a time-step of length one tenth of the natural period of the oscillator would give a satisfactory representation of the frequency content of the exact response. Figure 4.5 shows two simulation results for a typical waiting time distribution using the autoregressive process only. The one simulation conducted with a time step of one hundredth of the natural period, the other with time-step one tenth of the period. The results are within the same order of magnitude but not identical, implying a non-negligible amount of outcrossings of short duration occur between pulses. A simple improvement of the results obtained by the large time-step is possible without making the simulation

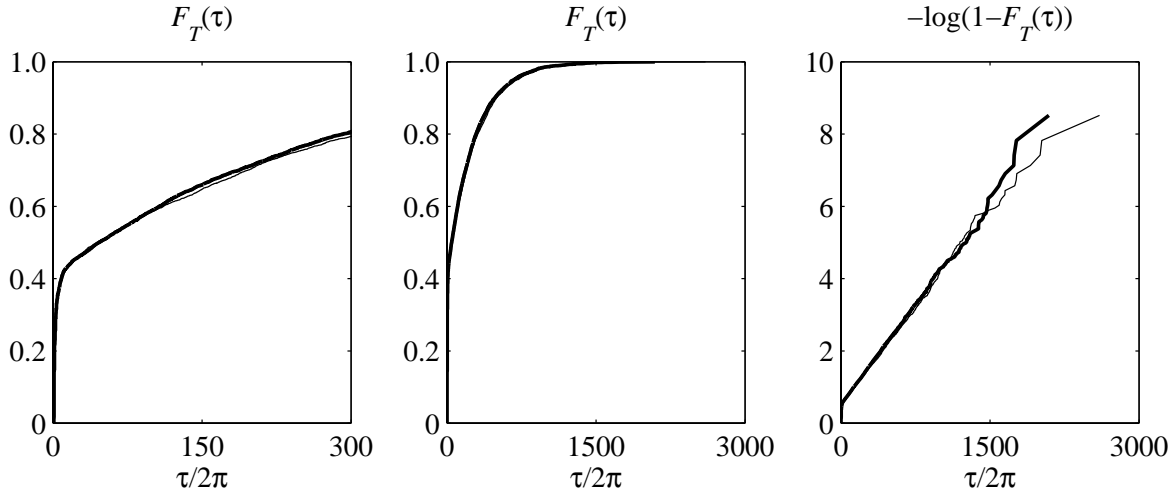


Figure 4.6: Waiting time distribution simulations by improved direct time integration with step size one tenth of the period (thin curves) compared with simple direct time integration using step size one hundredth of the period (thick curves). 5000 samples for $u = 3$ and $\zeta = 0.01$.

scheme become much more time costly. Whenever the response comes close to the elasticity limits it is checked if an outcrossing has taken place even though two successive states of the autoregressive process does not indicate an outcrossing.

The two issues: how one defines 'close to the elasticity limits', and how one checks if an outcrossing has occurred, require some remarks. The situation we are considering is when $X^* = X - X_p \approx |u|$ and the velocity is close to zero – otherwise there would be too much kinetic energy in the oscillator for it to cross out and cross in within one time-step. A simple calculation based on Eq.(4.4) shows that under the conditions $X^* = u$ and $\dot{X}^* = 0$ the oscillator, during on time-step, will at most displace approximately $\Delta X^* \approx (1 - \cos \Delta\tau)u$. So by close is meant

$$|X^* - u| \leq \delta = (1 - \cos \Delta\tau)u \quad (4.37)$$

The check of a possible outcrossing simply consists in shifting time-step to $\Delta\tau/10$, without changing the temporal density of the pulses. One steps ahead using the state transition matrix $\mathbf{A}_{\kappa=0.1}$ and checks if this more dense, but still discrete process, experiences an outcrossing. If it does not, simulation returns to the original step size $\Delta\tau$ and so on.

With $\Delta\tau$ equal to one tenth of the period one finds $\delta = 0.19u$. For the moderately low elasticity level $u = 2$ this implies that about 10% of the response is computed with time-step $\Delta\tau/10$. For $u = 3$ it is less than 2%. Consequently the extra time consumption is little – especially so for high levels which are the most relevant ones. Figure 4.6 compares, for the same waiting time distribution as in Fig. 4.5, a simple simulation with time-step one hundredth of the period with one using the improved simulation scheme with time-step one tenth of the period. A satisfactory agreement is obtained.

4.4.2 The Algorithm in Short

Up till now stepping through linear and non-linear states has been discussed separately. How to shift from linear states to non-linear states and back again has not been discussed. The subjects of this section are: discussion of shifting between states, and recapitulation of the algorithm. The latter subject is given in the form of a table.

Sometimes a higher resolution of the time-stepping algorithm is required. Like it was discussed above, it is needed when detecting outcrossings of less duration than one time-step. It is also needed when, after an outcrossing, an extreme is detected. The outcrossing and the response path from the outcrossing to the extreme have to be computed rather precisely, as they determine the size of the plastic displacement increment due to that particular outcrossing. Because the time from an outcrossing to the following extreme is typically less than one quarter of the natural period, time-steps of size one tenth of the period are too crude for the simulation of the response path after an outcrossing. So, when evaluating the plastic displacement increment, the point of outcrossing must be precisely determined as well as time-steps of size $\Delta\tau/10$ during non-linear stepping are required. The coupling between linear and non-linear time-stepping therefore becomes as follows. When an outcrossing is detected the step-size is either $\Delta\tau/10$ (as described in Sec.4.4.1) or $\Delta\tau$. In the latter case, go back one time-step $\Delta\tau$, shift to time-step $\Delta\tau/10$ and re-detect the point of outcrossing more precisely. Then shift to the non-linear time-stepping procedure and proceed stepping with step size $\Delta\tau/10$. Continue until the extreme is detected. Shift back to linear stepping, and carry on using time-step $\Delta\tau/10$ until the next pulse. Apply the pulse and continue with the original step size $\Delta\tau$. Note, that during all this the temporal density of the pulse application does not change. Table 4.2 (at the end of the chapter) presents the algorithm as explained here. For convenience it is assumed in this table that the initial conditions (which are not discussed in this chapter) are within or at the elasticity limits.

4.5 Summary

This chapter discusses an implementation of a direct numerical time integration scheme fit for the evaluation of the performance of the Slepian Model Simulation Method when used to simulate the response of an SDOF oscillator with hysteresis driven by white noise.

The numerical scheme implies a discretization of time and consequently a discretization of the driving white noise process. The white noise process has been represented by discrete pulses. The time discretization is characterized by the distance – the so-called time-step – between the discrete points in time. It has been shown that for a linear oscillator the simulated stationary response spectrum approximates the exact response spectrum very well. Especially the dominating resonant frequency, being important for the time scaling, has virtually no error.

Another virtue of the direct scheme is that the white noise discretization implies that an exact time-stepping formula exists as long as the oscillator is at elastic states. Due to the non-

linearities approximate time-stepping is generally inevitable, however, the errors do not matter much in the total picture as only relatively few time-steps take place in the non-linear domain.

Enhanced time-stepping improves waiting time and plastic displacement simulations but does not affect simulation time much.

Thus it may be concluded that the direct time integration scheme produces reliable results for a typical time-step that at the same time makes it a fair and realistic benchmark for the Slepian Model Simulation Method with respect to computation time consumption and accuracy.

Set initial conditions inside elasticity limits – deterministically or randomly.

DO

DO

Simulate linear time-step.

IF close to elasticity limits (see Eq.(4.37)):

Set step size to $\Delta\tau/10$.

DO

Simulate linear time-step.

UNTIL outcrossing or next pulse.

IF no outcrossing: Reset step size to $\Delta\tau$.

ENDIF

UNTIL outcrossing.

IF step size equals $\Delta\tau$:

Go back one step.

Set step size to $\Delta\tau/10$.

DO

Simulate linear time-step.

UNTIL outcrossing.

ENDIF

Set step size to $\Delta\tau/10$.

DO

Simulate non-linear time-step.

UNTIL extreme reached.

DO

Simulate linear time-step.

UNTIL next pulse

Reset step size to $\Delta\tau$.

UNTIL end of sample

Table 4.2: The simulation algorithm in pseudo code.

Chapter 5

Simulation Results

The previous chapters provide the background for the Slepian Model simulation method and the testing of it. In the present chapter simulations of plastic displacement processes are given. First examples with a bilinear EPO with hardening and softening are treated. Next a non-ideal EPO is treated. In all cases the combination of the Slepian modeling of the clumps of plastic deformations and the waiting time simulations for the inter-clump response gives good results.

5.1 The Plastic Displacement Process

Recapitulating definitions given in Chaps. 1 to 3, but also for use in the present chapter, Fig. 5.1 shows a sketch of the plastic displacement process as simulated by the Slepian model simulation scheme. One observes that there are – at least – two ways of describing the distributions of the plastic displacement process. One can consider the plastic displacement at a given time instant the sum of all the previous plastic displacements, or one can consider it the sum of the net plastic

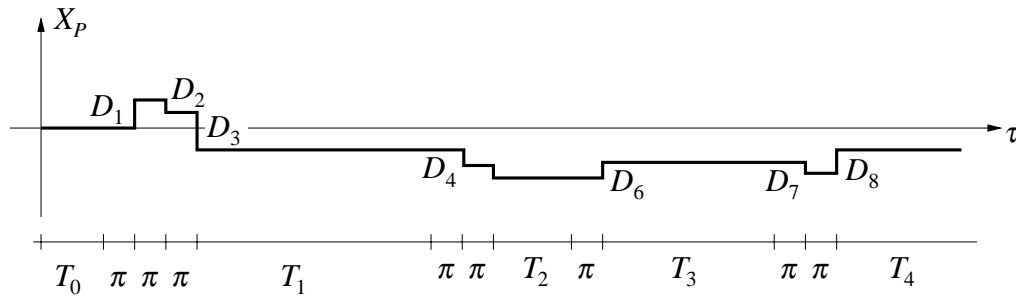


Figure 5.1: Sketch of the plastic displacement process for the Slepian simulation scheme.

displacements of each clump:

$$X_P = \sum_{\text{increment } i} D_i, \quad X_P = \sum_{\text{clump } i} D_{\text{net},i} \quad (5.1)$$

By the latter description generally less dependence of the terms in the sum is obtained. This is due to the time distance between the clumps being larger than the time distance between each plastic displacement.

5.2 Initial Conditions

Strain hardening has a stabilizing effect on the plastic displacement process. Physically this is easily understood, if one considers an ideal elastic-plastic beam subjected to a static tensional normal force as shown in Fig. 5.2. Regarding the transverse end point displacement it is clear that the tensional force will always attempt to straighten the beam, thus preventing the end point from displacing arbitrarily much. The plastic displacement processes is consequently continuously drawn back towards zero. The statistical moments of the plastic process therefore become stationary independent of the initial conditions of the oscillator. Intuitively this implies that $X_P(\tau)$ is, when stationarity is reached, an ergodic process. Generating just one very long sample of $X_P(\tau)$ would suffice to obtain the stationary statistical moments. However, in opposition to hardening, strain softening destabilizes the plastic displacement process why it becomes unstable leading to collapse of the oscillator. Thus stationarity is clearly not obtainable for strain softening and the statistical properties of the process must be obtained by simulating the process over and over again using the identically distributed initial conditions, and finally evaluating the ensemble average. The same holds true for ideal plasticity as the plastic displacement process can drift due to lack of hardening. So, in general the statistical properties of the plastic displacement process depend on the initial conditions of the oscillator, why this section is devoted to this subject.

In the present examples the random initial conditions are chosen as follows. It is assumed that the response at time $\tau = 0$ has reached approximate stationarity without any outcrossings. Therefore $X_P(0) = 0$ and $|X(0)| < u$, where u denotes the absolute value of the initially symmetric yield limits. Furthermore it is assumed that the oscillator at time $\tau = 0$ is at a crest/trough.

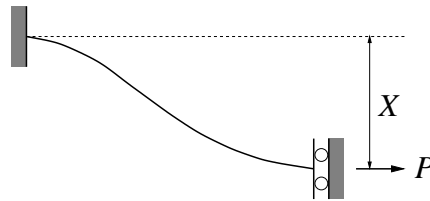


Figure 5.2: Column subjected to tensional static force.

This assumption is introduced as it simplifies the simulation of the waiting time to the first outcrossing when employing the amplitude model. As an approximation to the distribution of the extreme under these assumptions the truncated standard Rayleigh density

$$\frac{xe^{-\frac{1}{2}x^2}}{1 - e^{-\frac{1}{2}u^2}}, \quad 0 < x < u \quad (5.2)$$

is adopted. This approximation is used because the stationary distribution of the amplitude of the normalized response of a linear oscillator subjected to white noise is standard Rayleigh. The direct simulation is then initiated by generating an outcome from (5.2) and assigning it to $X(0)$ using, with equal probability, positive or negative sign. The velocity $\dot{X}(0)$ is set to zero. The Slepian model simulations are initiated by generating an outcome M_0 from (5.2) also. The time to the first outcrossing is then obtained by simulating the outcomes of the amplitude model according to Eq. (3.11) using M_0 as the initial amplitude.

5.3 Strain Hardening and Softening for the Bilinear EPO

In this section simulation results for the bilinear EPO are presented (the definition of the bilinear restoring force diagram is reviewed Appendix A.) As hardening and softening lead to different types of plastic displacement developments the results are presented in separate sections.

5.3.1 Hardening

The aim is to obtain the development in time of the statistical moments up to and including the fourth order. Due to the symmetry of the initial conditions and the restoring force diagram the mean and skewness is zero at all times. Therefore the plots in Figs. 5.3, 5.4 and 5.5 show only the time development of the standard deviation and the kurtosis for different values of the system parameters. These are as follows: u , which is the initial symmetric yield level, γ , which is the inclination of the hardening branch (see Fig. A.1 p. 119), and ζ , which is the damping ratio. The number of simulations performed is 5000, which is quite high. This was done in order to obtain reliable estimates of the higher order moments. Especially problems can arise for the time instances close to zero as only a few samples are non-zero close to zero. Consequently the statistical uncertainty in the estimation of the kurtosis is high there. From the plots in Figs. 5.3–5.5 it is seen how the uncertainty decreases with time. The clear step-shape of the kurtosis plots for the Slepian model simulations is due to the simulation of the waiting time to the first outcrossing by the discretized amplitude model. Therefore the Slepian model simulations cannot catch the very beginning of the time development of the kurtosis very well. However, the plateaus are generally well situated compared to the more smooth curves obtained by the direct simulations.

Before carrying on comparing direct and Slepian Model simulation results some remarks on the time development of the kurtosis are given. As mentioned above the value of the plastic displacement process at a certain time instant may be considered as either the sum of all the previous plastic displacement increments or the sum of the net plastic displacements in each clump. If the distributions of the terms in these sums are identical and independent the Central Limit Theorem states that the distribution of the plastic process approaches the Gaussian distribution as the number of terms tends to infinity, i.e. time tends to infinity. The terms are in general not independent and nor equally distributed. The separate plastic increments are dependent simply due to the clumping. When the yield limits are of similar size, i.e. almost symmetric, it is most likely that a negative increment follows a positive increment, if they belong to the same clump. When the limits are very asymmetric a positive increment usually precedes a positive increment and a negative precedes a negative. This concerns the dependence of the sign. Nor the magnitude of the plastic increments are in general independent. Regard first the second and following plastic increments in a clump. The size of these increments clearly depends on the yield limits u^+ and u^- which in turn depends on the foregoing plastic increment. Consider now the first increment in a clump. Due to the inter-clump oscillations the first plastic increment in a clump depends in a more complicated way on the last plastic increment of the previous clump. However, it is clear that it is not independent on this plastic increment. So much for dependence. Furthermore, since the plastic increment depends on u^+ and u^- which develop in time, the distribution of the increments are not identical. Some of the considerations given for the separate increments hold true for the distribution of the net plastic displacement of a clump as well. The net plastic displacements are however less dependent as the inter-clump oscillations separates them in time. This is an 'on the average' consideration, because inter-clump waiting times can be rather short, as discussed previously, why net plastic displacements in clumps closely positioned in time are highly dependent (a fact partially neglected in [12]). Again it follows from the fact that u^+ and u^- develop in time that the distributions of the net plastic displacements are not identical either. This is clearly illustrated by regarding the plots in Figs. 2.14 and 2.15 (pp. 50 and 51). When the yield limits are almost symmetric the distribution of the single increments and the net displacements become symmetric. On the other hand, when yield limits are asymmetric (for $|X_p|$ large) the corresponding distributions become very asymmetric.

All the above points in the opposite direction of the requirements for the Central Limit Theorem to be fulfilled. However, in the case of hardening and especially weak hardening approximate Gaussianity is obtained. To explain this let us consider the ideal EPO. The dependence of the sign of the separate plastic increments is of course the same as in the general case of hardening or softening. The magnitude of the increments are, on the other hand, equally distributed and independent for the following reason. Both limits u^+ and u^- have the same value independent of the foregoing plastic displacement increment and they do not develop in time, i.e. they are independent of the past history. Therefore the general features of the plastic process which led to the inter-dependence of the magnitude of plastic increments vanish in the special case of the ideal EPO. Likewise the net plastic displacement of the clumps are equally distributed (a thorough investigation of this distribution is given in [6]). As the net plastic increment of a clump

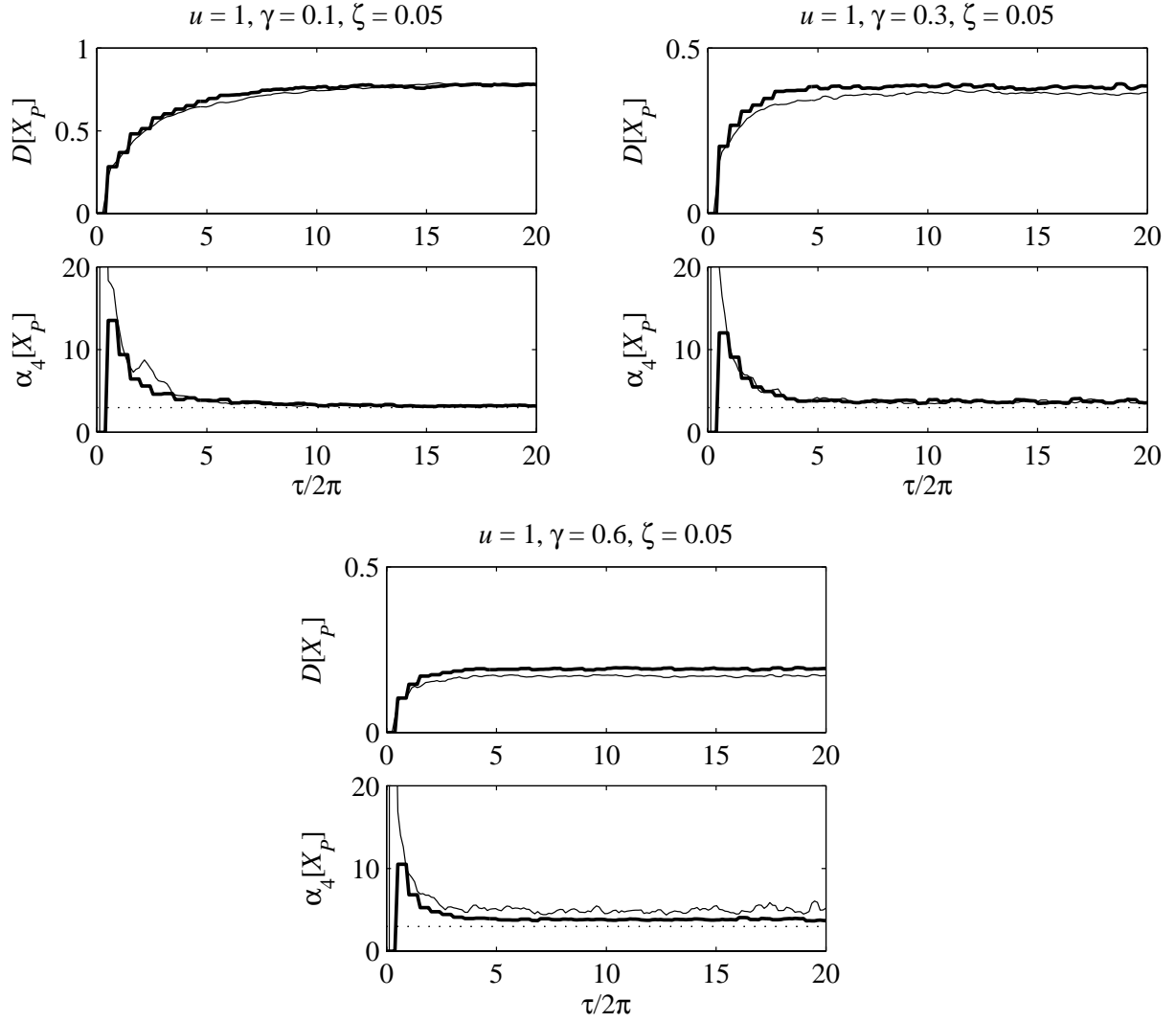


Figure 5.3: Comparison of plastic displacement process simulation results for the bilinear EPO obtained by Slepian simulation (thick curves) and direct simulation (thin curves). Parameters as defined in Chap. 2 are given at the plots. 5000 samples.

is obtained by adding the separate increments in a clump, much of the inter-dependence of the sign of the increments is accounted for by the distribution of the net plastic displacement. Still the net plastic displacements of the clumps is not independent either, as the sign of the first plastic increment in a clump depends on the previous clump. This dependence of course reduces for increasing inter-clump waiting time. In the long run a sufficiently large number of nearly independent net plastic displacements are encountered, so that the plastic displacement process will approach Gaussianity. Returning now to the case of a weakly hardening oscillator, it is clear that the net plastic increments of the clumps become approximately independent. Furthermore, in opposition to softening, the hardening ensures that extremely asymmetric distributions like

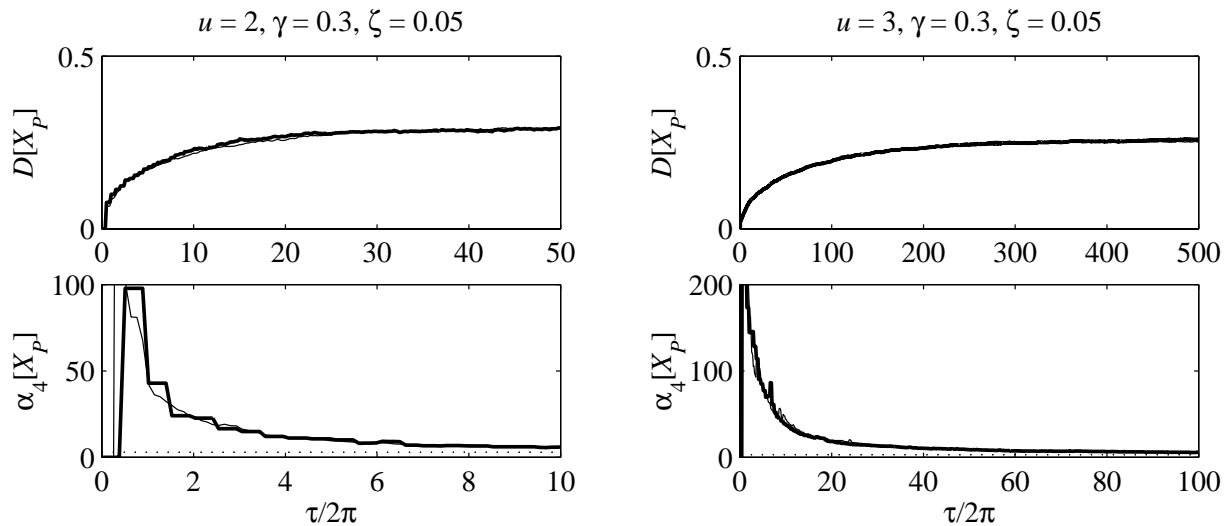


Figure 5.4: See the caption of Fig. 5.3

in Fig. 2.15 do not occur. Therefore the net plastic increments of the clumps become almost identically distributed too. It may therefore be concluded that in the case of hardening, stabilization leads to an approximately Gaussian distribution of $X_p(\tau)$ as time goes to infinity. The more so the weaker the hardening. All plots in Figs. 5.3 to 5.5 of the kurtosis show how a level close to 3 (the level 3 is shown by a dotted horizontal line) is approached. Especially the plots in Fig. 5.3 demonstrate the effect of increasing hardening causing larger and larger deviation from Gaussianity.

Results obtained by direct simulation and by Slepian model simulations are now compared. Generally good agreement between the results for the wide spread of parameters used in the plots is obtained. Anyway, for the initial yield level $u = 1$ and hardening parameter $\gamma = 0.6$ (Fig. 5.3) there is a notable error in the computation of the kurtosis when using the Slepian Simulation Method. The error is constant when first the kurtosis has reached a stationary level. This means that the error is due to the clump simulation and not the waiting time simulation. That errors may occur at such a low level is to be expected due to the assumptions behind the Karnopp-Scharton hypothesis. As explained at the end of Chap. 2 the simulation of the plastic displacement increment for low levels has errors, because the influence of the driving load after outcrossing is neglected resulting in a too small spread of the distribution of the plastic displacement obtained by the Slepian Model in combination with the Karnopp-Scharton hypothesis. As it is shown in the first row of Fig. 2.14 the Slepian model distribution is more steep than the true distribution, i.e. the kurtosis is smaller than the true kurtosis. This is exactly what is observed in the last plot in Fig. 5.3. The plot shows also that, for the same reason, the standard deviation is underestimated. The error is very pronounced because the high level of the hardening parameter causes crossings of even lower levels than 1 to become quite likely.

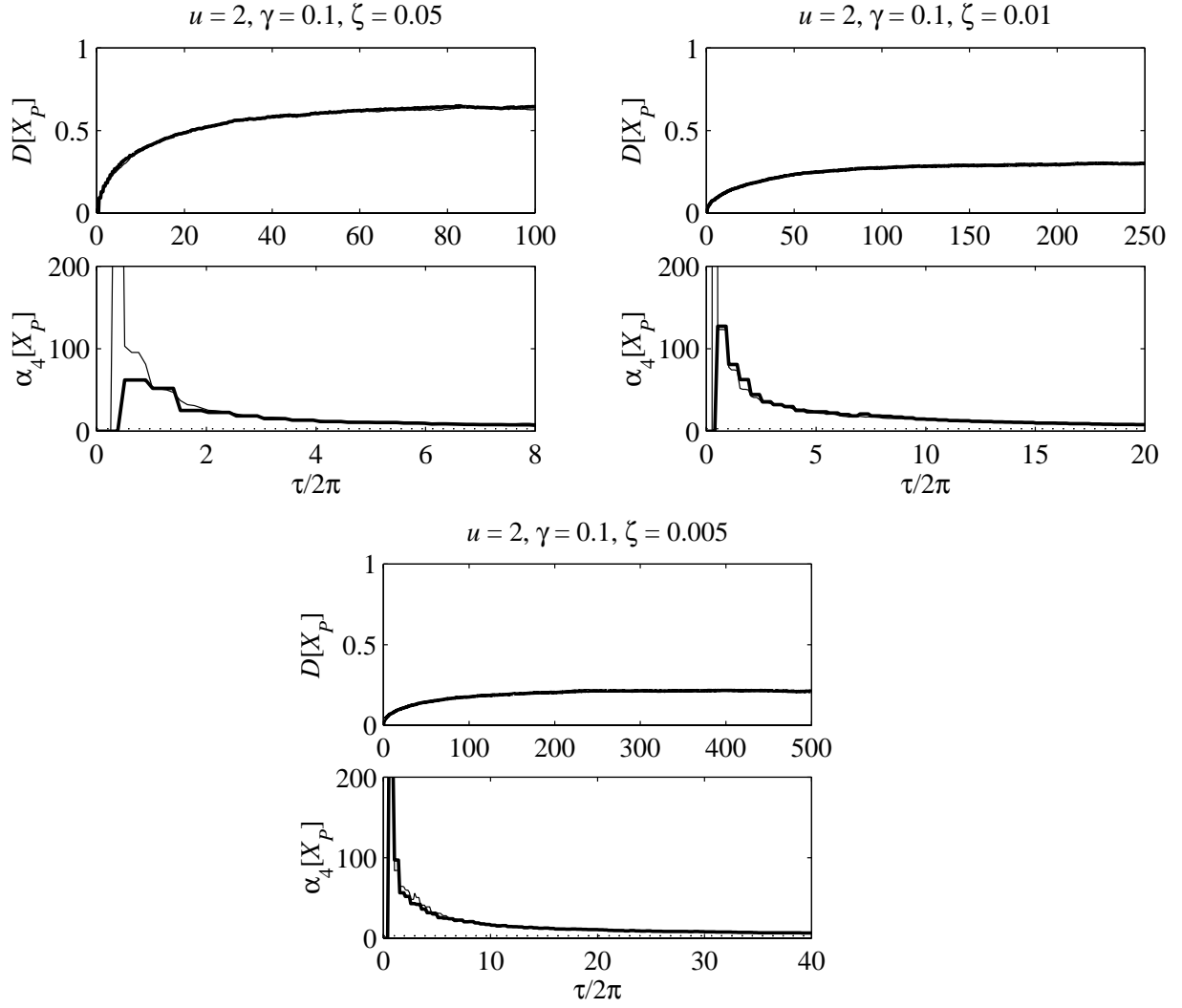


Figure 5.5: See the caption of Fig. 5.3

The error does not grow in time because the hardening causes the plastic displacement process to return to zero so that the symmetrized yield level stays close to the initial value giving a time independent error (this is not the case for softening as explained in the next section). For the other plots in Fig. 5.3, in which the hardening is smaller, the error is hardly visible, as it vanishes in statistical errors. However, a close look at the plots for $\gamma = 0.1$ and $\gamma = 0.3$ reveals that the standard deviation is underestimated in those cases too. After all the conclusion evidently is that the Slepian Simulation Model performs well even for low yield levels when the response of a system with hardening is simulated.

Further to these comments on errors, a few words regarding the time development of the standard deviation and the kurtosis in dependence of the parameters are given. As it has already been explained how the distribution of X_p approaches approximate Gaussianity the comments given here concerns the speed by which they do so. Because increasing hardening causes stronger restoring the distribution will stabilize faster. It causes also smaller plastic increments and therefore smaller standard deviation of X_p . Both effects appear clearly in Fig. 5.3. Contrary to this, a higher yield level will slow down convergence to stationarity as the mean inter-clump waiting time increases. Furthermore the spread of the plastic increments reduces too (as explained on page 35) resulting in a decreasing standard deviation with increasing yield level. Fig. 5.4 shows plots supporting these arguments. Finally decreasing damping causes slower convergence too, as it implies longer waiting times. The explanation for the influence of damping on the stationary level of the standard deviation is as follows. The higher the damping the less narrow banded the response and the more rapidly varying the mechanical energy process. Consequently, the higher the damping the larger the variance of the conditional distributions of the ALO extremes and the plastic increments. Thus the stationary variance increases with damping. The plots in Fig. 5.5 illustrate the dependence of $D[X_p]$ and $\alpha_4[X_p]$ on damping.

5.3.2 Softening

As softening destabilizes the response the variance of X_p grows in time and it does never assume a stationary level as in the hardening case. So, from a practical point of view, it is of more interest to have information about the first passage times T_p of plastic displacement levels than about the development of the plastic process itself. For the purpose of illustrating the applicability and limitations of the Slepian Model simulation method, Figs. 5.6 to 5.7 show plots of mean, coefficient of variation, skewness and kurtosis of the first passage times for different values of the system parameters u , γ and ζ . These statistical moments are plotted against the absolute value $|x_p|$ of the plastic displacement level as, due to symmetry, passing x_p or $-x_p$ is equally damaging to the oscillator. The number of simulations is 5000 in all plots.

Unlike the hardening case in which the stationary distribution depends on solely the distribution of the plastic displacement increments the distribution of the first passage times depends on both the distribution of the inter-clump waiting times and the distribution of the increments. Giving general statements about the type of the first passage distribution is therefore difficult. Statements about the dependence of $E[T_p]$ on the plastic displacement level $|x_p|$ can, however, be given. Due to destabilization the plastic displacement process develops as follows. In the beginning, when yield limits are symmetric, positive and negative plastic increments are nearly equally probable. Later, when the asymmetry of the yield limits becomes more pronounced, plastic increments solely of the same sign become more and more likely. Eventually plastic increments in only one direction appear and the plastic displacement begins growing faster and faster. As seen in all plots the mean of T_p grows faster with $|x_p|$ for small levels than for higher levels of $|x_p|$ where destabilization and asymmetry become dominant. Similarly, as seen from the plots of the coefficient of variation, the standard deviation $D[T_p]$ exhibits slow growth for

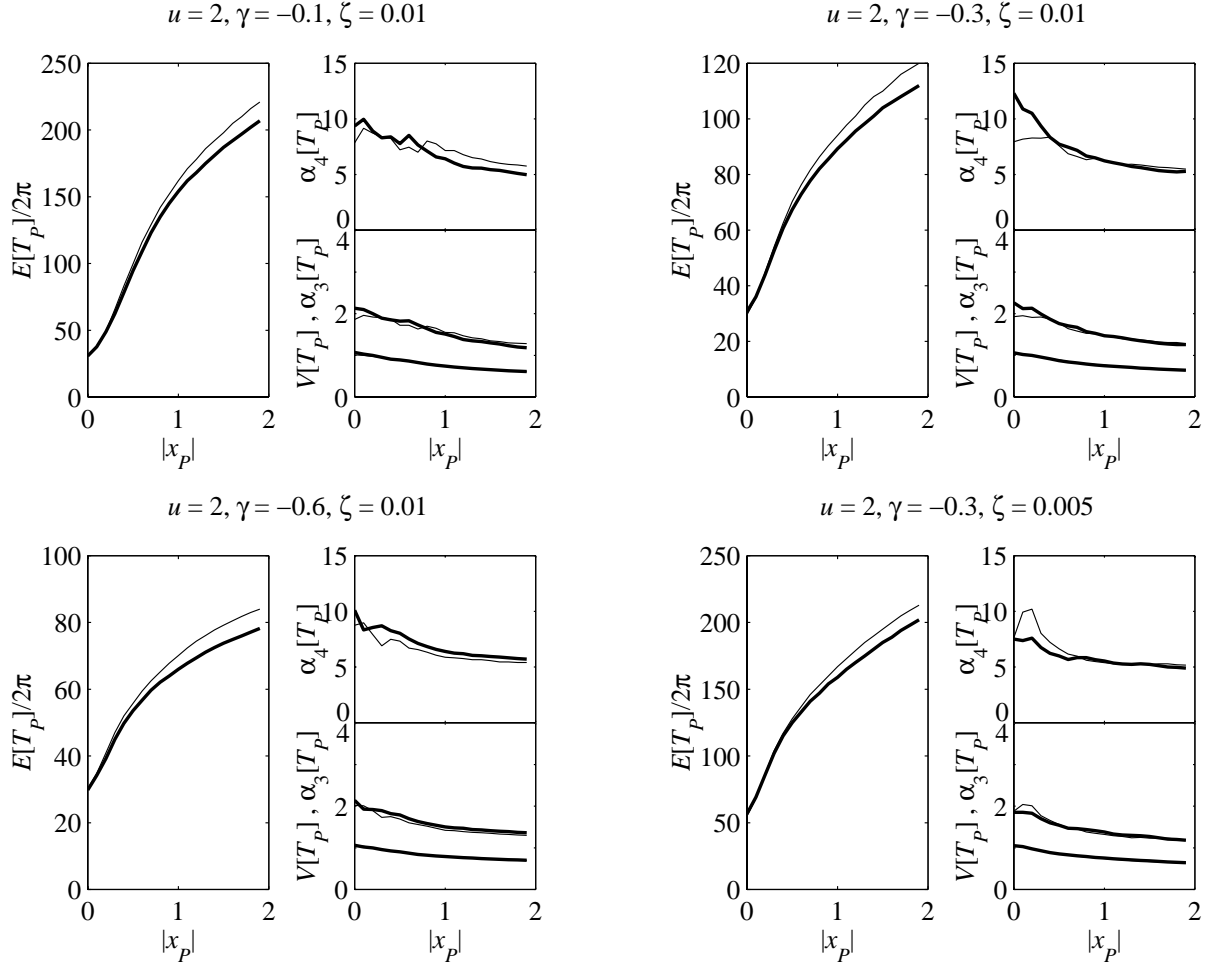


Figure 5.6: Statistics of the first passage times of plastic displacement levels for the bi-linear EPO. Comparison of simulation results obtained by Slepian simulation (thick curves) and direct simulation (thin curves). In the plots for the coefficient of variation V and the skewness the lower curves are always V . Parameters as defined in Chap. 2 are given at the plots. 5000 samples.

high levels of the plastic displacement. The time development of the three relative statistics are practically insensitive to the choice of parameters indicating some common features of the first passage time distributions. As the upper tail of the inter-clump waiting time distribution is exponential one may conjecture that this common feature – at least for small levels $|x_p|$ – is related to the exponential distribution. From the plots it is observed that for the plastic displacement level $|x_p|$ within a moderate range, i.e. around 1, the values of these relative statistics are $V \approx 0.9$, $\alpha_3 \approx 1.7$, and $\alpha_4 \approx 7$. These values are close to those of a random variable $S^{0.9}$, where S has an exponential distribution. That is, T_p is a distribution of Weibull type. A more general discussion of the first passage time distribution is not given herein.

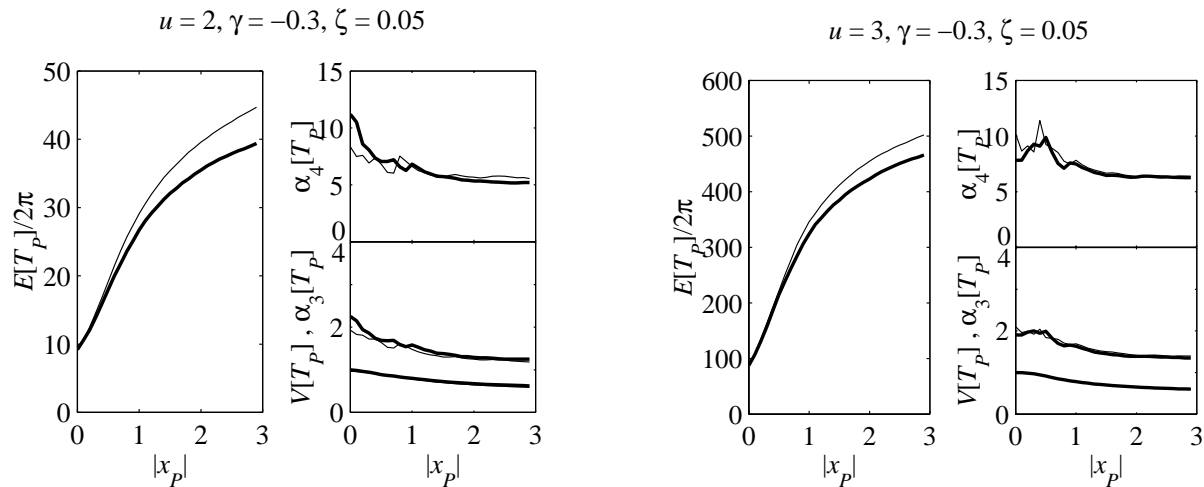


Figure 5.7: See the caption of Fig. 5.6

In opposition to the hardening case errors are present for all choices of parameters. These errors are present in the plots of $E[T_p]$ whereas the relative statistics show convincingly small deviations between the two sets of results. The small errors of the relative statistics may relate to the above observation that some general features of the first passage time distribution exist. The error in the mean value estimation can be explained as follows. Firstly, it is noted that errors are not due to the inter-clump waiting time simulation, as Fig. 3.10 (p. 72) shows that even for low yield levels the waiting time simulation performs well. Thus errors stem from the plastic increment simulations. Next it is seen that the error increases in time (opposite of what was seen in the case of hardening). Clearly it is the errors due to the Karnopp-Scharton hypothesis that give rise to the error in the computation of $E[T_p]$. As the asymmetry of the yield levels increases with time the symmetrized yield limit decreases accordingly and the error increases. Some rules for the dependence of the error on the system parameters can be deduced from the above. It is the relative error of $E[T_p]$, and not the absolute error, which is the proper measure of the error. It is so, because the inter-clump waiting time simulation does not give rise to any errors, but solely changes the time-scale. The relative error is approximately read from the plots because the ordinate axes are scaled such that the graphs fit in the plot area. For given softening parameter γ , increasing the initial yield level u implies that it takes longer time till the error due to the asymmetry of the yield limits become important. Thus, as seen in Fig. 5.7, the relative error in the estimation of $E[T_p]$ decreases with increasing yield level. Likewise one would expect that the relative error should increase with increasing softening. The first three plots in Fig. 5.6 show, however, that the increase of the relative error with γ is only weak. As a last comment on errors attention is drawn to Fig. 5.8 which shows plots for the low initial yield level 1. Unlike observed in hardening, the results from the Slepian Simulation Method exhibit notable errors for such a low level.

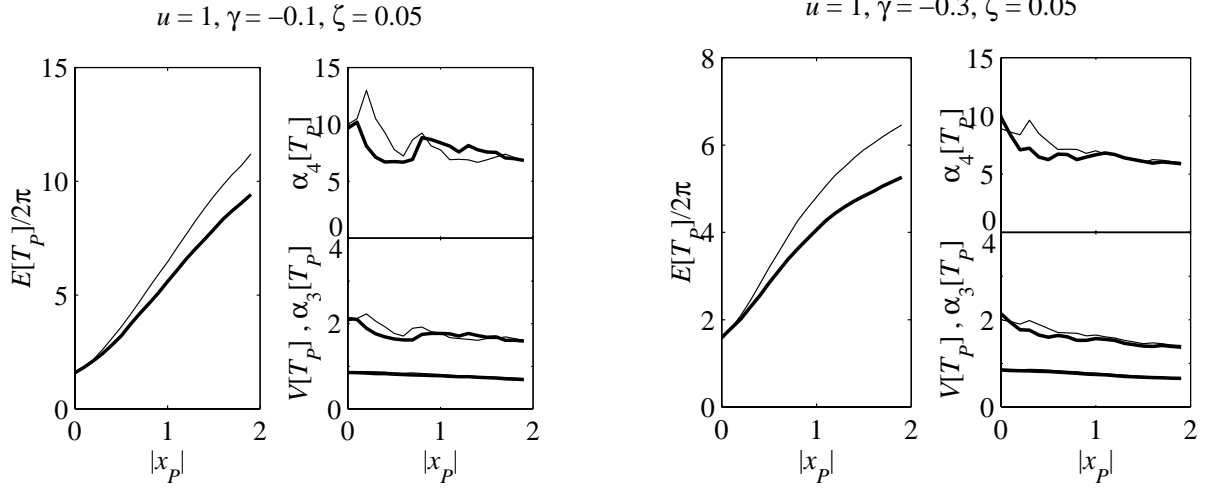


Figure 5.8: See the caption of Fig. 5.6

Here a few remarks on the dependence of the first passage time on system parameters are given. As the average inter-clump waiting time increases with decreasing damping the first passage time does so too – see the right column in Fig. 5.6. Figure 5.6 shows also that for increasing softening the average first passage times decrease. Clearly this is due to the increasing plastic increments for increasing softening (which in turn is in accordance with the large standard deviation appearing in the second row in Fig. 2.15 p. 51). Finally, increasing initial yield levels causes increasing inter-clump waiting times and decreasing standard deviation of the plastic increments leading to increasing average first passage times as verified by the plots in Fig. 5.7.

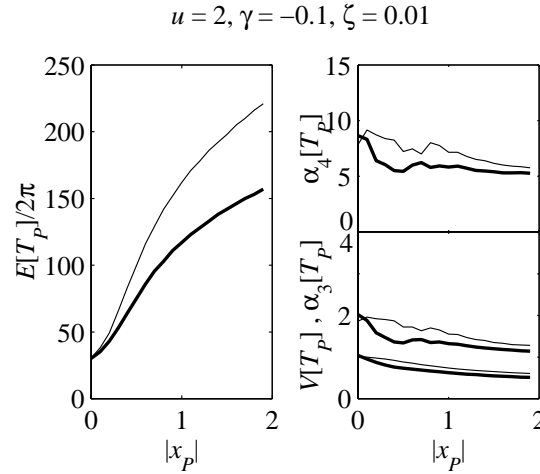


Figure 5.9: First passage time distributions obtained by use of fully exponentially distributed inter-clump waiting times in the Slepian model simulations. Compare with the first plot in Fig. 5.6

As an illustration of the influence of approximating the inter-clump waiting time distribution by an exponential distribution the plot shown in Fig. 5.9 is produced. The intensity used in the exponential distribution is the mean crossing rate of the Cramér-Leadbetter envelope corrected by the ratio of qualified crossings (see e.g. [6]). Note that the parameters used are most realistic. (It is noted that the waiting time to the first outcrossing has been simulated by the amplitude model (3.11) why no errors appear for $|x_p| = 0$.) Notable errors in the mean first passage time compared to the plot in Fig. 5.6 are present. As discussed previously the error is due to the neglected step-shape of the transient tail. Thus it is clear that the waiting time approximation suggested herein accounts much better for the clumping of clumps than the purely exponential distribution does. Or put in other words: The linkage of clump and waiting time simulation as described by Tables. 2.2-2.4 and 3.2 ensures that the inter-clump waiting time and the inter-clump dependence of plastic displacements in clumps of clumps is well modeled.

5.4 Non-Ideal EPO

The thorough treatment of the bilinear EPO in the previous section demonstrates and discusses the errors of the Slepian Model Simulation Method when combining waiting time simulations and clump simulations. As the waiting time simulation scheme is the same for all EPOs the treatment here of the non-ideal EPO focuses on the clump simulation. As long as the simplified non-ideal restoring force diagram suggested in Sec. 2.5 (see Fig. 2.10) is considered, no further errors than those due to the Karnopp-Scharton hypothesis are present in the clump simulation. Therefore the discussion here concentrates on the assumptions leading to the simplified restoring force diagram. For this purpose a not very general, but for illustration purposes quite useful, function $g(s)$ for the curved part of the restoring force diagram is used. The function considered here of course fulfills the requirement that a closed form analytical expression for the integral of the curved part exists. In addition to this it has convenient scaling and translation properties which allows a restoring force diagram which is not simplified to be constructed from g . Or, from another point of view: the simplified diagram may be regarded as derived from a more general diagram defined by g . Thus the considered simplified diagram is fit for comparisons between Slepian Model simulations using the simplified diagram and direct simulations using a diagram from which one can imagine that the simplified diagram is derived. In the following the diagram used in the direct simulation is termed the *non-simplified* restoring force diagram.

Figure 5.10 shows a schematic of the curved part of the simplified diagram (see Fig. 2.10) including some of the parameters appearing in the definition

$$g(s) = \gamma s + \eta - \frac{\kappa \rho}{(s + s_a)^{1+\kappa}} \quad (5.3)$$

As $g(0) = 0$ the abscissa $-s_a$ of the vertical asymptote is related to the other parameters through

$$s_a = \sqrt[1+\kappa]{\frac{\kappa \rho}{\eta}} \quad (5.4)$$

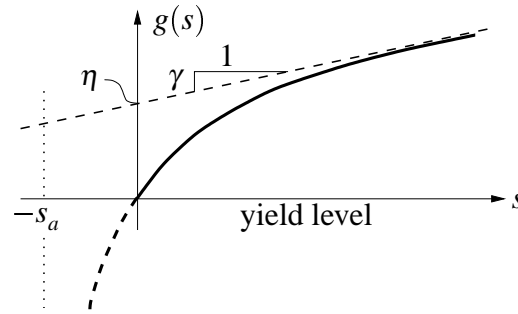


Figure 5.10: Schematic of the curved part of the simplified restoring force diagram (refer to Fig. 2.10 p. 38).

Recall that for the simplified restoring force diagram partial reloading is neglected and hardening/softening is assumed independent. Both these assumptions are loosened in the non-simplified model. In this model hardening is assumed kinematic and partial reversed loading is included. Details of the construction of the non-simplified diagram from $g(s)$ are given in Appendix A. Clearly, as η/u tends to zero the simplified diagram will approach the ideal bilinear diagram. Thus one will expect that for given η and increasing u the distribution of the plastic displacement increment D_i as obtained by the simplified model approaches the distribution obtained by the non-simplified model. As explained below, Figs. 5.12 and 5.13 (pp. 112 and 113) show that this really is the case. For $\eta = 1$, $\kappa = 0.8$, $\rho = 7.5$ and $\gamma = \pm 0.3$ the plots show the same type of distributions as those presented in Fig. 2.14 and 2.15 in Sec. 2.7. (Fig. 5.11 shows the simplified restoring force diagrams for $u = 2$). For the first plastic increment in the first clump the yield limits are symmetric and no plastic loading has yet been experienced, why the distribution of D_1 in the simplified and in the non-simplified model are, as seen in the figures, identical. The distributions of D_2 are of course affected by the differences in modeling hardening/softening and reloading. It is seen from the figures that as u increases the distributions

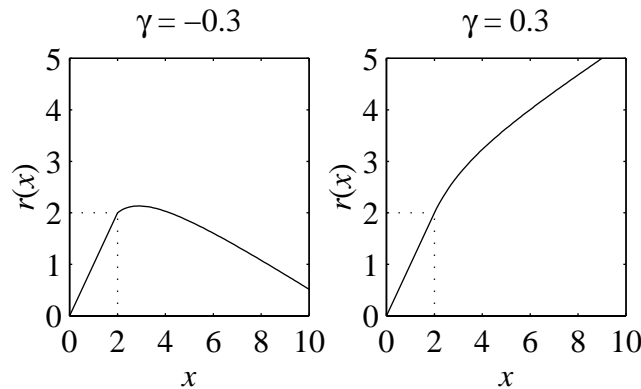


Figure 5.11: Plots of the simplified restoring force diagram in the initial configuration for $u = 2$, $\eta = 1$, $\kappa = 0.8$, $\rho = 7.5$ and $\gamma = \pm 0.3$.

for D_2 obtained by the simplified model and the non-simplified model approaches one another. Generally the agreement between the plots is good for levels larger than $u = 2$. Also clump length distributions and the number of empty excursions show good agreement. Mainly this is due to the oscillatory nature of the response. The oscillations ensure, especially in hardening, that neglecting partial reversed loading is not a very crude assumption. It is noted that the similarity between the plots in the last two rows of Fig. 2.15 and the plots in the last row of Figs. 5.12 and 5.13 is not a coincidence. Due to the large initial plastic displacement the yield limits are asymmetric and no reversed loading is experienced – only up-, un- and reloading. In that case the simplified and the non-simplified diagrams behaves identically.

The conclusion is that using the simplified restoring force diagram, developed to make the Slepian Model simulations of the clumps reasonably simple and fast, can give satisfactorily accurate approximations to the plastic response process of a non-simplified EPO.

5.5 Time Gain Factor

There is no doubt that the Slepian Simulation Method is faster than direct simulations, mainly due to the considerable computation time gain obtained by the inter-clump waiting time simulations. In Table 5.1 the time gain is quantified in terms of time gain factors denoted ε and defined as the average over a large number of simulations of the ratio of the time consumption by direct simulations to the time consumption by Slepian Model simulations. Time gain factors for the waiting time simulation and time gain factors for the clump simulation are regarded separately. Furthermore the time gain factor of a complete process simulation is regarded. Thereby a comparison showing the relative contribution of the waiting time and the clump simulations to the total time gain is possible.

All time gain factors shown in the table are computed for levels $u = 1, 2, 3$. The time gain factors $\varepsilon_{\text{wait}, 0.01}$ and $\varepsilon_{\text{wait}, 0.05}$ for the waiting time simulation are computed for damping ratios $\zeta = 0.01, 0.05$ and appear in the two first columns of the table. Clearly the time gain increases considerably with increasing level. This is to be expected for the following reasons. The average long waiting time grows rapidly as function of u causing a similarly rapidly growing time consumption of the direct simulation method. On the other hand the time consumption of the Slepian Model simulation of the long waiting times is constant independently of the average waiting time. As it appears from the table, the time gain reduces with increasing damping ratio. This is a consequence of the rule given by formula (3.12) (p. 65). For high damping it overestimates the extent of the transient lower tail, whereby too many steps for the simulation of the transient tail are carried out making the waiting time simulation a little too time costly.

In Sec. 2.6.1 the time gain of the clump simulation was discussed. It was underlined that possibly simulating the clumps by Slepian Model simulations would be more expensive than simulating them by direct simulation. The results shown in the third to the fifth column in Table 5.1 show that this is not the case for any of the relatively simple hysteresis models applied herein. The factor $\varepsilon_{\text{bilinear}}$ gives the time gain when using the bilinear model with $\gamma = 3$. The

u	$\varepsilon_{\text{wait}, 0.01}$	$\varepsilon_{\text{wait}, 0.05}$	$\varepsilon_{\text{bilinear}}$	$\varepsilon_{\text{non-ideal}, 1}$	$\varepsilon_{\text{non-ideal}, 2}$	$\varepsilon_{\text{hard. proc.}}$
1	3	2	5	6	6	6
2	7	5	4	5	5	6
3	43	33	3	3	4	15

Table 5.1: Gain factor for Inter-clump waiting time simulations, clump simulations and plastic displacement process simulations.

factor $\varepsilon_{\text{non-ideal}, 1}$ gives the time gain for the simplified model (5.3) with $\gamma = 3$, $\eta = 1$, $\kappa = 0.8$, $\rho = 7.5$. Finally the factor $\varepsilon_{\text{non-ideal}, 2}$ gives the time gain when the Slepian model simulations use the simplified model and the direct simulations follow the corresponding non-simplified model, both with parameters $\gamma = 3$, $\eta = 1$, $\kappa = 0.8$, $\rho = 7.5$. As discussed in Sec. 2.6.1 there are arguments pro and con that Slepian Model simulations for the simulation of clumps will be less expensive than direct simulations. The results given here show that for the applied models it turns out that the gain factors generally grows with the complexity of the hysteresis model, implying that the cost of the direct time integration increases faster than cost of the Slepian model. Furthermore all of the factors $\varepsilon_{\text{bilinear}}$, $\varepsilon_{\text{non-ideal}, 1}$ and $\varepsilon_{\text{non-ideal}, 2}$ decreases with increasing u because the duration of yielding decreases with increasing u causing the direct simulation to spend less time on simulating an excursion. For the Slepian Model simulations, however, the time cost of simulating an excursion is of course practically independent of u .

The last column in the table gives the time gain factor when simulating the plastic displacement process of a bilinear EPO with hardening. Parameters are $\gamma = 0.3$ and $\zeta = 0.01$. The gain factor $\varepsilon_{\text{hard. proc.}}$ is then a weighted mixture of the gain factors $\varepsilon_{\text{wait}, 0.01}$ and $\varepsilon_{\text{bilinear}}$. The process was run until stability was obtained. Stability occurs relatively early why fewer long waiting times than used to obtain $\varepsilon_{\text{wait}, 0.01}$ are encountered and therefore the gain factor $\varepsilon_{\text{hard. proc.}}$ for the high level $u = 3$ is smaller than $\varepsilon_{\text{wait}, 0.01}$. It is however still considerably large.

The conclusions that may be drawn from the results presented in this section is as follows. Recall that the time gain of the inter-clump simulation is not obtainable unless a stand-alone simulation procedure for the clumps exists (Sec. 2.6.1). The results show that even though the time gain during clump simulation for realistic levels is smaller than the time gain of the inter-clump simulation it is still well above 1 why the clump simulation is not prohibitive for the applicability of the Slepian Model Simulation Method. The process simulation, being a mixture of waiting time and clump simulations, may not exhibit as high time gain factors as the time gain factors obtained for the pure inter-clump simulation. The time gain is, however, still high and rapidly increasing with the increasing yield level.

5.6 Summary

In this chapter several simulation results are presented for the purpose of evaluating the performance of the Slepian Model Simulation Method with respect to accuracy and time consumption. On the basis of discussions of the main trends of the time development of the plastic displace-

ment process, in hardening as well as in softening, it is concluded that the results presented here are correct and reliable. That is, except for the approximation errors inherent in the simulation methods.

Simulation results for the bilinear EPO in hardening and softening are considered. The main purpose of these simulations is the study of how well the combined simulation of clumps and inter-clump waiting times reproduces the plastic displacement process. In the hardening case the time development of the standard deviation $D[X_p]$ and the kurtosis α_4 are considered. It is explained that the stationary distribution of X_p is close to Gaussian. Except for the low initial yield level 1 the kurtosis as obtained by Slepian Model simulations and by direct simulations approach the same value close to 3. Furthermore $D[X_p]$ reaches the same stationary value. The error at the level $u = 1$ is due to the errors of the Slepian Model simulations of the plastic displacement increments. Clearly the stationary values of $D[X_p]$ and α_4 do not depend on time. Therefore, except for the first short period until stationarity, the simulations with hardening do not give much information about how well the merging of waiting time simulations and clump simulations work. This is better revealed if one regards simulations with softening. However it is noted that, except for the statistical uncertainty of α_4 , there is virtually no error in the Slepian Model simulation results for the time development of $D[X_p]$ and α_4 until stationarity.

For softening there does not exist a stationary distribution of X_p . Instead the distribution of first passage times of plastic displacement levels are considered. Obviously these distributions reflect the merging of waiting time simulations and clump simulations. Contrary to the hardening case deviations between Slepian Model simulation results and direct simulation results are present for all initial yield levels, damping ratios and softening levels. These errors increase with the plastic displacement level and they are not due to the waiting time simulations but the clump simulations. The good approximation to higher order moments of the first passage time distribution underlines the strength of the Slepian Model Simulation Method. An example shows that using an exponential waiting time distribution model gives notably bigger errors than those obtained by the waiting time distribution model considered here.

A simplified non-linear restoring force diagram is considered too. It is shown that neglecting partial restoring and kinematic hardening are reasonable assumptions for near bilinear plastic hardening/softening.

Finally results show that the Slepian Model Simulation Method performs quite well with respect to time gain. Depending on the specific simulation problem (e.g. purely waiting time, separate clumps or the full response process), and depending on damping and the complexity of the restoring force diagram, time gain factors in the range from 5 to 45 were encountered in the examples given herein. In general the overall time gain of full process simulations is high and rapidly increasing with increasing yield level.

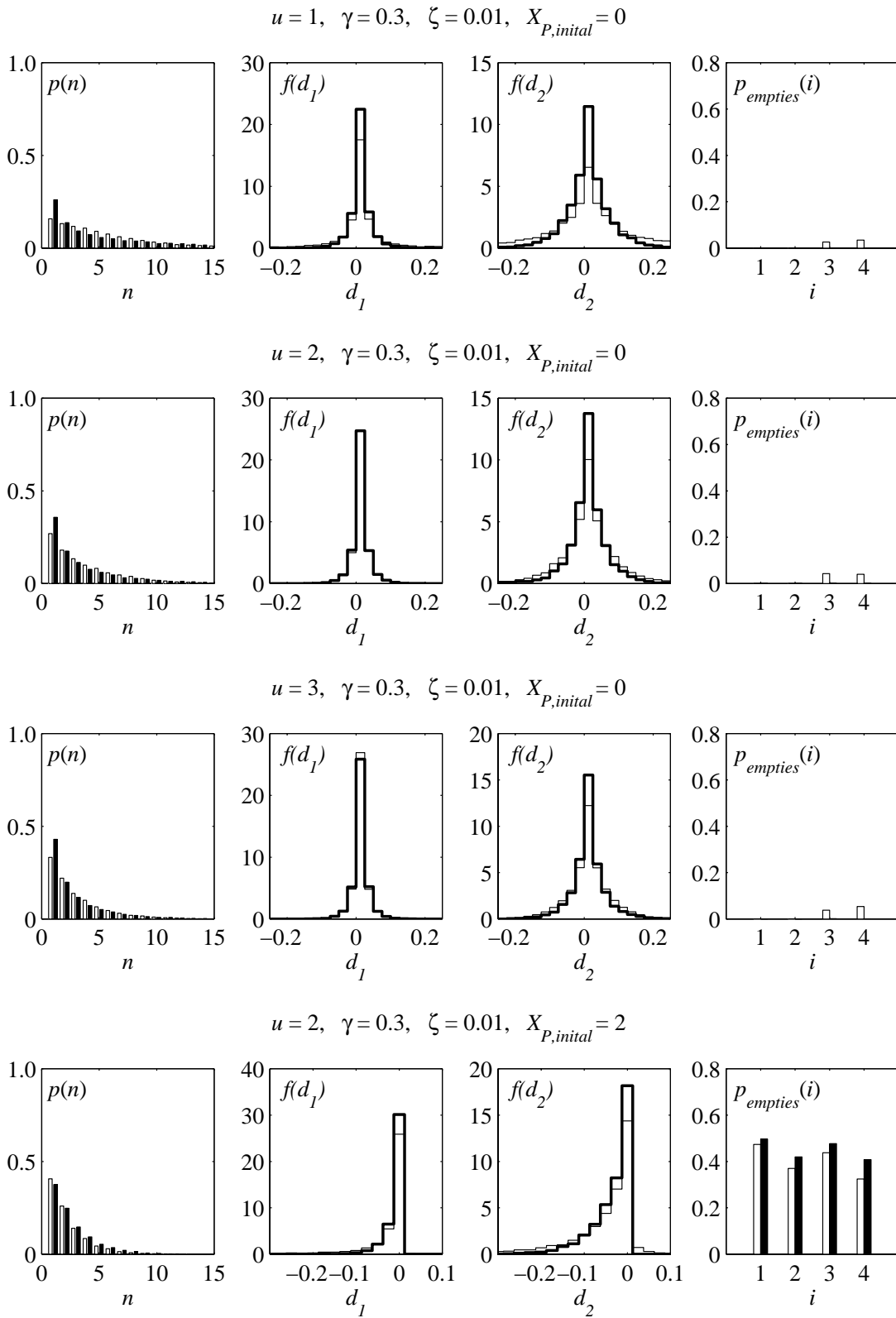


Figure 5.12: Comparison of clump simulation results obtained by Slepian simulation (thick curves) and direct non-simplified simulation (thin curves) for hardening. See p. 108.

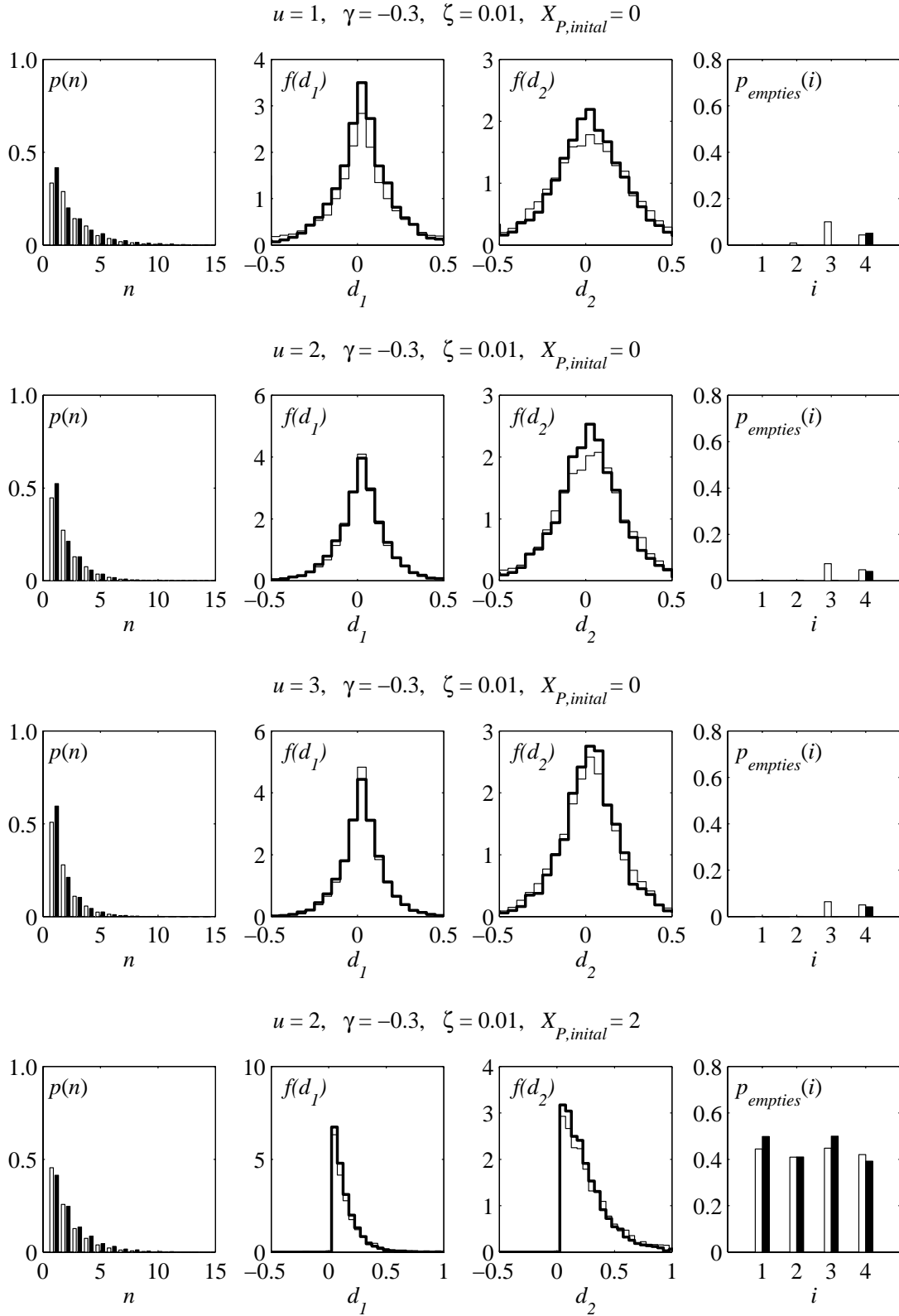


Figure 5.13: Comparison of clump simulation results obtained by Slepian simulation (thick curves) and direct non-simplified simulation (thin curves) for softening. See p. 108.

Chapter 6

Conclusions

In this first part of the thesis an effective scheme for the simulation of the time development of the degradation of a single degree of freedom (SDOF) hysteretic oscillator driven by white noise is developed. The presentation of the so-called Slepian Model Simulation Method, which is basically a time integration algorithm, is based on elasto-plastic oscillators (EPOs) for which the degradation in terms of the plastic displacement process is an important design issue. Such a simulation algorithm is of special interest for bilinear and non-linear EPOs. That is EPOs with hardening and softening, because, in opposition to the ideal EPO, only approximate analytical results exist for such EPOs – if any at all. Though the results obtained herein are based on EPOs, the results are valid for hysteretic systems in general.

The algorithm is based on three realistic assumptions about the loading and the constitution of the EPO. The oscillator is assumed lightly damped and with non-dominating hysteresis, i.e., high elasticity limits. Furthermore the load is assumed broad banded implying that it may be replaced by white noise. The consequences of these assumptions are that excursions of the elasticity limits are rare and that the response has a dominating frequency which is very close to the damped eigenfrequency of the associated linear oscillator (ALO) defined as the oscillator obtained by linearizing the EPO at the zero-point.

The simulation strategy consists in an approximate semi-analytical simulation scheme. The concept is quite simple. One observes that in certain regions of time the response experiences several, in time closely spaced excursions beyond the elasticity limits and in other time regions it does not. The regions of excursions are called *clumps* and the time between clumps is called the inter-clump waiting time. As degradation of the mechanical system is the result of the excursions, the simulation scheme divides the simulation procedure into the simulation of clumps and inter-clump waiting times.

Since the response is dominated by the eigenfrequency of the ALO the clumps are simulated in steps of half a natural period. One thus simulates one extreme after the other stepping directly from one extreme to another. This is possible due to former works [6] on the application of the so-called Slepian model to the ideal EPO. A plastic increment is obtained by simulating

an outcome of the Slepian model for the ALO response giving an extreme value of the ALO response conditional on an outcrossing. Each such outcome is termed a crest or a trough. The outcome is then transformed into a plastic increment and an elastic displacement of the EPO. The transformation uses an approximate energy consideration, regarding, during the excursion, only plastic work and elastic strain energy, i.e., neglecting damping and driving forces – the so-called Karnopp-Scharton hypothesis. In contrast to what is the case for an ideal EPO the elasticity limits change in time. Therefore they are generally asymmetric with respect to the equilibrium point of the oscillator and a new definition of clumps different from what is suggested in [16] and [6] is considered herein and found fruitful.

The simulation of the inter-clump waiting times simplifies greatly if excursions of symmetrized elasticity limits are considered. Therefore symmetrized elasticity limits defined by mirroring the elasticity limit closest to the equilibrium point and using it for both up- and downcrossings are introduced. Thus excursions of the symmetrized elasticity limits may or may not cause a plastic displacement increment, i.e. an excursion may be genuine or empty. Traditionally a clump is considered terminated when a crest/trough inside the real elasticity limits is encountered, that is, it contains only genuine excursions. In the present work it is necessary for the simplification of the inter-clump simulation that a clump is considered terminated the first time a crest/trough is inside the *symmetrized* elasticity limits. This means that clumps may contain empty excursions. Simulation results show that this new definition of the clump gives good results for the distribution of the plastic displacement increments in a clump. It is therefore concluded that introducing the new clump definition is not limiting to the applicability of the Slepian Model Simulation Method.

In Chap. 3 a discussion of the inter-clump waiting time distribution leads to an improved waiting time modeling better than the one presented in [6] and [12]. Outcrossings out of the (symmetrized) elasticity domain occur when the amplitude process, derived from the mechanical energy process, is close to the elasticity limits. As the energy level of the response drifts slowly in time the amplitude of the response builds up and fades away slowly too. This involves two implications: the amplitude process may drift around the symmetrized elasticity limit giving rise to short waiting times, or it may go far below the symmetrized elasticity limit giving rise to long waiting times. Therefore clumps arrive in clumps and one may think of the plastic displacement process in terms of clumps of clumps. This effect has not been properly accounted for in previous works like [6] and [12]. In these works it has been neglected because the tendency of clumping of clumps vanishes asymptotically as the elasticity limits tend to infinity. As pointed out herein the convergence to the asymptotic result is slow, why the clumping of clumps cannot be neglected for realistic elasticity limits and damping ratios.

In [6] the inter-clump waiting time was, in accordance with the asymptotic result, assumed exponential. As mentioned this is not realistic. The assumption however still holds true for the long waiting time between clumps of clumps which is approximately of exponential type as the waiting times are so large that approximate independence of the arrivals of clumps of clumps is obtained. Consequently the long waiting times are simulated by drawing from an exponential distribution. The waiting times within clumps of clumps are on the other hand not

governed by such a simple rule, why they cannot be simulated from a single distribution. Instead it is simulated by discretizing the amplitude process using time steps of half the natural period of the ALO. The discretization, giving rise to an amplitude model, involves the linear regressions of the displacement and the velocity on the amplitude half a period before, i.e. it involves Slepian models for the displacement and the velocity. Thus the amplitude model itself is not a Slepian model, but it is based on a Slepian model pair. This discretization gives results in very good agreement with results obtained by direct numerical time integration. The discretized amplitude process proves useful also for the computation of the parameter used in the exponential distribution of the long waiting times. This parameter is interpretable as the conditional mean crossing rate of the amplitude process given that outcrossings have not occurred for a time sufficiently large to obtain approximate independence between outcrossings. A very close approximation to the conditional mean crossing rate is obtained by a proposed numerical scheme resembling a numerical solution scheme for the Fokker-Planck equation of the amplitude process employing absorbing boundaries. The examples in Chap. 5 show that using an exponential distribution for the waiting time does not account as well for the clumping of clumps as the herein suggested waiting time approximation does.

The motivation for the application of the Slepian Model Simulation Method is twofold. First of all it provides a simulation scheme by which results concerning the response of systems with hysteresis can be obtained. Such results are, however, obtainable by direct numerical time integration too. The second motivation therefore is to provide a scheme that is faster than direct time integration. Clearly the time gain obtained by the inter-clump waiting time simulation is considerable as many time-steps are avoided. Especially for the long waiting times the time gain is large. The clump simulation involves a transformation of ALO displacements to EPO displacements. The energy equation used for this transform cannot be too complicated. Otherwise the time gain obtained by the waiting time simulation may be lost on time costly plastic increment simulations. The usefulness of the simulation scheme to non-ideal EPOs therefore depends on the complexity of the restoring force diagram. A simplified model for the restoring force diagram is suggested in Chap. 2. The corner stone of the simplification is the treatment of unloading/reloading and the Bauschinger effect. A specific implication of the Slepian Model approach is that the simplified non-ideal diagram must have a linear part of reasonable extend. In Chap. 5 it is verified that the simplifications introduced are acceptable. In general the results presented in Chap. 5 show how very well the Slepian model simulation scheme (under the given assumptions) reproduces the results obtained by direct time integration. Finally the results show that the method performs quite well with respect to time gain. Depending on the specific simulation problem (e.g. purely waiting time, separate clumps or the full response process), and depending on damping and the complexity of the restoring force diagram time gain factors in the range from 5 to 45 were encountered in the examples given herein. In general the overall time gain of full process simulations is high and rapidly increasing with increasing yield level. Apart from the time gain the author experienced another benefit of the Slepian Model Simulation Method. Though it does not appear so, it is simpler to code the Slepian Model Simulation Method than the direct simulation method because it is more difficult to extract from the samples obtained by direct simulations information about plastic displacement increments, clump

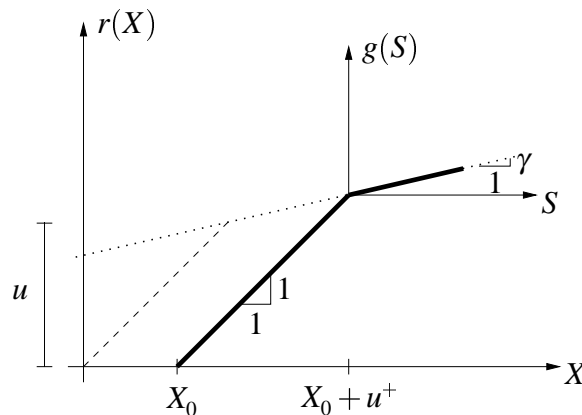
lengths etc. than it is from the samples obtained by Slepian simulations.

In closing, two remarks on possible future research in the field of application of the Slepian Model Simulation Method to EPOs seem appropriate. In this thesis only the response of non-ideal SDOF EPOs has been considered and fine time gain factors have been demonstrated. In [18] the applicability of the Slepian model to the modeling of the plastic displacement process in a multi storey frame by use of modal analysis has been considered. In that work the inter-clump waiting time distribution was modeled by an exponential distribution too. Application of amplitude model to inter-clump waiting times for an MDOF oscillator is an obvious subject of research. Especially so because the decoupling of modal energies under the assumption of modal damping makes it possible to add the mechanical energies of each of the modes. Simulating the amplitude process for a given degree of freedom as a sum of amplitude processes for each mode is then possible, provided eigenfrequencies, mode shapes and damping are so that independence of the amplitude processes may be assumed. Furthermore it is required that a mode dominating the response of the considered degree of freedom can be picked out. In this thesis the time development of the plastic process during uploading is not treated. The amplitude model applied here for the simulation of inter-clump waiting times is based on Gaussian white noise input and stationary ALO response. Clearly an investigation of the waiting time to the first excursion is a subject of interest. Regarding linear regressions of non-stationary ALO response due to Gaussian white noise input and defining on the basis of these regressions a discretized amplitude model could be a way to obtain a model for the first crossing time during uploading.

Restoring Force Diagrams

A.1 The Bilinear EPO

Compared to Fig. 2.10 the force diagram depicted in Fig. A.1 shows that some simplifications are obtained due to the idealization. The zero point X_0 (see Fig. 2.10) always equals the current



119

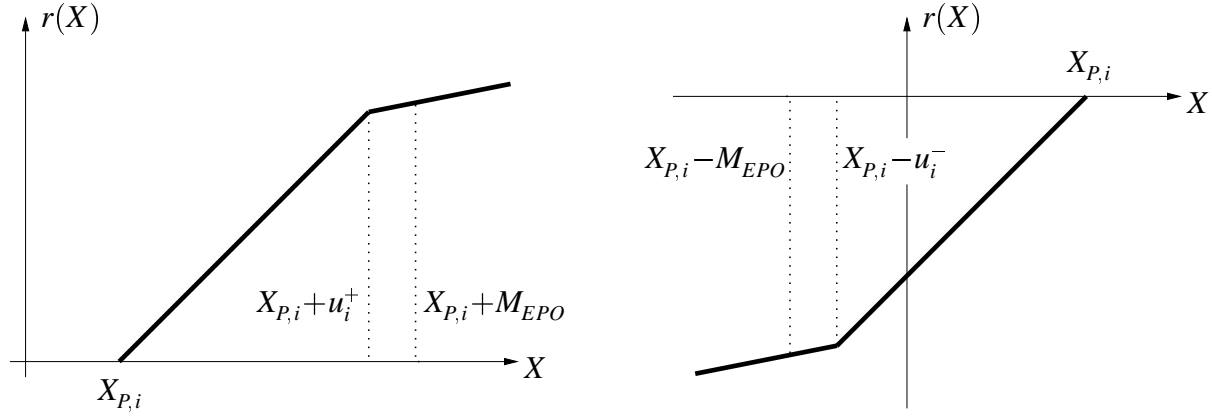


Figure A.2: The computation of M_{EPO} and updating of the plastic displacement and the yield levels using the idealized restoring force diagram.

plastic displacement and the yield limits u^\pm equal the assisting limits v^\pm (see Eq. (2.29) and Fig. 2.10). The force diagram of the bilinear EPO is so simple that the energy equations are directly derivable from the diagrams in Fig. A.2. There is no need to use formulas (2.31) and (2.34). After these few introductory remarks the relevant formulas are listed.

In the case of a maximum one derives the energy equation

$$u_i^+ (M_{EPO} - u_i^+) + \frac{1}{2} \gamma (M_{EPO} - u_i^+)^2 = \frac{1}{2} (M_{ALO}^2 - u_i^{+2}) \quad (\text{A.1})$$

leading to

$$\frac{M_{EPO}}{u_i^+} = \begin{cases} 1 + \frac{1}{\gamma} \sqrt{1 + \gamma \left(\frac{M_{ALO}^2}{u_i^{+2}} - 1 \right)} - \frac{1}{\gamma} & \text{for } \gamma \neq 0 \\ 1 + \frac{1}{2} \left(\frac{M_{ALO}^2}{u_i^{+2}} - 1 \right) & \text{for } \gamma = 0 \end{cases} \quad (\text{A.2})$$

The associated updating formulas read

$$X_{P,i+1} = X_{P,i} + (1 - \gamma) (M_{EPO} - u_i^+) \quad (\text{A.3a})$$

$$u_{i+1}^+ = u + \frac{\gamma}{1 - \gamma} X_{P,i+1} \quad (\text{A.3b})$$

$$u_{i+1}^- = u - \frac{\gamma}{1 - \gamma} X_{P,i+1} \quad (\text{A.3c})$$

and the plastic displacement increment becomes

$$D_i = (1 - \gamma) (M_{EPO} - u_i^+) \quad (\text{A.4})$$

For a minimum the energy equation correspondingly reads

$$u_i^- (M_{EPO} - u_i^-) + \frac{1}{2} \gamma (M_{EPO} - u_i^-)^2 = \frac{1}{2} (M_{ALO}^2 - u_i^{-2}) \quad (\text{A.5})$$

This energy equation leads to

$$\frac{M_{EPO}}{u_i^-} = \begin{cases} 1 + \frac{1}{\gamma} \sqrt{1 + \gamma \left(\frac{M_{ALO}^2}{u_i^{-2}} - 1 \right)} - \frac{1}{\gamma} & \text{for } \gamma \neq 0 \\ 1 + \frac{1}{2} \left(\frac{M_{ALO}^2}{u_i^{-2}} - 1 \right) & \text{for } \gamma = 0 \end{cases} \quad (\text{A.6})$$

and the associated updating formulas read

$$X_{P,i+1} = X_{P,i} - (1-\gamma)(M_{EPO} - u_i^-) \quad (\text{A.7a})$$

$$u_{i+1}^+ = u + \frac{\gamma}{1-\gamma} X_{P,i+1} \quad (\text{A.7b})$$

$$u_{i+1}^- = u - \frac{\gamma}{1-\gamma} X_{P,i+1} \quad (\text{A.7c})$$

from which it follows that the plastic displacement increment is

$$D_i = (1-\gamma)(u_i^- - M_{EPO}) \quad (\text{A.8})$$

Finally it is noted that the above formulas are valid also for strain softening: $\gamma < 0$. The only difference is that the oscillator may collapse. The exact bounds of collapse in this ideal bilinear model are given by

$$|X| = \frac{\gamma-1}{\gamma} u \quad (\text{A.9})$$

A.2 A Non-Idealized EPO

Figure A.3 taken from Sec. 2.5 shows the names used in characterizing the simplified restoring force diagram. The function $g(s)$ considered in Sec. 5.4 of course fulfills the requirement that a closed form analytical expression for the integral of the curved part exists. In addition to this it has convenient scaling and translation properties which allows also a non-simplified restoring force diagram to be constructed from g . Or from another point of view: the simplified diagram may be regarded as derived from a more general diagram defined by g . Here details of the construction of the non-simplified diagram are given.

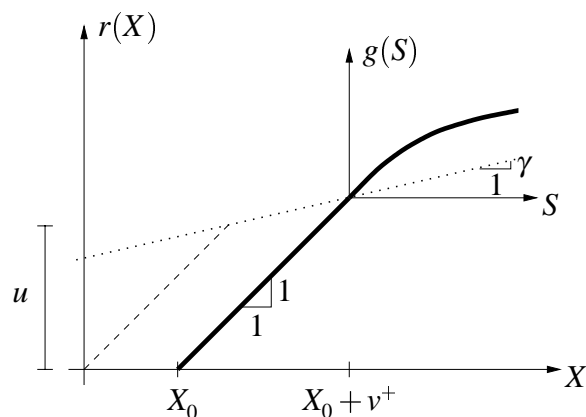


Figure A.3: The characterization of the simplified restoring force diagram.

A.2.1 The Simplified Restoring Force Diagram

Figure A.4 shows a schematic of the curved part including some of the parameters appearing in the definition

$$g(s) = \gamma s + \eta - \frac{\kappa \rho}{(s + s_a)^{1+\kappa}} \quad (\text{A.10})$$

As $g(0) = 0$ the abscissa s_a of the vertical asymptote is related to the other parameters through

$$s_a = \sqrt[1+\kappa]{\frac{\kappa\rho}{\eta}} \quad (\text{A.11})$$

The expression for the integral of g is easily obtained and has a simple form:

$$\int g(s)ds = \frac{1}{2}\gamma s^2 + \eta s + \frac{\rho}{(s+s_a)^\kappa} \quad (\text{A.12})$$

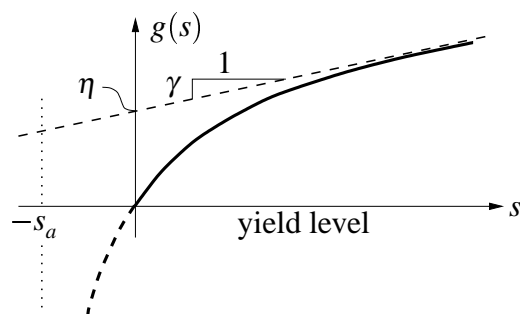


Figure A.4: Schematic of the curved part of the simplified restoring force diagram.

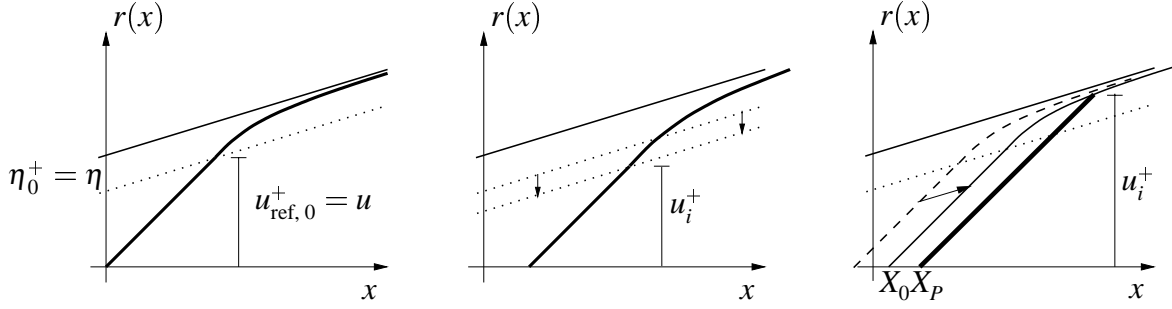


Figure A.5: Scaling (in the middle) and translating (to the right) the curved part of the non-simplified restoring force diagram. To the left the initial configuration.

A.2.2 The Non-Simplified Restoring Force Diagram

Two assumptions are introduced in the definition of the simplified restoring force diagram: hardening/softening is independent and partial reversed loading is neglected. Both these assumptions are loosened here. Now hardening is assumed kinematic and partial reversed loading is included in the model. Therefore, after a load reversal, yielding does not start at the inclined dotted line as shown in Fig. A.3. Yielding may onset either below or above the dotted line. This is shown in Fig. A.5 (showing the case of hardening). It is however still assumed that the inclined asymptotes do not change (the solid inclined line in Fig. A.5). The construction of the non-simplified diagram from g is carried out as follows. Consider a maximum as depicted in Fig. A.5. If the yield limit is below the inclined dotted line (the diagram in the middle) the dotted line is shifted downwards so that it coincides with the yield level. Thus the reference yield level u_{ref}^+ changes from $u_{\text{ref},i}^+$ to $u_{\text{ref},i+1}^+$. The curved part is scaled such that it fits in the space in between the two inclined lines. This scaling is equal in horizontal and vertical direction, so that the shape is not changed. Denoting the vertical extend of this space before and after shifting the inclined line, respectively, η_i^+ and η_{i+1}^+ , then one simply has

$$\eta_{i+1}^+ = \eta_i^+ - (u_{\text{ref},i+1}^+ - u_{\text{ref},i}^+) \quad (\text{A.13a})$$

$$\rho_{i+1}^+ = \rho_i^+ \left(\frac{\eta_{i+1}^+}{\eta_i^+} \right)^{2+\kappa} \quad (\text{A.13b})$$

$$s_{a,i+1}^+ = s_{a,i}^+ \frac{\eta_{i+1}^+}{\eta_i^+} \quad (\text{A.13c})$$

where

$$u_{\text{ref},i+1}^+ = u_i^+ - \frac{\gamma}{1-\gamma} X_{P,i} \quad (\text{A.14})$$

Further one sets $X_0 = X_{P,i}$ and $v^+ = u_i^+$. If, on the other hand, the onset of yielding is above the inclined line (to the right in Fig. A.5) but not on the curved part, then the curved part is

translated along the inclined line until the curved part includes the yield point. This corresponds to changing X_0 . After translation X_0 must fulfill the conditions:

$$v^+ + g(s) = u_i^+ \quad (\text{A.15})$$

$$s = (X_{P,i} + u_i^+) - (X_0 + v^+) \quad (\text{A.16})$$

$$v^+ = u_{\text{ref},i}^+ + \frac{\gamma}{1+\gamma} X_0 \quad (\text{A.17})$$

which, due to the simplicity of g , can be solved analytically giving

$$X_0 = (1 - \gamma) \left[b + s_{a,i}^+ - \sqrt[1+\kappa]{\frac{-\kappa \rho_i^+}{u_i^+ - u_{\text{ref},i}^+ - \eta_i^+ - \gamma b}} \right] \quad (\text{A.18})$$

where $b = X_{P,i} + u_i^+ - u_{\text{ref},i}^+$. After translation u_{ref}^+ , s_a^+ , η^+ and ρ^+ are all unchanged. Having scaled or translated the curved part, the computation and updating of yield levels and plastic displacement follow (2.32a-b) and (2.33). Due to kinematic hardening the lower yield limit u_{i+1}^- is given by

$$u_{i+1}^- = 2u - u_{i+1}^+ \quad (\text{A.19})$$

where u is the initial symmetric yield limit.

The above formulas were provided a maximum. For a minimum the formulas for scaling become

$$X_0 = X_{P,i} \quad (\text{A.20})$$

$$v^- = u_i^- \quad (\text{A.21})$$

$$u_{\text{ref},i+1}^- = u_i^- + \frac{\gamma}{1-\gamma} X_{P,i} \quad (\text{A.22})$$

$$\eta_{i+1}^- = \eta_i^- - (u_{\text{ref},i+1}^- - u_{\text{ref},i}^-) \quad (\text{A.23})$$

$$\rho_{i+1}^- = \rho_i^- \left(\frac{\eta_{i+1}^-}{\eta_i^-} \right)^{2+\kappa} \quad (\text{A.24})$$

$$s_{a,i+1}^- = s_{a,i}^- \frac{\eta_{i+1}^-}{\eta_i^-} \quad (\text{A.25})$$

And for translation the formula for the updating of X_0 reads

$$X_0 = (1 - \gamma) \left[-b - s_{a,i}^- + \sqrt[1+\kappa]{\frac{-\kappa \rho_i^-}{u_i^- - u_{\text{ref},i}^- - \eta_i^- - \gamma b}} \right] \quad (\text{A.26})$$

where $b = -X_{P,i} + u_i^- - u_{\text{ref},i}^-$. After translation or scaling the computation and updating of yield levels and plastic displacement follow (2.35a-b) and (2.36). Due to kinematic hardening the upper yield limit u_{i+1}^+ is given by (u is the initial symmetric yield limit)

$$u_{i+1}^+ = 2u - u_{i+1}^- \quad (\text{A.27})$$

It remains only to note that though the formulas presented on the previous pages were derived on the basis of hardening they are so general that they are also valid for softening.

A.3 A Few Phrases used in the Theory of Plasticity.

When subject to loads a plastic material experiences that its yield limits develop in time. If, after an uploading resulting in the material exceeding the yield limits, the material is unloaded, it generally behaves like a linear material. If the material is loaded up again its yield limit has changed due to the previous uploading. This course of events is called *uploading, unloading and reloading*. If after an uploading the load is reversed, the material will, provided the load is sufficiently strong, yield too at a yield level generally different from the one met during uploading. In the restoring force diagram this will appear as a hysteresis loop. The name for this phenomenon is the *Baushinger effect*.

There exist different models for how the yield limits develop in hardening/softening. In the present work knowledge of kinematic, isotropic and independent hardening/softening is required. Kinematic hardening/softening means that the distance from the lower yield limit to the upper yield limit is constant. That is, the sum $u^+ + u^-$ is independent of time. This corresponds to how the elasticity limits develop in time in bilinear hysteresis. Isotropic hardening means that the upper and the lower elasticity limits are always of the same absolute value, i.e. $u^+ = u^-$. Hardening/softening is said to be independent if there is not a rule, as there is for kinematic and isotropic hardening/softening, that relates u^+ and u^- to each other.

Part II

Vibrations in Systems with Fuzzy Sub-Systems

Chapter 1

Introduction

The background of the work presented in this part of the thesis and the basic governing equations of the considered problem are given in the present chapter.

1.1 Background and Mechanical Modeling

The problem treated here originates in the field of acoustics of submerged ship hulls, e.g. a submarine. One is typically interested in the acoustic field radiated from the submerged elastic structure due to internal dynamical loads stemming from engines etc. The ship hulls are equipped with numerous instruments and mechanical devices of small size compared to the size of the ship hull. It is a well-known experience that all these devices are never fully rigidly mounted on the hull structure, either because it is simply not the intention, or because vibrations of the hull will gradually loosen the joints by which the devices are attached to the structure. They may therefore affect the dynamical characteristics of the hull by more than a mere addition of mass. Accounting for the influence of the devices requires mechanical modeling of the devices as small elastic sub-structures. The precise assessment of the number of devices, their location within the hull, and their dynamical properties is a difficult task to carry out. This may be so for many reasons, for example: 1) devices may be added, changed or moved elsewhere after the design of the structure is completed, 2) the stiffness and damping characteristics of gradually loosened joints is known to be difficult to assess. Furthermore there may be so many devices that a detailed modeling of each device is too cumbersome a task. Appreciating all this, it is clear that a less detailed overall modeling of the devices may be a reasonable way to go. For this purpose the theory of the so-called *structural fuzzy*, initiated by Soize [20], has been developed in the literature. In this theory, all the devices, termed *fuzzy sub-structures*, are considered minor secondary mechanical structures attached to a primary major structure termed the *master structure*, e.g. the hull. In the remainder of this thesis the fuzzy sub-structures and the master structure are for short termed the *fuzzies* and the *master*, respectively.

Depending on the frequency content of the acoustic field relative to the eigenfrequencies of the fuzzies, the fuzzies will influence the dynamical properties of the master in different ways. If the frequency range of the acoustic field is situated below the eigenfrequencies of the fuzzies, i.e. in the so-called low-frequency range, the fuzzies will mainly contribute an added-mass effect to the hull as they experience essentially only static displacements relative to the master. When, on the other hand, the frequency range of the acoustic field coincides with the range of fuzzy eigenfrequencies, the fuzzies are excited and the interaction between the fuzzies and the master becomes important for the predictions of the acoustic field radiated from the master. In this medium-frequency range the effect of the fuzzies is that they absorb a lot of the vibratory energy, an effect similar to the basic principle of mass tuned dampers. For sound frequencies in the high-frequency range well above the fuzzy eigenfrequencies matters are simple like in the low-frequency. The fuzzies contribute added stiffness as they exhibit virtually no oscillations themselves.

The theory of structural fuzzy is relevant to other disciplines than that of acoustics. Damping of mechanical and structural systems is a vast field with many branches. As pointed out by Strasberg and Feit in [21], the source of the relatively large damping experienced in mechanical and structural systems, inexplicable by the inherent dissipation due to internal material damping, is known to be due to minor elements non-rigidly attached to a main structure. This is a situation similar to the devices inside the submerged ship hull. In their papers they treat the elements as resonant sprung masses and prove how the masses greatly increase the damping over a wide frequency range, that is, over the medium-frequency range. As implicitly noted earlier, this behaviour is not surprising since it has long been known that individual sprung masses can behave as dynamic vibration absorbers when tuned properly to the specific frequencies which need damping.

In this thesis, the focus is put on the investigation of the interplay of the fuzzies and the master when excitation is in the medium-frequency range where contributions to the damping of the master is high. As explained in [20] this is a relevant subject of investigation, since, up till now, the models used for the low- and high-frequency range analyses do not give satisfactory results for the medium range because of the neglected resonance of the fuzzies. The relevance is further supported by the applicability to structural and mechanical damping modeling in the area of which the authors of [22] see potential use of the herein presented results mainly taken from [22].

1.1.1 Modeling the Master and the Fuzzies

In [21] Strasberg and Feit investigates systems in which the fuzzies are discrete and deterministically given. They do so in order to focus on the demonstration of the influence of the fuzzies on damping. This model choice for the fuzzies is however not realistic, since information about the fuzzies in reality is uncertain. Soize suggests a probabilistic modeling of the fuzzies and a general numerical approach to the computation of the effects of the fuzzies on the master. Here the

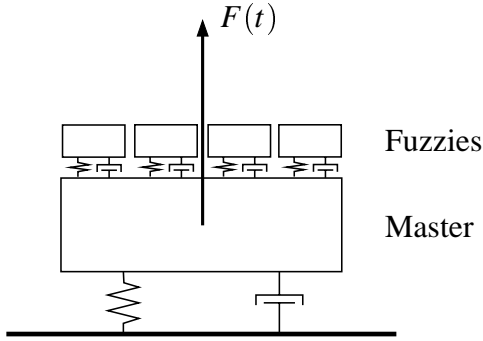


Figure 1.1: The model system of an SDOF master with SDOF fuzzies.

probabilistic approach is adapted too, as it is the most meaningful. Furthermore, as a case study, two specific types of random fields, of interest in many practical applications, are employed in modeling the distribution of the fuzzies over the master, namely, the homogeneous Poisson square-wave and the homogeneous Poisson impulse point fields. Hereby specific approximate results quantifying the effects of the fuzzies is obtained by application of the Winterstein approximation technique. The strength of these results is that, via the Winterstein approximation, a mapping from standard Gaussian variables is obtained opening for possible application in numerical reliability methods.

The specific simple model system investigated here is build out of single degree of freedom (SDOF) oscillators as depicted in Fig. 1.1. The system consists of a viscously damped linear SDOF master supporting an ensemble of likewise viscously damped linear SDOF oscillators. It is in this study, as a further simplifying step, assumed that the fuzzies are located along a line on the master such that line fields are sufficient to model the random properties of the fuzzies, i.e. mass, damping ratio and eigenfrequency. The aim of this simplified study is to demonstrate the validity of two different hypotheses about the influence on the damping effect of the specific modeling of the fuzzies. The response characteristics used to explore the damping effect of the fuzzies are related to the steady state response due to harmonic loading. As the driving point impedance of the master provides essential information about the damping effect of the fuzzies on forced response it is natural to consider the impedance. Whereas the impedance is much used in acoustics the frequency response function, easily obtainable from the impedance, is widely used in structural and mechanical engineering. Therefore the frequency response function, which will also reflect the damping effect of the fuzzies, is considered. Especially the phase angle and the amplification factor are regarded. The hypotheses to investigate are the following: 1) the standard deviation of the change in impedance due to the fuzzies cannot always be neglected, and 2) for this variance to be detected it is not a prerequisite that the fuzzies be modeled by a discrete system, they may as well be modeled by a non-discrete continuous field, provided it is not too rapidly fluctuating. These hypotheses relate to a paper by Lin [17] in which he points out that in former research ([20] and [21]) only the mean and not the variance of the

change in impedance has been examined. This is a limitation which can give misleading results in realistic cases where the standard deviation can easily be of the same order of magnitude as the mean value. The second hypothesis is due to the following argument by Lin: In [21] the sums resulting from the discrete fuzzy model are replaced by integrals. This being equivalent to converting the number of fuzzies to uncountable infinity implies that the most important effect of resonance when the excitation frequency coincides with the eigenfrequency of any single fuzzy is accorded with probability zero. Based on this argument he claims that the application of continuous fields give rise to errors. Here it is, however, argued that the dynamical damping effect of the fuzzies is also experienced if excitation frequencies within the eigenfrequency range of a continuous field of fuzzies appear. Though not optimal, a single fuzzy still exhibits a dynamical damping effect if it is excited at a near resonant frequency. Thus, if the field has reasonable correlation length there will be sufficiently high probability that fuzzies of eigenfrequencies close to a given excitation frequency is accorded, and consequently a non-zero and non-negligible set of fuzzies is excited at a near-resonant frequency, why the damping effect is still present.

1.1.2 Governing Equations, Impedance and Frequency Response

Driving Point Impedance of A single Sprung Mass

It is useful for the following derivations, and instructive for the understanding and discussion of results, to regard first the driving point impedance of a single sprung mass subjected to support motions. The situation is depicted in Fig. 1.2 in which x is the support motion and y the motion of the mass relative to the support. The impedance Z_{supp} is defined by the ratio of the force applied at the driving point and the velocity of the driving point, where the driving point in this case is the support:

$$Z_{\text{supp}} = \frac{f}{v_x} \quad (1.1)$$

where $v_x = \dot{x}$. Due to the reaction of the sprung mass on the support the force f required in (1.1) is given by:

$$\frac{f}{m} = -\omega_0^2 \int v_y dt - 2\zeta_0 \omega_0 v_y \quad (1.2)$$

where for convenience the expression is stated in terms of the relative velocity $v_y = \dot{y}$. Combining this expression with the equation of motion (expressed in terms of the velocities too)

$$\dot{v}_y + 2\zeta_0 \omega_0 v_y + \omega_0^2 \int v_y dt = -\dot{v}_x \quad (1.3)$$

an expression for Z_{supp} can be derived. In all that follows henceforward the harmonic steady state complex time dependence $e^{i\omega t}$, where ω is the driving frequency of $f(t)$, is implicitly

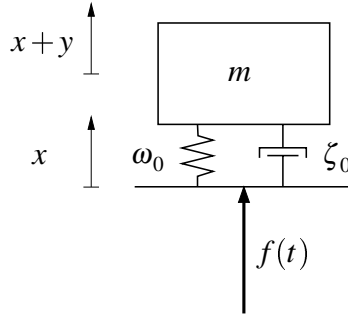


Figure 1.2: A single sprung mass subjected to support motions.

assumed. Denoting by \hat{f} and \hat{v}_x the phasors of f and v_x , respectively, and exploiting that the phasors of \dot{v}_x and $\int v_x$ are $i\omega\hat{v}_x$ and $-i\hat{v}_x/\omega$, respectively, one finds from (1.2) and (1.3) that

$$Z_{\text{supp}} = \frac{\hat{f}}{\hat{v}_x} = im\omega \left(1 + \frac{1}{a^2 - 1 + i2\zeta_0 a} \right) \quad (1.4)$$

in which $a = \omega_0/\omega$ is the ratio of the eigenfrequency to the driving frequency. It is from Eq. (1.4) that the damping effect of the fuzzies can be revealed. The power consumed by the sprung mass is largest if the force f and the velocity v_x are in phase, that is, if the impedance is real. At resonance $a = 1$ and $Z_{\text{supp}} \approx m\omega_0/2\zeta_0$ (for low damping) which shows that dynamical damping is most effective at resonance. Furthermore it shows that the driving force, due to resonance of the mass, is many times larger than the driving point velocity ensuring effective damping. It is noted that resonance means maximum velocity of the sprung mass, whereas it means minimum velocity of the driving point. That is, the driving point experiences antiresonance as the result of the dynamical damping. Finally it is noted that clearly Z_{supp} need not be purely real for the sprung mass to receive considerable dynamical power. This implies that near resonance, excitation still causes dynamic damping.

Frequency Response of Complete System

Using the above result, it is easy to derive expressions for the impedance and then also the frequency response function of the discrete system in Fig. 1.1. In the following M , ω_0 and ζ_0 denote the mass, the eigenfrequency and the damping ratio of the master, respectively, and F denotes the force applied to the master. Let further f_j denote the force acting on the support of the j 'th fuzzy, $j = 1 \dots N$. The equation of motion of the master is then given by

$$\ddot{x} + 2\zeta_0\omega_0\dot{x} + \omega_0^2x + \sum_{j=1}^N \frac{f_j}{M} = \frac{F}{M} \quad (1.5)$$

Rephrasing the equation of motion in terms of velocities one immediately sees that the impedance of the master is given by

$$Z = M \left[2\zeta_0\omega_0 + i\omega \left(1 - \left(\frac{\omega_0}{\omega} \right)^2 \right) \right] + \sum_{j=1}^N Z_{\text{supp},j} \quad (1.6)$$

Substituting Z_{supp} from (1.4) and rearranging terms gives

$$Z = M \left[2\zeta_0\omega_0 + V(\omega) + i\omega \left(1 - \left(\frac{\omega_0}{\omega} \right)^2 \right) + iR(\omega) \right] \quad (1.7)$$

in which $V(\omega)$ and $R(\omega)$, respectively, account for the real viscously resistive and the imaginary reactive contributions to the impedance from the fuzzies. Let η_j , Ω_j and ζ_j denote for the j 'th fuzzy the ratio of its mass to M , its eigenfrequency and its damping ratio. Furthermore let $a_j = \Omega_j/\omega$, then $V(\omega)$ and $R(\omega)$ are given by

$$V(\omega) = \omega \sum_{j=1}^N \chi(a_j, \zeta_j) \eta_j, \quad R(\omega) = \omega \sum_{j=1}^N \gamma(a_j, \zeta_j) \eta_j \quad (1.8)$$

The functions $\chi(a, \zeta)$ and $\gamma(a, \zeta)$ are intimately related to the driving point impedance of a single sprung fuzzy, as

$$\chi(a, \zeta) + i\gamma(a, \zeta) = i \left(1 + \frac{1}{a^2 - 1 + i2\zeta a} \right) \quad (1.9)$$

giving

$$\chi(a, \zeta) = \frac{2\zeta a}{(a^2 - 1)^2 + 4\zeta^2 a^2}, \quad \gamma(a, \zeta) = \frac{a^2(a^2 - 1 + 4\zeta^2)}{(a^2 - 1)^2 + 4\zeta^2 a^2} \quad (1.10)$$

As the impedance gives a relation between the forcing and the velocity response, the frequency response function $H(\omega)$ is of course closely related to the $Z(\omega)$. Since H gives the relation $\hat{x} = H \frac{\hat{F}}{M}$ between the phasor \hat{F}/M of the mass normalized forcing and the phasor \hat{x} of the response, one has the relation

$$H(\omega) = \frac{M}{i\omega Z} = \frac{1}{\omega_0^2 - \omega^2 - \omega R(\omega) + i(2\zeta_0\omega_0\omega + \omega V(\omega))} \quad (1.11)$$

The generalization of the above formulas to a continuous distribution of fuzzies is presented in chapter 2.

1.2 Outline of the Following Chapters

- Chapter 2.** discusses the modeling of the fuzzies by either a discrete or a continuous model.
- Chapter 3.** presents, for a specific example, results for the impedance and frequency response using Winterstein approximations and compares them with simulation results.
- Chapter 4.** presents the conclusions.
- Appendix A.** presents the derivation of the first four moments of integrals of Poisson fields as used in the Winterstein approximations.

1.3 Summary

It is explained why the change in dynamical characteristics of a major main structure due to the attachment of several minor elastic sub-structures is a relevant subject of research. Especially it is argued that the problem is of random nature as the knowledge about the sub-structures is uncertain, for what reason the sub-structures are termed structural fuzzy, or for short fuzzies. The main structure is termed the master structure. Depending on the excitation of the master, the fuzzies may have a damping effect on the response of the master. Here it is suggested to investigate the changes in the impedance and the frequency response function of the main structure due to the fuzzies. Both quantities, relevant to harmonic steady state response, will reveal possible damping effects.

It is argued that the structural fuzzy may be modeled by both discrete models and continuous field models, without losing the resonant dynamical damping effect of the fuzzies. This is provided that in the latter case the correlation length of the field is reasonable large. As a specific case study a viscously damped linear SDOF master equipped with likewise viscously damped linear SDOF fuzzies is suggested. In that case, deriving the statistical moments of the change in impedance, allowing semi-analytical computations based on Winterstein approximations, is practicable if the fuzzies are modeled by homogeneous Poisson fields.

Finally, formulas for the impedance and the frequency response function for a discrete fuzzy model are derived, whereas the formulas for the continuous model are postponed till later.

Chapter 2

Modeling the Fuzzies

Whether it is possible to obtain a dynamical damping effect when the field of fuzzies is modeled by a continuous field or not is the subject of the present chapter. That it is in fact possible is shown by demonstrating asymptotic equivalence between a specific discrete and a specific non-discrete piecewise continuous fuzzy field model. Furthermore the distributional properties of the reactive and resistive dissipative contributions of the fuzzies to the impedance, including their Winterstein approximations, are discussed.

2.1 A Discrete Fuzzy Model

For the SDOF master regarded herein, the distribution of the fuzzies over the master has no influence on the change in impedance due to the fuzzies. So, in the discrete fuzzy model no assumptions are made about the spatial distribution of the fuzzies. Consequently it seem natural to assume that there is no dependence between the dynamical characteristics of the fuzzies. Furthermore it is natural to assume that the number N of fuzzies is random. Following the notation introduced in Sec. 1.1.2, each fuzzy is represented by a triplet of random variables (η, Ω, ζ) . As two further simplifying assumptions all triplets are assumed equally distributed and the variables η , Ω , and ζ are assumed mutually independent. It is conjectured that in most cases this is realistic assumption. Finally it is for computational ease henceforth assumed that ζ is deterministic and equal for all fuzzies.

Due to the independence of the fuzzy eigenfrequencies one can, without loss of generality, imagine that for any realization of the discrete fuzzy field, the eigenfrequencies are sorted in ascending order. Plotting the sorted eigenfrequencies on an axis, it is clear that one can consider the eigenfrequencies as a realization of an inhomogeneous Poisson point field. Denote in the following this frequency axis the ν -axis, and let the Poisson counting process, counting the number of eigenfrequencies below ν , be denoted $N(\nu)$. Naming further the inhomogeneous

mean rate of the counting process $\lambda(v)$ then

$$\mu_N = E[N(\infty)] = \int_0^\infty \lambda(v) dv < \infty \quad (2.1)$$

where the inequality sign expresses a restriction put on $\lambda(v)$ ensuring similarity of $\lambda(v)$ to a density function. Since an infinity of fuzzies never occur this restriction is clearly not a limitation. Under the above assumption one finds that $R(\omega)$ has the mean (suppressing ζ in $\chi(a, \zeta)$ and $\gamma(a, \zeta)$ as ζ is assumed deterministic)

$$E[R(\omega)] = \omega E[\eta] \int_0^\infty \gamma\left(\frac{v}{\omega}\right) \lambda(v) dv \quad (2.2)$$

and the covariance

$$\text{Cov}[R(\omega_1), R(\omega_2)] = \omega_1 \omega_2 E[\eta^2] \int_0^\infty \gamma\left(\frac{v}{\omega_1}\right) \gamma\left(\frac{v}{\omega_2}\right) \lambda(v) dv \quad (2.3)$$

Similar expressions may be written for $V(\omega)$, the cross-covariance $\text{Cov}[R(\omega_1), V(\omega_2)]$, etc.

The above results may be obtained using the following approach. The conditional probability that the number N_u of fuzzy eigenfrequencies below u is less than n_u given $\mu_N = n$ is

$$P\{N_u \leq n_u \mid \mu_N = n\} = \frac{1}{n} \int_0^u \lambda(v) dv \quad (2.4)$$

Since $R(\omega)$ is given by the sum

$$R(\omega) = \sum_{j=1}^{N(\infty)} \eta_j \gamma\left(\frac{\Omega_j}{\omega}\right) \quad (2.5)$$

the mean and the covariance functions of $R(\omega)$ may be computed by

$$E[R(\omega)] = E[E[R(\omega) \mid N(\infty)]] \quad (2.6)$$

$$\begin{aligned} \text{Cov}[R(\omega_1), R(\omega_2)] &= E[\text{Cov}[R(\omega_1), R(\omega_2) \mid N(\infty)]] \\ &\quad + \text{Cov}[E[R(\omega_1) \mid N(\infty)], E[R(\omega_2) \mid N(\infty)]] \end{aligned} \quad (2.7)$$

Due to independence and equality of distributions one gets

$$E[R(\omega) \mid N(\infty) = n] = n E[\eta] E\left[\gamma\left(\frac{\Omega}{\omega}\right) \mid N(\infty) = n\right] = n E[\eta] \int_0^\infty \gamma\left(\frac{v}{\omega}\right) \frac{\lambda(v)}{n} dv \quad (2.8)$$

and thereupon, by substitution into Eq. (2.6), Eq. (2.2) is obtained. Following the same approach $\text{Cov}[R(\omega_1), R(\omega_2)]$ etc. are obtained by somewhat more involved, but simple, manipulations.

This section is closed by stating that the correlation coefficient between $R(\omega)$ and $V(\omega)$ is (note the change of integration variabel)

$$\rho[R(\omega), V(\omega)] = \frac{\int_0^\infty \gamma(a) \chi(a) \lambda(\omega a) da}{\sqrt{\int_0^\infty \gamma(a)^2 \lambda(\omega a) da \int_0^\infty \chi(a)^2 \lambda(\omega a) da}} \quad (2.9)$$

2.2 A Non-Discrete Field Fuzzy Model

For rigid bodies with more than one degree of freedom, or for flexible structures, e.g. a beam, the spatial distribution of the fuzzies over the master is of course important for the evaluation of the impedance of the whole system of master and fuzzies. Therefore field models for fuzzies are of interest too.

A field description of the fuzzies allows for a more general modeling. Instead of being represented by random triplets $(\eta_j, \Omega_j, \zeta_j)$ the system of fuzzies is now be described by a triplet of random fields $[\eta(\xi), \Omega(\xi), \zeta(\xi)]$, where $\xi \in I$ is the spatial coordinate. A discrete system of fuzzies is just a special case in which the triplet of random fields corresponds to randomly positioned Dirac delta functions. Under this general setting the equation of motion for the master is (suppressing in most terms the time argument)

$$\ddot{x} + 2\zeta_0\omega_0\dot{x} + \omega_0^2x - \int_I [2\zeta(\xi)\Omega(\xi)\dot{y}(\xi) + \Omega(\xi)^2y(\xi)]\eta(\xi)d\xi = \frac{1}{M}f(t) \quad (2.10)$$

in which $y(\xi, t)$ is the displacement field of the fuzzies relative to the master. The difference between (2.10) and (1.5) is that the finite sum is changed into an integral. The equation of motion of the single fuzzy does not change why the expression (1.7) stay unchanged. Due to the integral in (2.10) the formulas for $R(\omega)$ and $V(\omega)$ now read:

$$V(\omega) = \omega \int_I \chi\left(\frac{\Omega(\xi)}{\omega}, \zeta(\xi)\right) \eta(\xi) d\xi, \quad R(\omega) = \omega \int_I \gamma\left(\frac{\Omega(\xi)}{\omega}, \zeta(\xi)\right) \eta(\xi) d\xi \quad (2.11)$$

in which the functions $\chi(a, \zeta)$ and $\gamma(a, \zeta)$ have the same definition as in the discrete case (Eq. (1.10)). Again formulas for the mean and covariance of $R(\omega)$ and $V(\omega)$ are established. For the purpose of conciseness define the function $\Gamma(\xi, \omega) = \gamma(\Omega(\xi)/\omega, \zeta(\xi))$. Then the well-known formulas are

$$E[R(\omega)] = \omega \int_I E[\Gamma(\xi, \omega)\eta(\xi)] d\xi \quad (2.12)$$

and

$$\text{Cov}[R(\omega_1), R(\omega_2)] = \omega_1\omega_2 \int_{I \times I} \text{Cov}[\Gamma(\xi_1, \omega_1)\eta(\xi_1), \Gamma(\xi_2, \omega_2)\eta(\xi_2)] d\xi_1 d\xi_2 \quad (2.13)$$

Analogously expressions can be written for $V(\omega)$ and the cross-covariance of $R(\omega)$ and $V(\omega)$.

Before considering the non-discrete field to be defined herein, a discrete point field equivalent to the discrete model presented in the previous section is consider. Assume that the fuzzies are attached to the master along a line of length L and let the points of attachment be modeled by a homogeneous Poisson field of mean rate κ per unit length. Furthermore assign density function $f_\Omega(v) = \lambda(v)/\mu_N$ to the random fuzzy eigenfrequencies Ω , then, since the Ω 's are independent, the number of realizations of Ω in the interval $[v, v + \Delta v]$ is Poisson distributed with mean

$$\kappa L \int_v^{v+\Delta v} f_\Omega(w) dw = \frac{\kappa L}{\mu_N} \int_v^{v+\Delta v} \lambda(w) dw \quad (2.14)$$

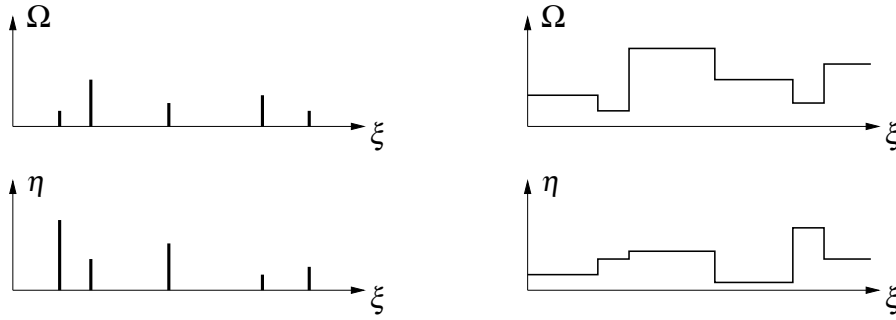


Figure 2.1: The Poisson point pulse and square-wave fields.

By choosing $\kappa L = \mu_N$, this alternative representation is equivalent to the representation discussed in the previous section.

Inspired by this Poisson point field the non-discrete piecewise continuous Poisson square-wave field is regarded (see Fig. 2.1.) One may picture that the square-waves as obtained from the point field by "smearing out" the discrete fuzzies over the intervals between the points. Essentially this smearing corresponds to giving the fuzzies of the point field finite extend. Thus, not surprisingly, asymptotic equivalence between the discrete fuzzy model from Sec. 2.1 and the square-wave field is obtained by scaling the distribution of $\eta(\xi)$ by the mean distance between two consecutive jumps $L/\mu_N = \kappa^{-1}$. It is emphasized that this kind of "smearing" is different from the kind of "smearing" applied in other works, e.g. [21] resembling that of the statistical theory of gases. By "smearing" is in that reference indicated a passage to a continuum of fuzzies similar to letting the occurrence rate κ tend towards ∞ and $E[\eta]$ tends to zero such that $\kappa E[\eta]$ tend to a positive constant. Then the variance $\text{Var}[R(\omega)]$ tends to zero. This approach is questioned in [17] because it sweeps out the variance which in realistic situations can be considerably larger than the mean. the example in Chapter 3 demonstrates this.

A homogeneous Poisson square-wave vector field $(\eta, \Omega, \zeta)(\xi)$, $\xi \in [0, L]$, is considered. To demonstrate the asymptotic equivalence with respect to second order moments the covariance function of $R(\omega)$ is considered. It shall be compared to Eq. (2.3). Using Eqs. (A.3) and (A.9) from the appendix one finds that the covariance given by (2.13) becomes

$$\text{Cov}[R(\omega_1), R(\omega_2)] = 2L^2 \omega_1 \omega_2 \frac{\mu_N + e^{-\mu_N} - 1}{\mu_N^2} \text{Cov}[\Gamma(\xi, \omega_1) \eta(\xi), \Gamma(\xi, \omega_2) \eta(\xi)] \quad (2.15)$$

Using that $\eta(\xi)$ and $\Gamma(\xi, \omega)$ are assumed mutually independent for each fixed ξ and that $\zeta(\xi)$ is assumed deterministic provide

$$\text{Cov}[\Gamma(\xi, \omega_1) \eta(\xi), \Gamma(\xi, \omega_2) \eta(\xi)] = E[\Gamma_1 \Gamma_2] E[\eta^2] - E[\Gamma_1] E[\Gamma_2] E[\eta]^2 \quad (2.16)$$

where $\Gamma_i = \Gamma(\xi, \omega_i)$, $i = 1, 2$. Combining Eqs. (2.15) and (2.16) and writing out in full the result

one has

$$\begin{aligned} \text{Cov}[R(\omega_1), R(\omega_2)] &= 2L^2 \omega_1 \omega_2 \frac{\mu_N + e^{-\mu_N} - 1}{\mu_N^2} \times \\ &\left\{ E[\eta^2] \int_0^\infty \gamma\left(\frac{\nu}{\omega_1}, \zeta\right) \gamma\left(\frac{\nu}{\omega_2}, \zeta\right) f_\Omega(\nu) d\nu - E[\eta]^2 \int_0^\infty \gamma\left(\frac{\nu}{\omega_1}, \zeta\right) f_\Omega(\nu) d\nu \int_0^\infty \gamma\left(\frac{\nu}{\omega_2}, \zeta\right) f_\Omega(\nu) d\nu \right\} \end{aligned} \quad (2.17)$$

As in the point field case, one sets $f_\Omega(\nu) = \lambda(\nu)/\mu_N$. Moreover, due to the scaling of η , $E[\eta^2]$ in (2.3) corresponds to $2E[(\eta(\xi)L/\mu_N)^2]$ in the present. Therefore, as $\mu_N \rightarrow \infty$, (2.17) tends asymptotically to (2.3) which proves the asymptotic equivalence of the discrete model and the present non-discrete Poisson square-wave field. It is noted that in the other limit $\mu_N \rightarrow 0$ the discrete model has no fuzzies whereas the square-wave field has no jumps but the field is with probability 1 non-zero. Therefore, (2.3) gives $\text{Var}[R(\omega)] = 0$ in the limit $\mu_N \rightarrow 0$ but $\text{Var}[R(\omega)] = \omega^2 \{E[\gamma(\frac{\Omega}{\omega}, \zeta)^2]E[\eta^2] - E[\gamma(\frac{\Omega}{\omega}, \zeta)]^2 E[\eta]^2\}$ showing that the fields are only asymptotic equivalent. The asymptotic second order moment equivalence prove that there exist non-discrete fields which can model the dynamical effect of the fuzzies.

As already mentioned the smearing applied to obtain the square-wave field essentially corresponds to giving the fuzzies of the point field finite extend. Thus it is essentially similar to the discrete field. Therefore, one may claim that the piecewise continuous square-wave field is not a very good counter example of the postulate by Lin based on continuous fields. Lin claimed that the probability of the coincidence of the excitation frequency and any single fuzzy eigenfrequency is zero, and therefore the most important effect of resonance is for continuous fields accorded with zero probability. Since the square-waves always have finite extend, there is always a non-zero probability that fuzzies of the same eigenfrequency exist, which is of course not in general the case for continuous fields. The square-wave process does, however, point out why continuous fields are nevertheless applicable as fuzzy models.

Also in the discrete model, the probability of hitting exactly the eigenfrequency of any fuzzy is zero if the frequencies are continuously distributed, but a damping effect is nevertheless experienced. So, the point it is not that in continuous fields the fuzzies have infinitesimal extend. The point is, as noted at the end of the first subsection of Sec. 1.1.2, that even near-resonant excitation of a fuzzy is sufficient to give a dynamical damping effect. Such an effect is only realizable if a fuzzy of non-vanishing mass is excited. Of course, in the discrete fuzzy model each fuzzy has finite mass giving rise to a non-vanishing damping effect of each fuzzy. Contrary to this the single fuzzies of the continuous field model has infinitesimal mass, why they cannot by themselves contribute to the dynamical damping effect. This is probably what is Lin's concern. Thus, the requirement that a field be a suitable fuzzy model is that a non-zero set of sufficiently many fuzzies excited at near resonance exists. Clearly, as demonstrated by the derivations given above, the square-wave field meets this requirement. A way that the requirement be met for continuous fields is if the field has a sufficiently large correlation length. Obviously this requirement is not unrealizable, proving that continuous field fuzzy models exist.

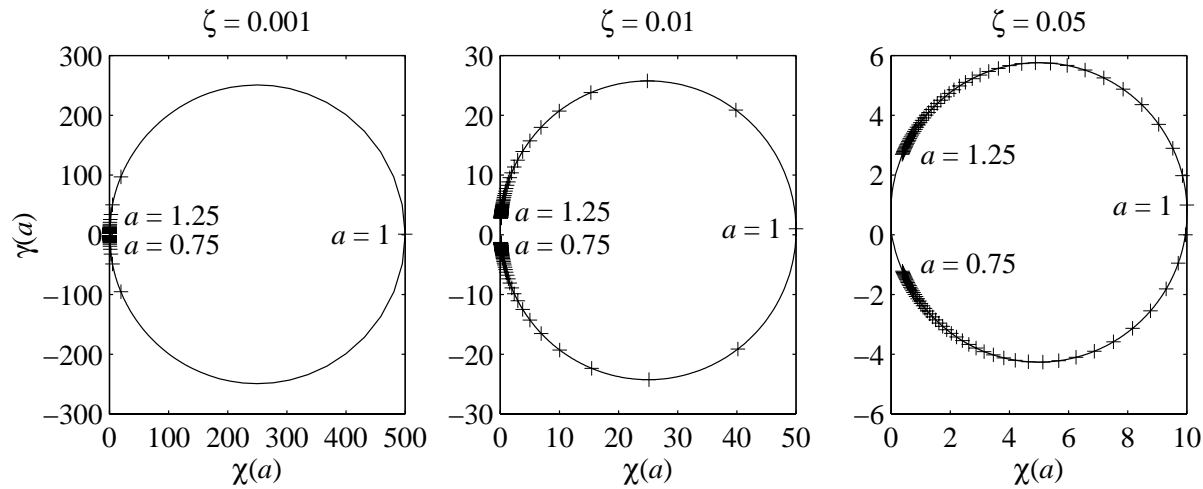


Figure 2.2: The complex number $\chi(a, \zeta) + i\gamma(a, \zeta)$ as function of $a \in [0, \infty]$ for different damping ratios.

2.3 Distributional Properties of R and V and Winterstein Approximations

From a reliability point of view it is necessary to know, at least approximately, the distributions of the reactive and the resistive dissipative contributions, $R(\omega)$ and $V(\omega)$, of the fuzzies. Especially having a mapping from a correlated pair $[U(\omega), W(\omega)]$ of zero mean unit variance Gaussian variables to $[R(\omega), V(\omega)]$ will be very convenient. The major problem one faces in this is, that a general solution for the distribution of an integral of a random field is difficult to obtain. However, some general considerations can be given.

Under suitable mixing conditions, any spatially separated events in a random field become asymptotically independent as the separating distance increases. If convergence towards independence is sufficiently fast when compared to the size of the integration domain, then a generalization of the central limit theorem implies that the integral of this field becomes asymptotically Gaussian. Thus both $R(\omega)$ and $V(\omega)$ can be asymptotically Gaussian. However obstacles for the application of central limit theorem are present. If the coefficient of variation $V_V(\omega)$ of $V(\omega)$ is not suitably small, the normal distribution will be a bad approximation for the distribution of $V(\omega)$ because $V(\omega)$ is a positive variable. Furthermore it is a premise of the central limit theorem that the distribution of the integrands in the expressions for $R(\omega)$ and $V(\omega)$ do not change drastically with ξ . Depending on the driving frequency ω the integrands may change drastically with ξ . If the driving frequency is such that practically none of the fuzzies are excited at near resonance they act either as purely mass or as purely stiffness contributors, why the distribution of the integrands is dominated by the distribution of $\eta(\xi)$, which is independent of ξ , and therefore the central limit theorem applies. An illustration of this is given in Fig. 2.2 which shows plots of the complex number $\chi(a, \zeta) + i\gamma(a, \zeta)$ as function of $a \in [0, \infty]$ for different damping ratios. To indicate how $\chi(a, \zeta) + i\gamma(a, \zeta)$ develops as function of a crosses are put on the graphs in the range from $a = 0.75$ to $a = 1.25$ and in steps of 0.05. Due to resonance

the range $a \in [0.75, 1.25]$ covers most of the graphs. Therefore, for non-resonant excitation $\chi(a, \zeta)$ and $\gamma(a, \zeta)$ concentrates in narrow regions of the graphs being in this way almost deterministic. If one instead consider excitation in the range of the fuzzy eigenfrequencies, i.e. medium-frequency range excitation, the absolute values of $\chi(a, \zeta)$ and $\gamma(a, \zeta)$ become large and important to the distribution of the integrands in $R(\omega)$ and $V(\omega)$. Thus, when the excitation is in the extremities of the fuzzy eigenfrequency range, few fuzzies are excited but they will dominate the distributions of $R(\omega)$ and $V(\omega)$, those being then in general far from Gaussian distributed. On the other hand, when the excitation is well within the medium-frequency range approximate Gaussianity of $R(\omega)$ and $V(\omega)$ is regained and the range of values that $R(\omega)$ and $V(\omega)$ may take is considerably larger than the range of values that $R(\omega)$ and $V(\omega)$ may take when the excitation frequency is outside the medium-frequency range.

The plots in Fig. 2.2 may also be used to give statements about the joint distribution of $R(\omega)$ and $V(\omega)$. Clearly, when the excitation is below the medium-frequency range there is an almost constant positive correlation coefficient between $R(\omega)$ and $V(\omega)$, independent of ω . Likewise, when the excitation is above the medium-frequency range, the coefficient of correlation is almost constant negative. Due to the almost symmetric shape of the graphs in Fig. 2.2 the correlation comes close zero when the excitation is in the medium-frequency range. When passing from non-resonant excitation to medium range excitation the correlation coefficient passes rapidly from the constant non-zero level to zero. This follows from the fast variation of $\chi(a, \zeta)$ and $\gamma(a, \zeta)$ with a when a is in the neighborhood of 1. On the premise that excitation is in the medium-frequency range the following approximate line of reasoning can now be followed. The marginal distributions of $R(\omega)$ and $V(\omega)$ are nearly normal and one may conjecture that $\text{Cov}[R(\omega), V(\omega)]$ gives much information about the joint distribution of $R(\omega)$ and $V(\omega)$. Thus it is conjectured that for medium frequency-range excitation $R(\omega)$ and $V(\omega)$ are virtually uncorrelated why there is only little need of a precise account for their joint distribution.

Supported on the above considerations about the approximate Gaussianity and the specific examples given in Chapter 3, $[R(\omega), V(\omega)]$ is approximated by $[\hat{R}(\omega), \hat{V}(\omega)]$ given by the mapping (suppressing the argument ω)

$$\hat{R} = E[R] + D[R] [aU + b(U^2 - 1) + c(U^3 - U)] \quad (2.18)$$

$$\hat{V} = f \exp(gW - \frac{1}{2}hW^2) \quad (2.19)$$

The coefficients a, b, c, f, g and h are determined such that $[\hat{R}(\omega), \hat{V}(\omega)]$ have the same first four marginal moments as those of $[R(\omega), V(\omega)]$. This type of approximation as applied to $R(\omega)$ has been successfully used in several different applications by Winterstein [23, 7]. Therefore (2.18) is called a Winterstein approximation and (2.19) a log-Winterstein approximation. The form of (2.18) is based on the conjecture that $R(\omega)$ is asymptotically Gaussian no matter what the distributions of the fuzzy eigenfrequencies and masses are. Thus the first term in the square bracket contributes to Gaussianity whereas the other terms account for the deviations from Gaussianity. For the distributions applied in the examples in the Chapter 3 this conjecture proves useful. Similarly one might conjecture that $V(\omega)$ be approximated by a polynomial of a Gaussian variable. However, $V(\omega)$ is positive, and for the specific examples in Chapter 3 ap-

proximately exponential distributions of $V(\omega)$ are obtained. Adding to this, that the exponential distribution approaches normality as the coefficient of variation $V_V(\omega)$ decreases, an exponential transform of the second degree polynomial in (2.19) seems a reasonable choice. Having assessed the coefficients a, b, c, f, g and h , the covariance of $[U(\omega), W(\omega)]$ is chosen such that $\text{Cov}[\hat{R}(\omega), \hat{V}(\omega)] = \text{Cov}[R(\omega), V(\omega)]$. This is in accordance with the discussion of the joint distribution of $[R(\omega), V(\omega)]$ given in the previous paragraph. For brevity the approximations to $[R(\omega), V(\omega)]$ will in the following be called the (joint) Winterstein approximation.

The polynomial degree used in formulas (2.18) and (2.19) are not completely arbitrarily chosen. There is no algebraic restrictions on the degree applicable in polynomials like (2.18). However moments of higher order than four are seldom obtainable, so usually only third degree Winterstein polynomials are used. Furthermore, in the current applications satisfactory approximations are obtained by (2.18). In formula (2.19) the random field W only appears up to the second degree. This is due to algebraic limitations. Since W is Gaussian the tail of its distribution is of type $e^{-\frac{1}{2}w^2}$ and therefore, if terms of the form kW^m with $m > 2$ are present in the exponent, then moments of \hat{V} do not exist for m odd and any k , or for m even and positive k . It turns out that in the present investigations (2.19) gives satisfactorily accurate approximations to the considered distributions.

The requirement that the first four moments of $R(\omega)$ and $\hat{R}(\omega)$ be equal gives rise to the following equations, [7, p. 119],

$$a^2 + 2b^2 + 6c^2 = 1 \quad (2.20)$$

$$2b(2 + a^2 + 18ac + 42c^2) = \alpha_{3,R} \quad (2.21)$$

$$15 + 288ac + 936c^2 - 12a^4 - 264a^3c - 864a^2c^2 - 432ac^3 - 2808c^4 = \alpha_{4,R} \quad (2.22)$$

in which $\alpha_{3,R} = E[(R - E[R])^3]/D[R]^3$ is the skewness of $R(\omega)$ and $\alpha_{4,R} = E[(R - E[R])^4]/D[R]^4$ is the kurtosis of $R(\omega)$. Setting $E[V^q] = E[\hat{V}^q]$ for $q = 1, 2, 3$ will give three equations to obtain f, g , and h . Using the density function of the normal distribution the n th order moment of $\hat{V}(\omega)$ is derived. One finds

$$E[\hat{V}^n] = \frac{f^n}{\sqrt{1+nh}} \exp\left(\frac{n^2g^2}{2(1+nh)}\right) \quad (2.23)$$

for $h > -1/n$. The correlation of the Gaussian pair $[U(\omega_i), W(\omega_j)]$, $i, j = 1, 2$ defining completely the correlation of pair $[\hat{R}(\omega_i), \hat{V}(\omega_j)]$, $i, j = 1, 2$ is obtained from one of the following equations, [7, pp. 116,120], where for short subscript i denotes "function of ω_i ", e.g. $U_i = U(\omega_i)$, $\rho[\cdot, \cdot]$ denotes the correlation coefficient, and $\phi(u, v; \rho)$ is the standard two-dimensional

normal density:

$$\rho[R_1, R_2] = a_1 a_2 \rho[U_1, U_2] + 2b_1 b_2 \rho[U_1, U_2]^2 + 6c_1 c_2 \rho[U_1, U_2]^3 \quad (2.24)$$

$$E[V_1 V_2] = f_1 f_2 \int_{-\infty}^{\infty} \int_{-\infty}^{\infty} e^{g_1 u + g_2 v - (h_1 u^2 + h_2 v^2)/2} \varphi(u, v; \rho[W_1, W_2]) du dv \quad (2.25)$$

$$\begin{aligned} \rho[R_1, V_2] D[V_2] = \\ f_2 \int_{-\infty}^{\infty} \int_{-\infty}^{\infty} [a_1 u + b_1 (u^2 - 1) + c_1 (u^3 - u)] e^{g_2 v - h_2 v^2/2} \varphi(u, v; \rho[U_1, W_2]) du dv \end{aligned} \quad (2.26)$$

subjected to constraint that of course

$$\begin{bmatrix} \text{Cov}[U_1, U_2] & \text{Cov}[U_1, W_2] \\ \text{Cov}[W_1, U_2] & \text{Cov}[W_1, W_2] \end{bmatrix} \quad (2.27)$$

is nonnegative definite.

The Winterstein approximation technique is obviously not of much use if not the first four moments of the integrals $R(\omega)$ and $V(\omega)$ are known. Examples employing the Poisson square-wave field and the Poisson point pulse field are given in Chap. 3. Formulas for the moments of $R(\omega)$ and $V(\omega)$ for these fields are derived in Appendix A.

A solution a, b, c to the Eqs. (2.20), (2.21) and (2.22), or a solution f, g, h to the three equations obtained from (2.23) may not exist, or there may be more than one solution. The existence of solutions $\rho[U_1, U_2]$, $\rho[W_1, W_2]$ and $\rho[U_1, W_2]$ to Eqs. (2.24), (2.25) and (2.26) such that the requirement (2.27) is satisfied is also a complicated problem. Nonexistence of solutions can occur when one or more of the correlation coefficients $\rho[R_1, R_2]$, $\rho[R_1, V_2]$ and $\rho[V_1, V_2]$ approach ± 1 , in particular, at ω values where $R(\omega)$ and $V(\omega)$ deviate much from the normal and the lognormal distributions, respectively. In Chap. 3 it is explained how these potential problems are overcome.

2.4 Summary

Three different fuzzy models are considered. First a discrete model not giving any information about the spatial distribution of the fuzzies is treated. Due to the assumed mutual statistical independence of the fuzzies in this model an equivalent one-dimensional Poisson point pulse field is constructed and shortly treated. Inspired by this field a Poisson square-wave field is obtained by smearing out the fuzzies of the Poisson point pulse field which essentially corresponds to giving the fuzzies of the point field finite extend. The hereby obtained field is shown to be asymptotically second order moment equivalent to the discrete model as it reproduces asymptotically the covariances $\text{Cov}[R(\omega_i), R(\omega_j)]$ etc., and of course the means too. Based on this result, showing that non-discrete and non-continuous fields may model the impedance contributions due to the fuzzies, it is explained that continuous fields may as well be used in modeling

fuzzies and still provide meaningful results. This is a contradiction to the consideration given by Lin.

In the last half of this chapter a discussion of the marginal distributions and the joint distribution of $R(\omega)$ and $V(\omega)$ is given. For medium-frequency range excitation the distributions are, as a consequence of the central limit theorem, approximately Gaussian. Furthermore, it turns out that the correlation coefficient is nearly zero in the medium-frequency range. It is based on these observations and because it from a reliability point of view is convenient to have a mapping from a pair of Gaussian variables to $[R(\omega), V(\omega)]$, that the so-called joint Winterstein approximation to the joint distribution of $[R(\omega), V(\omega)]$ is introduced. The joint Winterstein approximation consists of the well-known Winterstein approximation which is used here to approximate $R(\omega)$, and a so-called log-Winterstein approximation used to approximate $V(\omega)$. The latter, which is basically defined as the exponential of a conventional Winterstein approximation, is introduced here because the resistive contribution $V(\omega)$ from the fuzzies is positive, why a Gaussian-like approximation to its distribution may not be successful.

Chapter 3

Quantification of Vibration Damping

Using the Winterstein approximations suggested in the previous chapter the main goal of this chapter is to show the quantitative assessment of the second order moments of some quantities associated with the frequency response function is possible. In doing this, the dynamical damping effect of the fuzzies as modeled by the piecewise continuous Poisson square wave field is once again demonstrated.

3.1 Amplification Factor and Phase Angle

In structural engineering one usually considers the frequency response function rather than the impedance. Therefore this chapter focuses on the frequency response function. In Sec. 1.1.2 it was shown that the frequency response function is given by

$$H(\omega) = \frac{M}{i\omega Z} = \frac{1}{\omega_0^2 - \omega^2 - \omega R(\omega) + i(2\zeta_0\omega_0\omega + \omega V(\omega))} \quad (3.1)$$

For many practical purposes it is of more use to know the amplification factor A and the phase angle ψ defined by

$$A(\omega) = \frac{|\hat{x}|}{|\hat{F}/M\omega_0^2|} = |H(\omega)|\omega_0^2 \quad \text{and} \quad \psi(\omega) = \arg[H(\omega)] \quad (3.2)$$

One may want to know the mean and the standard deviation of these quantities. Especially the mean and the standard deviation of the amplification factor may be of interest. Either simply because they may be directly useful in a reliability assessment of the master, or because one seeks the mean and the variance of quantities which depend on $H(\omega)$. For instance the covariance function of the stationary response $X(t)$ of the master structure to a stationary excitation with spectral increment $dS(\omega)$ is given by

$$\text{Cov}[X(s), X(t)] = \int_{-\infty}^{\infty} e^{i\omega(s-t)} E[|H(\omega)|^2] dS(\omega) \quad (3.3)$$

It is noted that since the system of fuzzies on the master structure is some particular realization of the field of fuzzies, this stationary response $X(t)$ is a random process which is non-ergodic with respect to properties that concern the statistical nature of the fuzzy system. For example, a time average estimation of the covariance function from a single realization of $X(t)$ will not be an estimate of the covariance function as given by (3.3). It will rather be a realization of the random covariance function obtained from (3.3) when replacing $E[|H(\omega)|^2]$ by the random function $|H(\omega)|^2$. It therefore may be valuable to be able to compute $\text{Cov}[X(s), X(t)]$ from (3.3).

Herein $A(\omega)$ and $\psi(\omega)$ are mainly regarded for the purpose of illustrating the damping effect of the fuzzies by use of the frequency response function rather than by use of the impedance, less used in structural engineering. Furthermore $A(\omega)$ and $\psi(\omega)$ are considered to demonstrate the applicability of the Winterstein approximation suggested in Chapter 2. Since $A(\omega)$ and $\psi(\omega)$ are complicated nonlinear functions of $R(\omega)$ and $V(\omega)$, computing the mean and the variance of $A(\omega)$ and $\psi(\omega)$ requires the joint distribution of $[R(\omega), V(\omega)]$, and this is where the Winterstein approximation comes into the picture.

3.2 The Example

The Poisson point pulse field and the Poisson square-wave fields are considered. In order to show how different the variance of $R(\omega)$ and $V(\omega)$ may be, the mean fuzzy mass $E[\eta(\xi)]$ is kept constant while the mean number of fuzzies μ_N varies. For the rest of the chapter μ_N takes either one of the values 10 or 100, and the normalized fuzzy masses $\eta(\xi)$ are assumed to be Rayleigh distributed with mean 0.3. As mentioned in Chapter 2 the damping ratios of the fuzzies are for simplicity assumed deterministic and set to $\zeta(\xi) = 0.01$. Furthermore the fuzzy

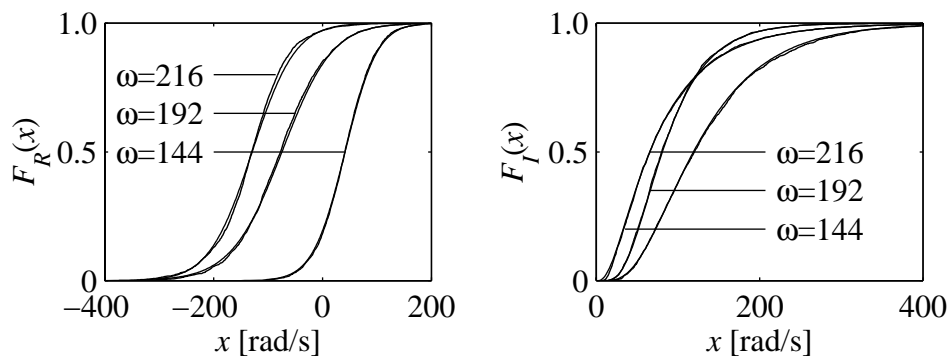


Figure 3.1: Marginal distributions of $\hat{R}(\omega)$ and $\hat{V}(\omega)$ compared to simulated distributions of $R(\omega)$ and $V(\omega)$ for the square-wave field model with $\mu_N = 100$.

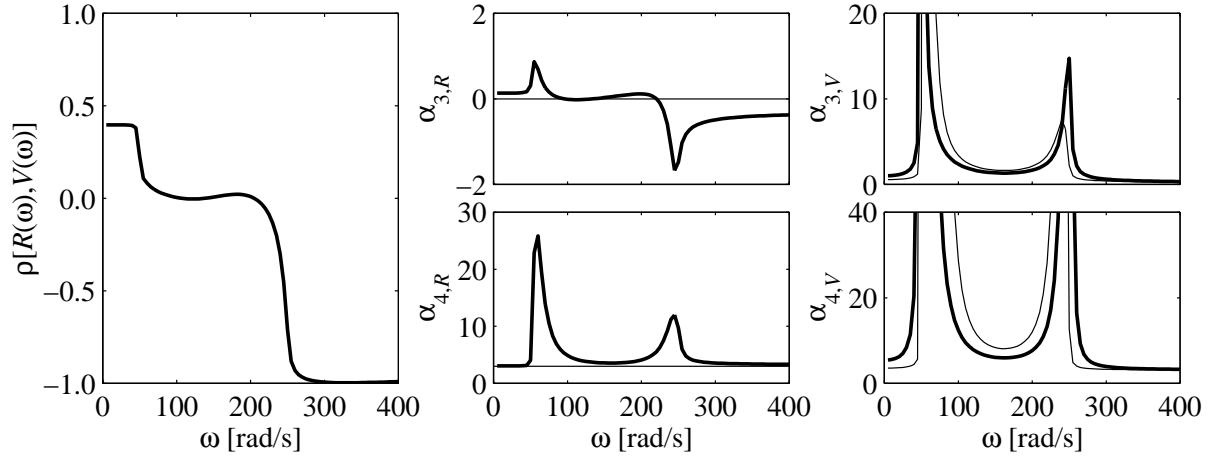


Figure 3.2: Correlation functions (invariant with respect to μ_N) and, for $\mu_N = 100$, skewness and kurtosis of $R(\omega)$ and $V(\omega)$ (thick curves) compared to the skewness and kurtosis of normal and log-normal distributions with the same mean and standard deviation as $R(\omega)$ and $V(\omega)$, respectively (thin curves). All results are for the square-wave field model.

eigenfrequencies $\Omega(\xi)$ are assumed to be distributed with symmetric density

$$f_{\Omega}(\omega) = \begin{cases} \frac{2}{\omega_U - \omega_L} \sin^2\left(\pi \frac{\omega - \omega_L}{\omega_U - \omega_L}\right), & \omega \in [\omega_L, \omega_U] \\ 0 & \text{otherwise} \end{cases} \quad (3.4)$$

where $\omega_L = 50$ and $\omega_U = 250$. All the above distributions and numerical values are chosen such that they match those presented in [17]. Based on these distributional assumptions, the results shown in Figs. 3.1 to 3.2 are obtained. Except for minor numerical inaccuracies, the results in Figs. 3.3 and 3.2 are exact, as they are obtained by use of the formulas in Appendix A.

Figure 3.1 shows plots of the Winterstein approximation $[\hat{R}(\omega), \hat{V}(\omega)]$ together with simulations of the marginal distributions of $[R(\omega), V(\omega)]$ for $\mu_N = 100$. It is recalled that the approximations are obtained independently of each other. The driving frequencies $\omega = 144, 192, 216$ considered in the plots vary from the center to the tail of the fuzzy eigenfrequency distribution, i.e. within the medium-frequency range. Clearly the Winterstein and the log-Winterstein approximations are good these conditions. The good agreement underlines the hypothesis brought forward in Sec. 2.3 that $R(\omega)$ and $V(\omega)$ are virtually independent under the given conditions. Supporting this, the left plot in Fig. 3.2 shows the correlation coefficient $\rho[R(\omega), V(\omega)]$ as function of ω . As explained earlier (with reference to Fig. 2.2) ρ is close to zero in the medium-frequency range and with steep changes near the medium-frequency range endpoints ω_L and ω_U . As also explained before, the center and the right plot in Fig. 3.2, respectively, show that the distribution of $R(\omega)$ and $V(\omega)$ deviate the most from Gaussianity and the log-normality, respectively, in the

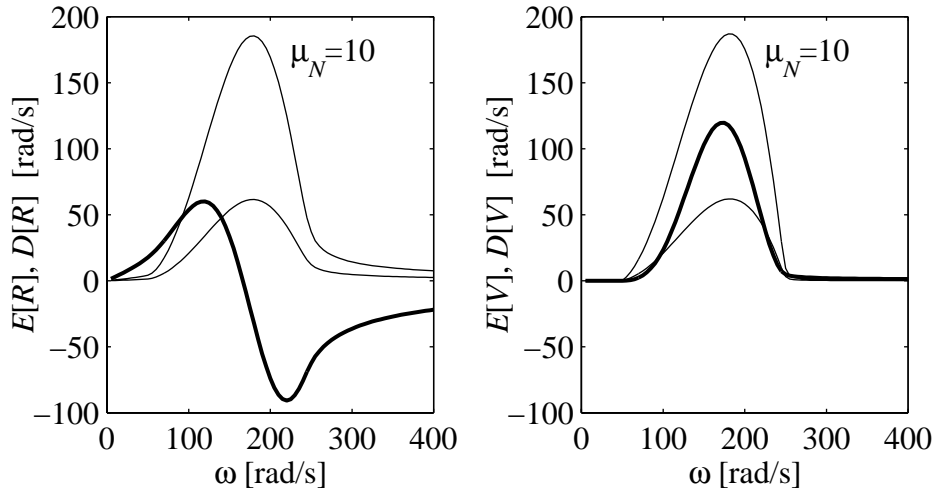


Figure 3.3: Mean (thick curve) and standard deviations (thin curve) of $R(\omega)$ and $V(\omega)$ for the square-wave field model for mean number of fuzzies $\mu_N = 10, 100$. The curves for $D[R]$ and $D[V]$ for $\mu_N = 10$ are marked.

neighborhood of the endpoints of the medium-frequency range. Thus, at the endpoints the Winterstein approximation may give considerable errors, if existing at all. However, at the endpoints the variance of $R(\omega)$ and $V(\omega)$ are relatively small (see. Fig. 3.3), why the potential errors of the Winterstein approximation will not have a dramatic influence on the final results for $A(\omega)$ and $\psi(\omega)$.

Together all the above observations suggest that using the Winterstein approximation in the medium-frequency range may provide good approximate results for the mean and the variance of $A(\omega)$ and $\psi(\omega)$. Outside the medium-frequency -range, the small variation of $R(\omega)$ and $V(\omega)$ imply that their randomness may be sufficiently accurately accounted for by assuming them normally and log-normally distributed, respectively, and independent. Since it is the medium-frequency range which is of interest, it is not a severe drawback that the applicability of the Winterstein approximation technique is limited to this frequency-range.

It is noted that some of the above conclusions are of empirical nature, why they may not be valid given some other distribution assumptions. Furthermore the nice plots in Figs. 3.1 and 3.2 are obtained for a high mean number of fuzzies, i.e. for $\mu_N = 100$. For $\mu_N = 10$ one must expect that e.g. $R(\omega)$ deviates more from Gaussianity than when $\mu_N = 100$. Later it is seen that, even for $\mu_N = 10$, reasonable results are obtainable by use of the Winterstein approximation.

Before discussing the frequency response function the impedance contributions of the fuzzies are considered. Figure 3.3 depicts the mean and standard deviation of $R(\omega)$ and $V(\omega)$. The means $E[R(\omega)]$ and $E[V(\omega)]$ show that on the average considerable contributions are present in the center of the medium-frequency range. On the other hand, the possible great variability of

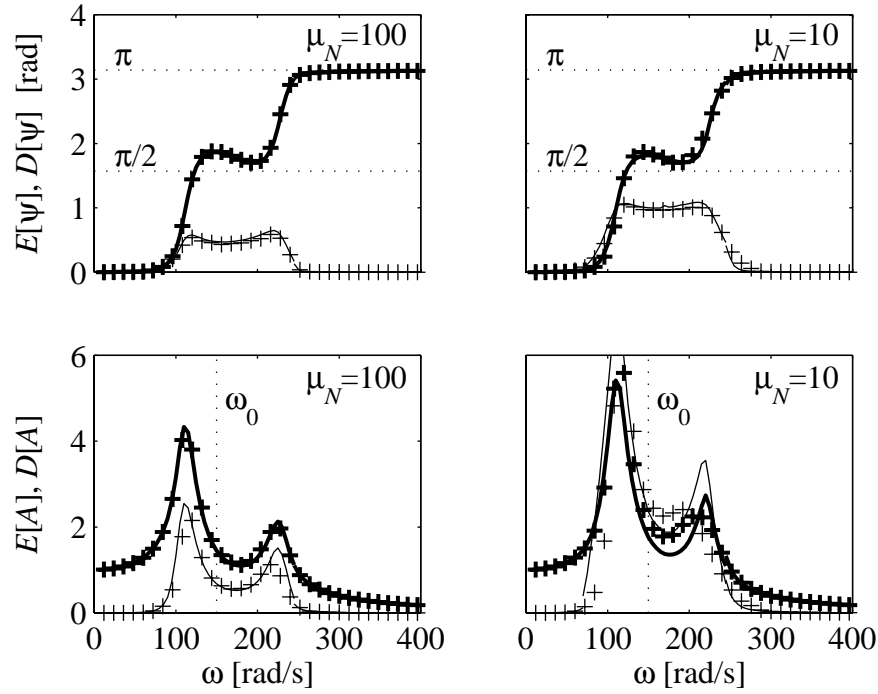


Figure 3.4: Simulated (crosses) and Winterstein approximated (solid lines) means (thick line) and standard deviations (thin line) of the amplification factor $A(\omega)$ and the phase angle $\psi(\omega)$, as obtained for the square-wave model and for $\mu_N = 10, 100$.

$R(\omega)$ and $V(\omega)$ indicates that the contributions may, or may not, be present. The plots show how much bigger than the mean, the standard deviation can be. As expected and in analogy to the theory of gases, increasing the number of fuzzies while keeping the mean mass constant reduces the variation of the damping effect makes the realization of the dynamic damping effect caused by the fuzzies less uncertain. It is noted that the dynamic damping effect is on the average the largest when the mean $E[R(\omega)]$ of the reactive contribution is close to zero and the mean $E[V(\omega)]$ of the resistive contribution is big. This is, due to the symmetry of f_Ω , not surprisingly seen to be very close to the center of the distribution of the fuzzy eigenfrequencies. Finally it is concluded that the plots give numerical proof that certainly the non-discrete square-wave model can account for the damping effect of the fuzzies.

For the square-wave model, Fig. 3.4 shows, along with simulation results, the mean and the standard deviation of $A(\omega)$ and $\psi(\omega)$ computed by use of the Winterstein approximation for the joint distribution of $[R(\omega), I(\omega)]$. Both $\mu_N = 100$ and $\mu_N = 10$ is considered. It is noted that in the graphs of $D[\psi(\omega)]$, as obtained by use of the Winterstein approximation, there are some gaps close to the endpoints ω_L and ω_U of the fuzzy eigenfrequency range. These gaps are explained by the shift from the Winterstein approximation applied in the medium-

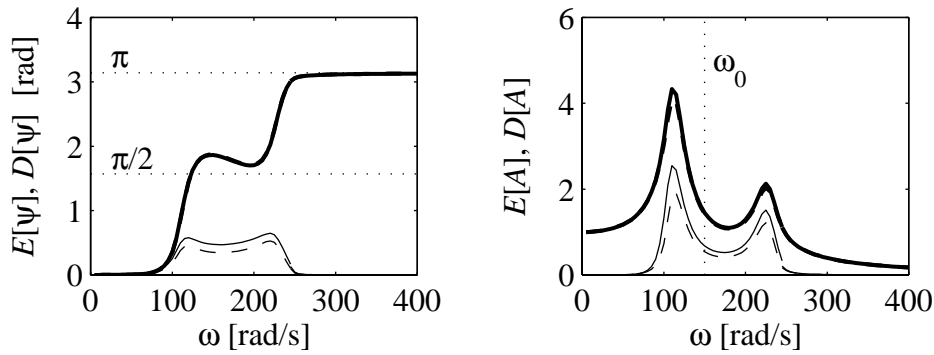


Figure 3.5: Means (thick curves) and standard deviations (thin curves) of the amplification factor $A(\omega)$ and the phase angle $\psi(\omega)$ obtained by Winterstein approximation for the Poisson square-wave field model (solid curves) and the Poisson point pulse field (dotted curves).

frequency range to the simplified distributional model applied outside this range. In order to demonstrate the influence of the dynamical damping effect of the fuzzies, the eigenfrequency of the master structure itself is chosen to be in the center of the fuzzy eigenfrequency range, i.e. $\omega_0 = \frac{1}{2}(\Omega_L + \Omega_U) = 150$ rad/s. It is seen that the determination of the main features of the dependence of the mean and the standard deviation on ω , as obtained from the Winterstein approximation, is quite accurate, and the largest errors occur only when the mean number of fuzzies is very small. It shows that accounting for the joint distributional characteristics of $[R(\omega), V(\omega)]$ by only requiring the covariance of the pairs $[R(\omega), V(\omega)]$ and $[\hat{R}(\omega), \hat{V}(\omega)]$ be equal gives satisfactory results. As mentioned above, the dynamical damping effect of the fuzzies in the current case has, on the average, the greatest effect at the center of the fuzzy eigenfrequencies. Since ω_0 equals the center point of the eigenfrequency distribution, it may be expected that on the average the entire fuzzy system will behave essentially as a mass damper. This is confirmed by the variation of the expectation of the amplification factor $A(\omega)$ as a function of ω with a local minimum close to ω_0 . However, it is again seen that the standard deviation of the amplitude is quite large, indicating that this mass damper effect may, or may not, be present for a particular realization of the fuzzy system.

In order to give a quantitative idea about the difference between results obtained by use of the Poisson square-wave model and the Poisson point pulse model, Fig. 3.5 compares, for $\mu_N = 100$, the mean and the standard deviation of $A(\omega)$ and $\psi(\omega)$ for these two models. The means $E[R(\omega)]$ and $E[V(\omega)]$ are for the two models identical, but due to the only asymptotic equivalence of the two models the standard deviations $D[R(\omega)]$ and $D[V(\omega)]$ are not identical. Consequently the moments of $A(\omega)$ and $\psi(\omega)$ will deviate from each other. Due to the asymptotic behavior the differences will, as it appears in the figure, be small for $\mu_N = 100$.

3.3 Summary

An example demonstrating the conclusions drawn in Chapter 2 is given. In this example the mean and standard deviation of the amplification factor and the phase angle, both quantities related to the frequency response function, has been obtained. The results demonstrate that the possible dynamic damping effect of the fuzzies can be modeled by use of a non-discrete field model. Furthermore they show that considerable standard deviations of the change-in-impedance can be present. The computation of the amplification factor and the phase angle required the joint distribution of the reactive and resistive contributions $[R(\omega), V(\omega)]$ due to the fuzzies. It was shown by comparison to results obtained by simulation that results coming quite close to the simulation results may be obtained by use of the joint Winterstein approximation suggested in Chapter 2. The Winterstein approximation performs especially well when excitation frequencies well within the eigenfrequency range of the fuzzies are considered.

Chapter 4

Conclusions

The subject of this part of the thesis is vibrations of a deterministically defined major main structure to which several minor stochastically defined sub-structures are attached. This kind of problem originates in the field of acoustics in which the resonant excitation of the substructures, the so-called *fuzzies*, has to be taken into consideration because the resonating fuzzies will exert a dynamical damping effect on the main structure, the so-called *master*. In structural and mechanical engineering the dynamical damping effect of minor sub-structures on major structures is also a relevant problem.

Information about the fuzzies is generally uncertain, why a stochastic modeling of the fuzzies is the most reasonable choice of model. Herein two issues connected to the damping effect of the fuzzies, as obtained by use of a the stochastic fuzzy model, are discussed. The damping effect is investigated by considering the change in impedance of the master due to the fuzzies. In computing the impedance, some authors choose to account for the fuzzies by letting the number of fuzzies tend to infinity in such a way that the mean total mass of the fuzzies stay constant and consequently the variation of the total mass tends to zero. Thereby a deterministic model neglecting possibly large variations of the change in impedance is obtained. This is not a reasonable result, and it is shown quantitatively by an example, that the variance can be considerable. The passage from a finite number of discrete fuzzies to an infinity of fuzzies may be considered a "smearing" of the fuzzies. The second issue concerns an alternative way of smearing. Instead of a discrete fuzzy model a continuous random field may be applied as a model for the fuzzies. Such a continuous random field represents a smearing since it consists of infinitely many infinitesimally small fuzzies. Because the fuzzies in such a model are infinitesimally small, Lin [17] questions that the damping effect of the fuzzies may be accounted for by continuous field models. Regarding a piecewise continuous field, obtained in a natural way from a discrete field, and showing asymptotic second order moment equivalence between the two fields it is herein argued that a damping effect may also be encountered when using a continuous field model provided that the field has a reasonably high correlation length.

In a reliability assessment of the master, the distribution of the change in impedance due to the fuzzies must somehow be assessed. Herein a simple tool for this purpose is developed. The simplicity follows from the field models applied. The fields are the Poisson square-wave field and the Poisson pulse point field which are of the often used Poisson field type. General statements about the distribution of the change in impedance in dependence of the fuzzy field model and the distribution of fuzzy eigenfrequencies, masses and damping ratios are quite weak. Therefore approximations are sought. Especially having a mapping from standard Gaussian variables to the random variables giving the change in impedance is convenient. From the general statements it follows that approximate Gaussian distributions of the random variables giving the change in impedance are to be expected. Therefore, and based on the specific example given in the last chapter, Winterstein approximations are applied with success. Based on the Winterstein approximations quite accurate evaluations of the statistics of the frequency response function is obtained. These results demonstrate a quantification of the damping effect of the fuzzies when these are modeled by a non-discrete field.

Under some simplifying assumptions this part of the thesis mainly gives a discussion of the modeling of the fuzzies in terms of a discrete model versus a continuous model. Future research must regard multiple degree of freedom masters such as beams. For such masters it is doubtful whether a simple analysis as the one carried out here can be applied. Probably a Finite Element approach is required. There is, however, no doubt that the considerations given in the present work about the applicability of the continuous fuzzy field models carry over to multiple degree of freedom masters.

Appendix A

Statistical Moments of Integrals of Poisson Fields

The first four central moments of integrals of homogeneous Poisson fields on a line are excessively used in this part of the thesis. A detailed derivation of the formulas for these moments has been postponed to this Appendix. Without loss of generality one can always scale the axis along the line why we consider integrals of the type

$$Y = \int_0^1 Z(\xi) d\xi. \quad (\text{A.1})$$

where $Z(\xi)$ is a homogeneous Poisson square-wave field or a Poisson point pulse process.

A.1 The Square-Wave Field

The square-wave field is shown in Fig. 2.1. Based on that figure the formulas presented here are obtained. First of all the well-known results for the mean and variance are repeated:

$$E[Y] = E[Z] \quad (\text{A.2})$$

$$\begin{aligned} \text{Var}[Y] &= \int_0^1 \int_0^1 \text{Cov}[Z_1, Z_2] d\xi_1 d\xi_2 \\ &= \text{Var}[Z] \int_0^1 \int_0^1 P\{\xi_1 \text{ and } \xi_2 \text{ inside the same square-wave}\} d\xi_1 d\xi_2 \\ &= \text{Var}[Z] \int_0^1 \int_0^1 \exp(-\mu_N |\xi_1 - \xi_2|) d\xi_1 d\xi_2 \end{aligned} \quad (\text{A.3})$$

where for brevity Z_i denotes $Z(\xi_i)$, μ_N is the mean number of jumps in the field and where $P\{\text{event}\}$ means the probability of *event*. Furthermore the coordinate ξ is suppressed in $E[Z]$ and $\text{Var}[Y]$ as the field is homogeneous. Henceforth the coordinate is suppressed when possible.

For the computation of the skewness the third central moment is required. If one defines an operator $\text{TriCov}[S, T, U]$ similar to the covariance operator by

$$\text{TriCov}[S, T, U] = E[(S - \mu_S)(T - \mu_T)(U - \mu_U)] \quad (\text{A.4})$$

the third central moment of Y becomes

$$E[(Y - \mu_Y)^3] = \int_0^1 \int_0^1 \int_0^1 \text{TriCov}[Z_1, Z_2, Z_3] d\xi_1 d\xi_2 d\xi_3 \quad (\text{A.5})$$

As $\text{TriCov}[Z_1, Z_2, Z_3]$ is zero if just one of the Z_i 's is independent of the two others one has

$$\begin{aligned} \text{TriCov}[Z_1, Z_2, Z_3] &= E[(Z - \mu_Z)^3] P\{\xi_1, \xi_2 \text{ and } \xi_3 \text{ inside the same wave}\} \\ &= E[(Z - \mu_Z)^3] \exp(-\mu_N \max_{i,j}(|\xi_i - \xi_j|)) \end{aligned} \quad (\text{A.6})$$

Proceeding to the fourth central moment a multilinear operator QuaCov is defined analogously to the multilinear operator TriCov providing

$$E[(Y - \mu_Y)^4] = \int_0^1 \int_0^1 \int_0^1 \int_0^1 \text{QuaCov}[Z_1, Z_2, Z_3, Z_4] d\xi_1 d\xi_2 d\xi_3 d\xi_4 \quad (\text{A.7})$$

The evaluation of QuaCov is a bit more complicated than the evaluation of TriCov . Letting $\{i_1, i_2, i_3, i_4\}$ denote a permutation of $\{1, 2, 3, 4\}$, then of course $\text{QuaCov}[Z_1, Z_2, Z_3, Z_4] = \text{QuaCov}[Z_{i_1}, Z_{i_2}, Z_{i_3}, Z_{i_4}]$. If the permutation $\{i_1, i_2, i_3, i_4\}$ is chosen such that it satisfies $\xi_{i_1} \leq \xi_{i_2} \leq \xi_{i_3} \leq \xi_{i_4}$ then one can state that the QuaCov is only non-zero in the two cases:

1. All the Z_i 's are inside the same wave, or
2. ξ_{i_1}, ξ_{i_2} are inside one wave and ξ_{i_3}, ξ_{i_4} are inside another wave.

Using the permutation renders

$$\begin{aligned} \text{QuaCov}[Z_1, Z_2, Z_3, Z_4] &= E[(Z - \mu_Z)^4] \exp(-\mu_N(\xi_{i_4} - \xi_{i_1})) \\ &\quad + (\text{Var}[Z])^2 \exp(-\mu_N(\xi_{i_2} - \xi_{i_1})) \exp(-\mu_N(\xi_{i_4} - \xi_{i_3})) \{1 - \exp(-\mu_N(\xi_{i_3} - \xi_{i_2}))\} \\ &= E[(Z - \mu_Z)^4] \exp(-\mu_N(\xi_{i_4} - \xi_{i_1})) \\ &\quad + (\text{Var}[Z])^2 \{ \exp(-\mu_N(\xi_{i_2} - \xi_{i_1} + \xi_{i_4} - \xi_{i_3})) - \exp(-\mu_N(\xi_{i_4} - \xi_{i_1})) \} \end{aligned} \quad (\text{A.8})$$

Though the integrands (A.6) and (A.8) look complicated, symmetry of these integrands over the domain of integration in formulas (A.3), (A.5) and (A.7) leads the following results

$$\begin{aligned}
 & \int_0^1 \int_0^1 \exp(-\mu_N |\xi_2 - \xi_1|) d\xi_1 d\xi_2 \\
 &= 2! \int_0^1 \int_0^{\xi_1} \exp(-\mu_N (\xi_2 - \xi_1)) d\xi_1 d\xi_2 \\
 &= \frac{2}{\mu_N} + \frac{2}{\mu_N^2} (e^{-\mu_N} - 1)
 \end{aligned} \tag{A.9}$$

$$\begin{aligned}
 & \int_0^1 \int_0^1 \int_0^1 \exp(-\mu_N \max_{i,j}(|\xi_i - \xi_j|)) d\xi_1 d\xi_2 d\xi_3 \\
 &= 3! \int_0^1 \int_0^{\xi_1} \int_0^{\xi_2} \exp(-\mu_N (\xi_1 - \xi_3)) d\xi_1 d\xi_2 d\xi_3 \\
 &= 6 \frac{2(1 - e^{\mu_N}) + \mu_N(1 + e^{\mu_N})}{\mu_N^3 e^{\mu_N}}
 \end{aligned} \tag{A.10}$$

$$\begin{aligned}
 & \int_0^1 \int_0^1 \int_0^1 \int_0^1 \exp(-\mu_N (\xi_{i_4} - \xi_{i_1})) d\xi_1 d\xi_2 d\xi_3 d\xi_4 \\
 &= 4! \int_0^1 \int_0^{\xi_1} \int_0^{\xi_2} \int_0^{\xi_3} \exp(-\mu_N (\xi_1 - \xi_4)) d\xi_1 d\xi_2 d\xi_3 d\xi_4 \\
 &= 12 \frac{6(1 - e^{\mu_N}) + \mu_N(4 + 2e^{\mu_N} + \mu_N)}{\mu_N^4 e^{\mu_N}}
 \end{aligned} \tag{A.11}$$

$$\begin{aligned}
 & \int_0^1 \int_0^1 \int_0^1 \int_0^1 \exp(-\mu_N (\xi_{i_4} - \xi_{i_3} + \xi_{i_2} - \xi_{i_1})) d\xi_1 d\xi_2 d\xi_3 d\xi_4 \\
 &= 4! \int_0^1 \int_0^{\xi_1} \int_0^{\xi_2} \int_0^{\xi_3} \exp(-\mu_N (\xi_1 - \xi_2 + \xi_3 - \xi_4)) d\xi_1 d\xi_2 d\xi_3 d\xi_4 \\
 &= 12 \frac{6(e^{\mu_N} - 1) + \mu_N(\mu_N e^{\mu_N} - 4e^{\mu_N} - 2)}{\mu_N^4 e^{\mu_N}}
 \end{aligned} \tag{A.12}$$

The covariance of the integrals of two different Poisson square-wave fields with simultaneous jumps but different, possibly correlated, amplitudes is needed too. Similarly to formula (A.3) (and using formula (A.9)) one finds that

$$\text{Cov}[\hat{Y}, \tilde{Y}] = \text{Cov}[\hat{Z}, \tilde{Z}] \left\{ \frac{2}{\mu_N} + \frac{2}{\mu_N^2} (e^{-\mu_N} - 1) \right\} \tag{A.13}$$

where

$$\hat{Y} = \int_0^1 \hat{Z}(\xi) d\xi \quad , \quad \tilde{Y} = \int_0^1 \tilde{Z}(\xi) d\xi \tag{A.14}$$

are the integral of the processes.

A.2 The Point Pulse Field

Deriving expressions for the skewness and kurtosis of the Poisson point pulse field is computationally much simpler than what was seen above. So, instead of computing the central moments up to and including the fourth order, expressions for the skewness and kurtosis are presented. As the process is a point pulse process the integral becomes a sum:

$$Y = \int_0^1 Z(\xi) d\xi = \sum_{i=1}^N Z_i \quad (\text{A.15})$$

where now the subscript i is simply a counter and not as before an indicator of the point ξ_i . The random variable N counts the random number of pulses in the interval $[0; 1]$. As the process is homogeneous N is Poisson distributed with parameter μ_N . Since the Z_i 's are independent the moments of the sum in (A.15) are easily obtained by use of the moment generating function $\phi(u)$ of the pulses. Conditioned on $N = n$ the moment generating function $\psi(u)$ of the sum is $\phi^n(u)$. Now, unconditioning by the Poisson probabilities gives

$$\begin{aligned} \psi(u) &= \sum_{n=1}^{\infty} \phi^n(u) e^{-\mu_N} \frac{\mu_N^n}{n!} \\ &= \exp [\mu_N (\phi(u) - 1)] \end{aligned} \quad (\text{A.16})$$

As skewness and kurtosis are unaffected by changes of mean and variance, assume that the pulses have zero mean and unit variance. Then the first four derivatives of $\phi(u)$ for $u = 0$ are 0, 1, skewness $\alpha_3[Z]$, and kurtosis $\alpha_4[Z]$ of the pulses. Then, by taking the first four derivatives at $u = 0$ of $\psi(u)$ the first four moments 0, μ_N , $\mu_N \alpha_3[Z]$ and $3\mu_N^2 + \mu_N \alpha_4[Z]$ of the integral are obtained. Thus the skewness and kurtosis of the integral become

$$\alpha_3[Y] = \frac{\alpha_3[Z]}{\sqrt{\mu_N}} \quad (\text{A.17})$$

$$\alpha_4[Y] = 3 + \frac{\alpha_4[Z]}{\mu_N} \quad (\text{A.18})$$

respectively (suppressing again the coordinate in $Z(\xi)$).

The covariance of the integrals of two Poisson point pulse fields with identically situated pulses of different possibly correlated pulse magnitude is also required. One easily finds by conditioning on $N = n$ and subsequent unconditioning by the Poisson probabilities that (compare with (2.3))

$$\text{Cov}[\hat{Y}, \tilde{Y}] = \text{Cov}\left[\sum_{i=1}^N \hat{Z}_i, \sum_{j=1}^N \tilde{Z}_j\right] = \mu_N \text{Cov}[\hat{Z}, \tilde{Z}] + \mu_N E[\hat{Z}] E[\tilde{Z}] = \mu_N E[\hat{Z}, \tilde{Z}] \quad (\text{A.19})$$

Bibliography

- [1] T. K. Caughey. Random excitation of a system with bilinear hysteresis. *J. Applied Mechanics, ASME*, 27:640–643, 1960.
- [2] H. Cramér and M. R. Leadbetter. *Stationary and Related Stochastic Processes*. John Wiley & Sons, New York, 1967.
- [3] O. Ditlevsen. *Uncertainty Modelling*. McGraw-Hill, 1981.
- [4] O. Ditlevsen. Elasto-plastic oscillator with gaussian excitation. *Journal of Engineering Mechanics*, 112(4):386–406, 1986.
- [5] O. Ditlevsen. Dimension reduction and discretization in stochastic problems by regression method. In F. Casciati and B. Roberts, editors, *Mathematical Models for Structural Reliability Analysis*, CRC Mathematical Modelling Series, pages 51–138. CRC Press, Boca Raton, 1996. ISBN 0-8493-9631-X.
- [6] O. Ditlevsen and L. Bognár. Plastic displacement distributions of the gaussian white noise excited elasto-plastic oscillator. *Probabilistic Engineering Mechanics*, 8:209–231, 1993.
- [7] O. Ditlevsen and H. O. Madsen. *Structural Reliability Methods*. Wiley, Chichester, 1996. ISBN 0-471-96086-1.
- [8] O. Ditlevsen and N. J. Tarp-Johansen. White noise excited non-ideal elasto-plastic oscillator. *Acta Mechanica*, 125:31–48, 1997.
- [9] O. Ditlevsen and N. J. Tarp-Johansen. Choice of input fields in stochastic finit elements. *Probabilistic Engineering Mechanics*, 14(1-2):63–72, 1999.
- [10] O. Ditlevsen and N. J. Tarp-Johansen. Slepian modeling as a computational method in random vibration analysis of hysteretic structures. In *Proc. of the 3’rd Int. Conf. on Computational Stochastic Mechanics, Thera – Santorini, Greece, June 14-17, 1998*, pages 67–78, Rotterdam, 1999. A.A. Balkema.
- [11] O. Ditlevsen, N. J. Tarp-Johansen, and H. Denver. Bayesian soil assessments from prior censored samples. *Computers And Geotechnics*, 2000. Accepted for publication.

-
- [12] O. Ditlevsen, N. J. Tarp-Johansen, and S. Randrup-Thomsen. Elasto-plastic frame under horizontal and vertical gaussian excitation. In *Proc. of the 4'th Int. Conf. on Stochastic Structural Dynamics, Notre Dame, August 6-8, 1998*, pages 429–438, Rotterdam, 1999. A.A. Balkema. To appear in slightly revised version in *Journal of Nonlinear Dynamics*.
- [13] C. Gardiner. *Handbook of Stochastic Methods, for physics, Chemistry and the natural sciences*. Springer, Berlin Heidelberg, 1997. 2'nd Ed., 4'th printing.
- [14] M. Geradin and D. Rixen. *Mechanical Vibrations, Theory and Applications to Structural Dynamics*. Wiley, Chichester, 1997. 2'nd Ed.
- [15] A. M. Hasofer, O. Ditlevsen, and N. J. Tarp-Johansen. Positive random fields for modeling material stiffness and compliance. In *Proc. of ICOSSAR'97 – the 7'th Int. Conf. on Structural Safety and Reliability, Kyoto, November 24-28, 1997*, pages 723–730, Rotterdam, 1998. A.A. Balkema.
- [16] D. Karnopp and T. D. Scharon. Plastic deformation in random vibration. *J. of the Acoustical Society of America*, 39(6):1154–1161, 1966.
- [17] Y. K. Lin. On the standard deviation of change-in-impedance due to fuzzy subsystems. *J. Acoust. Soc. Am.*, 101(1):616–618, 1997.
- [18] S. Randrup-Thomsen. *Analysis of the White Noise Excited Elasto-Plastic Oscillator of Several Degrees of Freedom*. PhD thesis, Dept. of Structural Engineering and Materials, Tech. University of Denmark, Build. 118, Brovej, Tech. University of Denmark, DK-2800 Kgs. Lyngby, Denmark, December 1996.
- [19] J. B. Roberts. The yielding behaviour of a randomly excited elasto-plastic structure. *J. Sound Vibrations*, 72:71–85, 1980.
- [20] C. Soize. A model and numerical method in the medium frequency range for vibroacoustic predictions using the theory of structural fuzzy. *J. Acoust. Soc. Am.*, 94(2):849–865, 1993.
- [21] M. Strasberg and D. Feit. Vibration damping of large structures induced by attached small resonant structures. *J. Acoust. Soc. Am.*, 99(1):335–344, 1996.
- [22] N. J. Tarp-Johansen, O. Ditlevsen, and Y. K. Lin. Secondary systems modeled as fuzzy sub-structures. In *Proc. of ICOSSAR'97 – the 7'th Int. Conf. on Structural Safety and Reliability, Kyoto, November 24-28, 1997*, Rotterdam, 1998. A.A. Balkema.
- [23] S. R. Winterstein. Nonlinear vibration models for extreme and fatigue. *J. Engrg. Mech., ASCE*, 114:1772–1790, 1988.